

METAMORPHIC REACTIONS IN SOME

SCOTTISH BASIC INTRUSIONS

PANJAWAN MONGKOLTIP

A thesis submitted for the degree
of DOCTOR OF PHILOSOPHY at
the University of Aston in Birmingham
DEPARTMENT OF GEOLOGICAL SCIENCES

JULY, 1983

To My Parents

THE UNIVERSITY OF ASTON IN BIRMINGHAM

METAMORPHIC REACTIONS IN SOME SCOTTISH BASIC INTRUSIONS

PANJAWAN MONGKOLTIP

THESIS SUBMITTED FOR THE DEGREE OF DOCTOR OF PHILOSOPHY

JULY, 1983

SUMMARY

Three main mineralogical alterations were studied in two syn-orogenic basic igneous suites, the 'Younger' basic complex and the Glen Scaddle intrusion. They were examined using optical microscopy, electron probe microanalysis, scanning and transmission electron microscopy and x-ray diffraction.

Olivine and plagioclase reacted to form coronas comprising a layer sequence olivine-orthopyroxene - amphibole - (amphibole + spinel symplectite) - plagioclase, separated by a sharp boundary. In some specimens, discontinuous layer of amphibole + anorthite symplectite is developed. Quantitative model reactions are written based on the evidence of restricted movements of Al and Si in plagioclase when made over to symplectites. This is shown by the inheritance of Al/Si ratios of plagioclase in both symplectites. Fe, Mg and O released from olivine \longrightarrow orthopyroxene transformation moved into the amphibole + spinel symplectite, causing the boundary to move towards olivine.

Igneous clinopyroxene changed to metamorphic compositions of higher Ca while reacting to actinolite by exchanging Ca, Mg and Fe with the environment. At the initial stage, when metamorphic pyroxene predominated over actinolite, the reaction consumed Ca and released Fe, Mg. Ca was released when more actinolite was produced. Ca may partly come from the simultaneous reaction actinolite + plagioclase \longrightarrow hornblende + quartz. Orthopyroxene is pseudomorphed by cummingtonite which simultaneously reacts with plagioclase forming hornblende rims. Possible model reactions for each system are proposed. They suggest variable degrees of open - system behaviour. Although Fe and Mg partition approaches metastable equilibrium between actinolite and hornblende in the Glen Scaddle area, in which hornblende closely approaches equilibrium with plagioclase, the abruptness of the actinolite core/hornblende rim transition is interpreted as due to sluggishness of Al diffusion. Thus this boundary may be inherited from the original plagioclase/pyroxene interface and is not an equilibrium feature.

Primary hornblende of high Ti content is equilibrated at lower temperature by exsolving oriented ilmenite and rutile in approximately a closed system. The orientations of ilmenite are controlled by semi-coherent relations of oxygen atom packing to the hornblende.

Key words: Corona, pyroxenes, actinolite, hornblende, cummingtonite.

ACKNOWLEDGEMENTS

The author is deeply grateful to her supervisor, Dr J. R. Ashworth for his kind and invaluable assistance, guidance and encouragement throughout the course of this study as well as many discussions and useful suggestions in the fulfilment of this work.

Acknowledgements are made to the technicians in the Departments of Geological Sciences and Metallurgy and Materials, particularly to Mr J. H. Williams for his technical advice, Mr R. G. Howell in the SEM and electron probe work, Mr K. Murthy for the Mössbauer work and Miss G. Thomas, Department of Civil Engineering for digitizer.

The author would like to express her deepest thanks to Drs D. J. Vaughan, R. A. Ixer and A. D. Chambers for their advice and useful suggestions, and to Mr C. Limpichotikul for his help in the preparation of some tables and corrections to the typescript.

Finally, her sincere gratitude is dedicated to her parents for their financial support, patience and encouragement without which, this work would have never been possible.

CONTENTS

	<u>Page</u>
Summary	i
Acknowledgements	ii
Contents	iii
List of Figures	vii
List of Tables	xii
Chapter 1 Introduction	1
1.1 Scope of the study	1
1.2 Method	2
Chapter 2 General geology and petrography of the Glen Scaddle intrusion and the 'Younger' basic complex in Scotland	3
2.1 Glen Scaddle intrusion	3
2.1.1 Geological setting	3
2.1.1 Petrography	5
2.2 The 'Younger' basic igneous complex in NE Scotland	10
2.2.1 General geological setting	10
2.2.2 Belhelvie mass	12
2.2.3 Morven-Cabrach mass	16
2.2.4 Huntly-Portsoy masses	23
Chapter 3 Formation of coronas around olivine in 'Younger' basic complex in Aberdeenshire and Banffshire, NE Scotland	25
3.1 Introduction	25

	<u>Page</u>
3.2 Previous work on corona formation between olivine and plagioclase	26
3.3 Description of areas	29
3.4 Petrographic descriptions	30
3.5 Mineral chemistry	34
3.5.1 Electron probe microanalyses	34
3.5.1.1 Method	34
3.5.1.2 Results	35
3.5.2 Semi-quantitative analyses using SEM	45
3.5.3 Energy-dispersive electron probe results	46
3.6 SEM study of symplectite	48
3.6.1 The secondary electron image and X-ray maps	48
3.6.2 Back scattered electron image	51
3.7 Estimation of volume proportion of corona minerals	53
3.7.1 Method	53
3.7.2 Results	57
3.8 Interpretation and discussion	57
3.9 Conclusion	76
 Chapter 4 Compositional characteristics of pyroxenes and amphiboles, and relationships among these minerals.	 79
4.1 Introduction	79
4.2 Detailed petrographic relationships between pyroxenes and replacing amphiboles	

	<u>Page</u>
and among coexisting amphiboles.	83
4.2.1 Glen Scaddle area	83
4.2.2 Morven-Cabrach area	89
4.2.3 Belhelvie area	
4.3 Estimation of Fe ³⁺ in amphibole analyses by Mössbauer spectroscopy	100
4.4 Mineral compositions	106
4.4.1 Glen Scaddle intrusion	107
4.4.2 Morven-Cabrach intrusion	124
4.4.3 Belhelvie intrusion	138
4.5 Interpretation and discussion	145
4.5.1 Soldus and subsolidus compositional relationships of some coexisting pyroxenes from the studied areas	145
4.5.2 Replacement of clinopyroxene by actinolite	154
4.5.3 Replacement of hypersthene by cummingtonite	158
4.5.4 Model reactions for the formation of actinolite, cummingtonite and hornblende	162
4.5.5 Coexisting actinolite and hornblende	172
4.5.6 Coexisting cummingtonite and calcic amphibole	189
4.5.7 Hornblende-plagioclase relations	194
4.6 Conclusions	197

	<u>Page</u>
Chapter 5 Exsolution of ilmenite and rutile in hornblende	199
5.1 Introduction	199
5.2 Specimen localities	200
5.3 Petrography	200
5.4 Scanning electron microscopy	202
5.5 Mineral compositions	205
5.6 Estimation of volume proportions of ilmenite inclusions in a hornblende	207
5.7 Orientation relationships between ilmenite and hornblende host	208
5.7.1 Universal-stage measurement	208
5.7.2 Transmission electron microscopy	210
5.7.3 Single crystal X-ray diffraction	212
5.8 Comparison of ilmenite and hornblende crystal structures	218
Appendix 1 Specimen lists and locality maps	221
Appendix 2 Supplementary pyroxenes and amphibole analyses	229
References	252

LIST OF FIGURES

<u>Figure</u>	<u>Page</u>
2.1 Locality and boundary of the Glen Scaddle intrusion	4
2.2 Optical micrograph showing primary brown hornblende surrounding actinolite	7
2.3 Geological sketch map of NE Scotland	11
2.4 Geological map of the Belhelvie mass	13
2.5 Geological map of the Morven-Cabrach mass	17
2.6 Optical micrograph of discrete cummingtonite grain enclosing hypersthene	19
2.7 Optical micrograph of hypersthene and replacing cummingtonite with primary and secondary hornblende	22
3.1 Optical micrograph showing typical corona between olivine and plagioclase	32
3.2 Optical micrograph showing corona with the third layer of amphibole-anorthite symplectite	33
3.3 Comparison of Fe/Mg partition in olivine and orthopyroxene between literature and studied areas	38
3.4 Electron-microprobe line scans across coronas of specimen 710 C	43
3.5 Electron-microprobe line scans across coronas of specimen 15/18763	44
3.6 Energy dispersive X-ray spectra of spinel	47
3.7 SEM micrographs showing secondary electron image and X-ray maps of typical corona	49
3.8 SEM micrographs showing secondary electron image and X-ray maps of 2 types of symplectite	50

<u>Figure</u>	<u>Page</u>
3.9 BSE images of symplectites	52
3.10 Digitizer equipment	54
3.11 Graphical display of number of atoms across the typical corona of 53 P	59
3.12 Graphical display of number of atoms across corona with amphibole + anorthite symplectite of 15/18763	60
3.13 Element diffusion model of corona reaction	77
4.1 Optical micrograph showing relict clinopyroxene in pseudomorphing actinolite and surrounding hornblende	85
4.2 Optical micrograph showing gradational contact between actinolite and hornblende	86
4.3 Optical micrograph showing actinolite aggregates with sharp contact with rimming hornblende	88
4.4a Optical micrograph showing relict clinopyroxene set next to cummingtonite, both are edged by continuous hornblende	91
4.4b Optical micrograph relict orthopyroxene with blebby clinopyroxene exsolution and replacing cummingtonite	91
4.5 Optical micrograph showing acicular grains of edging hornblende around cummingtonite	93
4.6 Optical micrograph showing sharp contact between cummingtonite core and rimming hornblende	94
4.7 Optical micrograph showing interlocking grains of hornblende aggregates	96
4.8 Optical micrograph showing deformed hypersthene which is replaced along margins by cummingtonite	98

<u>Figure</u>	<u>Page</u>
4.9 Optical micrograph showing orthopyroxene completely replaced by cummingtonite aggregates with thin zone of fringing hornblende	99
4.10 Mössbauer spectrum of hornblende	104
4.11 Electron probe line-scan across actinolite and hornblende of specimen 603 C	108
4.12 Electron probe line-scan across actinolite and hornblende of specimen 652 C	109
4.13 Ca-Fe-Mg diagram of pyroxenes from the Morven-Cabrach area and associated areas	146
4.14 Ca-Fe-Mg diagram of pyroxenes from the Belhelvie area	147
4.15 Ca-Fe-Mg diagram of pyroxenes from the Glen Scaddle area	148
4.16 Graphical pyroxene geothermometer	152
4.17 Fe/Mg partition between clinopyroxene and actinolite	157
4.18 Fe/Mg partition between orthopyroxene and cummingtonite	161
4.19 Schematic diagram showing directions of Ca ²⁺ and (Mg, Fe) ²⁺ movements related to the amount of metamorphic pyroxene produced	166
4.20 Plot of actinolite and hornblende pairs in terms of 100 Mg/Mg + Fe and Si according to nomenclature	174
4.21 Plot of coexisting actinolite-hornblende in actinolite and hornblende fields of Shido and Miyashiro	176
4.22 Intimately coexisting actinolite-hornblende pairs plotted in the diagram of Shido and Miyashiro	177

<u>Figure</u>	<u>Page</u>
4.23 The Mg-Fe-Al ^{iv} diagram of coexisting actinolite-hornblende	179
4.24 Fe-Mg partition between coexisting calcic-amphiboles	180
4.25 Plot of A site occupancy, Al ^{vi} and Al ^{iv} verses Fe/(Fe + Mg) for Glen Scaddle actinolite and hornblende	181
4.26 Coexisting actinolite and hornblende across compositional gap suggested by the data of Misch and Rice	182
4.27 Plot of total alkalis against tetrahedral Al for calcic amphiboles	184
4.28 Plot of tetrahedral Al against total Al for calcic amphiboles in Glen Scaddle area	185
4.29 Plot of tetrahedral Al against total Al for calcic amphiboles in Morven-Cabrach area	186-
	187
4.30 Plot of tetrahedral Al against total Al for calcic amphiboles in Belhelvie area	188
4.31 Ca-Mg-Fe plots of coexisting cummingtonite and calcic amphiboles	191
4.32 Mg-Fe partition between cummingtonite and hornblende	192
4.33 Plot of K_D hb-cum against Al ^{iv} content in hornblende	193
4.34 Relationships between hornblende and associated plagioclase	195
4.35 Relations between Al ^{vi} and Si in hornblendes	196

<u>Figure</u>	<u>Page</u>
5.1 Optical micrographs of oriented inclusions in hornblende	201
5.2 Energy dispersive X-ray spectra of ilmenite and rulite inclusions	203
5.3 SEM photographs showing ilmenite and rulite inclusions	204
5.4 Stereographic projection showing the orientation relationships of ilmenite inclusions to host hornblende	209
5.5 Electron diffraction patterns of hornblende host and ilmenite inclusions	211- 212
5.6 TEM micrographs showing shapes and sizes of ilmenite inclusions	213
5.7 X-ray oscillation photographs of hornblende	216
5.8 The arrangement of oxygen atoms in hornblende and ilmenite	219

APPENDIX 1

1 Specimen locality map of Glen Scaddle area	222
2 Specimen locality map of Morven-Cabrach area	225
3 Specimen locality map of Belhelvie area	227

LIST OF TABLES

<u>Table</u>	<u>Page</u>
3.1 EPMA of olivine	36
3.2 EPMA of orthopyroxene	37
3.3 EPMA of amphibole	40
3.4 EPMA of plagioclase	42
3.5 Estimated volume proportions of corona minerals	56
3.6 Comparison of numbers of atoms in corona minerals before and after volume corrections in specimen 53 P	61
3.7 Comparison of numbers of atoms in corona minerals before and after volume corrections in specimen 15/18763	62
3.8 Comparison of Al: Si in symplectite and primary plagioclase	66
3.9 Estimated coefficients in the corona reaction	75
4.1 EPMA of the amphibole used in Mössbauer work	102
4.2 EPMA of clinopyroxene and amphiboles in 603 C	104
4.3 EPMA of amphiboles in 685 C	111
4.4 EPMA of clinopyroxenes and amphiboles in 683 C and 678 C	112
4.5 EPMA of primary and secondary amphibole in 687 C	113
4.6 EPMA of clinopyroxenes and amphiboles in 604 C and 655 C	114
4.7 EPMA of clinopyroxene and amphiboles in 657 C	115
4.8 EPMA of clinopyroxene and amphiboles in 652 C	116
4.9 EPMA of clinopyroxene and amphiboles in 603 C	117

<u>Table</u>	<u>Page</u>
4.10 EPMA of clinopyroxene, pseudomorphous actinolite and surrounding primary brown hornblende of 602 C	118
4.11 EPMA of clinopyroxene and amphiboles of 601 C	119
4.12 Partial analyses of plagioclase in Glen Scaddle area	122
4.13 Analyses of epidote of specimen 678 C	123
4.14 EPMA of orthopyroxene and amphiboles of 62 P	125
4.15 EPMA of orthopyroxene and amphiboles of 724 C	126
4.16 EPMA of clinopyroxene and amphiboles of 84 P	127
4.17 EPMA of clinopyroxene and amphiboles of 81 P	128
4.18 EPMA of amphiboles of 741 C	129
4.19 EPMA of clinopyroxene and amphiboles of 757 C and 758 C	130
4.20 EPMA of orthopyroxenes and amphiboles of 725 C, 67 P and 65 P	131
4.21 EPMA of clinopyroxenes and amphiboles of 73 P and 733 C	132
4.22 EPMA of orthopyroxenes and amphiboles of 746 C and 735 C	133
4.23 Partial analyses of plagioclase of the Morven- Cabrach area	137
4.24 EPMA of pyroxenes and amphiboles of 19 D and 19 E	139
4.25 EPMA of pyroxenes and amphiboles of 38 P	140
4.26 EPMA of pyroxenes and amphiboles of 33 P	141
4.27 Partial analyses of plagioclase in the Belhelvie area	144
4.28 Estimated temperature of coexisting pyroxenes	151

4.29	Comparison between clinopyroxene and replacing actinolite in terms of differences in numbers of atoms of each elements per 240 (OH)	156
4.30	Comparison between orthopyroxene and replacing actinolite in terms of differences in numbers of atoms of each elements per 240 (OH)	160
5.1	EPMA of hornblende of 612 C, 659 C and ilmenite of 612 C	206
5.2	Indexed ilmenite spots of single crystal X-ray oscillation photographs	

APPENDIX 2

1.	Supplementary pyroxenes and amphiboles analyses of the Glen Scaddle specimens	230
2.	Supplementary pyroxenes and amphiboles analyses of the Morven-Cabrach specimens	237
3.	EPMA of pyroxenes and amphiboles in 625 C, 626 C, the Portsoy intrusion	249
4.	EPMA of primary clinopyroxene from coronite specimens of the Belhelvie mass	251

CHAPTER ONE

INTRODUCTION

1.1 SCOPE OF THE STUDY

This study focuses on some reactions which occurred in two main syn-orogenic basic igneous suites; the "Younger" basic complex and the Glen Scaddle intrusion. The "Younger" basic complex was intruded into the Dalradian Terrain of NE Scotland during the main Caledonian Orogeny or M₃ metamorphism (Stewart and Johnson 1960, Munro 1970, Stewart 1970, Fettes 1970 and Pankhurst, 1970). The complex comprises the Huntly, Inch, Haddo House, Arnage, Morven-Cabrach and Belhelvie masses. The Glen Scaddle intrusion which has originally been termed "epidiorite" (Drever, 1940) due to the plagioclase composition, was emplaced into the already regionally metamorphosed Moine series of SW Scotland between D1 and D2 deformation events during a very slow regional uplift period (Stoker, 1980). The metamorphism in these intrusions is mainly due to introduction of volatiles, mainly water. So, primary anhydrous minerals were modified by hydrous mineral pseudomorphing.

The present study reports on three main mineralogical changes during this period. The second chapter is intended to provide a general idea of the geology and petrography of the studied intrusions. An early stage of metamorphism is shown by the development of coronas around olivine against plagioclase. Such coronas are composed of two main layers, separated by a sharp boundary. The inner layer next to olivine is orthopyroxene, while the outer layer is made up of consecutively amphibole and amphibole + spinel symplectite

with occasional occurrence of patches of hornblende + anorthite symplectite as a third discontinuous layer. Attention is focussed on the reactions involved in corona formation in the Belhelvie and Huntly intrusions. Chapter 3 is devoted to them.

One of the most characteristic features in all the studied basic intrusions is the pseudomorphing of pyroxenes by amphiboles, which are actinolite after clinopyroxene and cummingtonite after orthopyroxene. Both amphiboles are surrounded by a thin zone of hornblende. Their relationships along with the pyroxene - amphibole transformation will be described in detail, both texturally and chemically, in three intrusions; the Glen Scaddle, the Morven-Cabrach and the Belhelvie. This is the subject of chapter 4. Chapter 5 deals with the development of oriented oxide inclusions in hornblende from the Glen Scaddle intrusion, and the Glen Loy intrusion which is also of Caledonian syn-orogenic age.

1.2 METHOD

The main technique used in the present study was electron probe microanalysis to estimate compositions of minerals as well as produce concentration profiles across mineral grains. Scanning electron microscopes were employed to study symplectites, which are very fine-grained intergrowths, and tiny inclusions in hornblende. Particularly, this technique is very useful in identifying and distinguishing mineral phases. Transmission electron microscopy was used to study the orientation relationships between oxide inclusions and hornblende host, as well as the single crystal X-ray oscillation technique. Fe^{3+}/Fe^{2+} ratio in a hornblende was estimated by Mössbauer spectroscopy.

CHAPTER TWO

GENERAL GEOLOGY AND PETROGRAPHY OF GLEN SCADDLE INTRUSION AND THE 'YOUNGER' BASIC COMPLEX IN SCOTLAND

2.1 GLEN SCADDLE INTRUSION

2.1.1 Geological Setting

Drever (1940) regarded the sheet-like Glen Scaddle mass as a large massive coarse-grained epidiorite (metagabbro) which intruded into the psammitic or semi-pelitic gneiss of the Moine Series of the SW Scottish Highlands after the regional metamorphism. The intrusion forms an oblong-shaped outcrop trending NW from the shores of Loch Linnhe, for some 10 km (Fig. 2.1). Recent detailed work by Stoker (1980) suggested that this Caledonian intrusion was emplaced as a sub-horizontal sheet during the interval between D_1 and D_2 deformation which was the period of very slow regional uplift. The mass was folded after consolidation, during D_2 , so it is now the core of the Glen Scaddle Synform.

Stoker (1980) further proposed to support Drever's idea that the emplacement of the sheet post-dated the peak of the regional metamorphism of the country rocks which were probably still very hot, hence the narrow metamorphic aureole. The metagabbro was subsequently regionally metamorphosed at amphibolite facies during D_2 deformation, although retrogression zones occur locally.

The physical conditions during the Glen Scaddle intrusion were estimated, based on the contact metamorphic cordierite-garnet

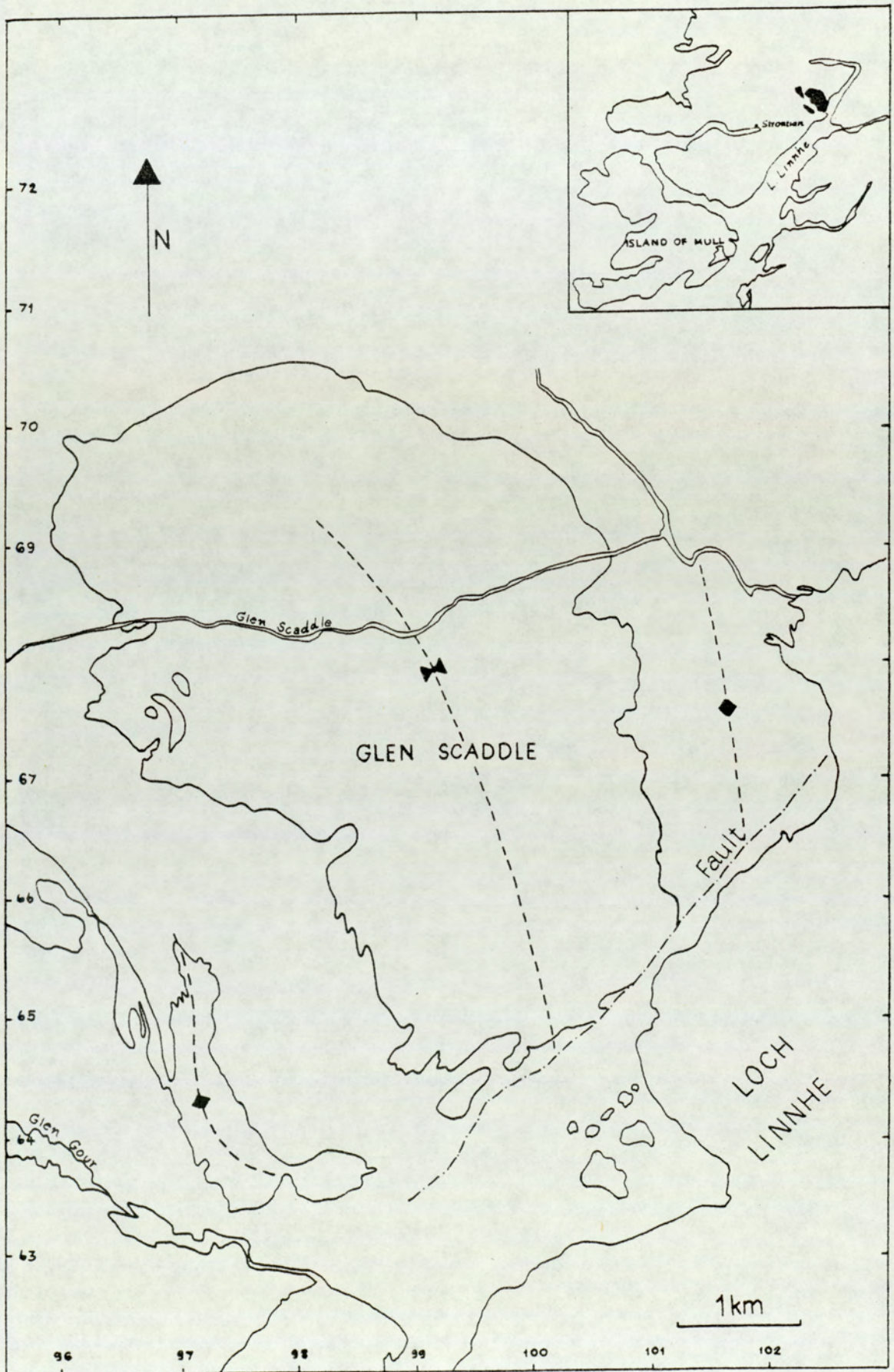


Fig. 2.1 Locality of the Glen Scaddle intrusion. The boundary of the mass after Geological Survey of Great Britain sheet 53 (Ben Nevis). The major structures from Stoker (1980).

coexistence in the aureole by Ashworth and Chinner (1978) who suggested T of 790 - 820°C and a pressure estimate of 5.2 - 6 kbar.

2.1.2 Petrography

Although the Glen Scaddle intrusion has suffered from subsequent deformation and metamorphism, during the waning phase of the regional orogenic events, its original minerals and textures are still widely preserved. The majority of textures in the Glen Scaddle rocks are the typical hypidiomorphic granular texture associated with plutonic rocks rather than a metamorphic texture with polygonal grain intersections at 120° triple points.

In rocks that have been intensely sheared, foliation texture developed with characteristic augen of blastoporphyrritic relic plagioclase and amphibole surrounded by oriented clusters of quartz, chlorite, ilmenite and sphene.

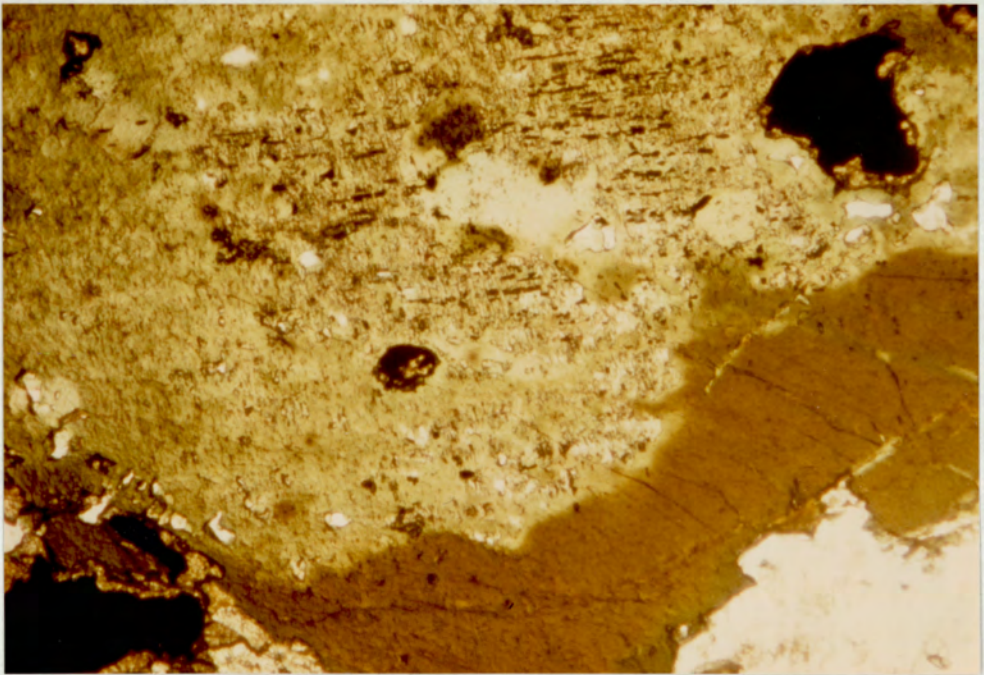
The major minerals of the metabasic rocks found in this study are plagioclase, amphibole and clinopyroxene with variable amounts of quartz, biotite, chlorite, microperthite and myrmekite. Accessory minerals include sphene, ilmenite, apatite and epidote.

Plagioclase laths are medium-coarse grained with well-developed albite, Carlsbad and pericline twinning. Bent, irregular and wedge-shaped twinning lamellae are often formed by strain effects. Zoning is easily seen under the microscope. This is normal zoning from a more calcic core (An 32-50) to a sodic margin (An 23-45). The compositions of plagioclase were determined by the combined albite-Carlsbad twinning method and EPMA. It is interesting to

note that the plagioclase composition is generally consistent within the andesine range, throughout the mass, both in rocks that are highly deformed and those in which primary minerals and textures are predominant. The margins of plagioclase laths are generally irregular and sometimes diffuse suggesting corrosion by intergranular fluid which is now represented by interstitial granophyric quartz. Myrmekite of quartz-plagioclase is developed dominantly along plagioclase margins and rarely within plagioclase grains. Associated with myrmekite is microperthite which is often present in variable amount. Alteration to fine-grained mica (sericitization) is also a common feature of plagioclase.

The primary pyroxenes that still survive^y as relics in some specimens are clinopyroxene usually containing small platy ilmenite inclusions. Replacement of pyroxene by amphibole is found in various stages of alteration and deformation. In specimens where primary minerals and textures are well preserved (602C), pyroxenes are surrounded by primary large homogeneous deep greenish-brown hornblendes with deep green margins. Pyroxene is being pseudomorphed along edges and cleavages by colourless pale green actinolite showing optical continuity with surrounding brown hornblende (Fig.2.2). Contacts between actinolite and hornblende are generally sharp.

In deformed and metamorphosed rocks, pyroxene is completely replaced by small, multi-crystal aggregates of pale green actinolite with fine opaque inclusions. Many characteristics of the original pyroxene are retained by the secondary amphibole: these include stubby prismatic growth, simple twinning, and patterns of opaque inclusions. Wrapped around these actinolite aggregates is a thin



0.25 mm.

Fig 2.2 Primary deep brown hornblende surrounding relict clinopyroxene which is almost entirely replaced by actinolite. Ilmenite is marginally replaced by sphene (specimen 602 C).

zone of green hornblende which becomes olive green or bluish-green against plagioclase. Gradational changes in colour correspond to relative enrichment in Fe and Al towards the rim. The thin hornblende margins occur only where actinolite aggregate is in contact with plagioclase suggesting the source of Al to form hornblende is plagioclase.

The habit and grain size of replacing amphiboles are quite variable. They range from small fibrous varieties to large ragged porphyroblasts with quartz inclusions. More rarely, there are traces of relict brown hornblende as patches within actinolite aggregates. The aggregated habit, small grain size, thin hornblende margin and a large amount of quartz inclusions made it difficult to trace the boundary between actinolite core and thin hornblende rim. However, universal-stage observation accompanied by probe profiling indicates that their boundaries are commonly sharp with occasional gradation. The expansion of replacing amphibole into surrounding plagioclase is also a common feature.

Cummingtonite has been found in only 2 specimens (601C, 651C). They are fine-grained quartz-biotite norite. Cummingtonite forms an inner fibrous or prismatic core often containing opaque inclusions, mantled by very narrow, green hornblende when in contact with plagioclase. Cummingtonites could have derived from primary orthopyroxene which is noticed by Drever (1940) and Stoker (1980). Unfortunately it has not been found in this study.

In the least altered rocks, biotite forms coarse deep brown flakes occasionally enclosing pyroxene; biotite is also associated with the thin hornblende margin around actinolite and cummingtonite as

parallel, small overgrowth flakes. At a more advanced metamorphic stage, biotite is altered to fibrous assemblages of chlorite which are present in various amounts throughout the intrusion. Partial replacement of hornblende along the margins by chlorite and/or epidote, suggesting a retrogression process, is locally found.

Chlorite is pale green with anomalous blue to purplish blue interference colour, and is usually developed as massive aggregates between hornblende and plagioclase grains, sometimes growing into plagioclase along cracks.

Quartz is present mainly as fine to medium grained interstitial "granophyre" between plagioclase laths and less commonly as myrmekitic intergrowth with plagioclase. Ilmenite and sphene occur as conspicuous accessories. Sphene forms skeletons around or complete pseudomorphs after ilmenite, set in amphibole, pyroxene and chlorite. Accessory apatite is typical in various sizes. Prehnite may occur between biotite cleavages. Epidote is negligible, absent or locally abundant.

The Glen Scaddle metagabbro is mineralogically commensurate with the amphibolite facies of regional metamorphism. It is uncertain to what extent the plagioclase composition changed during metamorphism. Replacement of hornblende by chlorite accompanied by abundant epidote in some rocks could be the result of localized retrograde metamorphism to green-schist facies. The survival of primary minerals and igneous textures prevailing in the metagabbro indicate incomplete reactions and non-attainment of equilibrium during metamorphism.

2.2.1 General Geological Setting

The Younger Basic intrusions include the masses of Huntly, Inch, Haddo House, Arnage, Morven-Cabrach and Belhelvie (Fig. 2.3). It has been generally accepted that they intruded into the Dalradian hot country rocks during or very soon after the climax of regional metamorphism (M_3) as a thick single-sheet body which was folded after emplacement and consolidation but perhaps while still hot, by the major F_3 Caledonian (Boyndie-Buchan) movements. (Shackleton in discussion of Read and Farquhar 1956, Stewart and Johnson, 1960, Munro 1970, Stewart 1970, Fettes 1970 and Pankhurst 1970). However, there is no clear evidence of any effect of the F_3 movement on the deformation and shearing in these younger basic masses (Munro, 1970, Boyd and Munro, 1978).

The geochronological work by Pankhurst (1970, 1974) indicates that the Younger igneous complex is dated at 501 ± 17 Ma, an early Ordovician age. The deformation and metamorphic history of the complex's long cooling together with the country rocks has been interpreted in terms of fundamental orogenic processes such as the waning of the metamorphic climax and subsequent uplift. Pankhurst gave the conclusion (based on his interpretation of the K-Ar, Rb-Sr minerals ages taken together) that the long cooling period from 650°C or more to $\sim 400^\circ\text{C}$ was maintained for 20-30 Ma. Subsequently the cooling was relatively rapid to $150^\circ\text{C} - 200^\circ\text{C}$. Slow crystallization at high temperature has been supported by the gravity differentiation and cryptic layering in some masses. (Munro 1970, Clarke and Wadsworth 1970, Ashcroft and Boyd, 1976).

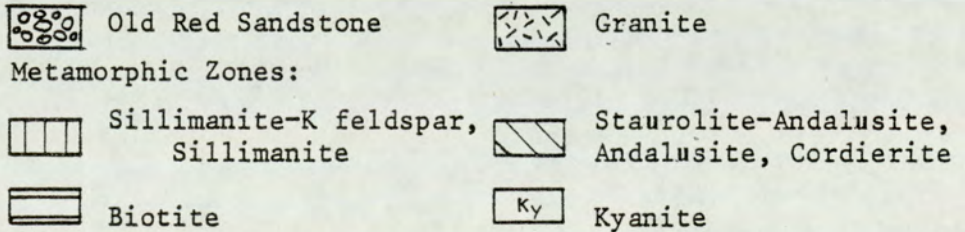
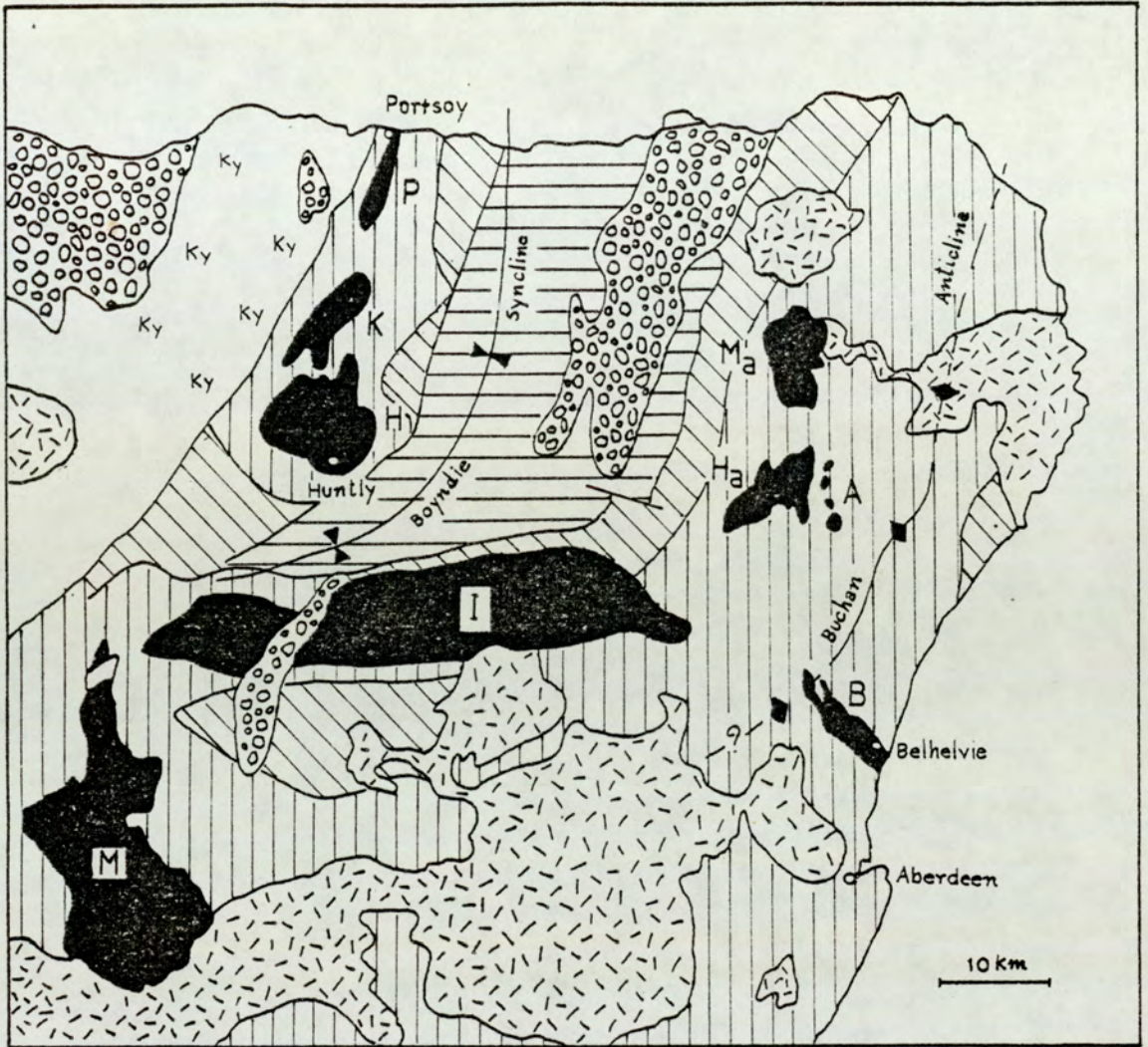


Fig. 2.3 Geological sketch-map of NE Scotland, showing distributions of the 'younger' basic complex.

H - Huntly mass	I - Insch mass	M - Morven-Cabrach
P - Portsoy mass	B - Belhelvie mass	A - Arnage mass
K - Knock mass	Ma - Maud mass	Ha - Haddo House mass

Based on Johnson & Stewart (1960), with additional metamorphic information from Read & Farquhar (1956), Fettes (1970), Ashworth (1975), Chinner & Heseltine (1979) and Hudson (1980). 'Younger' basic boundaries modified after Munro (1970), Ashcroft & Boyd (1976) and Allan (1970).

Gribble (1966) also suggested that the unusual large-scale partial melting of the country rocks around the Arnage and Haddo House complexes strongly indicated the long hot environment with repeated pulses of magma. As well in most of the large layer intrusions, the repeated injection of more than one pulse of magma is possible (Stewart 1970, Weedon, 1970, Ashworth, 1975).

2.2.2 Belhelvie Mass

The Belhelvie igneous mass is a gravity stratified intrusion composed of ultrabasic rocks, troctolite and gabbro/norite. It intruded into the Ellon Gneiss of the lower Dalradian and is exposed over the area of about 25 km² lying between 8 and 16 km north of Aberdeen. (Ashcroft and Boyd 1976). This mass was described in some detail by Stewart (1946) and Wadsworth et al (1966). Recently, Ashcroft and Boyd (1976) have revised the map of the intrusion based on a magnetic survey and shallow drilling. This map shows that the intrusion can be sub-divided into three parts (Fig. 2.4). The two northern areas are elongated lithological units with strike uniformly NNW-SSE. They are separated from each other by a septum of country rock. Both units contain a similar sequence of cumulate rocks of ultrabasic, troctolite and gabbro/norite from west to east with nearly vertical boundaries. The southern area consists mainly of ultrabasic cumulates. It is separated from the northern units by the NE-striking Belhelvie fault.

Cryptic layering is a prominent feature of the mass which has been turned through an angle of about 90° so that the layering is now vertical (Ashcroft and Boyd 1976). McGregor and Wilson (1967) gave the idea that the mass may be folded into an asymmetrical

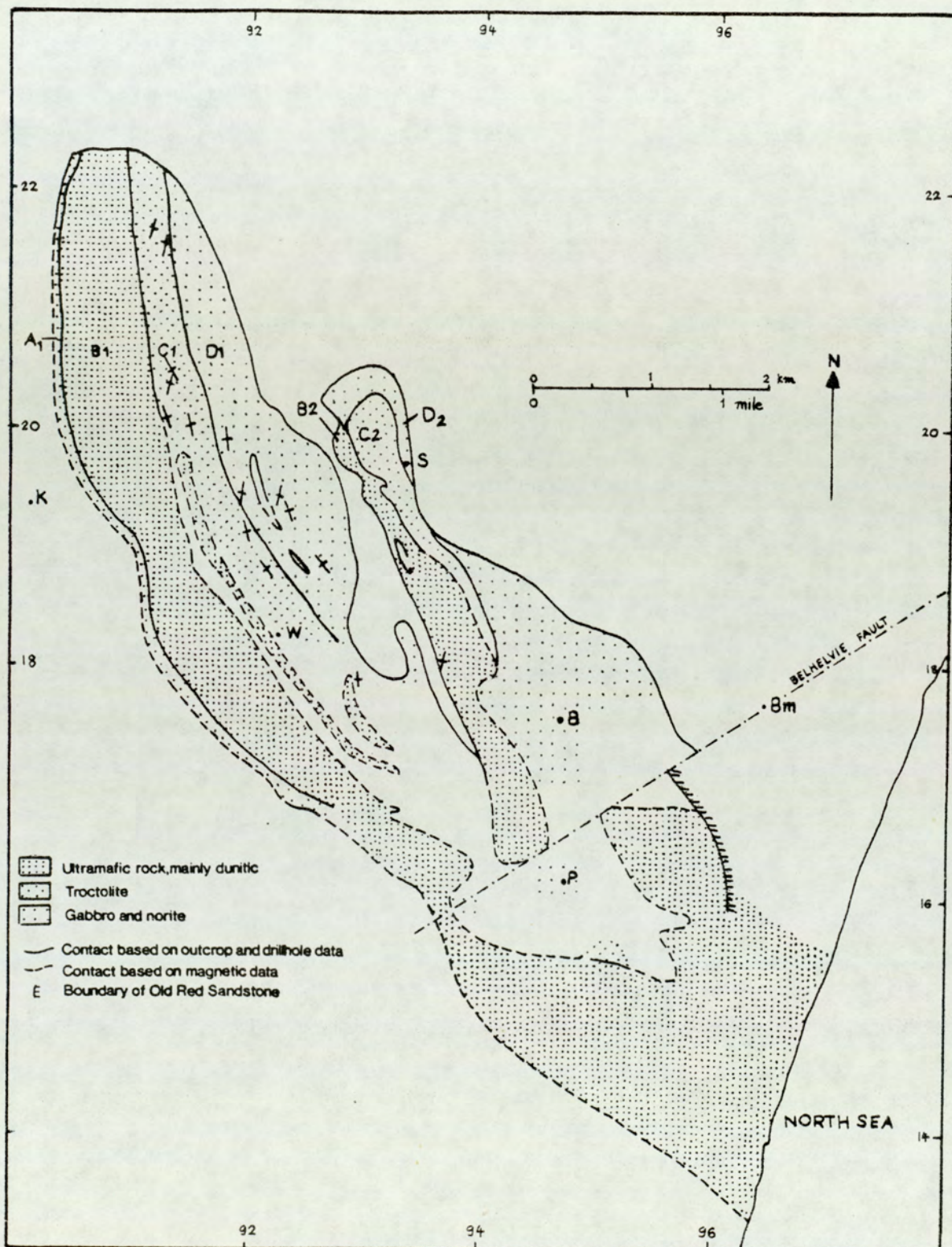


Fig. 2.4 Geological map of the Belhelvie mass based on Ashcroft and Boyd (1976).

syncline with a vertical limb which formed the portion exposed at present. The widespread shearing and mylonitization suggest amphibolite or hornblende-hornfels facies conditions. (Boyd and Munro, 1978).

Ultrabasic rocks (dunitic olivine cumulate)

Under the microscope, the mesh structure of serpentine after olivine is very common.

Troctolite (olivine - plagioclase cumulate)

Olivine and plagioclase are major minerals with small amounts of clinopyroxene and accessory chromite, pyrite and ilmenite. Olivine usually occurs as rounded grains and is largely serpentized. There is no zoning in olivine, with composition of Fo 80-85. Clinopyroxene is present as an intercumulate mineral, forming ophitic texture, in small amounts. Plagioclase is generally tabular in habit with composition of An 77-85. The outline of olivine has been modified by a corona or reaction rim of orthopyroxene and hornblende-spinel symplectite, when it is ⁱⁿ contact with plagioclase. The development of coronas around olivine is particularly common in troctolitic and olivine-gabbroic rocks of the complex. These have been studied in detail, and chapter 3 is devoted to them. Pseudomorphous cummingtonite and fine talc after coronitic olivine is occasionally found in some specimens.

These rocks grade from troctolite by the gradational disappearance of olivine and the incoming of pyroxene to become olivine gabbro, gabbro and norite. Most of the samples from this unit, which were

collected from the Balmedie Quarry, are highly deformed and uralitised rocks.

The primary minerals in this unit are (in approximate order of abundance) plagioclase, clinopyroxene, orthopyroxene, opaques, brown hornblende and rarely biotite. The relative proportions of orthopyroxene and clinopyroxene vary greatly, often within a short distance. The original igneous texture has been progressively broken down by the localized bending and marginal granulization and recrystallization of original minerals in the initial stage of cataclasis. Plagioclase tends to remain unaltered as large porphyroclasts with undulose extinction, deformation twinning or twisted twin planes. Pyroxenes are first bent and twisted, then marginally frayed by amphibole replacement. Orthopyroxenes react to fibrous aggregates of cummingtonite and talc which is surrounded by a thin zone of hornblende. Clinopyroxene is partially or completely pseudomorphed by fibrous actinolite with patchy marginal hornblende.

With continued recrystallization and shearing, in some cases actinolite and cummingtonite aggregates are replaced by crudely dimensionally oriented euhedral grains of green hornblende. These ferromagnesian minerals tend to form lensoid clusters, while plagioclase crystals frequently occur as isolated porphyroclasts set in a finer-grained matrix of these ferromagnesian minerals. In rare cases, brown hornblende with oriented opaque inclusions like those described in Chapter 5 forms rounded porphyroclasts. Composition of primary plagioclase is An 70-85 while the recrystallised ones are much more sodic, An 45-50. Quartz, occurs as fine-grained granular groundmass. Although uralitization is developed

very well in these deformed rocks, it also occurs extensively in undeformed rocks from elsewhere in the mass.

2.2.3 Morven-Cabrach mass

The Morven-Cabrach mass crops out in the counties of Aberdeen and Banff, extending some 15 miles in the N-S direction from the district of Cabrach towards Deeside (Fig. 2.5). Although this mass belongs to the same period of basic activity as the other 'younger' basic masses, there are certain differences from the others. The Morven-Cabrach basic intrusion was intruded in its present position, since there is no large scale shearing except in an east-west zone running through Strathdon and lower Glen Ernan (Allan, 1970). The characteristics of near-vertical attitude and lack of cryptic variation have been interpreted by Allan (1970) as indicating a feeder pipe body and very slow cooling of magma.

The northern part of the mass has been described in detail by Henry (1938) as quartz-biotite norite with uralitized veins. The unaltered rocks are characterized by short prismatic crystals of pyroxene which is mainly hypersthene, and often exhibit a strong exsolution of opaque oxides as thin plates or rods. Clinopyroxene is present in small amounts and usually as small crystals. Quartz is abundant in coarse grains. Plagioclase is labradorite (An 50-60). Biotite forms reddish-brown, large flakes enclosing apatite, pyroxene and plagioclase. Hornblende is generally pleochroic from olive-green to brownish-green. It occurs as big plates enclosing pyroxene and plagioclase, forming poikilitic textures. The other poikilitic mineral is colourless cummingtonite with or without coarse hornblende intergrowth (specimen 63 P). It is clear

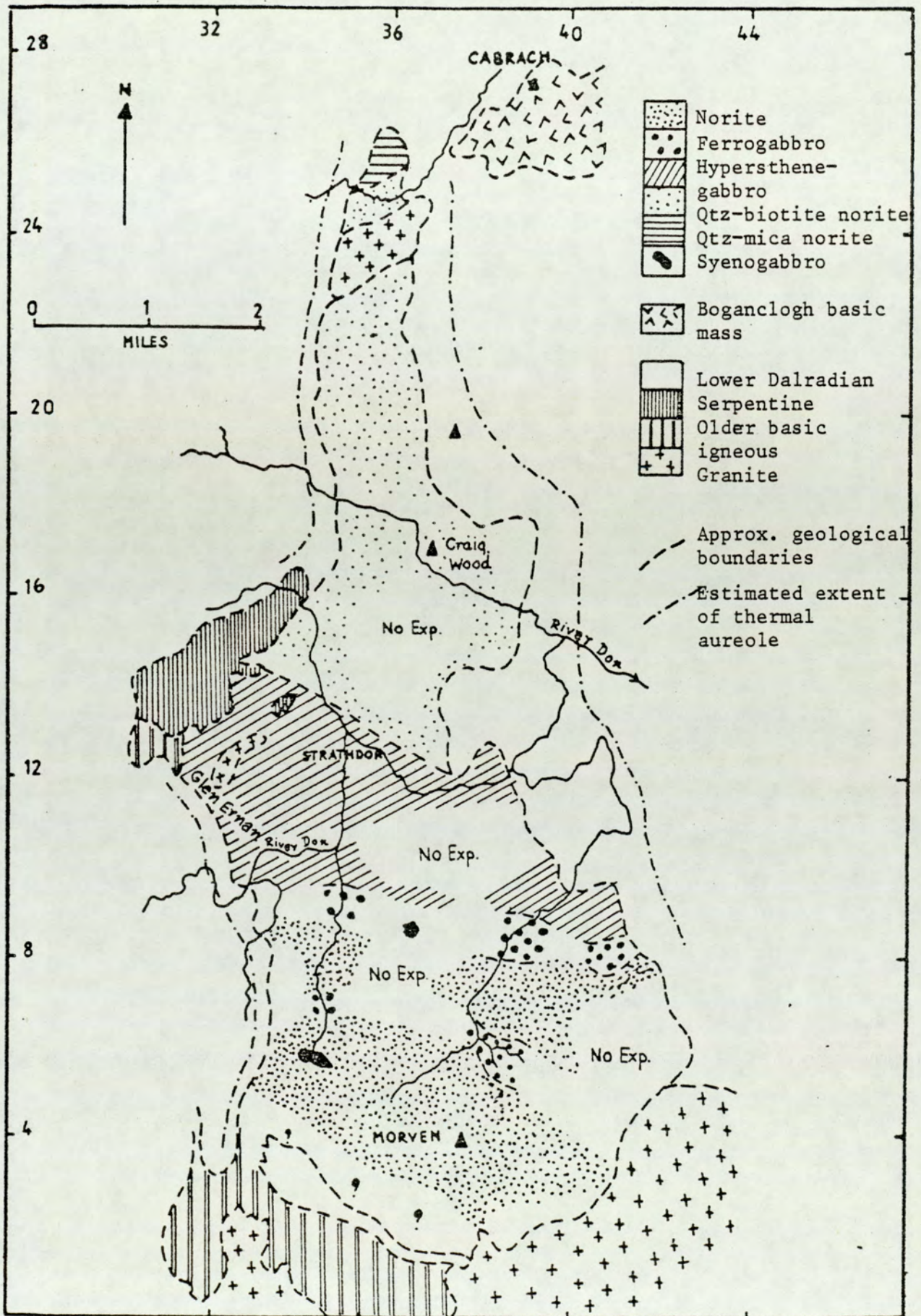
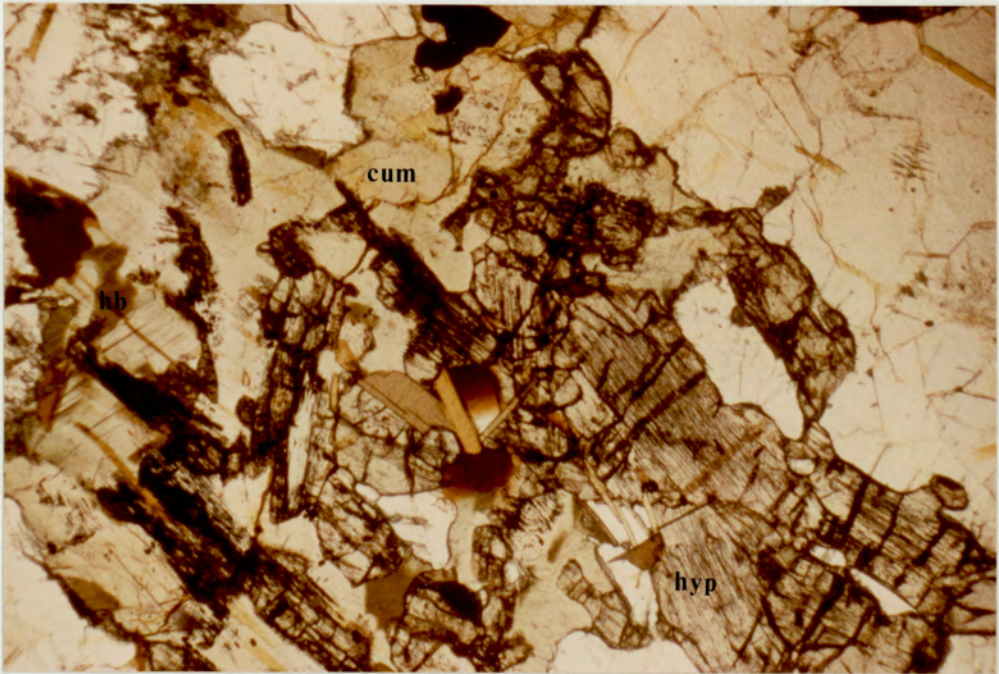


Fig. 2.5 Sketch map showing the geology of the Morven-Cabrach mass (after Allan, 1970).

that these uniform, discrete crystals of cummingtonite are not an alteration product of hypersthene, since hypersthene in the same rocks is still fresh, and secondary cummingtonites from hypersthene in most cases are fibrous aggregates (Fig. 2.6). These cummingtonites are also fringed by thin zones of green hornblende. The intergrowth of cummingtonite and hornblende can be seen clearly in amphibole-plagioclase rocks from Craig Wood Quarry (specimen 64 P). This rock is composed mainly of hornblende, cummingtonite and plagioclase (An 52-60) with small amounts of biotite flakes and opaque oxide. Hornblende and cummingtonite form homoaxial intergrowth and occasionally occur as separate grains. Cummingtonite fairly commonly forms cores partly or wholly surrounded by hornblende with sharp boundaries. Less commonly, hornblende occurs as thin lamellae and blebs in cummingtonite. In crystals where {110} cleavages are present, their traces are continuous between these two minerals. Multiple twinning is also a common characteristic of cummingtonite.

The quartz-biotite norite grades into hypersthene gabbro in the south by disappearance of quartz and decrease in amounts of biotite. The hypersthene-gabbro is generally medium grained with roughly equal amounts of orthopyroxene and clinopyroxene. One exposure on the bank of the River Don, south of Strathdon is sheared and foliated. In thin sections, these rocks are amphibolite consisting of relicts of cummingtonite aggregates, clinopyroxene and plagioclase remaining as porphyroclasts in a foliated groundmass. The matrix contains granular brownish-green hornblende, plagioclase and lesser amounts of quartz and crystals of magnetite. Associated with these sheared rocks are foliated hornblende-pegmatite veins (used in Mössbauer work, Chapter 4).



0.50 mm.

Fig. 2.6 Uniform, discrete cummingtonite (CUM) grain with patches and lamellae of hornblende (HB). Cummingtonite encloses hypersthene (HYP) and biotites (BIO). (specimen 63 P).

The most widespread rock type in the southern part of the Morven-Cabrach mass is norite with two strips of ferrogabbro and a few patches of syenogabbro (Allan 1970). Mineralogically, magnetite tends to increase, and biotite and quartz to decrease, from quartz-biotite norite in the north towards hypersthene gabbro and norite in the south. Compositions of plagioclase are remarkably consistent within the range An 50-65 throughout the mass.

Unaltered rocks, which are seldom found, consist chiefly of hypersthene and plagioclase with small amounts of clinopyroxene. Magnetite is an important accessory accompanied by apatite, biotite and zircon. In some samples, (70P, 636C, 745C and 746C) hypersthene contains two sets of augite exsolution. The first, dominant set is coarse, blebs lying along (001) of pre-existing pigeonite. The second set, which is uncommon, forms lamellae parallel to (100) of the hypersthene grains. The coarser set is generally curved.

Most of the specimens from this mass are highly altered, by later retrograde regional metamorphism during cooling and uplifting, particularly in the southern part in which the original minerals are totally obscured. The significant mineralogical changes are replacements of pyroxene by fibrous amphibole, often loosely called 'uralitization' or 'amphibolitization' which is the major study in this thesis (cf. Chapter 4). A similar process has been briefly described in Glen Scaddle and Belhelvie intrusions.

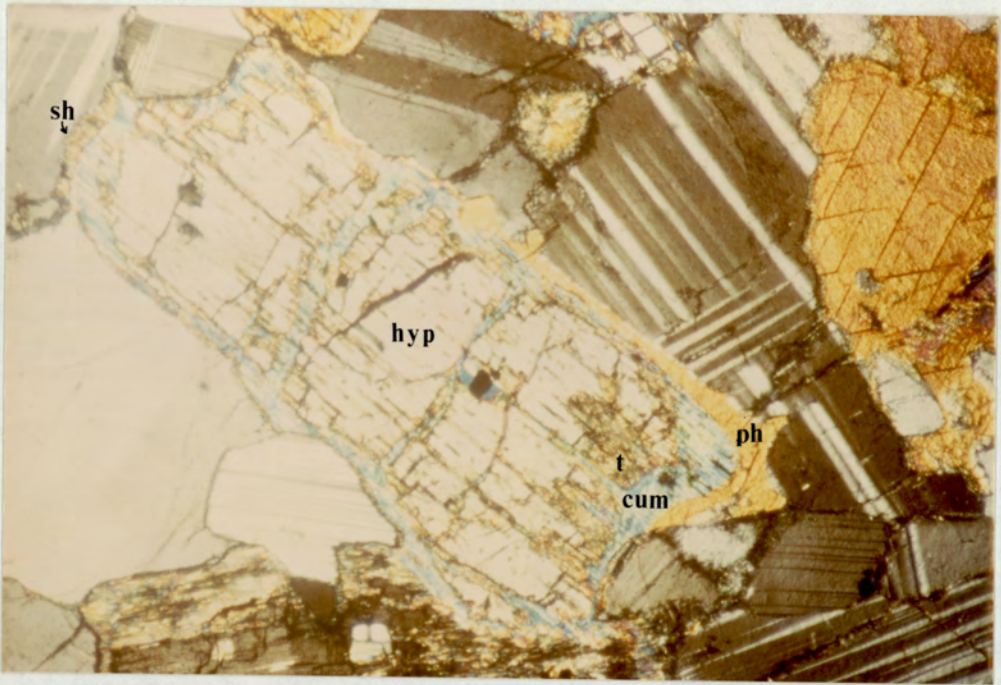
In the Morven-Cabrach mass, closely packed fibres of pseudomorphing cummingtonites are the dominant constituent, since primary pyroxenes are mainly hypersthene. Bluish-green or pale-green

amphibole zones are generally found between plagioclase and cummingtonite.

Contacts between fibrous or small, disoriented, prismatic aggregated cummingtonite cores and marginal hornblende are sharply defined, and show the original shapes of former hypersthene grains (Fig. 4.4b). Very narrow zones of dark bluish-green amphibole fringing cummingtonite are made up of acicular grains. As cummingtonite progressively reacts with plagioclase, these zones become paler and grow into surrounding plagioclase and occasionally along plagioclase boundaries as clots of disoriented prismatic grains. Eventually, they form radial prismatic crystals around cummingtonite cores.

In many cases, primary orthopyroxenes which are embedded in plates of primary brownish-green hornblende are made over to cummingtonite while the surrounding primary hornblende remains unaffected, suggesting that hypersthene made its way to cummingtonite without help from plagioclase. Primary hornblende can be distinguished from secondary by its uniform brownish-green colour, sometimes containing numerous, very small opaque inclusions, and its sharp, simple contact with not only plagioclase but also quartz and opaques. Fig. 2.7 shows part of cummingtonite bordered by uniform primary brownish-green hornblende, while the other part is rimmed by bluish-green hornblende showing highly irregular contact with plagioclase.

At more advanced stages of retrograde metamorphism, fibrous amphibole is marginally replaced by pale-green chlorite flakes which progressively occupy fibrous amphibole cores. Accompanying chloritisation is replacement of plagioclase by sericite and epidote.



0.25 mm.

Fig. 2.7 Hypersthene (HYP) with replacing cummingtonite (CUM) and talc (T) surrounded by primary homogeneous brown hornblende (PH) and secondary hornblende (SH). (specimen 635 C).

Primary hornblendes remain unaffected.

One of the most characteristic features of Morven-Cabrach rocks is the widespread occurrence of thin green amphibole veins which can be seen in both unaltered and altered rocks. These veins consist of disoriented, fine and well-developed crystals of green hornblende which frequently are replaced by fibrous chlorite. Ramification from the veins as veinlets forming a network linking one ferromagnesian mineral grain with another, growing along plagioclase boundaries or cutting through plagioclase grains in a sub-parallel fashion is also a common feature.

2.2.4 The Huntly-Portsoy masses

The ultrabasic and basic igneous rocks of the Huntly-Portsoy areas previously regarded as a single Huntly mass have been divided into 3 smaller isolated masses, named the Portsoy mass, the Knock mass and the Huntly mass based on the borehole evidence by Munro (1970). The Portsoy mass consists largely of layered olivine-plagioclase cumulate and rare quartz-biotite gabbro with an absence of xenolithic rocks while the Knock mass is troctolite, olivine-pyroxenite, norite and xenolithic rocks (Munro 1970). The Huntly mass has been studied in detail by Watt (1914), Read (1923) and Weedon (1970). They stated that the Huntly mass comprises a complex which varies in composition from olivine-gabbro and norite to troctolite and picrite.

These masses produced an obvious sillimanite aureole overprinting on the regional Andalusite and Kyanite zones (Ashworth, 1975). The temperature and pressure conditions during the emplacement

were estimated based on the coexisting garnet and cordierite from the innermost part of the aureole by Ashworth and Chinner (1978) as 720 - 730°C and 4.8 - 6.0 kbar respectively.

A detailed petrographic description of the Huntly rocks was given by Watt (1914) and Read (1923). Mineral compositions of main cumulus phases were determined by Weedon (1970). However, for the purpose of this study, attention should be paid to the development of coronas or reaction rims between olivine and plagioclase in olivine-gabbros. Resembling coronas in the Belhelvie mass, they consist of an inner shell of orthopyroxene and outer shell of hornblende-spinel symplectite, but their widths in each shell are generally narrower and less uniform than the Belhelvie coronites. Detailed study of these coronas is^{described} in Chapter 3.

CHAPTER THREE

FORMATION OF CORONAS AROUND OLIVINE IN 'YOUNGER' BASIC COMPLEX IN ABERDEENSHIRE AND BANFFSHIRE, NORTH EAST SCOTLAND

3.1 INTRODUCTION

Troctolitic and gabbroic rocks from Belhelvie and Huntly intrusions in Aberdeenshire and Banffshire, NE Scotland, usually developed corona structures or reaction rims between olivine and plagioclase. Such coronas are product of re-equilibration by reaction between plagioclase and olivine when physical conditions of the rocks are changed. These coronas consist of two sequences of mineral assemblages separated by sharp boundaries:-

- (1) Olivine - orthopyroxene - (amphibole + spinel) - plagioclase.
- (2) Olivine - orthopyroxene - (amphibole + spinel) - (amphibole + anorthite) - plagioclase.

The (amphibole + spinel) shell and the (amphibole + anorthite) shell are symplectites, that is fine intergrowths. The fineness of this texture must reflect limited diffusion range of one or more components in the reaction producing the two minerals. This aspect will be dealt with in this study.

Sequence (1) of corona minerals is typical in the studied areas and has been described by Read (1923), Stewart (1947) and Read et al (1961) and has been further discussed in terms of the pressure at which reaction occurred, by Weedon (1966) and O'Hara and Stewart (1966), without great detailed study. The second corona assemblages have never been reported in the literature.

Although extensive works on types similar to the first corona formation have been done from other areas (Murthy 1958, Reynolds and Frederickson 1962, Mason 1967, Frodesen 1968, Starmer 1969, Grieve and Gittins 1975, Sapountzis 1975, Esbensen 1978 and van Lamoen 1979 and Emmett 1982), the chemical reaction model is still not completely satisfactory.

This study particularly represents an attempt to define the chemical reactions involved in both sequences of corona formation. Textural observations and microprobe analyses have been combined to describe the series of corona forming reactions. Optical and SEM photographs have been digitized to estimate the proportions of each mineral concerned in corona assemblages including spinel.

3.2 PREVIOUS WORK ON CORONA FORMATION BETWEEN OLIVINE AND PLAGIOCLASE

Since Shand (1945) summarized the occurrence and origin of the corona structure between olivine and plagioclase, various hydrous as well as anhydrous assemblages have been discovered and studied. The typical hydrous assemblages generally consist of olivine - orthopyroxene - (amphibole + spinel) - plagioclase. Additional minerals in coronas such as cummingtonite (England 1974, Nishiyama, 1983), garnet (Murthy 1958, Grieve and Gittins 1975, Emmett 1982) have also been reported. Shand (1945) stated that the formation of coronas is due to the instability of olivine and its conversion to orthopyroxene in an open system. Murthy (1958) favoured the corona reaction as diffusion processes along the minerals interface with introduction of H₂O. He concluded that the first corona of orthopyroxene is formed by the rearrange-

ment of the SiO_4 tetrahedra of olivine into chains of linked tetrahedra (SiO_3) and the second corona of amphibole - spinel symplectite is developed by replacement of plagioclase, so that the original olivine-plagioclase contact is represented by the sharp orthopyroxene and amphibole contact. Reynolds and Frederickson (1962) considered the corona reactions on the principle of volume for volume replacement with addition of Si and water. A simple process of two way diffusion across the original interface between olivine and plagioclase in the solid state was introduced by Mason (1967). His hypothesis assuming the diffusion of magnesium and iron into the plagioclase and a little calcium and aluminium diffusing out of the plagioclase has been supported by many later workers (e.g. Sapountzis 1975, Grieve and Gittins 1975).

Grieve and Gittins (1975) attempted to quantify this diffusion model based on equal volume replacement of olivine by orthopyroxene and plagioclase by amphibole and spinel, but it failed to yield a satisfactory chemical balance. However, a reasonable approximation to a chemical reaction can be written if it is assumed that the symplectite/orthopyroxene boundary migrates towards the olivine during the reaction (Grieve and Gittins, 1975). This raises the problem of how the symplectite, whose texture is controlled by limited diffusion, can propagate across the system. In this study, the problem is tackled quantitatively. van Lamoen (1981) in describing three types of coronas from Susimake and Riuttama, Finland, claimed that individual coronas developed as allochemical systems, while in the bulk rock only a net gain of water and a loss of Na are involved in the overall reaction. It seems that in most, if not all, cases the corona formation has been approximately isochemical at least within the volume of a hand specimen,

even though there is no clear balanced equation for individual corona formation.

Corona in an anorthositic gabbro, in which olivine crystallized after plagioclase, producing similar type of corona in this study, were studied in some detail by Magruder (1981). He proposed corona model reactions and concluded that ^{the} system was closed to Al_2O_3 and SiO_2 and open with respect to Ca_2O , Na_2O , MgO and FeO . Recently, a steady ^{state} diffusion model has been applied to explain an olivine-plagioclase corona (Nishiyama, 1983). His model is very attractive in producing hornblende - (hornblende + spinel) by restricted diffusion of Al and Si compared with Mg.

Reactions between olivine and plagioclase can also produce coronas of anhydrous mineral assemblages. These assemblages usually contain two pyroxenes with garnet and/or spinel (Whitney and McLelland 1973, Griffin and Heier 1973, Miller 1974, McLelland and Whitney, 1980).

Various pressure-temperature conditions of corona formation have been proposed in different geological settings. Shand (1945), Huang & Merritt (1954) and Friedman (1955) regarded their coronas as the result of thermal metamorphism. Corona formation has been found in areas that have undergone regional metamorphism (Murthy 1958, Mason 1967, Starmer 1969, Whitney and McLelland 1973 and England 1974). However, many deuteritic or late-stage magmatic origins of corona have also been reported. (Griffin and Heier 1973, Sapountzis 1975 and Esbensen 1978). The term deuteritic strictly refers to interaction with residual water of igneous origin, during post-magmatic stages of cooling of an

intrusion (Frodesen, 1968). It is likely that many coronas originate at this stage, particularly when cooling is slow because the intrusion was emplaced into a metamorphic terrain undergoing slow regional cooling (Frodesen 1968, Esbensen 1978 and Mersmann 1981). Prograde metamorphism tends to reconstitute a rock completely rather than merely inducing the partial reactions preserved in coronites. The two-stage corona formation involving the deuteritic origin for orthopyroxene and amphibole (without spinel) coronas and the regional metamorphic origin for iron-ore rich orthopyroxene and amphibole - spinel symplectite has been suggested by Frodeson (1968).

3.3 DESCRIPTION OF AREAS

The present study concerns corona formation in the Huntly and Belhelvie intrusions which belong to the Younger Basic complex (Fig. 2.1). These masses comprise various rock types from ultrabasic and troctolitic rocks to gabbro and norite. (Stewart 1947, Munro 1970, Weedon 1970, Ashcroft and Boyd 1976).

The history of these intrusions has already been described in detail in Chapter 2. However, it is worth mentioning their conditions of intrusion again, as this is an important part for interpretation of their corona formation. Pankhurst (1970, 1974) demonstrated the clear evidence to support the view of Johnson (1962) and Fettes (1970) that these Younger Basic intrusions were emplaced into the hot country rocks during the climax of metamorphism (M_3) and were deformed by major F_3 folds. Water apparently moved into the basic masses from the dehydration reactions in hot country rocks (Gribble, 1967). Nearby shearing may be the pathway

of water into the intrusions, especially in the Belhelvie mass (c.f. Boyd and Munro 1978). This evidence strongly suggests that coronas in the studied areas are retrograde, regional metamorphic in origin.

The six samples described are troctolites and olivine gabbros. Three specimens (53 P, 710 C and 15/18763) are from Belhelvie area and three specimens (773 C, 774 C and 28/19763) came from the Huntly intrusion. Their precise localities are listed in Appendix 1.

3.4 PETROGRAPHIC DESCRIPTIONS

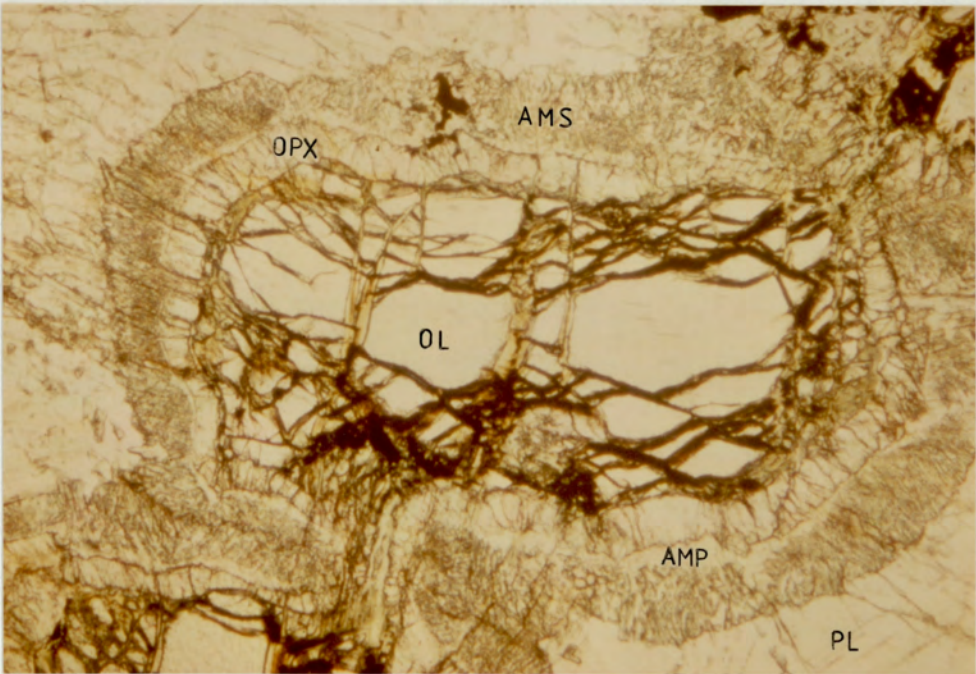
The troctolite and gabbro are medium-grained rocks. Ophitic and sub-ophitic textures with clinopyroxene enclosing, either partially or wholly, plagioclase and olivine are frequently developed. Some clinopyroxenes are bordered by deep brown hornblende.

Olivine is subhedral and largely serpentized. In specimen 710 C, olivine is pseudomorphed by fine talc and cummingtonite aggregates. Plagioclase is generally fresh. In some rocks, it shows a grey clouded core with very fine-grained inclusions, leaving the margin clear. This is not always developed and it can be found in corona free samples as well as corona-containing samples. Olivine in both areas is usually surrounded successively by typical coronas of orthopyroxene and amphibole-spinel symplectite when in contact with plagioclase, but never at contacts with primary clinopyroxene. The narrow spinel-free amphibole zone showing optical continuity with the outer spinel-amphibole symplectite shell is frequently seen.

The inner shell of radially arranged orthopyroxene can be distinguished optically from the outer shell of spinel-amphibole symplectite by their optical discontinuity and sharp boundary (Fig. 3.1). Amphibole is typically pale green with fine-grained rods or vermicular spinel intergrowths. Generally each of these shells developed uniformly with constant width. Occasionally the spinel-amphibole symplectite failed to develop in some parts of the corona, even if the orthopyroxene is well developed. This observation suggests that the formation of orthopyroxene is necessary for the development of spinel amphibole symplectite (c.f. Murthy, 1958).

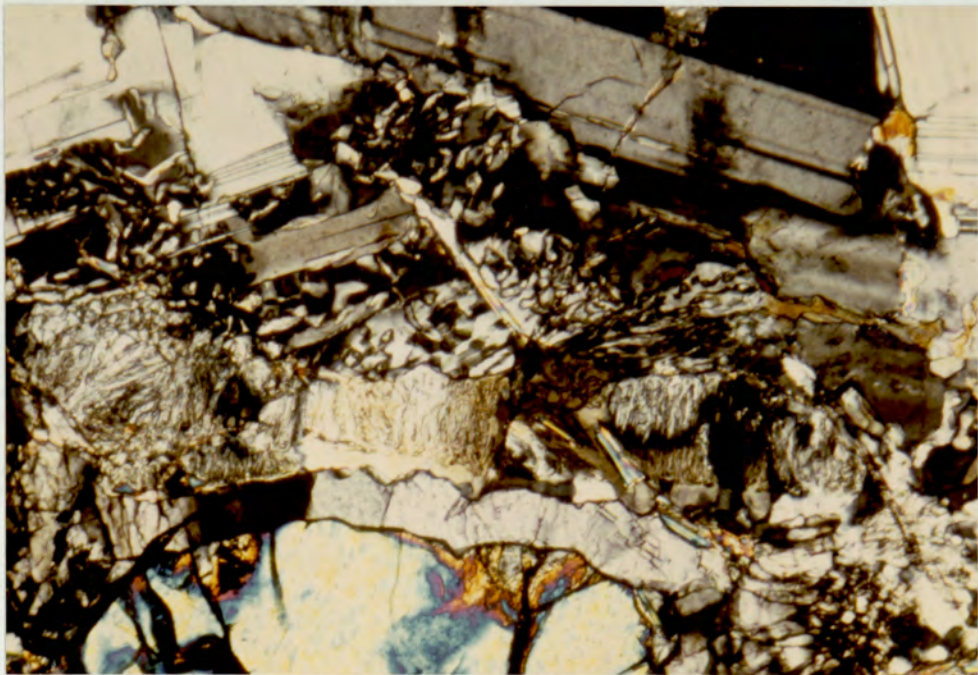
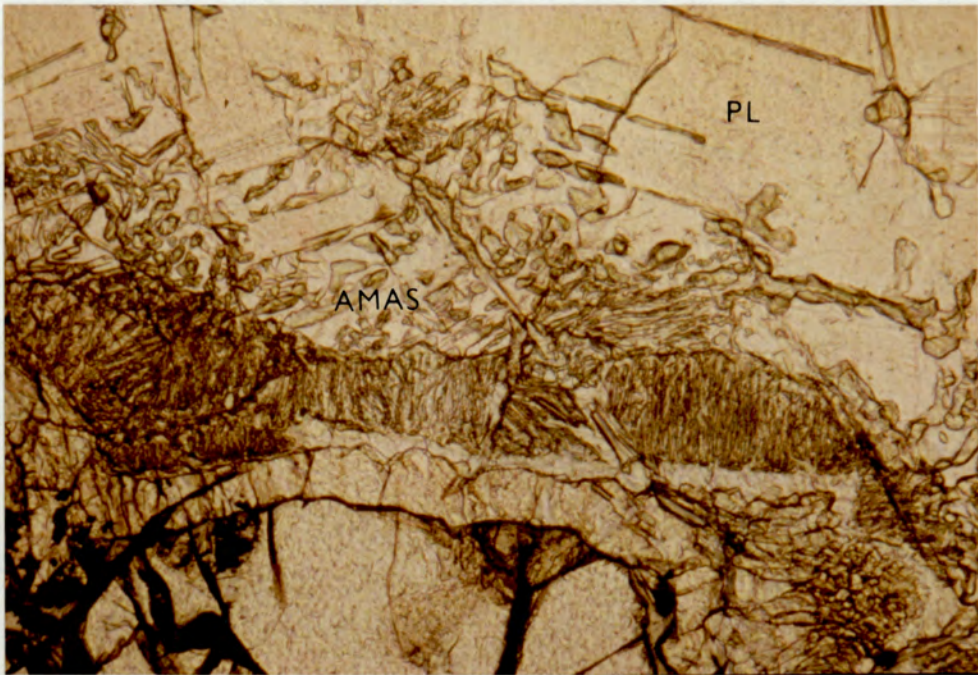
The third shell of hornblende and anorthite symplectite is occasionally developed in some specimens (15/18763 and 774 C) without continuity around the second shell. The irregular shape and size of this symplectite can be seen in Figure 3.2; in general it forms big bleb shapes or grows along plagioclase grain boundaries. There are no optical continuities between amphibole in both shells and between anorthite in the third shell and surrounding plagioclase. It has been found that in these specimens, orthopyroxene is slightly replaced by fibrous crystals of pale green, parallel extinction amphibole which is anthophyllite (Fig. 3.2), confirmed by EPMA analysis (analysis 3.4 Table 3.3).

Coronas are generally narrower in the Huntly specimens, with wider amphibole layer relatively to orthopyroxene layer compared with those in the Belhelvie specimens. Within the amphibole layer, spinel free amphibole is also greater than amphibole-spinel symplectite area for the Huntly specimens. It seems likely on textural grounds that the difference between amphibole-spinel



0.25 mm.

Fig 3.1 The typical olivine-plagioclase corona in the studied areas. Olivine (OL) is surrounded successfully by orthopyroxene (OPX) amphibole (AMP) and amphibole-spinel symplectite (AMS) when in contact with plagioclase (PL) in specimen 710 C.



0.10 mm.

Fig 3.2 Development of amphibole-anorthite symplectite (AMAS) between plagioclase (PL) and amphibole-spinel symplectite, with amphibole grains also developing on a grain boundary in plagioclase. There is no optical continuity between amphibole in each symplectite layer, nor is the anorthite in optical continuity with primary hornblende. (specimen 15/18763 C).

and orthopyroxene shells is inherited from the difference between plagioclase and olivine. So, the amphibole - spinel symplectite and the amphibole - anorthite symplectite are a result of replacement of the plagioclase and orthopyroxene formed from olivine.

The growth of hornblende from second and third shells along grain boundaries or cracks of plagioclase suggests solid-state corona formation rather than a magmatic origin. It can be seen clearly that coronas were destroyed by amphibolization (the cummingtonite which also replaces olivine), which was a later metamorphic effect.

3.5 MINERAL CHEMISTRY

3.5.1 Electron Probe Microanalyses

3.5.1.1 Method

Most of the mineral compositions reported on this thesis were determined by the wavelength-dispersive electron probe microanalyser (Cambridge Microscan 5) at the Department of Metallurgy and Materials, University of Aston. Operating conditions typically included an accelerating potential of 20 Kv, specimen current of 0.05 microamperes except for potassium where the specimen current was 0.02 microamperes.

Polished thin sections were coated with carbon at the same thickness as polished standards. Nine elements including Fe, Mg; Ca, Si; Mn, Al; Ti, Na and K were analysed in pairs using two detectors.

Standards that have been used throughout the study are as follows; Fe and Ti pure metal; wollastonite with concentration of Ca 34.51% and Si 24%; Al_2O_3 of Al concentration 52.91%; MgO containing 60.31% Mg; jadeite of 11.34% Na; 12.40% K containing orthoclase and Mn_3O_4 with concentration of Mn 72.03%.

Instrumental drift was corrected by frequently adjusting the condenser lens current. Corrections for dead time, background, fluorescence, absorption and atomic number were carried out by the computer programs after methods described by Reed (1975).

The accuracy of the analyses as determined by the instrument error is about $\pm 1.5\%$ for total weight percent. Concentration profiles for each element (Fig. 3.4 and Fig. 3.5) are also performed by scanning the focused-beam slowly across the corona.

3.5.1.2 Results

Olivine

The olivine analyses shown in Table 3.1 are averages of 3-5 measurements. Olivine in both intrusions are Mg-rich, ranging in composition from F080-85. No significant zoning is detected. These olivines have higher Mg content compared with corona olivine from other areas in the literature (Fig. 3.3) except Sultijelma, Norway (Mason, 1967) and Otzal Alps, Austria (Miller, 1974) where the olivine compositions are F082 and F079-85 respectively.

Orthopyroxene

The compositions of corona pyroxenes range from Eng2.6 to Eng5 and have low Ca, Al contents. In each grain of orthopyroxene,

TABLE 3.1 Electron microprobe analyses of olivine

SPECIMEN No.	53 P	710 C	15/18763	773 C	774 C	18/19763
MgO	42.93	45.26	43.04	42.79	42.96	41.63
Al ₂ O ₃	0.31	0.00	0.00	0.00	0.00	0.00
SiO ₂	39.33	39.51	39.23	39.09	38.66	38.91
CaO	0.03	0.00	0.00	0.00	0.00	0.00
MnO	0.18	0.20	0.22	0.21	0.22	0.27
FeO*	17.51	14.91	17.09	17.71	18.66	18.95
Total	100.29	99.88	99.58	99.80	100.50	99.76
Formula to 4 oxygens						
Si	1.00	0.99	1.00	1.00	0.99	1.00
Al	0.00	0.00	0.00	0.00	0.00	0.00
	1.00	0.99	1.00	1.00	0.99	1.00
Mg	1.62	1.70	1.63	1.64	1.63	1.59
Fe	0.37	0.31	0.36	0.38	0.40	0.41
Mn	0.00	0.00	0.01	0.01	0.01	0.01
Ca	0.00	0.00	0.00	0.00	0.00	0.00
	1.99	2.01	2.00	2.03	2.04	2.01
% Fo	81.4	84.6	81.9	81.2	80.3	79.5

*FeO = Total Fe

TABLE 3.2 EPMA of orthopyroxene.

SPECIMEN		53 P		710 C		15/18763		773 C		774 C		18/19763	
No.		2.1	2.2	2.1	2.2	2.1	2.2	2.1	2.2	2.1	2.2	2.1	2.2
ANALYSES		No.		No.		No.		No.		No.		No.	
MgO		31.96	30.99	31.96	31.16	31.34	30.73	30.85	30.41	30.51	29.93	30.27	29.36
Al ₂ O ₃		0.70	1.73	1.77	1.91	0.51	1.02	0.96	1.36	1.80	2.36	0.98	2.96
SiO ₂		56.46	54.87	55.81	54.78	56.22	55.42	55.48	55.03	53.97	53.38	56.20	55.83
CaO		0.10	0.24	0.11	0.18	0.09	0.18	0.19	0.23	0.30	0.74	0.36	0.19
MnO		0.28	0.26	0.22	0.21	0.23	0.22	0.30	0.26	0.35	0.35	0.29	0.29
FeO*		11.25	11.98	9.66	10.39	11.24	11.66	11.45	11.64	11.80	12.04	12.09	12.52
Total		100.75	100.07	99.53	98.63	99.63	99.23	99.23	98.93	98.73	98.80	100.19	101.15
Formula to 6 oxygens													
Si		1.97	1.94	1.96	1.95	1.99	1.97	1.97	1.97	1.94	1.92	1.98	1.95
Al		0.03	0.06	0.04	0.05	0.01	0.03	0.03	0.03	0.06	0.08	0.02	0.05
		2.00	2.00	2.00	2.00	2.00	2.00	2.00	2.00	2.00	2.00	2.00	2.00
Al		0.00	0.01	0.03	0.03	0.01	0.02	0.01	0.02	0.01	0.02	0.02	0.07
Mg		1.67	1.64	1.67	1.65	1.65	1.63	1.64	1.62	1.63	1.60	1.59	1.53
Fe		0.33	0.36	0.28	0.31	0.33	0.35	0.34	0.35	0.35	0.36	0.36	0.37
Mn		0.01	0.01	0.01	0.01	0.01	0.01	0.01	0.01	0.01	0.01	0.01	0.01
Ca		0.00	0.01	0.01	0.01	0.00	0.01	0.01	0.01	0.01	0.03	0.01	0.01
		2.01	2.03	2.00	2.01	2.00	2.02	2.01	2.01	2.01	2.02	2.00	1.99
100 Mg		83.5	81.6	85.2	83.8	83.3	82.3	82.8	82.2	82.3	81.6	81.5	80.5
Mg + Fe													

*FeO = Total Fe

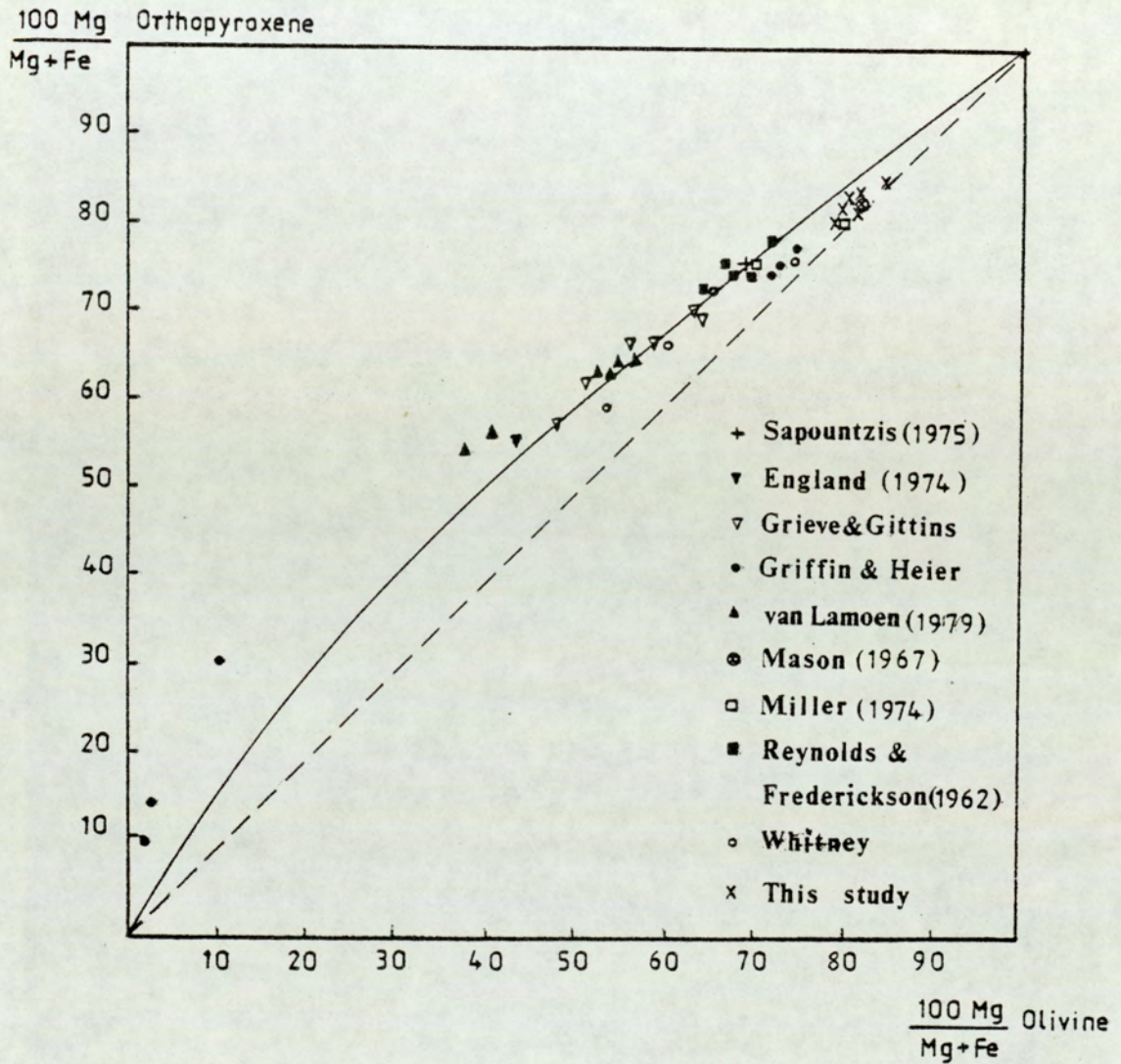


Fig 3.3 Comparison of olivine and coexisting corona orthopyroxene compositions from various localities and this study, suggesting that the initial olivine controls the composition of orthopyroxene. The solid curve represents the theoretical partitioning of Fe and Mg of synthetic olivine and orthopyroxene at 900°C (after Medaris, 1969).

two analyses were made across the grain in order to detect any zoning. The result (Tables 3.2) indicates that Mg slightly decreases while Fe shows a tendency to rise, which can be expressed by the minor decreasing of $Mg/(Mg + Fe)$ ratio towards the amphibole interface. The concentration profiles of Fe and Mg across the pyroxene (Fig. 3.4) also support the analytical data. Al and Ca do not significantly increase in the direction of amphibole. The higher Al and Ca content of orthopyroxene near amphibole (analysis 2.2 in Table 3.2) may partly be contamination (cross boundary fluorescence) from amphibole which is rich in Al and Ca, rather than actual zoning in orthopyroxene, but the profiles across orthopyroxene (Figs. 3.4, 3.5) also suggest a real increase in Al towards the amphibole. The effect is a small one. Generally the $Mg/(Mg + Fe)$ ratio of orthopyroxene is slightly greater than associated olivine. This compositional interdependence is expressed by a plot of their $Mg/(Mg + Fe)$ ratios in Figure 3.3.

Amphibole

Although the Fe^{3+} amount in amphibole is not determined, it is assumed that the Fe^{3+} is probably low, since the rocks are not oxidized and the analyses make sense without invoking a lot of Fe^{3+} . So, the amphibole is classified as pargasite according to Leake (1978). Again two areas within one grain of amphibole were analysed, the spinel free area (analysis 3.1 in Table 3.3) and the amphibole in spinel-amphibole symplectite. (analysis 3.2 in Table 3.3). Although fine-grained intergrowth of spinel caused difficulty in getting pure amphibole composition, analyses of symplectite amphibole from two specimens (53 P and 710 C) were obtained. The high Al in analysis 3.2 of 710 C may reflect slight spinel contamination.

TABLE 3.3 Electron probe microanalysis of corona amphiboles H₂O calculated from ideal formula with 22 O and 20 H.

SPECIMEN		53 P			710 C			15/18763			773 C			774 C			28/19763		
No.		3.1	3.2	3.1	3.1	3.2	3.1	3.1	3.2*	3.3	3.4**	3.1	3.1	3.1	3.1	3.1	3.1		
ANALYSES																			
No.		3.1	3.2	3.1	3.1	3.2	3.1	3.1	3.2*	3.3	3.4**	3.1	3.1	3.1	3.1	3.1	3.1		
Na ₂ O		2.50	2.38	2.29	2.41	2.41	2.03	1.89	1.58	-	2.60	2.38	2.40						
MgO		16.81	16.68	17.32	16.28	16.28	16.94	17.52	17.61	27.38	16.59	16.32	16.13						
Al ₂ O ₃		16.32	16.51	14.84	17.53	14.68	14.68	16.23	13.14	2.60	16.39	16.46	17.19						
SiO ₂		43.46	43.54	44.62	42.86	42.86	45.15	43.81	46.53	52.74	43.12	41.40	42.85						
K ₂ O		0.35	0.18	0.05	0.12	0.12	0.19	0.31	0.20	-	0.21	0.29	0.39						
CaO		12.36	12.16	11.44	11.38	12.12	12.12	11.54	12.12	1.17	11.86	12.05	11.79						
TiO ₂		0.13	0.09	0.11	0.03	0.03	0.02	0.06	0.06	0.27	0.06	0.12	0.07						
MnO		0.10	0.11	0.10	0.11	0.11	0.10	0.14	0.08	0.31	0.12	0.08	0.12						
FeO		6.35	5.99	5.91	6.30	6.30	5.65	7.14	5.54	13.31	5.53	5.66	6.01						
H ₂ O		2.11	2.11	2.10	2.14	2.14	2.10	-	2.11	2.14	2.09	2.02	2.09						
Total		100.52	99.81	98.79	101.15	98.96	98.64	99.88	98.97	99.88	98.58	96.74	99.04						

Formula to 23 oxygens (anhydrous)																			
		6.16	6.19	6.38	5.99	6.43	6.18	6.61	6.19	7.40	6.19	6.08	6.14						
Si		1.84	1.81	1.62	2.01	1.57	1.82	1.39	1.81	0.43	1.81	1.92	1.86						
Al		8.00	8.00	8.00	8.00	8.00	8.00	8.00	8.00	7.83	8.00	8.00	8.00						
Al		0.88	0.96	0.87	1.21	0.90	0.88	0.81	-	-	0.97	0.93	1.04						
Ti		0.01	0.01	0.01	0.00	0.00	0.01	0.01	0.03	0.03	0.01	0.01	0.01						
Mg		3.55	3.53	3.69	3.39	3.60	3.69	3.73	5.73	5.73	3.55	3.57	3.44						
Fe		0.76	0.71	0.71	0.74	0.67	0.84	0.66	1.56	1.56	0.66	0.70	0.72						
Mn		0.01	0.01	0.01	0.01	0.01	0.02	0.01	0.04	0.04	0.02	0.01	0.02						
Na		5.21	5.22	5.29	5.35	5.19	5.44	5.22	7.36	7.36	5.21	5.22	5.23						
Ca		0.69	0.66	0.64	0.65	0.56	0.52	0.44	-	-	0.72	0.68	0.67						
K		1.88	1.85	1.75	1.71	1.85	1.75	1.84	0.18	0.18	1.83	1.90	1.81						
		0.06	0.03	0.01	0.02	0.04	0.06	0.04	-	-	0.04	0.06	0.07						
		2.63	2.54	2.40	2.18	2.44	2.33	2.32	0.18	0.18	2.56	2.64	2.55						
100 Mg		82.4	83.3	83.9	82.1	84.3	81.5	85.0	79.0	84.0	83.6	82.7							
Mg + Fe																			

(3.1) Spinel free amphibole

(3.2) Amphibole in spinel amphibole symplectite

(3.3) Amphibole in anorthite-amphibole symplectite

* Analysed by R Wilson, using energy-dispersive electron probe at Leicester University

** Anthophyllite flake in orthopyroxene

In specimen 53 P, there is little difference in amphibole compositions in both analyses, probably indicating equilibrium amphibole. For specimen 710 C, olivine is partly or wholly replaced by cummingtonite which suggests ^{the} advanced metamorphic effect of more water getting into the system at a late stage. In this rock, both point analyses (Table 3.3) and concentration profiles (Fig. 3.4) show an increase in Si and Mg and decrease in Fe and Al from the symplectic to non-symplectic amphibole. The latter is pargasitic hornblende rather than pargasite, showing that amphibole composition changes towards ordinary hornblende of amphibolite facies.

The composition of amphibole in the third (amphibole-anorthite) layer of specimen 15/18763 (analysis 3.3, Table 3.3) is magnesio-hornblende (Leake, 1978) with higher Si, Mg and lower Al than pargasitic hornblende in the second layer. Amphibole in the second layer of coronas in Huntly specimens has also been classified as pargasite. The composition of amphibole in the third layer was analysed by energy-dispersive electron microprobe (cf Section 3.5.3 below), but the result shows a great contamination from anorthite.

Plagioclase

Zoning is very common in plagioclase usually with decreasing An content toward grain boundaries by amounts up to 5 mole % An. This zoning can be better ascribed ^{to} an igneous origin because it is not confined to grain edges showing metamorphic reactions. The average composition of plagioclase in the specimens from Belhelvie intrusion is An₇₄₋₇₉, and An₆₅₋₇₀ in the Huntly samples. The compositions of plagioclase which are given in Table 3.4

TABLE 3.4 Electron probe microanalyses of plagioclase.

SPECIMEN		53 P	710 C	15/18763	773 C	774 C	18/19763			
ANALYSES		1	2	3	4*	5	6	**7*	8	
Na ₂ O		2.48	2.33	2.68	0.31	3.56	3.74	0.98	3.35	
MgO		0.42	0.09	0.00	0.08	0.00	0.01	1.58	0.01	
Al ₂ O ₃		32.36	32.69	32.26	35.89	31.41	31.27	33.40	31.00	
SiO ₂		47.95	47.15	48.89	43.32	50.42	51.13	45.00	50.46	
K ₂ O		0.02	0.13	0.02	0.05	0.03	0.08	0.00	0.04	
CaO		16.04	16.15	15.19	19.37	14.08	13.52	17.91	14.23	
TiO ₂		0.03	0.01	0.00	0.00	0.00	0.01	0.07	0.09	
MnO		0.02	0.01	0.03	0.03	0.01	0.00	0.12	0.02	
FeO†		0.21	0.16	0.06	0.15	0.14	0.15	0.84	0.10	
Total		99.53	98.72	99.13	99.18	99.61	99.91	99.90	99.30	
Formula to 32 oxygens										
Si		8.84	8.77	9.00	8.09	9.22	9.30	8.35	9.25	
Al		7.03	7.17	7.00	7.90	6.77	6.71	7.30	6.70	
Fe		0.03	0.02	0.01	0.02	0.02	0.02	0.13	0.02	
Ti		0.01	0.00	0.00	0.00	0.00	0.00	0.01	0.01	
Mg		15.91	15.96	16.01	16.01	16.01	16.03	15.79	15.98	
Na		0.12	0.02	0.00	0.02	0.00	0.00	0.44	0.00	
Ca		0.89	0.84	0.96	0.11	1.25	1.32	0.35	1.19	
K		3.17	3.22	3.00	3.88	2.76	2.64	3.56	2.80	
		0.01	0.00	0.01	0.01	0.01	0.02	0.00	0.01	
		4.19	4.08	3.97	4.02	4.02	3.98	4.35	4.00	
% An		79	79	74	96	69	66	91	69	

* Anorthite in hornblende-anorthite symplectite.

** Analysed by R Wilson, using energy-dispersive electron probe.

† FeO as total Fe

Fig 3.4 Electron-microprobe line scans across corona of specimen 710 C. Traced from chart plotter output scaled in counts per second; the approximate scales of oxide weight % are obtained using correction factors averaged over the major minerals.

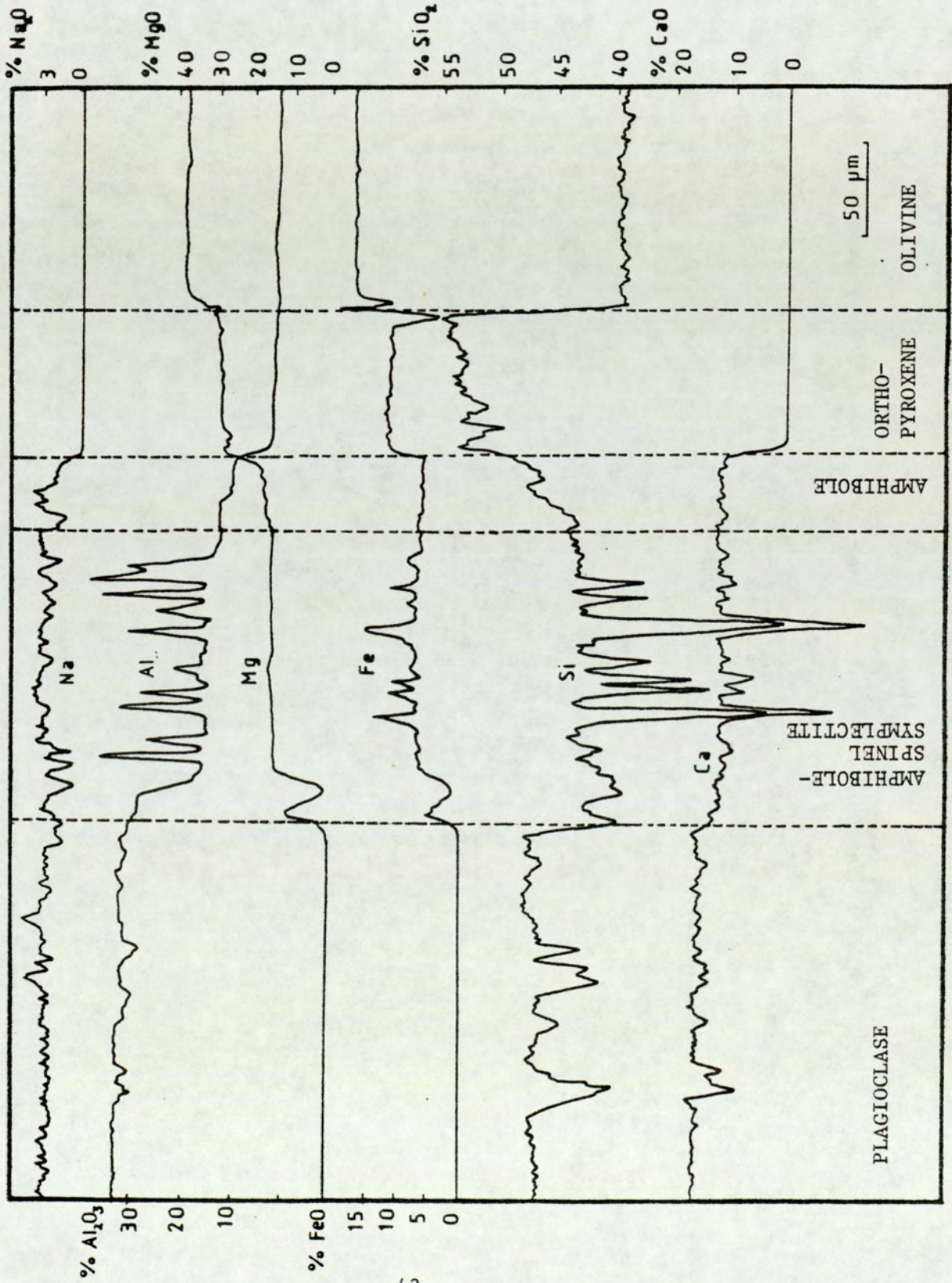
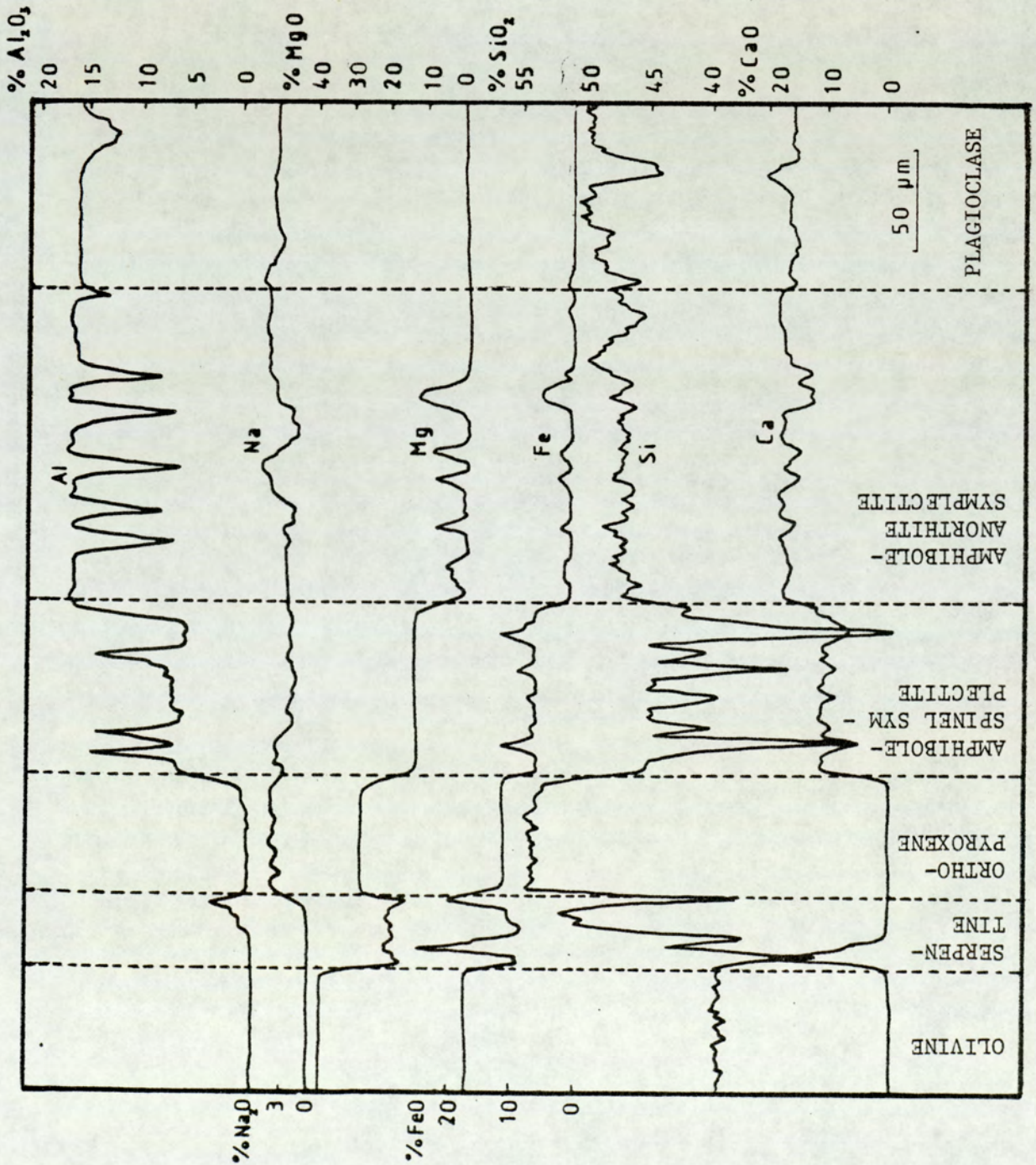


Fig 3.5 Electron microprobe line scans across corona of specimen 15/18763 without non-symplectite amphibole. The serpentine represents late replacement of olivine and contains iron oxide particles.



represent analyses next to studied coronas. Anorthite in hornblende-anorthite symplectite of specimen 15/18763 is also presented in Table 3.4 (analyses 4 and 7).

3.5.2 Semi-Quantitative Analyses Using SEM

Since it is difficult to determine the composition of fine grained spinel in symplectite by EPMA, analyses of spinel in polished specimens were carried out using SEM where the very small beam diameter down to 25\AA can be achieved (Wells, 1974). However, resolution remains limited by the diffusion of the electrons beneath the specimen surface. Since the SEM has not been designed for quantitative analysis purposes, the analyse of spinel composition is then only semi-quantitative.

This technique has the same principle as analyses by EPMA. The X-ray intensity data measured on samples and standards of known composition are compared. In the SEM, the X-ray spectra of every element in spinel can be produced as a line profile (Fig. 3.6) simultaneously within^a very short time using the energy dispersive X-ray detector (Wells, 1974). Therefore, the height of each X-ray peak above back ground is compared to standard peaks after counting time and dead time corrections. The choice of counting times which were timed by operator, depends on the intensity of an individual X-ray peak. In general, they are within the range 10-30 seconds. Three major elements in spinel, Fe, Mg and Al were determined. Standards are synthetic MgAl_2O_4 with Mg 17.09%, Al 37.93%; and pure Fe metal.

Obviously, this method should be able to give reasonable analyses.

But in practice, there are many difficulties. Since it is very hard to move specimens and standards to the exact position with the same take off angle or keeping constant working distance. Qualitatively, the method succeeds in isolating the spinel mineral and showing that it is simply a Mg, Fe spinel (Fig. 3.6A). After the ZAF correction, the result gives the atomic ratio Mg:Fe in spinel of specimen 53P as approximately 5:3. This indicates a molar % Mg/(Fe + Mg) approximately 0.6, that is lower than in the coexisting silicates. (Tables 3.1-3.3). This result agrees with those of previous workers (Mason 1967, Grieve and Gittins 1975, van Lamoen 1979), and is consistent with the expected equilibrium behaviour of these minerals under Amphibolite facies conditions (Medaris, 1975). Since the ratio may be in error by $\sim 10\%$ in the spinel, it is not used in the quantitative modelling below, where it is found to be adequate to treat Fe and Mg together, as (Fe + Mg).

3.5.3 Energy-Dispersive Electron Probe Result

An attempt to get compositions of spinel and amphibole was carried out using energy dispersive electron probe analyser at Leicester University by R. Wilson. It is possible to use a finer beam than in wavelength - dispersive work, which requires higher beam currents. However, all spinel analyses from six specimens have high content of Si and Ca which are contaminations from amphibole. The reasonable analyses are amphibole in amphibole-spinel symplectite of specimen 15/18763 (analysis in 3.2 Table 3.3) and anorthite in specimen 774 C (analysis 7 in Table 3.4).

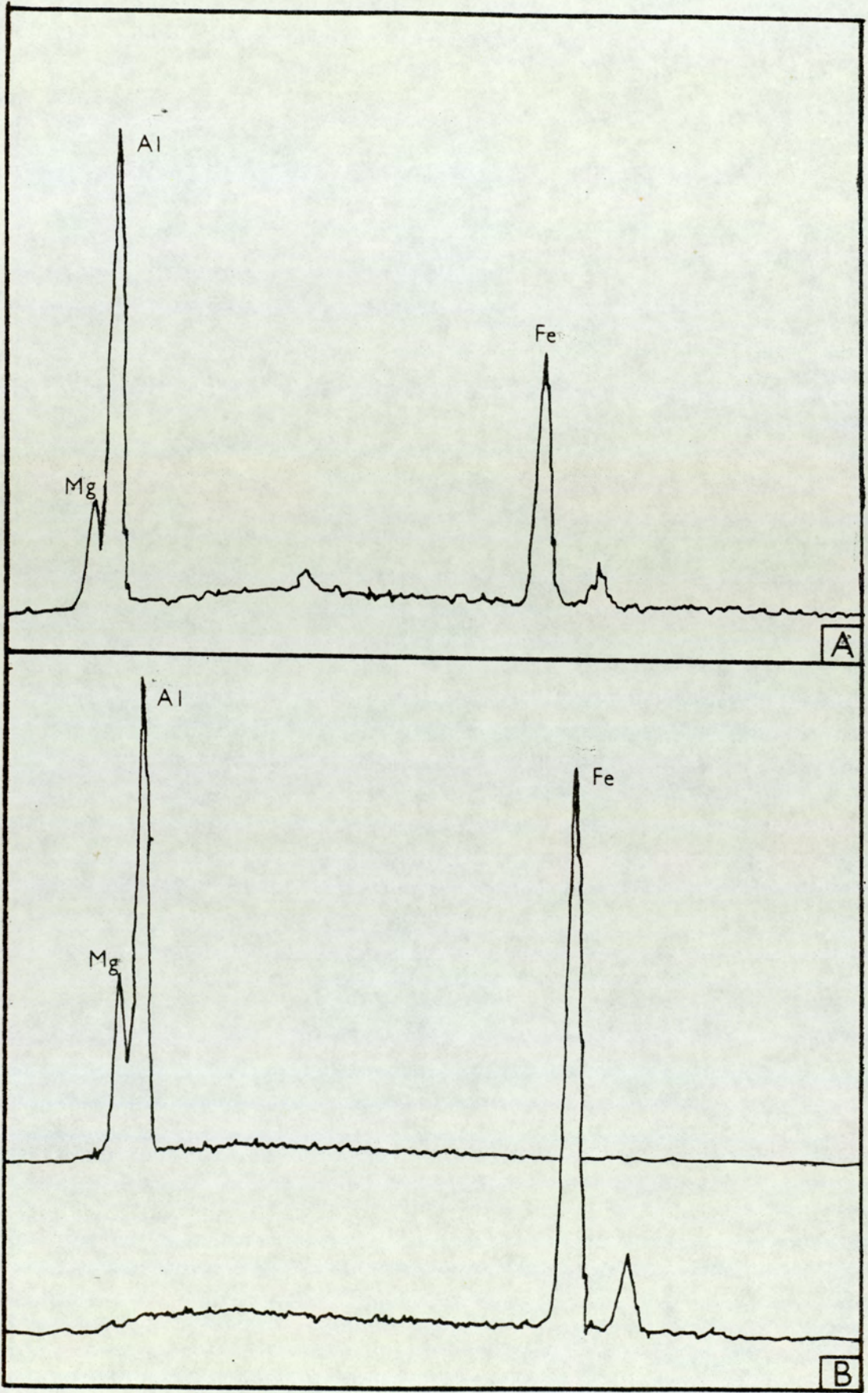


Fig 3.6 Comparison of energy-dispersive x-ray spectra of spinel: (A) taken in 10 seconds with 40% dead time and $MgAl_2O_4$ standard (B) taken in 25 seconds with 25% dead time and Fe metal (B) taken in 10 seconds with 50% dead time.

3.6 SEM STUDY OF SYMPLECTITE

In the course of examining fine-grained spinel-amphibole symplectite and hornblende-anorthite intergrowths, the capability of the optical microscope is limited. Therefore the scanning electron microscopes (SEM) which have great advantage for high resolution work were applied. Polished thin sections were coated with carbon. They were investigated by Cambridge Instruments Stereoscan S150 and 2A at the Department of Metallurgy and Materials, University of Aston.

3.6.1 The Secondary Electron Images and X-Ray Maps

The shape and distribution of spinel in spinel-amphibole symplectite and hornblende in hornblende-anorthite can be seen clearly from the secondary electron image (Figs. 3.7, 3.8). The sizes of rod, worm-like or irregular spinel vary from $0.5 \mu\text{m}$ to $5 \mu\text{m}$ in width and from a length of a few μm up to $30 \mu\text{m}$.

Hornblende intergrowths in anorthite usually form irregular rod shapes with smoothly curved surfaces (Fig. 3.8) indicating no crystallographic control. Its size ranges from $2-10 \mu\text{m}$ in width and the length is $5-20 \mu\text{m}$. Less commonly, within the same specimen but not within the same corona, remarkably perfect crystal shapes of symplectic hornblende suggest crystallographic control (Fig. 3.9). These hornblendes with perfect form are also coarser than the irregular form. It has been found that the development of the perfect form of hornblende occurs only when the primary plagioclase is mostly or completely surrounded by olivine. This difference can be explained in terms of the ability of water to



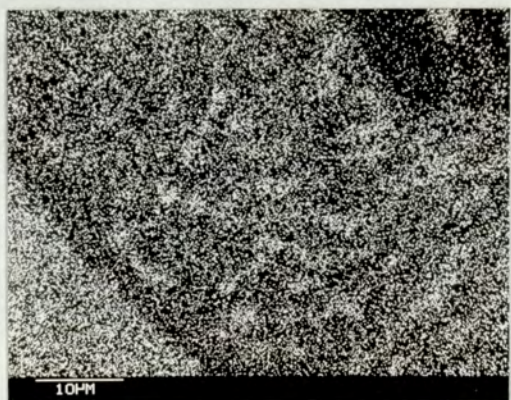
Al



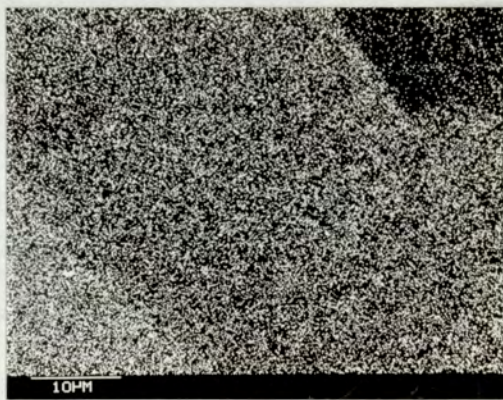
Si



Ca



Fe



Mg

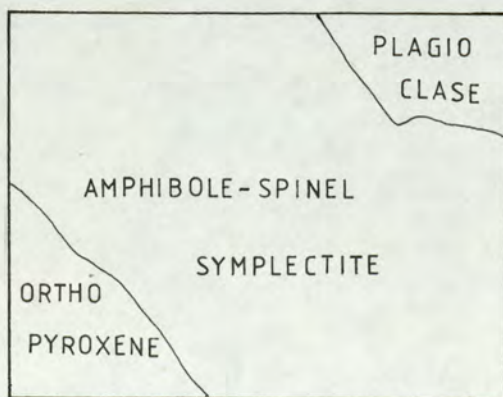


Fig 3.7 Secondary electron image and x-ray maps showing chemical variations within corona minerals (specimen 53 P).

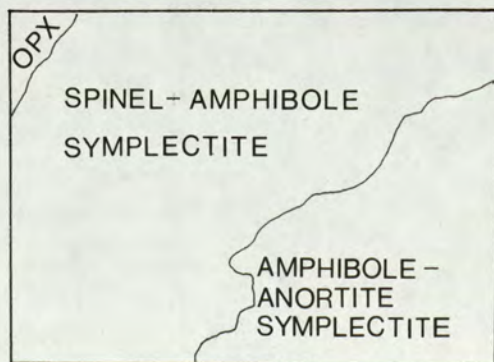
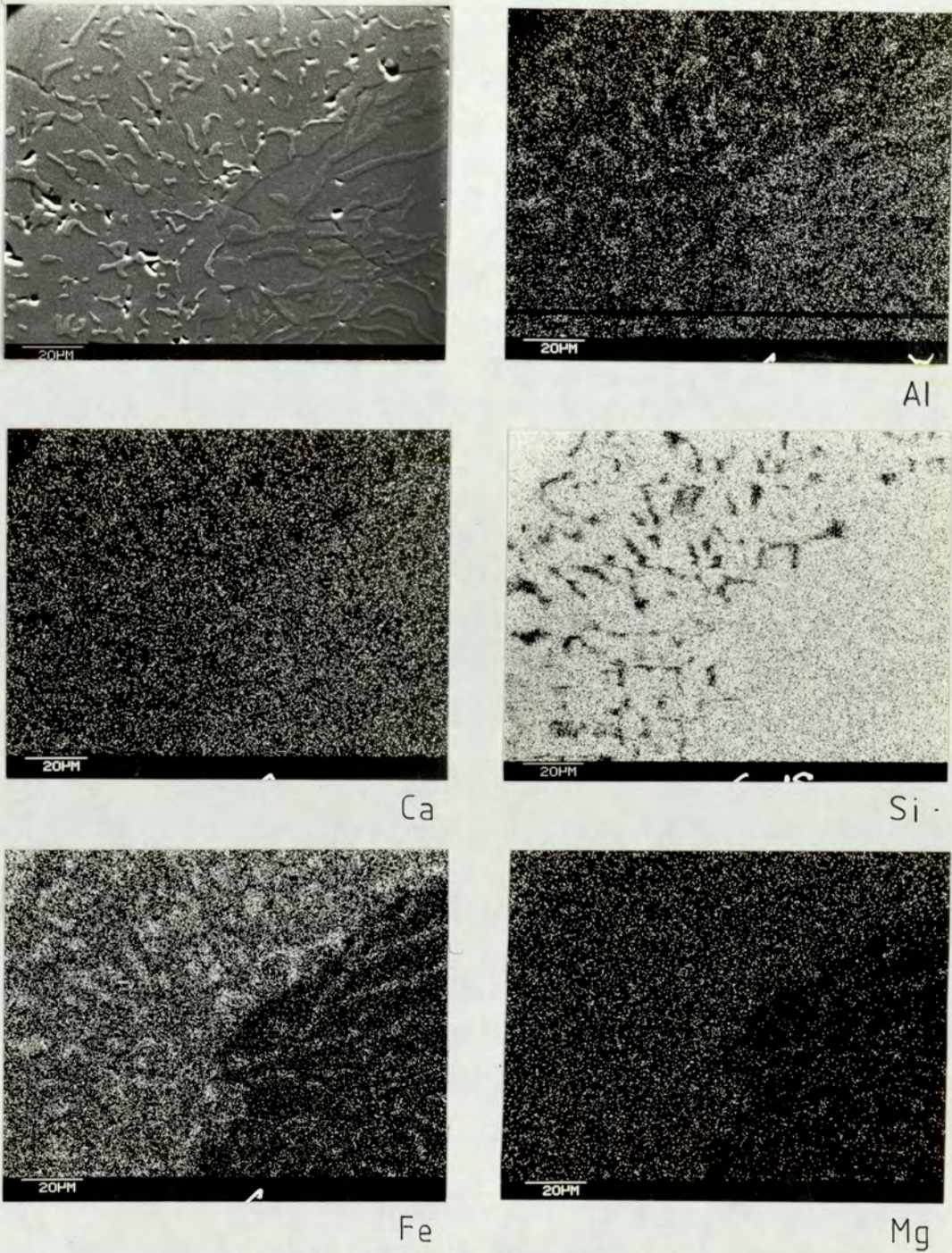


Fig 3.8 Secondary electron images and x-ray maps of corona in specimen 15/18763 in which the third layer of amphibole and anorthite symplectite is developed.

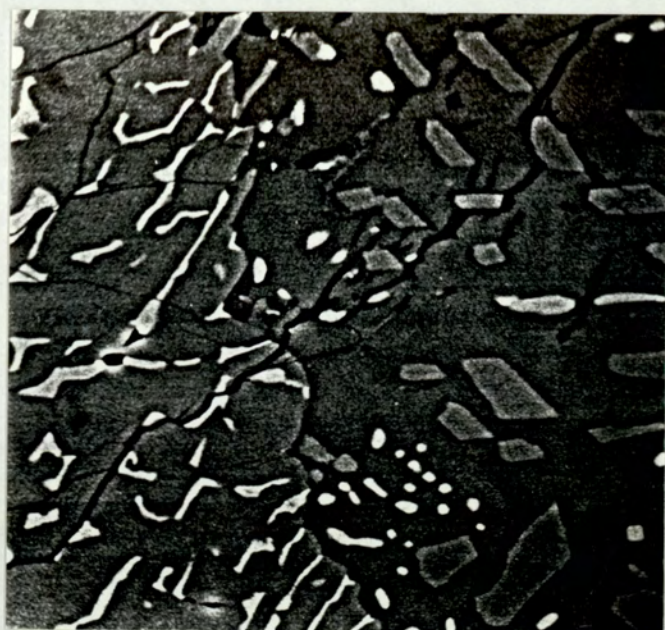
diffuse. Since the movement of water in the area surrounded by olivine is limited, the crystallization of hornblende takes a longer time than hornblende outside this area (where the diffusion of water is much easier), and slow growth promotes coarse good crystal form.

The proportions of spinel in amphibole and hornblende in anorthite in an individual specimen are generally consistent, not only within the scale of one corona, but also throughout the specimen. This characteristic makes it possible to estimate the volume proportions of each symplectic mineral. No tendency was found for spinel to be concentrated near the orthopyroxene interface or near the plagioclase interface. Many representative areas of symplectite were photographed for digitizing which will be described later (section 3.7).

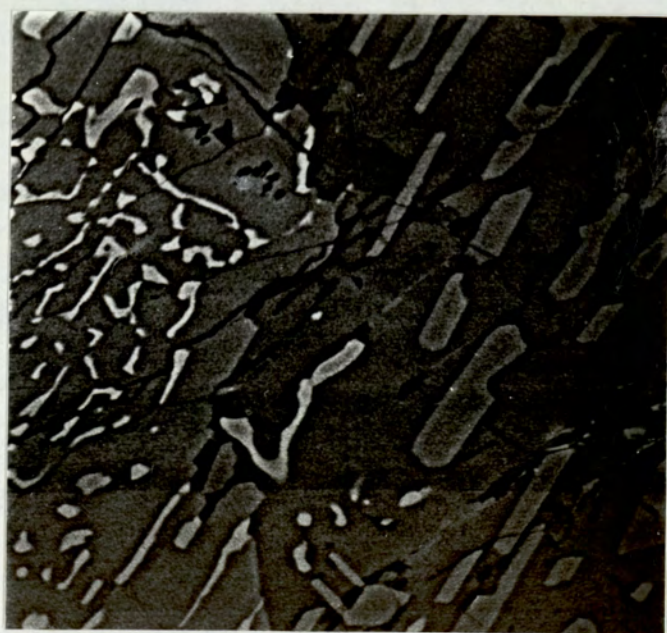
One other method to illustrate chemical variations between corona minerals from SEM is the X-ray maps. Figure 3.7 shows the distribution image for Ca, Si, Al, Fe and Mg of orthopyroxene, spinel-amphibole symplectite and plagioclase. The X-ray maps also help to identify the two different types of symplectite which are hard to distinguish in ordinary secondary electron images (Fig. 3.8).

3.6.2 Back Scattered Electron Images (BSE)

Although the secondary electron images have been widely appreciated for high resolution work, it is advantageous to use back-scattered electrons (BSE) which have relatively higher energy to produce much higher contrast. The back scattered electron image can be



10 μm



10 μm

Fig 3.9 The back scattered electron images of spinel-amphibole symplectite (left) and anorthite amphibole symplectite (right). Amphiboles in anorthite amphibole symplectite, which in this case is completely surrounded by olivine, show perfect crystal forms.

achieved by connecting the conventional SEM to the back scattered electron detector. This technique has also been used in combination with EPMA to study some symplectite intergrowths replacing cordierite by Vernon and Pooley (1981).

In the examination of spinel-amphibole symplectite and hornblende-anorthite symplectite, the solid state silicon diode (Hall and Lloyd, 1981), which has great ability to distinguish minerals with small differences in mean atomic number, was employed. From the BSE images (Fig. 3.9), spinel appears to be brighter than hornblende which has lower atomic number. It can be seen clearly that blebs or rods of spinel are present in hornblende-anorthite symplectite, but only near the interface with the amphibole-spinel symplectite, and only in very small amount.

3.7 ESTIMATION OF VOLUME PROPORTIONS OF CORONA MINERALS

3.7.1 Method

The volume proportions of corona minerals were estimated from area proportions in photographs, using the Hewlett-Packard 9874A Digitizer and the 9825A Desktop Computer (Fig. 3.10) at the Department of Civil Engineering, University of Aston.

Because it is not commonly used in mineralogy, the equipment will be described briefly. The digitizer comprises three main parts, the platen, keypad and the cursor controls (Fig. 3.10).

The platen is a sheet of laminated glass with the x, y conductor placed between the layers of glass. The top surface of the glass



9825A Desktop Computer and 9874A Digitizer

Fig 3.10 The digitizing equipment.

- (1) Platen
- (2) Keypad
- (3) Cursor with switches A and D

is lapped to provide uniform smoothness for the cursor vacuum feature. The active digitizing area on the platen is 315 x 435 mm². The keypad is used to program the unit. The cursor ring has two switches; one (labelled A) controls the vacuum applied to the cursor for fixing to the platen. The digitize switch on the right hand (labelled D) is used to enter data points. By pressing and releasing this switch, the co-ordinate value of the centre dot on the glass section of the cursor are recorded in the digitizer.

Continuous measurements are made simply by tracing this centre dot along and around the outline of each mineral grain. The positions of the centre dot are recorded simultaneously with maximum data rate of 30 points/second during the movement of the cursor. The connected microcomputer then converts this data into area (mm²). In each photograph, the total area of each mineral can also be measured from this microcomputer, giving an estimate of volume proportion.

The measurements were carried out for volume proportions of orthopyroxene: amphibole: amphibole - spinel symplectite where optical photographs were used, except for 710 C, in which widths of minerals were measured directly from the optical microscope; the volume proportions of spinel: amphibole within amphibole-spinel symplectite, and amphibole: anorthite symplectite. The last two cases were measured on SEM photographs. The photographs were enlarged as far as practicable before digitizing. The accuracy of the digitizer result depends mostly on the accuracy of the cursor movement along the grain boundaries. This again is the subject of human error. The digitizer itself has an

TABLE 3.5 Volume proportions of corona minerals determined by digitizing except specimen 710 C in which the width of orthopyroxene:amphibole:symplectite were measured by optical microscope.

LOCALITY	SPECIMEN No:	OPX:AMP:SYMPLECTITE	TOTAL MEASURED AREAS (μm^2)	SPINEL:AMP IN SYMPLECTITE	TOTAL MEASURED AREAS (μm^2)	HORNBLende: ANORTHITE IN SYMPLECTITE	TOTAL MEASURED AREAS (μm^2)
BELHELVE	53P	1: 0.22+0.076:	493,500	1:6.85+0.016	40770	-	
	710C	1: 0.21+0.04:	-	1:7.97+0.06	52360		
	15/18763	1: 0.31+0.09:	2,677,600	1:8.07+0.13	44660	1:3+0.13	29920
HUNTLY	773C	1: 1.23+0.08:	521,840	1:8.88+0.012	19714		
	774C	1: 0.30+0.10:	609,280	1:9.71+0.15	19800		
	18/19763	1: 1.16+0.086:	1,874,500	1:10.2+0.10	37580		

* Standard deviation

accuracy within ± 125 micrometres.

3.7.2 Results

Measurements were made in 6-16 photographs of several coronas in each specimen and optical measurements in 7 coronas in 710 C. The average and standard deviation over the several photographs and over the 7 coronas in the optical measurements of 710 C are given for each specimen in Table 3.5.

The three specimens from Belhelvie all have similar ratios of the orthopyroxene: amphibole: symplectite. These ratios vary among the Huntly samples, usually showing a greater area of spinel-free amphibole than the Belhelvie specimens, probably suggesting that H₂O was more abundant in the Huntly mass during corona formation.

The ratio of spinel and amphibole in symplectite is also uniform within each specimen. In general, spinel occupied 9-16% of the total areas. The irregular occurrences of the hornblende-anorthite symplectite cause difficulty in estimating their volume relations to the other corona minerals. However, the volume proportions of hornblende: anorthite in this symplectite were obtained as shown in Table 3.5. The variations noted (standard deviations, Table 3.5) are mostly real variation between the areas photographed, as distinct from measurement errors.

3.8 INTERPRETATION AND DISCUSSION

The digitizing data show that the volume proportion of ortho-

pyroxene: symplectite is reasonably steady in each studied area. The spinel: amphibole volume proportion in symplectite is also remarkably consistent, not only within each corona, but throughout the specimen. This is evidence that there must be restricted movements of some elements in corona reactions. The symplectite formation, which is the key to the interpretation of coronas, is reviewed in Mongkoltip and Ashworth, 1983 (in press).

In order to understand the movement of materials concerning corona formation, it should be easier to compare the chemistry of different minerals in a corona. From the analytical and digitizing data, the chemical variations across the corona can be graphically displayed as in Figure 3.11, where there are only two shells of corona in specimen 53P, and Figure 3.12 where the third (hornblende-anorthite) layer is also developed in specimen 15/18763. Since each mineral has different density, the volume correction by recalculating the analyses in terms of atoms per unit volume is essential. Tables 3.6 and 3.7 compare the atom proportions per unit volume with those per formula unit having 24 oxygens. Tables 3.6.2 and 3.7.2 give numbers of atom per unit volume of corona minerals relative to unit volume of orthopyroxene. Fe and Mg are treated together since the composition of spinel is unknown. It is reasonable to treat Fe and Mg as one component since their ratio is so similar in all the ferromagnesian silicates; relative to the reactant olivine, the small increase in Mg/Fe in orthopyroxene and hornblende is presumably roughly balanced by the larger decrease in the smaller volume of spinel. Data on molar volumes used in the calculations are from Robie et al (1966), except for amphibole, where the data on unit cell volume come from Papike et al (1969).

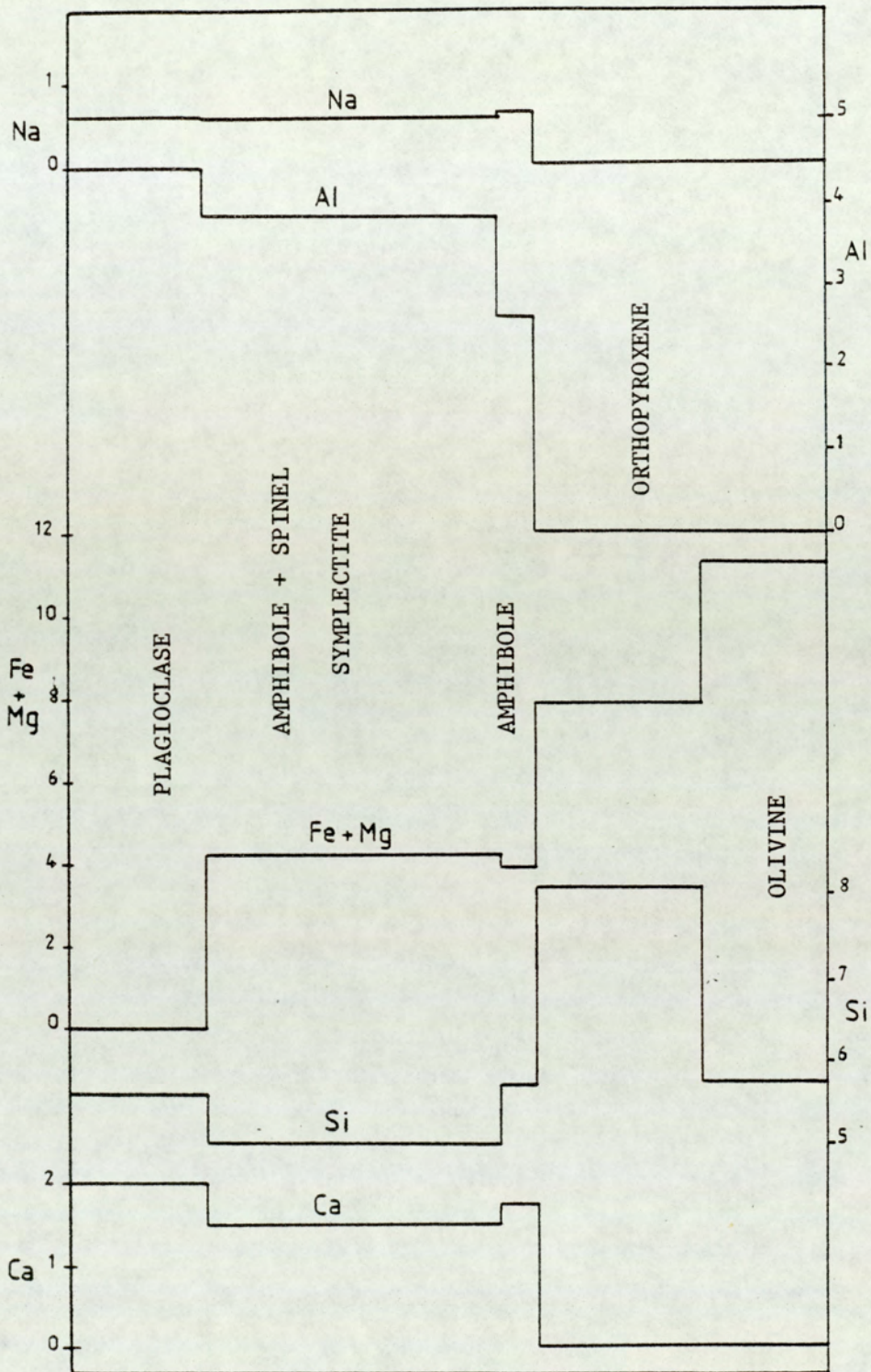


Fig 3.11 Volume corrected atomic concentrations across corona of specimen 53 P. The volume unit corresponds to 24 oxygen atoms in orthopyroxene.

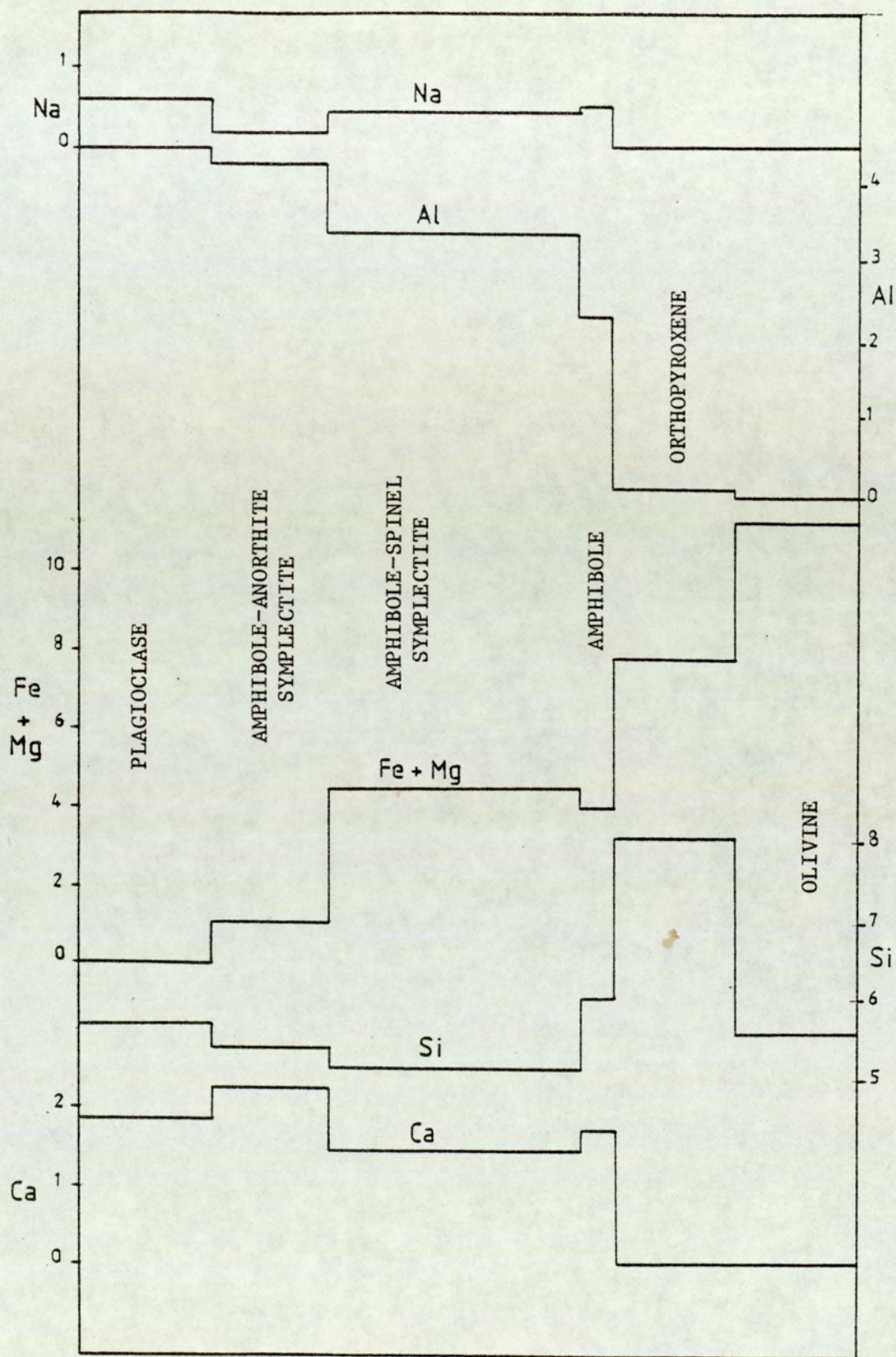


Fig 3.12 The chemical variations across an example of an evolved stage in corona evolution (specimen 15/18763), in terms of numbers of atoms after volume corrections.

TABLE 3.6.1 Numbers of atoms in corona minerals before the volume corrections in specimen 53 P.

MINERAL	Ca	Na	Mg + Fe	Al	Si	O	OH
OLIVINE	-	-	11.97	-	6.02	24	-
ORTHOPYROXENE	-	-	8.08	-	7.96	24	-
AMPHIBOLE	1.89	0.69	4.32	2.73	6.18	22	2
SPINEL	-	-	6.00	12.00	-	24	-
PLAGIOCLASE	2.38	0.67	-	5.27	6.63	24	-

TABLE 3.6.2 Numbers of atoms in corona minerals after the volume corrections in specimen 53 P.

MINERAL	Ca	Na	Mg + Fe	Al	Si	O	OH
OLIVINE	-	-	11.37	-	5.72	22.80	-
ORTHOPYROXENE	-	-	8.08	-	7.96	24	-
AMPHIBOLE	1.734	0.635	3.974	2.511	5.685	20.24	1.84
SPINEL	-	-	6.31	12.62	-	25.24	-
PLAGIOCLASE	1.99	0.56	-	4.41	5.55	20.08	-
SYMPLECTITE (87% AMP)	1.513	0.552	4.278	3.825	4.946	20.89	1.60

TABLE 3.7.1 Illustration of number of atoms in corona minerals in specimen 15/18763 before volume corrections.

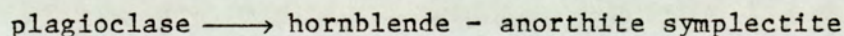
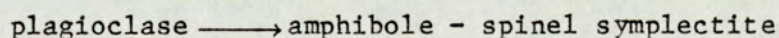
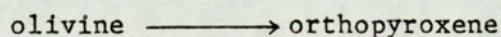
MINERAL	Ca	Na	Mg + Fe	Al	Si	O	OH
OLIVINE	-	-	12.00	-	6.00	24	-
ORTHOPYROXENE	-	-	7.933	0.08	7.973	24	-
AMPHIBOLE ₁	1.853	0.561	4.277	2.474	6.440	22	2
AMPHIBOLE ₂	1.754	0.521	4.540	2.706	6.193	22	2
AMPHIBOLE ₃	1.842	0.441	4.396	2.203	6.619	22	2
PLAGIOCLASE	2.251	0.720	-	5.253	6.754	24	-
ANORTHITE	2.946	0.120	-	5.872	6.093	24	-
SPINEL	-	-	6.00	12.00	-	24	-

TABLE 3.7.2 Number of atoms in corona minerals in specimen 15/18763 after volume corrections.

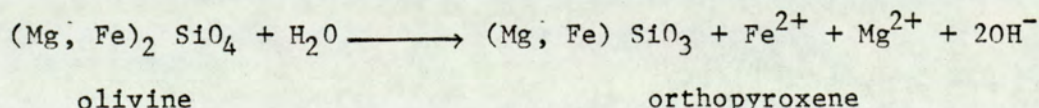
MINERAL	Ca	Na	Mg + Fe	Al	Si	O	OH
OLIVINE	-	-	11.396	-	5.700	22.80	-
ORTHOPYROXENE	-	-	7.933	0.08	7.973	24	-
AMPHIBOLE ₁	1.705	0.516	3.935	2.276	5.925	20.24	1.84
AMPHIBOLE ₂	1.614	0.479	4.177	2.489	5.697	20.24	1.84
AMPHIBOLE ₃	1.695	0.406	4.044	2.027	6.089	20.24	1.84
PLAGIOCLASE	1.884	0.603	-	4.396	5.652	20.08	-
ANORTHITE	2.463	0.100	-	4.910	5.094	20.07	-
SPINEL	-	-	6.31	12.62	-	25.24	-
AMP + SPINEL SYMP (89% AMP)	1.436	0.426	4.412	3.603	5.070	20.79	1.64
AMP + ANORTHITE SYMP (75% AMP)	2.271	0.177	1.011	4.189	5.343	20.57	0.46

In an attempt to write the corona reactions, there is still the question whether each corona forms as^a closed or open chemical system. From the graphical display (Figs. 3.11 and 3.12) showing chemical variations across the coronas, it is evident that olivine and plagioclase can supply the materials needed for corona formation. Then, as a starting working hypothesis, it should be reasonable to examine the proposition that coronas can probably form in approximately closed systems except for H₂O, without other components entering and leaving the system in large amounts.

As noted previously from textural observation, orthopyroxene could have formed directly from olivine and symplectites from plagioclase; the formation of the corona can be expressed by the following simplified partial reactions:



Evidently, orthopyroxene can form from olivine by rearrangement of SiO₄ tetrahedra to SiO₃ (SiO₄ → SiO₃ + O). These reaction models also require the movement of Fe and Mg from olivine into plagioclase to form amphibole and spinel by the following simplified reaction:-



From this reaction, two oxygen atoms are released from SiO₄ and presumably from OH⁻. The main chemical change in this stage is a loss of Fe, Mg and O. Where orthopyroxene is the only product, Fe, Mg and O must be lost. Corona formation probably starts this way, perhaps localised at olivine-plagioclase contacts

by their greater reactivity than olivine-pyroxene ones (inferred from the greater structural disorder required in olivine at a contact with the structurally very different feldspar; Murthy 1958). Usually, reaction proceeds further; plagioclase becomes a reactant and some of the Fe, Mg and O released from olivine is consumed in the reaction to produce spinel - amphibole symplectite.

The development of spinel - amphibole symplectite requires not only Fe, Mg, O from olivine, but also Si, Al, Ca and minor Na from plagioclase. Although the covalent Si-O and Al-O bonds which are the main framework of plagioclase are stronger than the bonds between other cations in silicate minerals, MacKenzie (1957) showed that water can provide enough energy necessary for weakening or breaking the strong Si-O and Al-O bonds. This can be applied for the breakdown of plagioclase to form spinel-amphibole and anorthite-hornblende symplectites, which according to Murthy (1958), need higher concentrations of water than the formation of orthopyroxene. It is therefore, in some coronas where the availability of water is limited, there is only orthopyroxene of the first shell without the development of spinel-amphibole symplectite.

The shapes and consistent proportions of spinel of high Al content, in spinel-amphibole symplectite strongly suggest the restricted movement of Al in plagioclase. The immobility of Si and Al in this part of the corona is revealed by comparing Al/Si ratios of symplectite and plagioclase. Table 3.8 shows that symplectite appears to have inherited the Al/Si of plagioclase in each specimen. This relationship is believed to be strong evidence in support of the assumed immobility of Al and Si.

But the fact that the narrow spinel free amphibole has higher Si and lower Al (analysis 3.1 in Table 3.3) than amphibole in spinel-amphibole symplectite (analysis 3.2) shows that Al and Si in plagioclase can not be completely immobile and may indicate that amphibole changes towards the composition of typical hornblende of amphibolite facies rather than pargasitic. It is noteworthy that this change occurs only in specimens 710C and 15/18763 where the amphibolisation of olivine is also developed. This picture indicates that at an advanced stage of metamorphism or when more water gets into the system, the corona evolves further by the inward growth of the pargasitic hornblende without spinel. In other words, spinel-free amphibole shells would thus represent an additional growth. It is most likely that this growth requires the outward movement of Si and the inward migration of Al from plagioclase to the orthopyroxene-amphibole contact. The significant Al content of orthopyroxene also suggests some mobility of this component. However, the strong relation of Al/Si ratio in plagioclase and spinel-amphibole symplectite (Table 3.8) indicates that assumption of relative immobility of Al and Si appears valid.

In the third layer present in some coronas, parts of plagioclase crystals are transformed to the symplectite of anorthite and hornblende. A likely source of Fe and Mg is provided by the remaining Fe, Mg from the formation of spinel-amphibole symplectite. The reason for the partial replacement of plagioclase by the irregular shapes of anorthite and hornblende symplectite is obscure. It may be speculatively interpreted as a kinetic effect, the contact between plagioclase and anorthite being the kinetic barrier. The compositional discontinuity slightly resembles the Huttenlocher miscibility gap, but is not consistent with

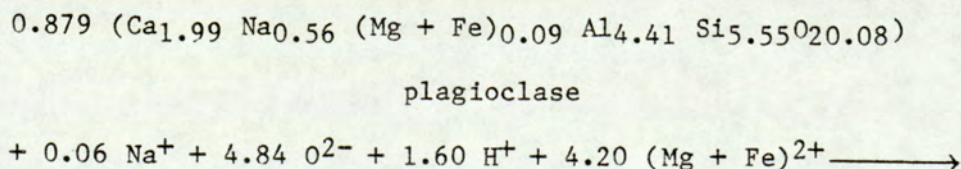
TABLE 3.8 Relationships between Al/Si in plagioclase, spinel-amphibole symplectite and hornblende-anorthite symplectite, indicating that Si and Al are relatively immobile during corona development.

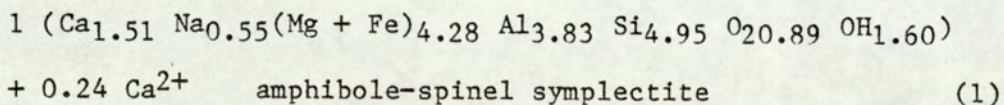
LOCALITY	SPECIMEN No.	An IN PLAGIOCLASE	Al/Si IN PLAGIOCLASE	Al/Si SPINEL-AMPHIBOLE SYMPLECTITE	Al/Si IN HORNBLLENDE-ANORTHITE SYMPLECTITE
BELHELVIE	53 P	79	0.79	0.77	
	710 C	79	0.82	0.82	
	15/18763	74	0.78	0.71	0.78
HUNTLY	773 C	69	0.73	0.70	
	774 C	66	0.72	0.70	
	28/19763	69	0.72	0.69	

this solvus (Grove, 1977). At this stage the Al/Si ratios of anorthite and hornblende symplectite and primary plagioclase are virtually identical (Table 3.8). This suggests that ^{the} anorthite-hornblende symplectite inherits the Al and Si content of plagioclase, at a stage when the amphibole-spinel symplectite is evolving away from this constrained condition.

To test the hypothesis described above, the analyses and volume proportions data of corona minerals from two examples (specimen 53P and 15/18763) are used to determine whether chemical mass balance in corona reactions is achieved. In the least evolved coronas (specimen 53P), a model which predicts the relative proportions of orthopyroxene and symplectite produced can be proposed by starting from the hypothesis that Al and Si are immobile in symplectite at this stage.

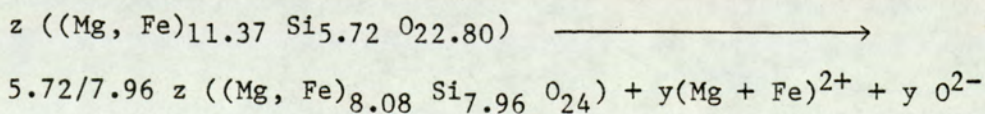
Let (x) be the number of volume units of plagioclase that react to produce 1 volume unit of amphibole-spinel symplectite. Non-symplectite hornblende is neglected, as it would make the problem intractable; this is justified because its amount is very small at this stage. (x) is estimated from the ratio of Si atoms in symplectite to Si atoms in plagioclase ($4.946/5.550 = 0.891$) or from the equivalent ratio for Al ($3.825/4.410 = 0.867$). Taking the charge weighted average estimate $x = 0.879$ preserves charge balance in the following equation, where the small residuals for Al and Si have been neglected:





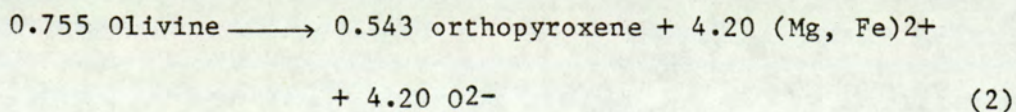
Oxygen is here expressed as O^{2-} for convenience, without necessarily implying that this is the reactant species. The large influx of oxygen as well as Mg, Fe leads to the increase in volume from 0.879 to 1 unit. The hypothesis of Al, Si immobility requires this addition of oxygen to make over the plagioclase to the symplectite formula. The source of most of the added oxygen and (Mg, Fe) must be the breakdown of adjacent olivine to a smaller volume of orthopyroxene. The mobility of other elements, implied by Si, Al immobility, thus explains the moving interface mechanism inferred by Grieve and Gittins (1975). We can assess quantitatively whether the model fits our observations by now calculating the volume of orthopyroxene that should be produced from olivine to supply the (Mg + Fe) for symplectite formation. This assumes that the system is approximately closed to (Mg + Fe). We assume this rather than closure to oxygen, which can be added to the system along with hydrogen from the aqueous fluid phase.

Let y be the amount of $(\text{Fe}, \text{Mg})^{2+}$ required to form the symplectite by reaction (1). In volume terms:-

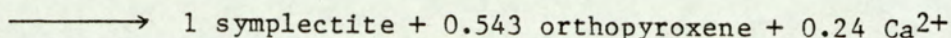
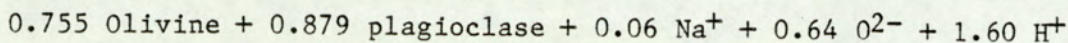


where $(11.37 - 5.72/7.96 \times 8.08) z = y$

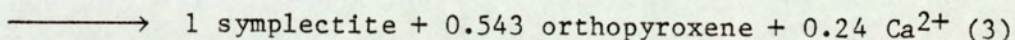
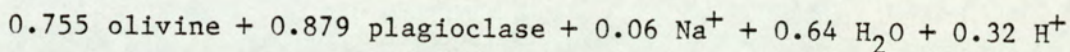
From equation (1) $y = 4.20$, giving:



Combining (1) and (2) gives the total model reaction, in terms of volumes of minerals:

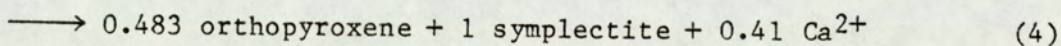
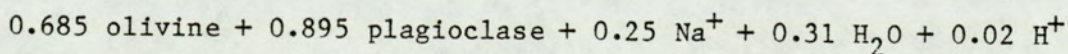


or, more realistically as regards the ions likely to be added from the fluid (Gresens, 1974),



This reaction appears to be very attractive as it yields the volume proportion of orthopyroxene: symplectite to be 1:1.84 which is very close to the measurement, particularly as the spinel-free amphibole was not modelled. The amount of plagioclase needed for the formation of corona is slightly greater than olivine. Moreover, the overall reaction is likely to involve only a net gain of water and H^+ and a loss of a very small amount of Ca^{2+} . These features strongly support the approximately closed chemical system of corona in the studied rock.

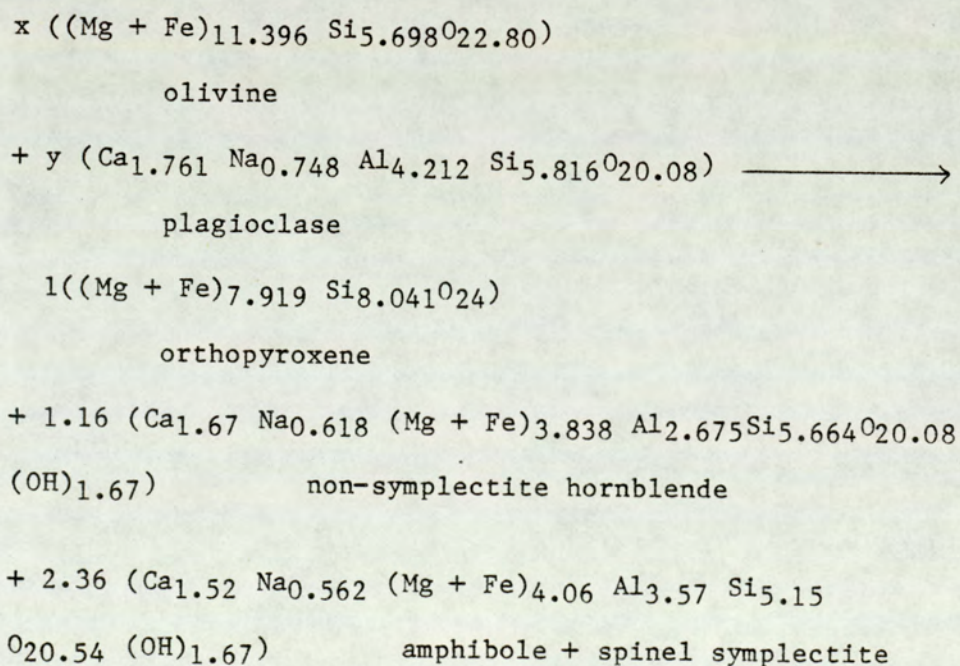
Using the same method of calculation on the data from specimen 710 C gives the overall reaction as:-



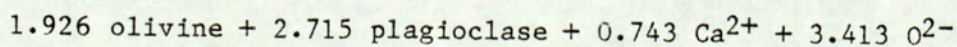
In more evolved coronas, there are too many variables for the prediction of shell proportions to be attempted. The large proportions of non-symplectite hornblende in specimens from the Huntly intrusion indicate that this part of the corona can not be omitted. It is impossible to tell precisely what represents the original (pre-migration) olivine-plagioclase boundary, probably somewhere within the non-symplectite hornblende zone. In this sense, non-symplectite hornblende could be derived from both

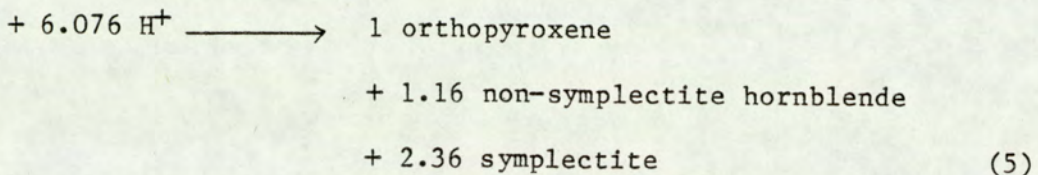
plagioclase and olivine. Therefore, the model can not be written as partial reactions like the previous model. The model also requires some movements of Al and Si. However, the Al/Si inheritance from primary plagioclase in the outer shell (amphibole + spinel symplectite) and the Mg/(Mg + Fe) similarity of the olivine and orthopyroxene and the middle shell (non-symplectite hornblende) suggest the corona model with closed system for these elements. We can write equations by using the measured volume proportions of layers.

An example for the model proposed here is based on the data of specimen 18/19763. Let (x) and (y) be the numbers of volume units of olivine and plagioclase respectively to form 1 orthopyroxene, 1.16 non-symplectite hornblende and 2.36 amphibole + spinel symplectite.



As we assume that the reaction is closed to Mg + Fe, Al and Si, it yields:

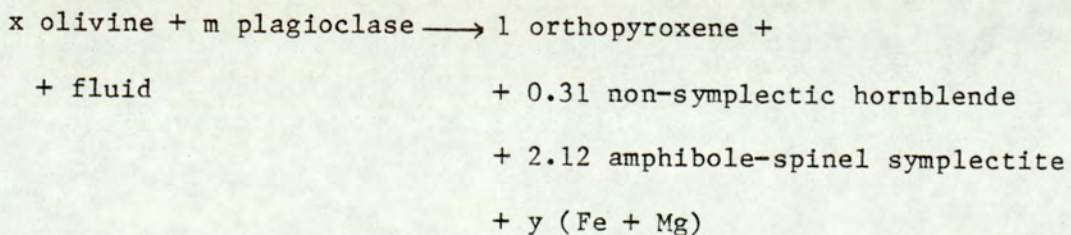




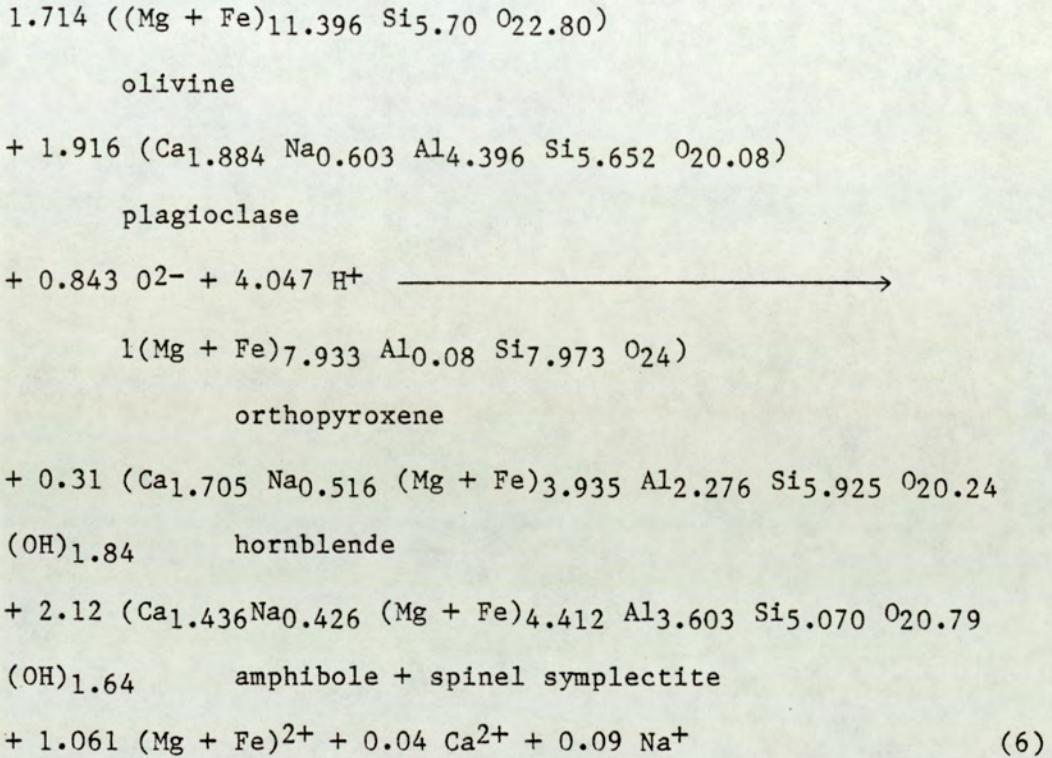
From this reaction, it appears that a great amount of plagioclase is involved, when ^ahigher proportion of non-symplectite hornblende is produced. Compared with reaction (3), in which the non-symplectite hornblende is neglected, a great amount of O^{2-} and H^+ or water is also required in reaction (5).

Since the anorthite-hornblende symplectite shell is often incomplete and occasionally lacking, the volume proportions of this shell to other minerals then vary from corona to corona. However, we can erect model reactions using the measured volume proportions as well as the chemical analyses. As an example, consider specimen 15/18763 in which hornblende-anorthite symplectite is developed and non-symplectite hornblende will also be modelled. The formation of hornblende-anorthite symplectite implies that (Fe, Mg) enter the system from other parts of the rock or from other parts of corona. The non-symplectite hornblende requires some Al, Si, mobility within this system, but we assume that as a whole it is closed to Al, Si explaining the inheritance of primary plagioclase Al/Si in the hornblende-anorthite region outside it.

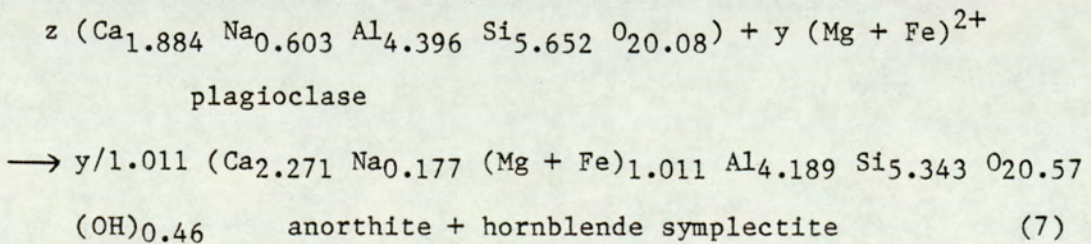
The reaction between olivine and plagioclase to form 1 orthopyroxene, 0.31 non-symplectite hornblende and 2.12 amphibole spinel symplectite may be expressed in terms of unit volume as:



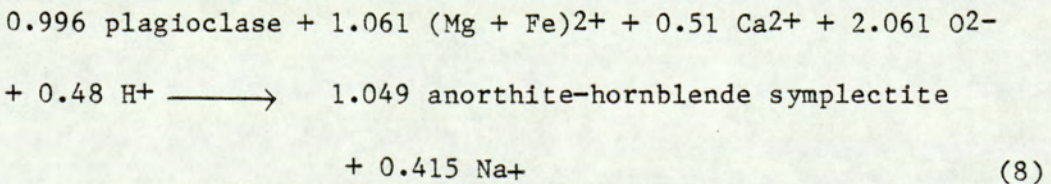
From the assumption that the system is closed to Si, Al but not closed to $(Mg + Fe)^{2+}$, Na^+ , Ca^{2+} , O^{2-} and H^+ , at this stage, we have:



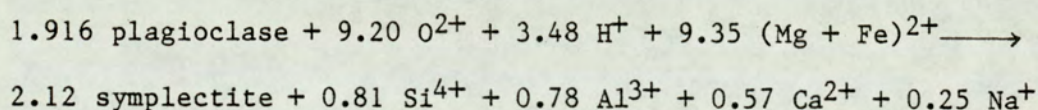
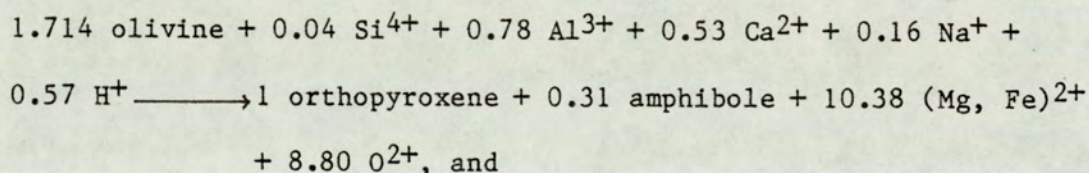
Let z be the number of volume units of plagioclase that react with $(Mg + Fe)^{2+}$ released from reaction (6) to form anorthite and hornblende symplectite. With the extension of Al, Si immobility theory, the amount of anorthite and hornblende, symplectite produced by the $(Mg + Fe)^{2+}$ lost in equation (6) then can be estimated by:-



From equation (6), $y = 1.061$,



Equation 8 can not be considered as realistic as equation 6, because the amount of anorthite - hornblende symplectite produced in equation 8 is small compared with those seen in the specimen. Moreover, the amount of this symplectite is uncertain; it varies from corona to corona. The development of anorthite-hornblende symplectite then should require the introduction of further $(\text{Fe} + \text{Mg})^{2+}$. In fact the amount of $(\text{Fe} + \text{Mg})^{2+}$ released in reaction 5 is comparable with the uncertainty in estimating it. This amount is also small compared with those moving between layers which can be seen by the following half reactions:-



By writing equations analogous to reaction 6 for all studied specimens, the coefficients for each specimen were derived (Table 3.9), along with the volume ratios between products and reactants. In all specimens, coronas can not be modelled as essentially closed except to H_2O , but the gains and losses of elements are small compared with the amounts of elements involved in the reactions. In the Huntly samples, in which the proportions of spinel-free amphibole are high, the gains of O^{2-} and H^{+} as well as $(\text{Mg} + \text{Fe})^{2+}$ and Ca^{2+} are higher than the Belhelvie samples. This can be related to the approximately constant volume for corona formation in the Huntly specimens while there is a small volume decrease in the Belhelvie specimens.

Oxygen is not entirely introduced into the system as H_2O .

Additional oxygen is represented in all equations (Table 3.9), and it always accommodates the charge balance for cation movements. Apart from oxygen, which is a mobile element, Ca^{2+} and Na^+ are also required to move. ~~Some of the~~ The Ca^{2+} and Na^+ to be added and/or released probably are exchanged with plagioclase at a distance from the corona, during the growth. It is evident that during the formation of more spinel-free amphibole, the system also required some Mg^{2+} and Fe^{2+} .

From table 3.9, it is evident that orthopyroxene can definitely not be derived from olivine by volume for volume replacement, nor the spinel-amphibole symplectite from plagioclase. In all cases, orthopyroxene produced is much lower than olivine consumed, strongly supporting the hypothesis of a migrating boundary by Grieve and Gittins (1975) and in a more general context Joesten (1977). This phenomenon is analogous to the Hartley-Kirkendall Effect (Brophy et al, 1964), which stated that the diffusion process is controlled by the relative rates of diffusion of material from each phase. If the differences in flux of material between two phases are high, it will cause the rapid migration of the material out of one phase, then the initial boundary may actually migrate. In the case of coronas, the flux of material is related to the high concentration of $(Fe + Mg)^{2+}$ in olivine compared with plagioclase. Fe^{2+} and Mg^{2+} , perhaps with O^{2-} , then diffuse into plagioclase. The corona reaction is then controlled by diffusion rates between the products although initially it was controlled by free-energy gradients between olivine and plagioclase.

TABLE 3.9 Estimated coefficients of corona reactions.

LOCALITY	SPECIMEN	REACTANT		GAINS AND LOSSES OF ELEMENTS*					VOLUME RATIOS OF PRODUCTS: REACTANTS
		OLIVINE	PLAGIOCLASE	Na	Ca	Mg, Fe	O	H	
BELHELVE	53 P	1.53	1.67	-0.18	+0.30	+0.86	-0.49	-3.25	0.94
	710 C	1.40	1.91	-0.15	+0.80	-0.23	-1.27	-3.52	0.94
	15/18763	1.71	1.92	+0.09	+0.04	+1.06	-0.84	-4.05	0.95
HUNTLY	773 C	1.97	3.40	+0.01	-0.92	-2.96	-7.54	-7.41	0.99
	774 C	1.49	2.58	+0.40	-0.61	-3.28	-6.25	-5.15	0.99
	28/19763	1.84	2.78	+0.04	-0.64	-0.85	-4.56	-6.08	0.98

*Negative sign indicates gains, positive sign indicates loss.

It is clear that water has an important role for the corona formation, in the studied areas, initially as the catalyst for the breaking down of bonds between Fe^{2+} and Mg^{2+} and the oxygen atoms in olivine to form orthopyroxene. Water, perhaps as OH (Dowty, 1980), is also necessary to facilitate the movement of materials into and within olivine and plagioclase for corona formation. Furthermore, water takes part in the amphibole formation. The local low water content must have prohibited the growth of amphibole-spinel symplectite which is occasionally absent in some coronas. The conversion of plagioclase to amphibole is also increased by increasing water activity which raises the stability of amphibole (Cawthorn, 1976). Since the availability of water in basic magma is limited and there is no hydrous mineral in the primary phases, the source of water in corona formation is likely to be the country rocks. Gribble (1967) also suggested that water released from the dehydration reactions during metamorphism in the hot country rocks moved into the basic intrusions. Thus the reaction is not strictly deuteritic but is retrograde metamorphic.

3.9 CONCLUSION

In summary, corona reactions in the studied areas can be quantitatively calculated in a nearly closed system except for H_2O and some cation exchange involving H^+ . The basis of volume for volume replacement of olivine by orthopyroxene and plagioclase by amphibole + spinel symplectite, as frequently interpreted by previous workers is rejected. Immobility of Al and Si in symplectite is inferred from the inheritance of Al/Si ratios from reactant plagioclase. Corona formation can be demonstrated by the ion diffusion model in Figure 3.13. It starts with the intro-

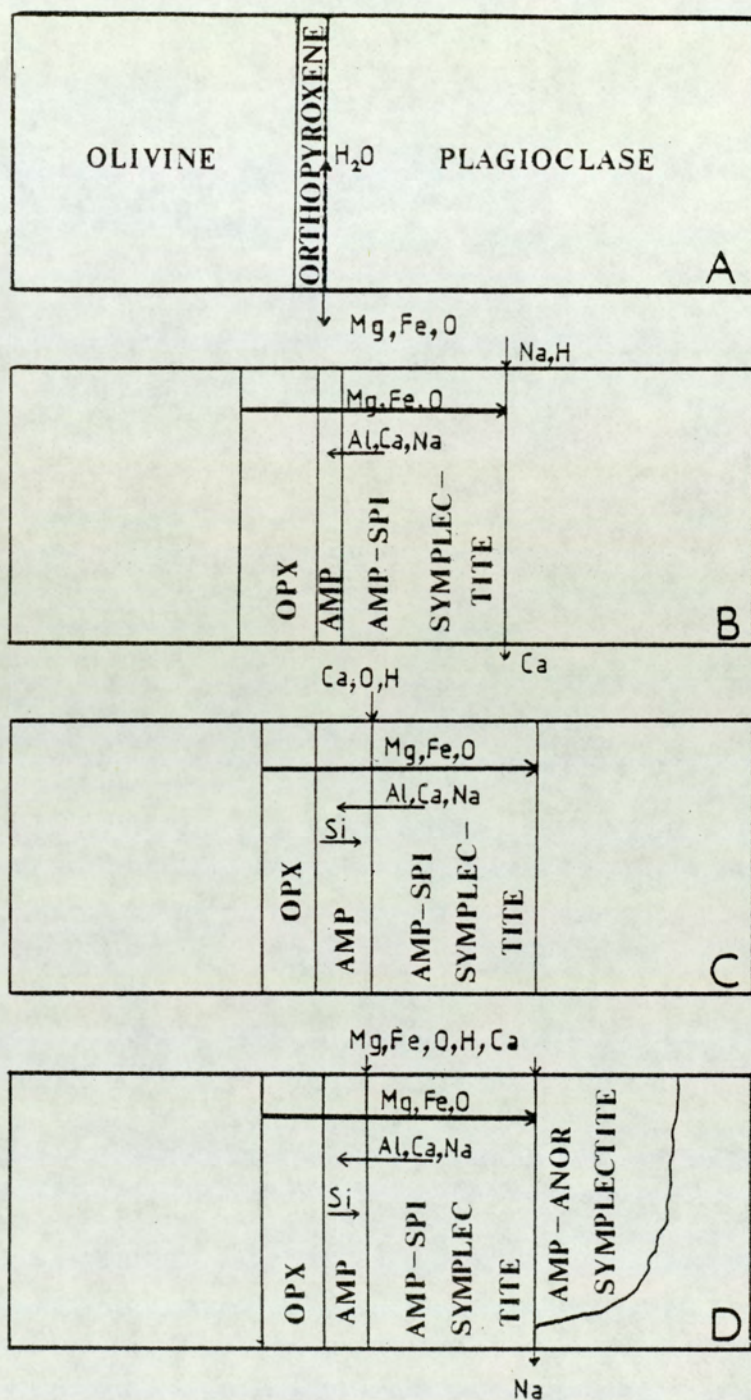


Fig 3.13 Ion diffusion model in various stages of the corona formation. (A) Reaction olivine \rightarrow orthopyroxene (B) Development of three-layer corona with amphibole poor from the Belhelvie volumetric data; referred to reaction 3. (C) With amphibole rich layer from the Huntly specimens, referred to reaction 5. (D) Additional development of amphibole-anorthite symplectite.

duction of H_2O along olivine and plagioclase boundary, the H_2O acting as catalyst for the transformation of olivine to orthopyroxene releasing Fe, Mg and O. Since olivine and orthopyroxene have almost the same density, the loss of Fe, Mg and O causes the volume reduction in the conversion of olivine to orthopyroxene. These ions diffuse into plagioclase, accompanied by Ca, Na, Al and Si in plagioclase producing amphibole-spinel symplectite, while Al, Si are completely immobile in this part of corona at this stage. The influx of Fe, Mg and O causes the increase in volume on the conversion of plagioclase to amphibole-spinel symplectite, although spinel has greater density than plagioclase.

When the availability of water in the system is high, the corona evolves further by the movements of Al from symplectite into and Si away from the orthopyroxene-symplectite interface to form hornblende of high Al and low Si, approaching amphibolite facies. The corona reaction producing more spinel-free amphibole occurs at approximately constant volume while the amphibole poor corona is produced with decrease in volume. In some cases, part of the plagioclase is replaced by hornblende-anorthite symplectite in the outer most part of corona. This conversion takes place with approximately volume for volume replacement in which Al and Si act as the inert elements while Fe, Mg and O, partly released from the formation of amphibole-spinel symplectite and small amounts of Ca from surrounding plagioclase move into this part of plagioclase.

CHAPTER FOUR

COMPOSITIONAL CHARACTERISTICS OF PYROXENES AND AMPHIBOLES, AND RELATIONSHIPS AMONG THESE MINERALS

4.1 INTRODUCTION

The formation of usually fibrous, secondary amphibole pseudomorphs after pyroxene is a common phenomenon in the hydrothermal and late stage alteration of basic igneous rocks and rocks that have undergone retrograde or dynamic metamorphism. Such a replacement process has long been recognised as "uralitization", or less frequently called "amphibolitization" when the replacement takes place under the amphibolite facies conditions. Pyroxenes that have been completely replaced by aggregates of slender prisms or fibrous amphibole are often referred to as "uralite". The term "uralite" was originally used by Rose in 1831 to describe a mineral with the habit of pyroxene but the structure of amphibole in green porphyritic rocks from the Ural Mountains (Rose, 1831 in Ford, 1946). Uralite is however not a stable product of pyroxene alteration, and so is in turn altered to chlorite, talc or other minerals which could be other types of amphibole.

In more recent years, much of the attention on the replacement of pyroxenes by amphiboles has been focused on reaction mechanism on the scale observable with TEM methods. Veblen and Buseck (1981) concluded that transformation from pyroxenes to amphiboles can take place either by a bulk replacement mechanism along a broad reaction front that advanced through the primary pyroxene, as previously stated by Dana (in Ford, 1946) in the case of uraliti-

zation, or by the nucleation and growth of narrow lamellae as suggested by Nakajima and Ribbe (1980). The latter phenomenon, however can form by exsolution from pyroxene that originally had some degree of solid solution toward amphibole composition (Papike et. al. 1969, Smith 1977, Yamaguchi et. al. 1978, Isaacs et. al. 1981).

Several types of amphibole may have been derived from different types of pyroxene. In general, the nature and composition of amphibole have a definite relation to the original pyroxene. Ca-pyroxene generally gives way to Ca-amphibole; e.g. augite to actinolite and hornblende. (Grapes, et. al. 1976, Piispanen and Alapieti, 1977), endiopside to actinolite (Rodgers, 1973) diopside to tremolite (Veblen and Buseck, 1981), whereas Ca-poor pyroxene preferably altered to Ca-poor amphibole: hypersthene to cummingtonite. (Stewart 1947, Himmelberg and Phinney 1967, Bonnicksen 1969, Austrheim and Robins 1980), aluminous hypersthene to aluminous anthophyllite (Vernon, 1972); for instance. Unusual cases have also been reported when Ca-poor pyroxene is replaced by Ca-amphibole (Oliver, 1951) or alternatively, Ca-pyroxene by Ca-poor amphibole (Allen and Fahey, 1957).

Although various papers concerning uralitization have been published and it is quite clear that most of the uralites form by alteration involving chemical exchange between pyroxenes and their surroundings, surprisingly the chemical changes associated with this process have received only occasional attention. Chemical changes involving uralitization have been discussed in terms of chemical variations within the mineral itself or on a larger scale (as the whole-rock chemistry) whether the process

behaves as a closed or open system. Based on the former case, the changes in chemical compositions in passing from pyroxene to secondary amphibole, apart from incoming of H₂O which is definitely necessary in all cases, can be increase in Si, Al, Fe, Ti and Mn and decrease in Ca (Allen and Fahey, 1957); introducing of Ti, Al, Fe, Na, K and simultaneous releasing of Ca (Piispanen and Atapieti, 1977) or a removing of Ca with small net loss in Si, Mg and a slight increase in Al (Rodgers, 1973). The effect of uralitization upon the whole rock composition has been proposed as a closed system except for water (Oliver, 1951 and Allan, 1970). It is strongly argued by Rodgers (1973) that uralitization can not be regarded as a closed-system even though both orthopyroxene and clinopyroxene are involved. Hanan (1976) also suggested a marked increase in the whole rock FeO/MgO ratios in uralitized rocks relative to unuralitized rocks. Various occurrences and natures of uralite described above, clearly indicate that uralitization is not a simple and unique process but rather complicated.

The most world-wide type of secondary amphibole replacing clinopyroxene is actinolite which is usually bordered by hornblende. The chemical relationships between coexisting actinolite and hornblende have been extensively studied in various localities from low-pressure to high-pressure metamorphic facies series. (e.g. Wiseman 1934, Shido and Miyashiro 1959, Klein 1969, Cooper and Lovering 1970, Brady 1974, Misch and Rice 1975, Tagiri 1977, Choudhuri 1974, Graham 1974, Grapes 1975, Sampson and Fawcett 1977, Grapes and Graham 1978). In spite of their great variety of occurrences, there has been considerable debate in the literature over whether or not a miscibility gap exists in the actinolite-

hornblende series. Their sharp contacts both optically and chemically have been cited as strong evidence of a miscibility gap or equilibrium by many workers. (e.g. Shido and Miyashiro 1959, Klein 1968, Cooper and Lovering 1970, Brady 1974, Choudhuri 1974, Kuniyoshi and Liou 1976, Tagiri 1977). Alternatively, it has been argued by Grapes (1975), Graham (1974), Sampson and Fawcett (1977), Grapes and Graham (1978) and Thomson et. al. (1981) that the typically abrupt change from actinolite to hornblende is the result of a continuous, but rapid gradation coupled with incomplete reaction or non-equilibrium rather than to the existence of an underlying miscibility gap. Graham (1974) also pointed out that both sharp and gradational contacts between actinolite and hornblende can occur within the same thin section or even within the same grain. Recently, Hynes (1982) shows that the compositional gaps between actinolite and hornblende are generally wider and more consistent in medium pressure terrains than in low-pressure terrains and due to the amount of tschermakite substitution which is related to the compositions of associated plagioclase. Perhaps the most fruitful approach to the problem is the experimental work by Oba (1980) on phase relations between tremolite and pargasite which can be related to the actinolite-hornblende miscibility gap. He stated that at 1 kbar there is a well-defined miscibility gap between pargasite and tremolite, but at 5 kbar tremolite and pargasite forms a continuous series of solid solution above 800°C and if the miscibility gap exists at this pressure, it must be below 800°C. However the experimental study in CaO-MgO-Al₂O₃-SiO₂-H₂O-CO₂ system by Pluysnina and Ivanov (1981) indicated that amphibole compositions change consistently along the equilibrium curve from tremolite to hornblende with increasing T from 400°-600°C and P at 2, 4, 6 and 8 kbar. Misch and Rice

(1975), working on natural assemblages, also inferred complete miscibility between tremolite and hornblende at temperatures greater than 600°C.

For the aim of the present study, we will examine the replacement of pyroxenes by amphiboles in some of the 'Younger' basic intrusions and Glen Scaddle mass. The uralitization process in the Morven-Cabrach intrusion and Belhelvie intrusion have been studied in some petrographic detail by Henry (1938) and Stewart (1946) respectively. Orthopyroxene is replaced by cummingtonite which is in turn bordered by hornblende when in contact with plagioclase. This is interpreted by Henry (1938) as further reaction of cummingtonite and plagioclase producing hornblende. Clinopyroxene^{is} altered to actinolite which is also rimmed by hornblende. Specifically, this study will be focused on detailed petrographic and chemical relationships between original pyroxenes and replacing amphiboles, primary and secondary^a amphibole, and among coexisting secondary amphiboles themselves. The most interesting feature is the coexisting actinolite and hornblende. Rather special interest attaches to the development of hornblende zones between cummingtonite and plagioclase which will be discussed in some detail in terms of their compositional controls.

4.2 DETAILED PETROGRAPHIC RELATIONSHIPS BETWEEN PYROXENES AND REPLACING AMPHIBOLES AND AMONG COEXISTING AMPHIBOLES

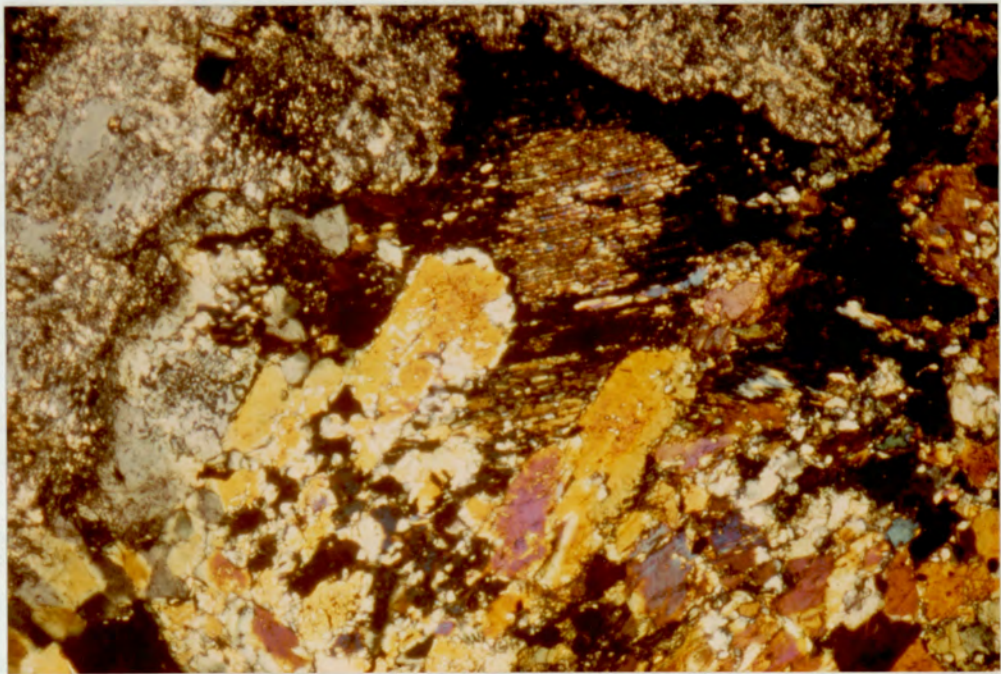
4.2.1 Glen Scaddle area

The only primary pyroxene still preserved in some thin sections as unstable relict mantled and partly replaced by amphibole is

clinopyroxene. In general, it occurs as individual grains or clusters of medium to coarse-grained, stumpy crystals with well-developed {100} parting. Clinopyroxene always contains small ilmenite plates exsolved along {100} planes. Twinning is also a common feature in clinopyroxene.

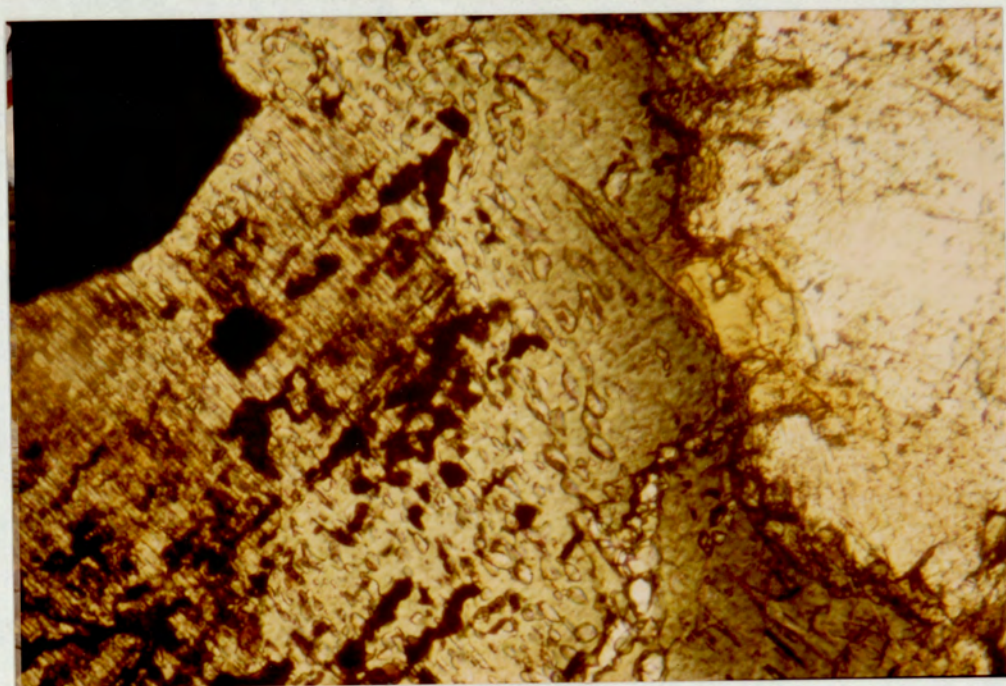
In quartz-biotite norite (specimens 610 C, 651 C), pyroxene grains are finer than those in metagabbro and are well preserved. There are only very narrow zones of green amphibole developed along the margins. Cummingtonite also occurs in these rocks as a acicular or fibrous aggregates pseudomorphing small, short prismatic shapes which appear to be inherited from the pre-existing orthopyroxene. Cummingtonite has unusually low birefringence. It is bordered by thin bluish-green hornblende zones when in contact with plagioclase.

In meta-gabbroic rocks, pyroxene is generally preserved as irregular grains being replaced along margins and cleavages by colourless to pale green, high birefringence actinolite. Both original pyroxene relicts and replacing actinolite are surrounded by a more or less continuous zone of green to bluish-green hornblende, blue green (γ), green (β) and light green (α), against plagioclase. At the initial stage of the pseudomorph or when most of the pyroxene grains still survive, actinolite forms single grains showing optical continuity or sharing crystallographic axes with edging hornblende (Fig 4.1). In this case, contacts between actinolite and hornblende are usually sharply defined by abrupt changes in colour and birefringence. Diffuse and gradational contacts may also be observed (Fig 4.2). Universal stage measurements indicate that b and c crystallographic axes of relict pyroxene and alteration amphiboles are in alignment.



0.20 mm.

Fig 4.1 Relict clinopyroxene (cpx) with single actinolite and hornblende zones in optical continuity. In the lower part of the photograph, pyroxene is completely replaced by actinolite aggregates (specimen no. 604 C).

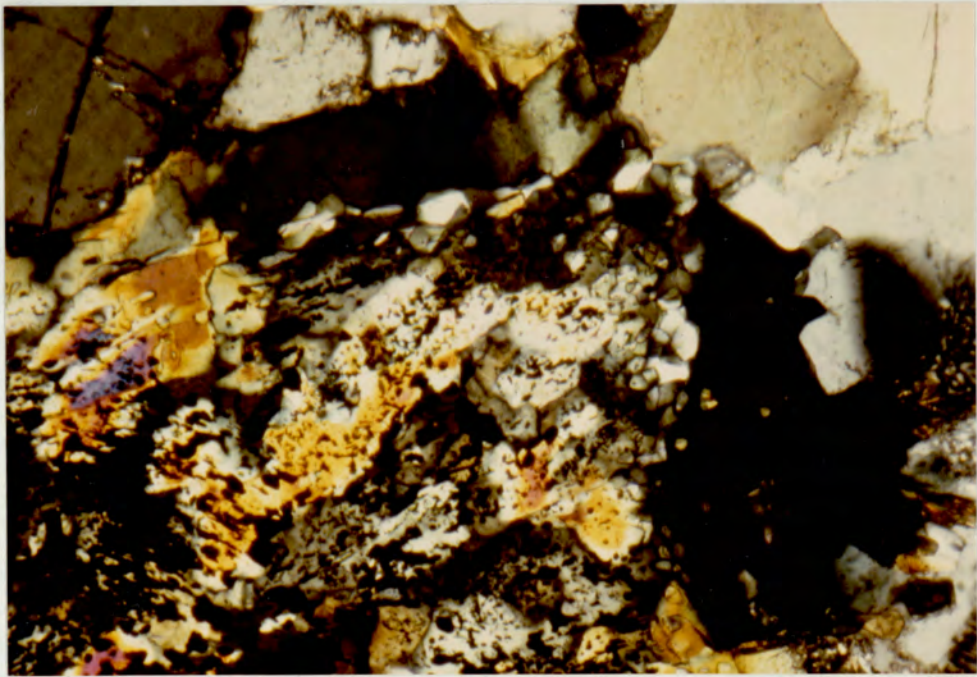
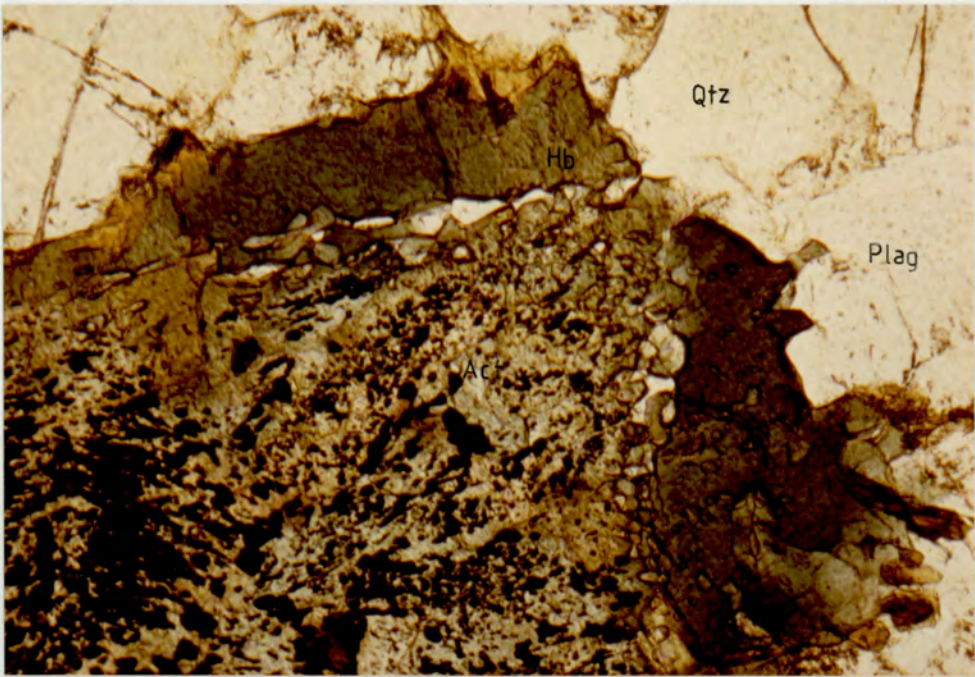


0.05 mm.

Fig 4.2 Gradational contact between actinolite and hornblende. Actinolite contains relict pyroxenes with ilmenite inclusions. There are quartz blebs in actinolite (specimen no. 603 C).

Replacement of pyroxene by actinolite occurs in various degrees, even within the same grain of pyroxene. Sometimes, one side of pyroxene is completely pseudomorphed by actinolite aggregates while the other side is still fresh showing sharp, regular contact with fringing bluish-green hornblende. Usually, the transformation begins along the outer parts of pyroxene and works progressively inwards. However, it is not necessary that the edges of pyroxene have to be completely occupied before the conversion grows further. Occasionally, a relict of edging pyroxene still survives as strings or blebs while the inner part is almost entirely occupied by actinolite. Associated with the bulk replacement along pyroxene margins is the simultaneous alteration along (010) planes of pyroxene. In some cases, when pyroxene is converted to actinolite solely by this mechanism, replacing actinolite forms closely packed aggregates of oriented, long fibres and pyroxene relicts remain as long, straight threads parallel to these fibres.

At later stage, when pyroxene disappears, actinolite sometimes becomes an aggregate of fibrous or disoriented short, prismatic crystals, but sometimes still remains as a single grain. Contacts between surrounding hornblende and actinolite aggregates are sharp in all cases; they may be marked by inclusions of quartz blebs. Many characteristics of original pyroxene are still discerned in actinolite pseudomorphs, but have never been found in enclosing hornblende. The patterns of oriented opaque inclusions in original pyroxene are well-preserved, even though actinolite is in fibrous or multi-disoriented forms. At later stages, these opaque inclusions are redistributed into individual grains of actinolite (Fig 4.3). Twinning, both simple and multiple, is occasionally seen in a single replacing actinolite, which



0.10 mm.

Fig 4.3 Actinolite aggregate pseudomorphing clinopyroxene. In this example the opaque inclusions form different patterns in different parts of the aggregate (specimen no. 656 C). Hornblende does not develop at the actinolite-quartz contact.

continues to rimming hornblendes. Texturally, it is suggested that pyroxene is replaced only by actinolite and contacts between actinolite and hornblende probably represent original pyroxene plagioclase boundaries. Primary deep greenish-brown hornblende often dusty with acicular opaque inclusions, previously developed in pyroxene, is still conserved as patches in actinolite (Fig 2.2). Most of the actinolite pseudomorphs are ragged with numerous blebs of quartz inclusions, which are occasionally developed in edging hornblende. The enclosing green to bluish-green hornblende are commonly clean forming continuity optically and in colour around actinolite cores, or composed partly of multiple rhomb-like crystals with corners growing towards plagioclase.

In specimen 602C, coarse pyroxene is embedded in big, homogeneous grains of deep greenish-brown hornblende which grades into deep-green hornblende at the margins. Pyroxene itself is partly or wholly converted into actinolite (Fig 2.3) like those described previously. This rock is fresh and the deep greenish-brown hornblende, which sometimes occurs as blebs in pyroxene, is considered to be a primary mineral.

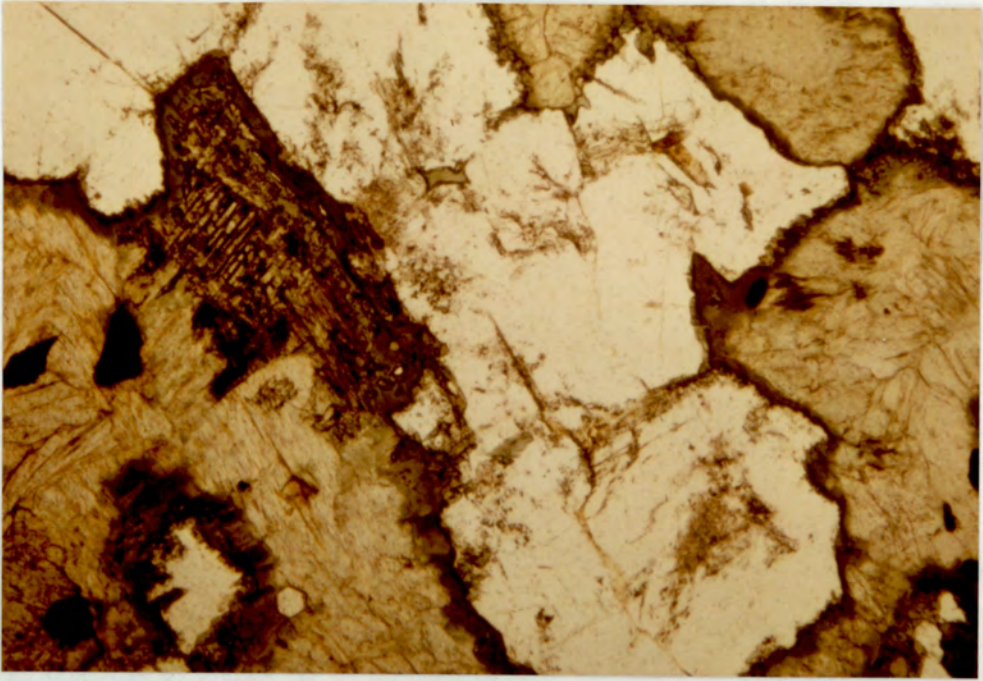
4.2.2 Morven-Cabrach area

The most characteristic feature of the Morven-Cabrach meta-noritic rocks is the alteration of orthopyroxene to fibrous aggregates of colourless cummingtonite which is in turn fringed by bluish-green or blue hornblende. Clinopyroxene, which is a minor constituent or absent in most of the rocks, has also undergone "uralitization". Orthopyroxene is always more easily altered to amphibole than clinopyroxene. In some specimens (722 C, 724 C), there are only

small remnants of remaining orthopyroxene while clinopyroxene, next to it, is entirely unaffected. Generally clinopyroxene is either unaltered or marginally replaced by pale green actinolite set next to cummingtonite aggregates. Complete replacement of clinopyroxene by actinolite has never been observed. Both actinolite containing pyroxene relics and associated cummingtonite aggregates are enveloped by a continuous zone of bluish-green hornblende (Fig 4.4).

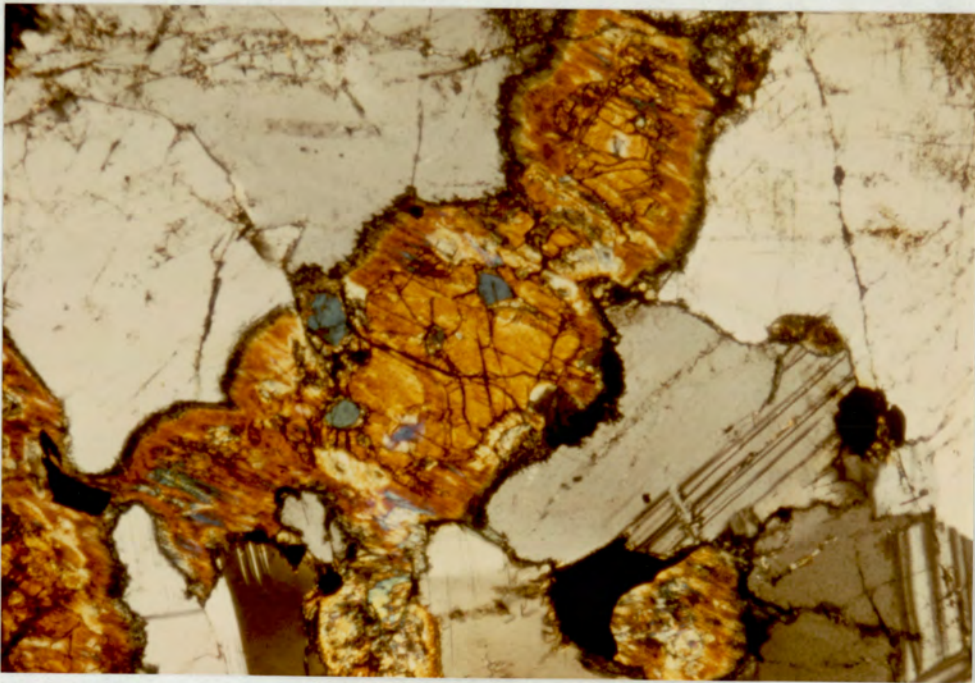
Orthopyroxene contains 2 sets of extremely thin, small rectangular plates of reddish brown inclusions, lying parallel to (100) and (210) planes. Orthopyroxene shows strong pleochroism from pale green to pale pink. In some noritic rocks (70 P, 636 C, 745 C and 746 C), orthopyroxene displays a characteristic development of broad and blebby clinopyroxene exsolution approximately parallel to (001) plane, indicating that these orthopyroxenes are inverted pigeonites. In the other specimens, exsolution of clinopyroxene was not found.

At the initial stage of uralitization, orthopyroxene is marginally frayed by replacing disoriented fibres of cummingtonite which is also developed, but in much lesser extent, as small blebs along cleavages and cracks of orthopyroxene. Cummingtonite gradually grows inward at more or less constant rates around original pyroxene. So the orthopyroxene relicts generally remain as their original shapes set in the middle of cummingtonite pseudomorphs. Eventually, this mineral is completely replaced by very fine-grained, disoriented fibrous cummingtonite aggregates. At this stage, the oriented opaque inclusions in orthopyroxene are still well-preserved or form a dust of very fine grains in cummingtonite.



0.25 mm.

Fig 4.4a Relict clinopyroxene is still present while cummingtonite is recrystallised to coarser, more perfect forms. (specimen 757 C).

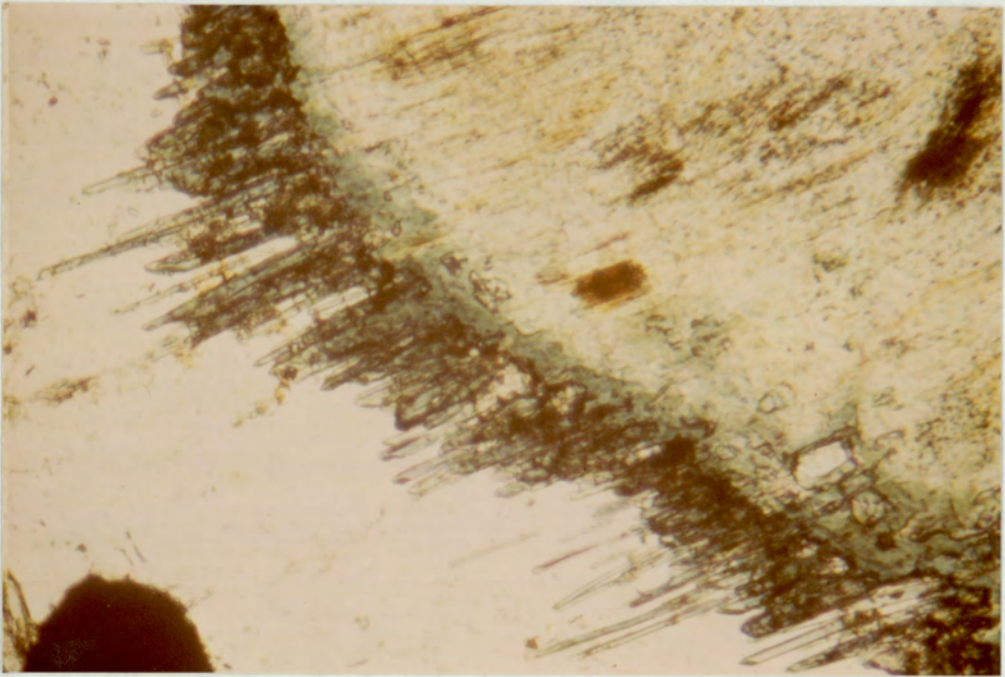


0.50 mm.

Fig 4.4b Relict orthopyroxene with blebby clinopyroxene exsolution, replaced by cummingtonite. (specimen 746 C).

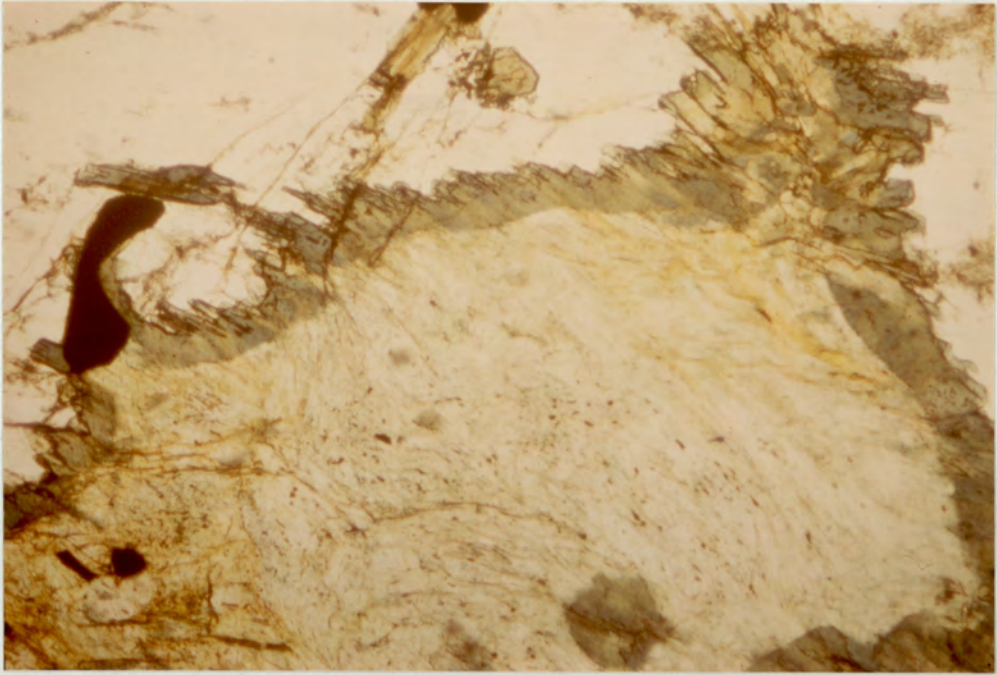
Pre-existing, coarse exsolution clinopyroxene in original pyroxene is now represented by blebs or patches of pale-green actinolite.

Cummingtonite pseudomorphs, with or without orthopyroxene cores, are always rimmed by bluish-green hornblende zones against plagioclase. Contacts between cummingtonite and hornblende are very sharp and remarkably parallel to the outlines of orthopyroxene relicts. This zone occurs only along cummingtonite/plagioclase contacts and has never been found along orthopyroxene/plagioclase boundaries even within the same orthopyroxene grains. Specimen 77 P, in which most orthopyroxenes is fresh, shows clear evidence of its development. This strongly indicates that the formation of enclosing hornblende occurs simultaneously with or soon after, but never before the development of cummingtonite. Where most orthopyroxene is still well-preserved or only small areas of cummingtonite occur, this zone is very narrow and composed of acicular grains of deep-bluish green hornblende lancing towards plagioclase. (Fig 4.5). As cummingtonite grows further, these acicular grains become coarser and develop further into plagioclase, but never lose their sharp and parallel contacts with cummingtonite. Sometimes, the fringing hornblende occurs as an optically continuous zone around cummingtonite and loses its rough contacts with plagioclase. In this case, contacts between plagioclase and hornblende are smooth and parallel to cummingtonite-hornblende contacts. When orthopyroxene is completely replaced, fibrous cummingtonite recrystallises to coarser, more perfect prismatic forms of disoriented aggregates. The fine-dusted oxide inclusions disappear, probably being resorbed into the recrystallised cummingtonite. The enclosing acicular hornblende becomes coarser forming radial prismatic crystals around cummingtonite cores (Fig 4.6). Sometimes



0.05 mm.

Fig 4.5 Acicular grains of hornblende lancing toward plagioclase.
Part of hornblende also grows into cummingtonite.
(specimen 725 C).



0.25 mm.

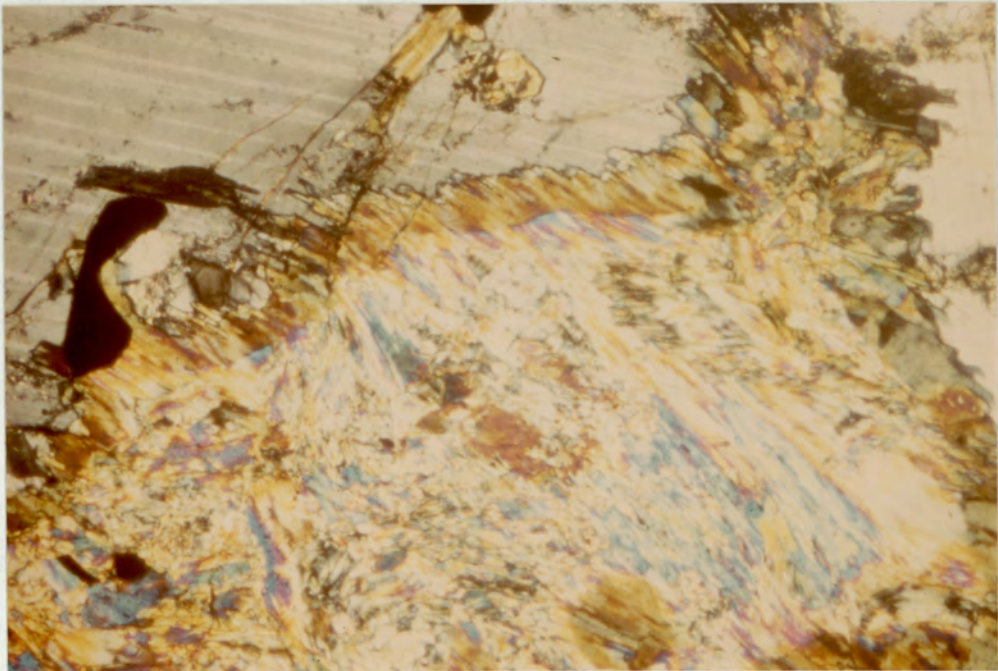
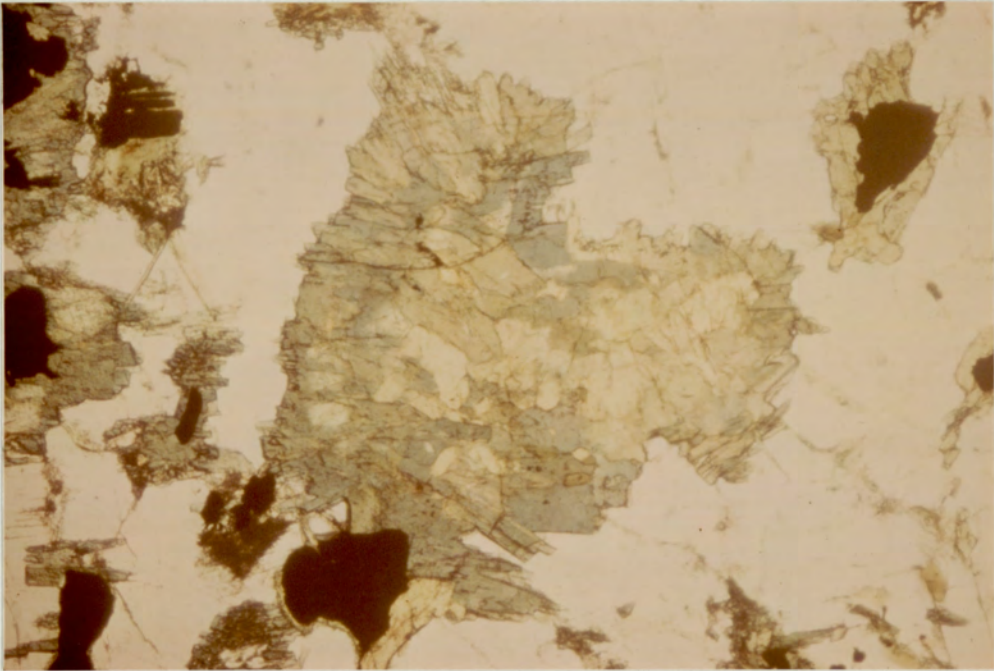


Fig 4.6 Aggregate of cummingtonite with sharp contact with hornblende. The bleb of hornblende inside cummingtonite was previously plagioclase which is now completely replaced by hornblende (specimen 67 P).

they share the same prismatic grains showing sharp contact and optical continuity (Fig 4.6). Some prismatic hornblende grains grow into cummingtonite at this stage. Patches of green hornblende also developed in cummingtonite aggregates. Finally, the whole cummingtonite aggregate recrystallises into an aggregate of interlocking bluish-green hornblende prismatic crystals (Fig 4.7) showing irregular contact with surrounding plagioclase.

Unfortunately, the fibrous and aggregate habit of cummingtonite and thinness of fringing hornblende caused difficulty in measuring orientation relationships between these minerals and relict pyroxene. However, optical continuity between these three minerals is noticed. In specimens 62 P and 84 P, in which some cummingtonites lose their aggregate habit and rimming hornblende is quite homogeneous, the universal stage observations indicate that they share the b and c crystallographic axes. Sometimes, (110) cleavages can be traced between the two amphiboles.

Primary olive-green to brownish green hornblende occurs as discrete grains, along pyroxene and plagioclase boundaries or forming poikilitic texture, enclosing pyroxene. In some specimens (757 C, 758 C) hornblendes are dusted with very tiny acicular opaque inclusions accompanied by some coarse apatite grains. Sometimes, these opaque inclusions are so dense as to make hornblendes look like opaque minerals under the microscope. Embedded as cores in these hornblendes are aggregates which are composed mainly of short, coarse prismatic grains of cummingtonite and less commonly of green hornblende. These rocks perhaps have undergone nearly the last stage of "uralitization" since cummingtonites are coarse grained and being partly replaced by green hornblende. Numerous



0.25 mm.

Fig 4.7 Interlocking grains of hornblende completely replacing cummingtonite (specimen 67 P).

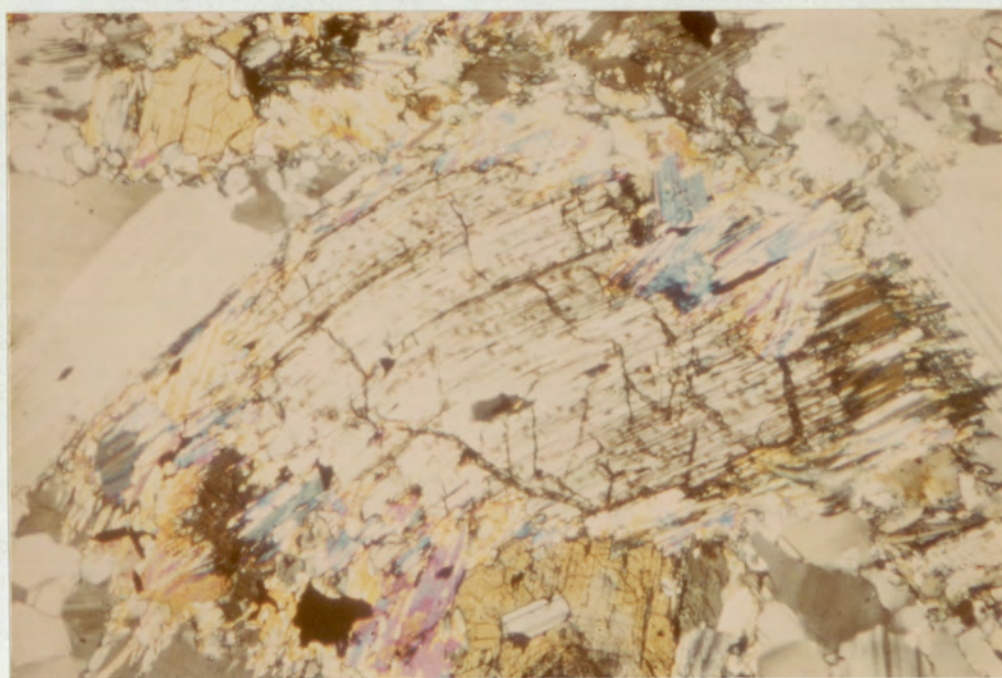
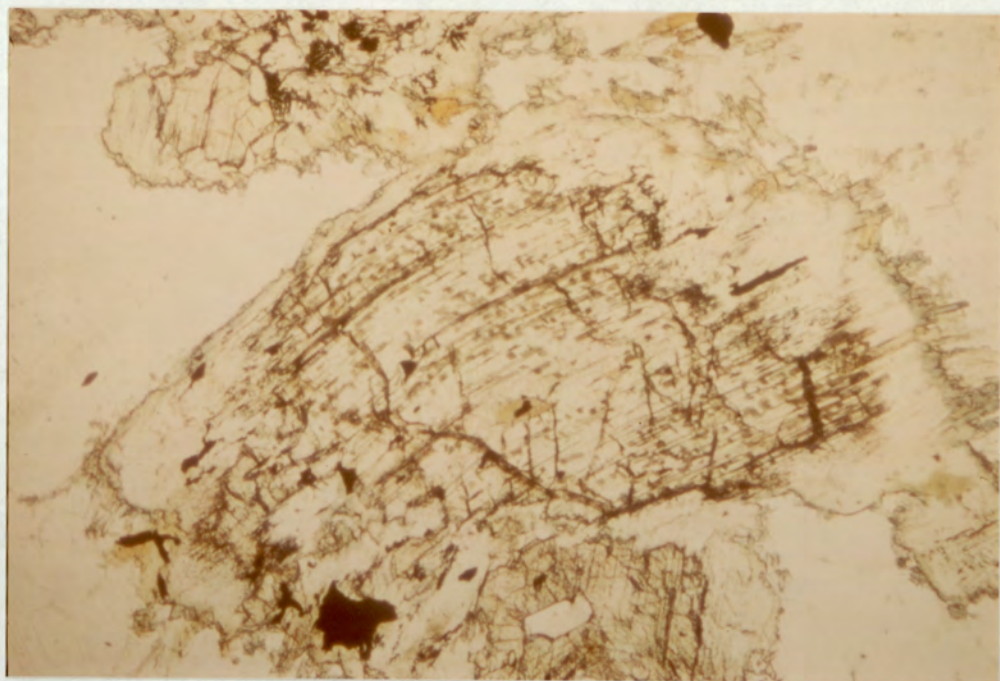
opaque inclusions in hornblende are thought to have been exsolved from magmatic brown hornblende during cooling, while pyroxene cores are being replaced by cummingtonite.

4.2.3 Belhelvie area

Noritic and gabbroic rocks of the Belhelvie intrusion display a marked mineralogical similarity in "uralitization" to the rocks from the Morven-Cabrach mass. Despite the similarity in uralitization process, the Belhelvie rocks are highly deformed especially in the Balmedie Quarry from which most of the specimens come.

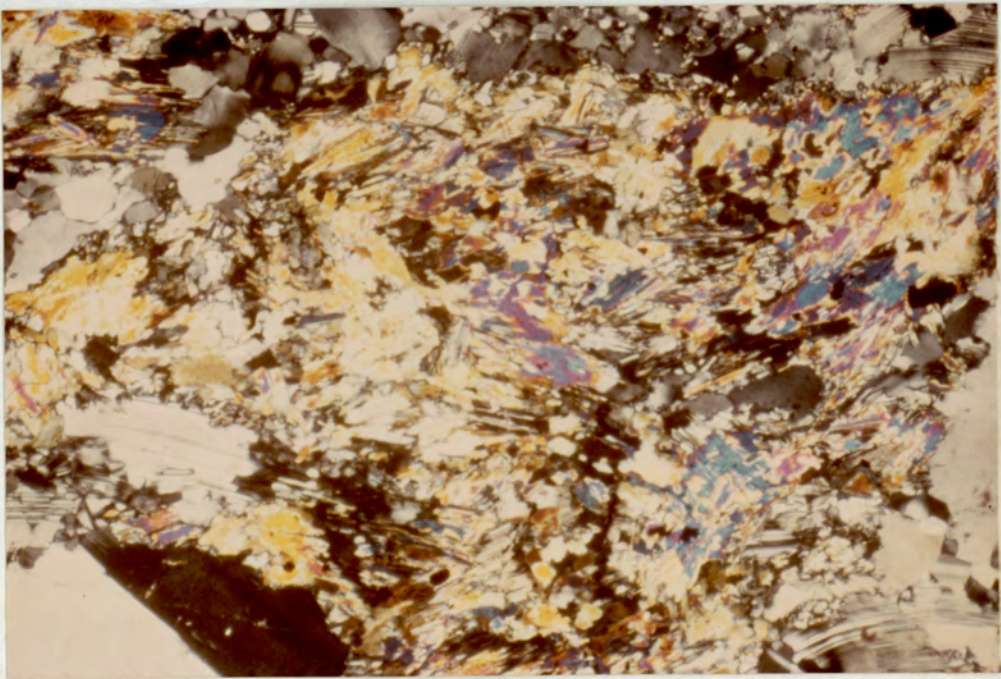
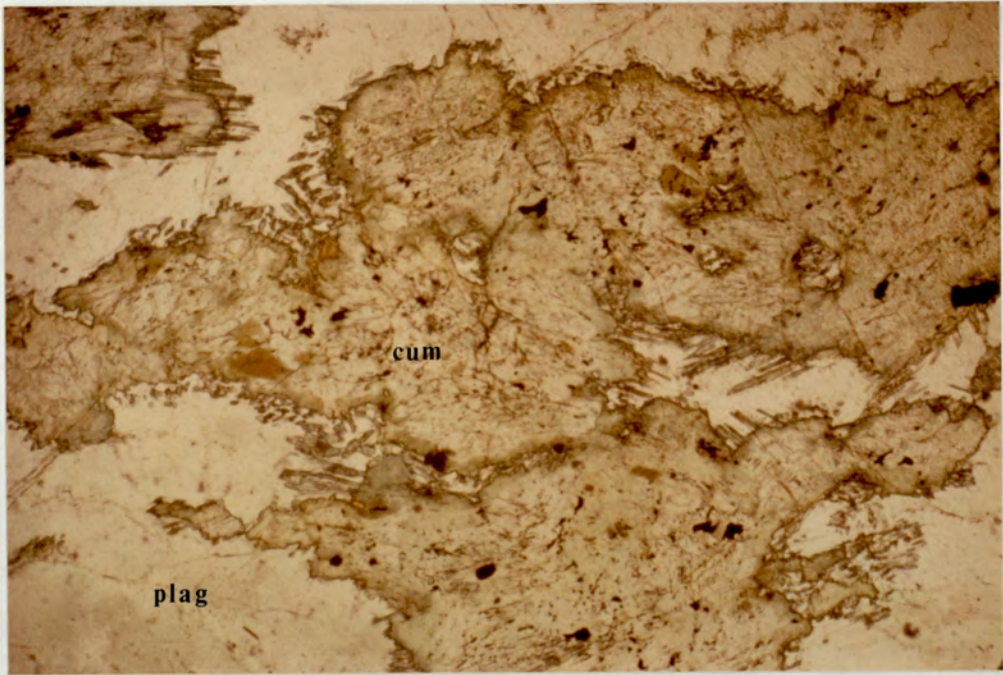
In the least altered rocks, both orthopyroxene and clinopyroxene are present in variable proportions, even within a short distance. Generally the former is dominant. Orthopyroxene contains as inclusions small, rectangular, brown transparent plates like those described in the Morven-Cabrach mass, (Fig 4.8). Clinopyroxene is sometimes surrounded by primary big grains of homogeneous brown hornblende. Once again orthopyroxene is more sensitive to alteration than clinopyroxene which still survives even in rocks that have undergone almost complete amphibolitization. (e.g. specimen 32 P, 33 P).

Although it is obvious that development of amphiboles from pyroxenes generally becomes more pronounced as the dynamic metamorphism becomes more advanced, uralitization can not be invariably related to deformation, since undeformed rocks from elsewhere in this mass^{are} also affected by uralitization (e.g. specimen 52 P). Moreover, the evidence can be demonstrated clearly in specimens 10 P and 19 P from the Balmedie Quarry. Both rocks display mortar texture (a largely unaltered primary mineral surrounded by finely granular



0.50 mm.

Fig 4.8 Bent orthopyroxene containing opaque inclusions, replaced along grain boundaries by cummingtonite aggregates rimmed by thin hornblende (specimen 17 P).



0.50 mm.

Fig 4.9 Complete pseudomorphing of orthopyroxene by cummingtonite aggregates. A thin zone of rimming hornblende also grows as acicular grains into plagioclase groundmass. (specimen 17 P).

material) which is an initial stage of shearing. In specimen 10 P, orthopyroxene is completely replaced by cummingtonite aggregates forming porphyroclasts and only a few grains of clinopyroxene are preserved, while in specimen 19 P which is slightly foliated, there are only slight alterations of orthopyroxene and clinopyroxene. This observation suggests that replacement of pyroxene by amphibole in some rocks is nearly completed before the deformation occurs while in other rocks this process has just started. This effect can be seen over short distances. However, replacements of cummingtonite and actinolite by hornblende are strongly related to shearing. With further shearing, hornblende becomes dominant and forms small equigranular texture, sometimes foliated, while cummingtonite and actinolite are completely replaced.

Typically the contact between plagioclase and the thin zone of enveloping hornblende around cummingtonite aggregates is very irregular, flame or worm-like hornblende growing into plagioclase, while cummingtonite/hornblende contacts are smooth parallel to the outline of orthopyroxene relics, (Fig 4.9). Primary brown hornblendes usually remain as patches in cummingtonite aggregates.

4.3 ESTIMATION OF Fe³⁺ IN AMPHIBOLE ANALYSES BY MÖSSBAUER SPECTROSCOPY

One of the obvious problems in comparing analyses of coexisting amphiboles is the lack of a direct method for the determination of Fe³⁺ using electron-probe micro-analysis. There have been a number of methods devised to determine the amount of Fe³⁺ in amphiboles, although none of them can solve the problem with certainty. These methods include wet chemical analysis (Hietanen

1974, Grapes et. al. 1977); Mössbauer spectroscopy (Bancroft et. al. 1967, Burns and Greaves 1971, Bancroft and Brown 1975 and Goldman 1979) and the recalculation method. (Stout 1972 , Papike et. al. 1974 and Neumann, 1976).

In this study, the pegmatite vein containing coarse amphibole crystals (specimen 78 P) in the Morven-Cabrach intrusion provides a good opportunity to estimate the amount of Fe^{3+} in the studied hornblendes by the Mössbauer spectroscopy method. This is the type of pegmatite described by Henry (1938) as associated with "end-stage alteration" of the norites. Therefore this rock-type is relevant to the present study; it is also easy to separate the hornblende cleanly from the coarse-grained rock: part of a single crystal of hornblende was sawn from the specimen and then crushed. Under the microscope, the hornblende is fresh and mostly clean with a very small quantity of opaque inclusions. Most of the hornblende is homogeneous and a greenish brown colour which grades into green at the edges. Electron probe microanalyses also indicate a homogeneous composition in the brown areas (Table 4.1). There is a slight increase in Al, Mg and Ca with a slight decrease in Si and Ti towards the green edges. (analysis 2, Table 4.1).

Experimental Method

Measurement of the Mössbauer spectrum was made at room temperature on a sample prepared as a powder disc containing 200 milligrams of pure, fresh hornblende. The source of γ -rays for the experiment was ^{57}Co in a palladium matrix and the vibrator and detector systems employed were designed by the Harwell Group. The spectrum was accumulated in 512 channels of an Ino-Tech 5200 multichannel analyser and run for about 4 days. The spectrometer was calibrated

TABLE 4.1 Electron probe microanalysis of the amphibole used in Mössbauer work.

Analysis 1 is brown hornblende and analysis 2 is green hornblende at the margin. Comparison between Fe as Total Fe (1.1), recalculation method after Stout giving minimum Fe³⁺ (1.2) and maximum Fe³⁺ (1.3) Fe³⁺ in 2 is Stout minimum.

SPECIMEN		78 P			
NO.		FERRO-EDENITIC HB			FERRO-TSCHERMALITIC HORNBLLENDE
ANALYSIS NO.	1.1	1.2	1.3	2	
Na ₂ O	1.43	1.43	1.43	1.25	
MgO	8.53	8.53	8.53	7.21	
Al ₂ O ₃	10.18	10.18	10.18	12.59	
SiO ₂	42.87	42.87	42.87	41.52	
K ₂ O	0.45	0.45	0.45	0.54	
CaO	9.80	9.80	9.80	11.09	
TiO ₂	1.68	1.68	1.68	0.64	
MnO	0.40	0.40	0.40	0.30	
Fe ₂ O ₃	-	0.27	11.89	2.09	
FeO	21.19	20.95	10.49	18.60	
H ₂ O*	1.94	1.94	1.94	1.93	
Total	98.47	98.50	99.66	97.76	
Si	6.61	6.61	6.42	6.43	
Aliv	1.39	1.39	1.58	1.57	
	8.00	8.00	8.00	8.00	
Alvi	0.46	0.45	0.21	0.72	
Ti	0.19	0.19	0.18	0.08	
Fe ³⁺	-	0.03	1.34	0.24	
Mg	1.96	1.96	1.90	1.66	
Fe ²⁺	2.73	2.70	1.31	2.41	
Mn	0.05	0.05	0.05	0.04	
	5.39	5.38	4.99	5.15	
Na	0.43	0.43	0.42	0.38	
Ca	1.62	1.62	1.57	1.84	
K	0.09	0.09	0.09	0.11	
	2.14	2.14	2.08	2.33	
100 Mg Mg + Fe ²⁺ **	41.8	42.1	59.2	40.8	

* H₂O calculated from ideal formula

** Fe = Fe Total

using Fe foil. The spectrum was fitted using a computer programme originally written by A.J. Stone and following methods described in Bancroft (1973). Four doublets, three arising from ferrous iron in octahedral coordination and one from octahedral ferric iron were fitted to the spectrum.

Results

The Mössbauer spectrum of the hornblende is shown in Figure 4.10 and the spectral parameters are listed in Table 4.2. The un-equal areas of peaks A and A' may be caused by a non-random orientation of grains in the powder. The peaks in the hornblende spectrum can be readily assigned following the work of previous authors (e.g. Burns and Greaves 1971, Bancroft and Brown 1975, Goldman 1979 and Thomas 1982):- peaks A and A', B and B', C and C' to Fe²⁺ in the M₁, M₃ and M₂ position respectively and peaks D and D' to Fe³⁺ in these three positions, although Fe³⁺ is known to be predominantly in M₂ position. Theoretically, the half-widths of all doublets should be equal, but a fit could not be obtained for the present data under that constraint.

The relationships between the area ratios and atomic ratios of Fe³⁺/(Fe³⁺ + Fe²⁺) can be expressed as:-

$$\frac{A_{Fe^{3+}}}{A_{Fe^{2+}}} = C \frac{N_{Fe^{3+}}}{N_{Fe^{2+}}} \quad (\text{Bancroft, 1973})$$

where A is Mössbauer absorption peak area and N is the number of Fe atoms per formula unit.

$$C = \frac{T_{Fe^{3+}} G (X_{Fe^{2+}}) f_{Fe^{2+}}}{T_{Fe^{2+}} G (X_{Fe^{2+}}) f_{Fe^{2+}}}$$

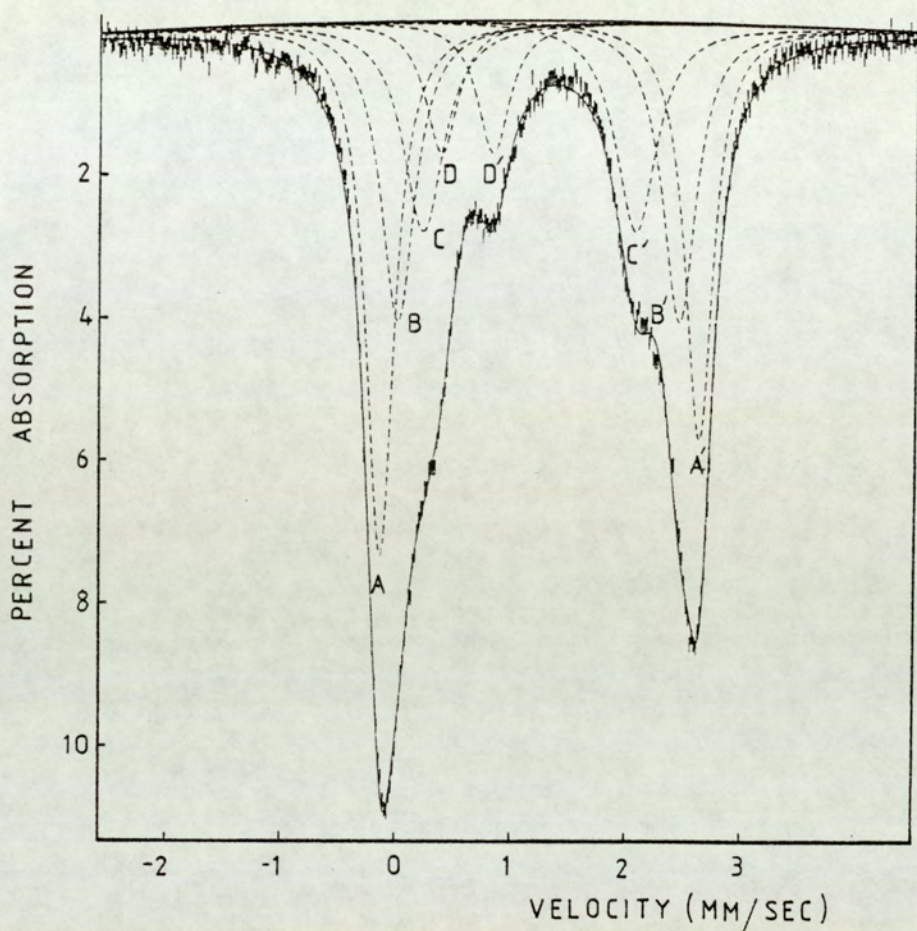


Fig 4.10 Mössbauer spectrum of hornblende with computer-fitted peaks.

TABLE 4.2 Mössbauer Parameters - Hornblende specimen 78 P.

PEAKS AA' (M_1)			PEAKS BB' (M_3)			PEAKS CC' (M_2)			PEAKS DD' (Fe^{3+})		
I.S	Q.S	H.W	I.S	Q.S	H.W	I.S	Q.S	H.W	I.S	Q.S	H.W
mms ⁻¹			mms ⁻¹			mms ⁻¹			mms ⁻¹		
1.23	2.84	0.30	1.22	2.51	0.36	1.14	1.89	0.44	0.59	0.46	0.35

I.S = Isomer Shift (relative to the centre of gravity of an iron foil spectrum as zero)

Q.S = Quadrupole Splitting

H.W = Full width of half height

where T = full width at half height
 $G(X)$ = saturation correction
 f = recoil free fractions

Bancroft (1973) suggested that f factors in this case should be very nearly equal. The saturation effect on the derived $Fe^{3+}/(Fe^{3+} + Fe^{2+})$ ratio has been found to be very small in pure samples of 100 mg to 600 mg of amphibole (Bancroft and Brown 1975). Hence, it is reasonable to assume that the areas of the resolved Mössbauer doublets are in approximately the same proportion as the iron atoms responsible for them. According to the method described above, the $Fe^{3+}/(Fe^{2+} + Fe^{3+})$ in the study hornblende is equal to 13.8%. However, this is only semiquantitative analysis, since it has been widely suggested recently that the Mössbauer spectra of amphibole containing tetrahedral Al must be considered inaccurate due to the influence of the next-nearest-neighbour tetrahedral Al of octahedral Fe (Seifert 1977, Goldman, 1979 and Thomas, 1982). This effect will broaden the Fe^{2+} absorptions especially in M_1 and M_2 sites and reduce the intensity of the Fe^{2+} doublets. Moreover, there are also large differences in $Fe^{3+}/(Fe^{3+} + Fe^{2+})$ ratios between Mössbauer doublet areas and expected areas predicted by infrared and x-ray studies (Burns and Greaves, 1971).

The Mössbauer result, bearing in mind the uncertainties, is consistent with the wet-chemical data of Henry (1938) for two pegmatite hornblendes, giving 7.8 and 10.0% of the iron as ferric. Henry (1938) also separated a hornblende from a rock where it has replaced pyroxenes and quoted 8.1% of the iron as ferric. His analyses are consistent with the present work in other respects. In summary, it is suggested that roughly 10% of the iron in the hornblende is ferric.

4.4 MINERAL COMPOSITIONS

In selected specimens, pyroxene, amphibole, plagioclase and a few grains of epidote were analysed by EPMA. The analytical method was carried out in the same conditions as previously described in Chapter 3. Twelve specimens from the Glen Scaddle intrusion, fourteen specimens from the Morven-Cabrach intrusion and four specimens from the Belhelvie mass were studied. Their specimen numbers and localities are listed in Appendix 1.

Amphibole analyses have been recalculated utilizing chemical and stoichiometric constraints to estimate the Fe^{3+} amounts after Stout (1972). Two recalculations can be made based on different assumptions:- based on 15 cations excluding Na and K by assigning all Na to the A site giving the maximum amount of Fe^{3+} , and based on 13 cations excluding Ca, Na and K by providing the maximum amount of Na enters the M_4 site yielding the minimum amount of Fe^{3+} consistent with stoichiometry. Using the hornblende analyses in the Mössbauer specimen (78 P), in order to compare these two assumptions with the Mössbauer result, it is found that the recalculation giving minimum Fe^{3+} value (analysis 1.2 Table 4.1) is best suited for the hornblende studied here, since the result is closer to the value determined by Mössbauer than is the maximum Fe^{3+} value of 50% approximately (analysis 1.3 Table 4.1). This method is also suggested by Stout (1972) in dealing with metamorphic amphibole and it has been used in some of the literature. The Mössbauer result is not applicable to actinolite or cummingtonite. For the purpose of this study, the minimum Fe^{3+} recalculation will be tabulated for actinolite and hornblende throughout. Actinolite typically shows somewhat less Fe^{3+} than hornblende.

Analyses of cummingtonite show zero value of Fe^{3+} in this calculation. This is in agreement with Klein (1968) and Stout (1972). Mössbauer study of the cummingtonite-grunerite series also indicated that there is no Fe^{3+} in their crystal structures (Bancroft et. al. 1967) or they contain only one percent of Fe^{3+} (Hafner and Ghose, 1971). The cummingtonite analyses, then are treated as if containing no ferric ion. The "Stout minimum" Fe^{3+} ranges up to about 30% in some hornblendes, which are suspected to be too high on the basis of the Mössbauer work and literature data for comparable assemblages. The Stout recalculation is sensitive to error in the analytical data. All amphibole analyses are classified after Leake (1978). For convenience in comparing the compositions of relict pyroxene, replacing amphibole and rimming amphibole, their analyses across the grains are presented in the same tables. Table 4.3 to 4.27 give selected mineral analyses. Further analyses are tabulated in Appendix 2. In all cases, for pyroxenes and amphiboles, analyses are tabulated in order from core to edge of grain or aggregate.

4.4.1 Glen Scaddle intrusion

The analyses listed in Tables 4.3 - 4.9 have been selected from 9 specimens as representative of 46 amphibole grains (across actinolite core and rimming hornblende), some containing relict clinopyroxenes, from 12 specimens. Figs 4.11 and 4.12 show typical traverses, with a slight compositional break or discontinuity between actinolite and hornblende. The table headings indicate the two point analyses between which this break occurs. Table 4.10 shows analyses of clinopyroxene, pseudomorphous actinolite and primary brown hornblende in specimen 602 C. Table 4.11 is

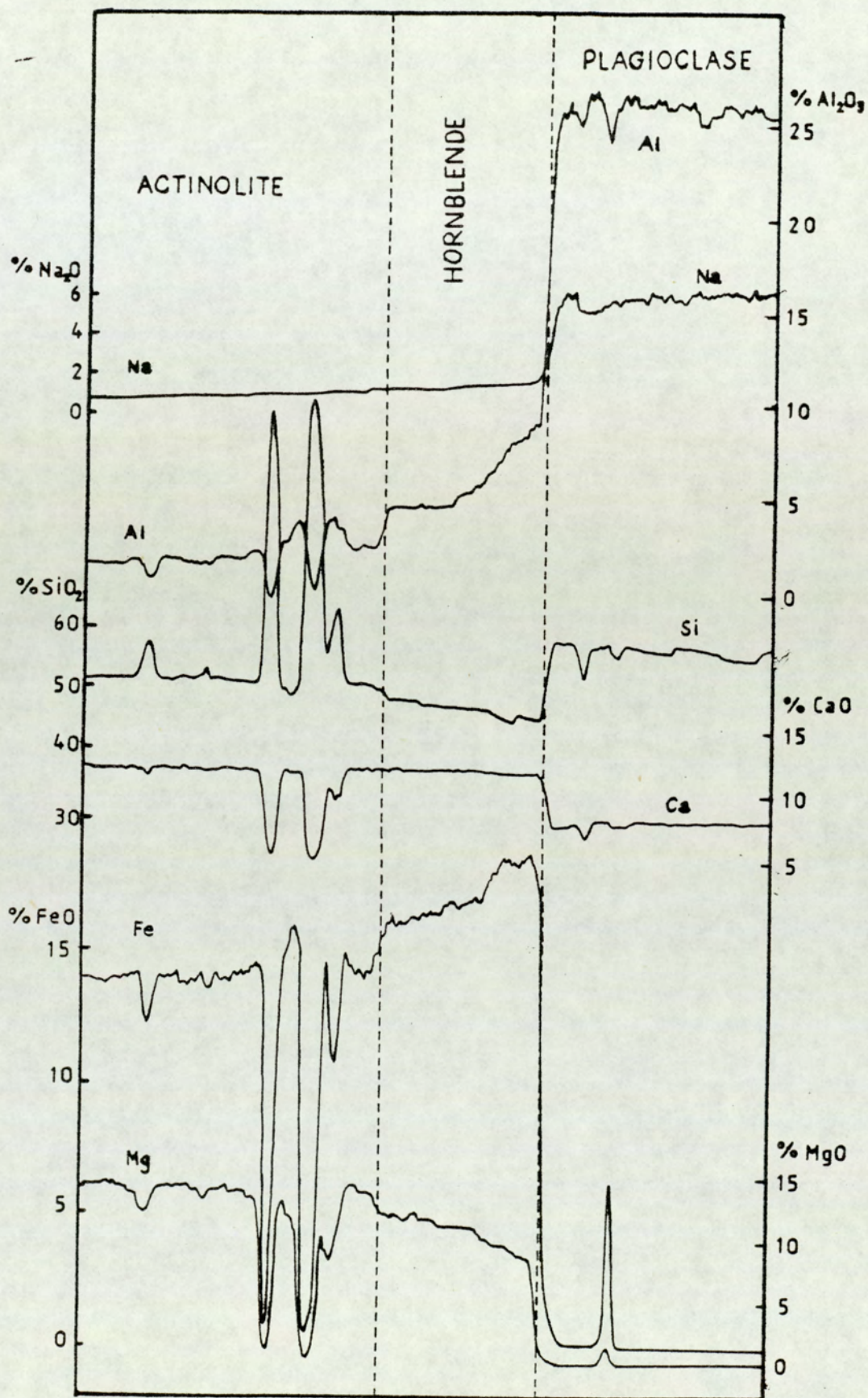


Fig 4.11 Electron probe line scan across actinolite and rimming hornblende in specimen 603 C. Line length 340 μ m. Actinolite has quartz inclusions.

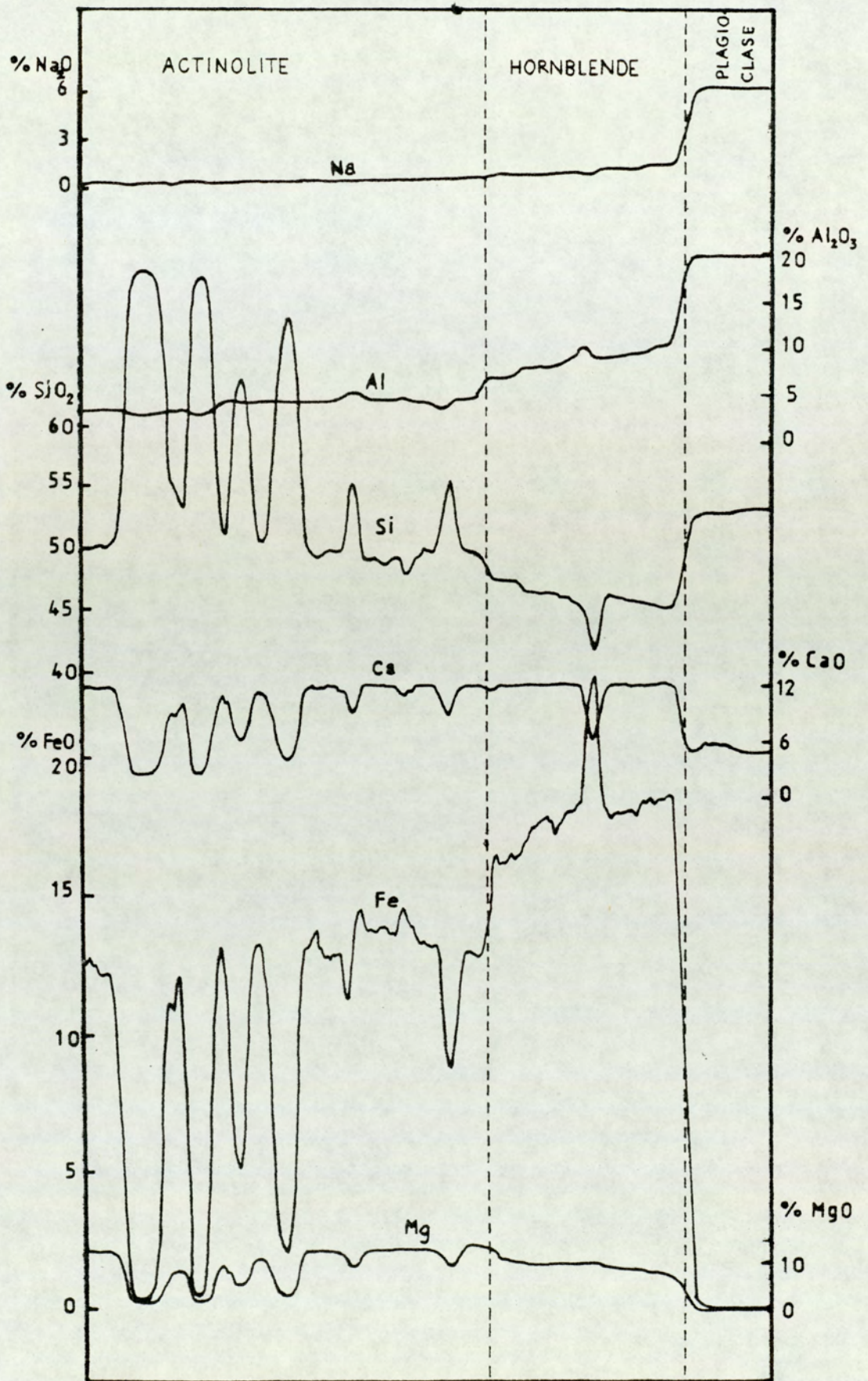


Fig 4.12 Electron probe line-scan in specimen 652 C. Line length 270 μ m. Actinolite contains quartz inclusions.

analyses of cummingtonite and rimming bluish-green hornblende of specimen 601 C.

Clinopyroxene

Average clinopyroxene in the Glen Scaddle intrusion is classified as salite of average composition $Wo_{48} En_{34} Fs_{18}$. No zoning was detected. Some selected analyses are presented in Table 4.4, analyses 1 and 5; Table 4.6, analyses 1 and 5; Table 4.6, analysis 6, Table 4.8, analysis 6 and Table 4.9 analysis 1. They show that there is only very slight variation in clinopyroxene compositions. The salite contains small amounts of Al which is generally more Al^{iv} than Al^{vi} , and very small amounts of Na, Mn and Ti. It is found that there is no compositional difference between the least altered pyroxene (specimen 601 C) and those with only small patches or blebs preserved.

Actinolite

Many analyses were made across actinolite grains from blebs or lamellae inside relict pyroxene (where analysible) through the contact with hornblende. Tables 4.3 - 4.9 show some representative analyses of actinolite compared with their primary pyroxene and co-existing hornblende. Apart from a large decrease in CaO and increase in MgO between pyroxene and actinolite, there is only slight increase in FeO and SiO_2 while Al_2O_3 seems to be inherited from the pseudomorphed pyroxene. $100 Mg^{2+}/(Mg^{2+} + Fe^{total})$ ratios in actinolite are very similar to relict pyroxene.

Actinolite is continuously zoned (Figs. 4.11, 4.12) with similarity in all analyses. There are slight decreases in MgO and SiO_2 with simultaneous slight increases in FeO, Al_2O_3 , Na_2O , K_2O and TiO_2

TABLE 4.3 Electron probe microanalysis of traverse across actinolite and hornblende of specimen 685 C. Oxides in weight %, number of atoms per formula unit calculated on the basis of 23 (0) anhydrous. A compositional break occurs between points 3 and 4.

SPECIMEN		685 C				
NO.						
ANALYSIS						
NO.	1	2	3	4	5	
MINERAL	ACTINOLITE	ACTINOLITE	ACTINOLITE	MAGNESIO- HORNBLLENDE	MAGNESIO- HORNBLLENDE	
Na ₂ O	0.28	0.35	0.39	0.78	0.93	
MgO	16.71	15.97	15.86	13.03	12.51	
Al ₂ O ₃	2.76	3.83	4.05	8.01	8.57	
SiO ₂	52.96	51.87	51.41	46.67	45.81	
K ₂ O	0.06	0.10	0.11	0.47	0.47	
CaO	12.16	12.04	12.27	12.16	12.04	
TiO ₂	0.19	0.26	0.26	0.71	0.64	
MnO	0.29	0.27	0.25	0.25	0.25	
Fe ₂ O ₃	0.85	0.56	0.84	2.17	2.71	
FeO	10.16	10.89	10.66	11.99	12.06	
H ₂ O	2.07	2.06	2.05	2.01	1.99	
Total	98.49	98.20	98.15	98.25	97.98	
Si	7.655	7.55	7.495	6.93	6.84	
Al ^{iv}	0.345	0.45	0.505	1.07	1.16	
	8.00	8.00	8.00	8.00	8.00	
Al ^{vi}	0.13	0.21	0.19	0.34	0.36	
Ti	0.02	0.03	0.03	0.08	0.07	
Fe ³⁺	0.09	0.06	0.09	0.24	0.31	
Mg	3.60	3.47	3.44	2.89	2.79	
Fe ²⁺	1.23	1.33	1.30	1.49	1.51	
Mn	0.04	0.03	0.03	0.03	0.03	
	5.11	5.13	5.08	5.07	5.07	
Na	0.08	0.10	0.11	0.23	0.27	
Ca	1.89	1.88	1.92	1.94	1.93	
K	0.01	0.02	0.02	0.09	0.09	
	1.98	2.00	2.05	2.26	2.29	
100 Mg	73.2	71.4	71.2	62.6	60.5	
Mg + Fe*						

* Fe = Fe Total

TABLE 4.4 Electron probe microanalysis of specimen 683 C and 678 C showing compositional break in calcic amphibole between 3/4 and 7/8.

SPECIMEN NO.	683 C				678 C			
	1	2	3	4	5	6	7	8
ANALYSIS NO.	CPX	ACTINOLITE (IN CPX)	ACTINOLITE	TSCHERMAKITE HORN- BLENDE	CPX	ACTINOLITE (IN CPX)	ACTINOLITIC HORN- BLENDE	FERROAN- PARGASITIC HORN- BLENDE
Na ₂ O	0.38	0.13	0.25	0.95	0.46	0.31	0.32	1.14
MgO	14.43	17.25	17.47	10.82	13.04	17.21	15.16	7.48
Al ₂ O ₃	1.83	1.76	1.96	11.70	3.45	1.41	3.62	11.42
SiO ₂	51.72	53.67	53.56	42.85	50.92	53.50	50.62	40.03
K ₂ O	0.01	0.05	0.05	0.80	0.00	0.00	0.00	0.97
CaO	21.02	12.59	11.92	12.05	20.92	12.40	12.35	12.11
TiO ₂	0.27	0.11	0.09	0.35	0.31	0.11	0.20	0.49
MnO	0.27	0.19	0.31	0.20	0.33	0.27	0.25	0.28
Fe ₂ O ₃	-	2.55	1.70	4.82	-	3.10	5.29	6.95
FeO	8.78	9.00	9.77	12.09	10.43	9.62	10.36	15.31
H ₂ O	-	2.08	2.08	1.97	-	2.08	2.04	1.89
Total	98.71	99.38	99.16	98.60	99.86	100.01	100.21	98.07
Si	1.95	7.70	7.69	6.43	1.91	7.65	7.33	6.23
Al ^{iv}	0.05	0.30	0.31	1.57	0.09	0.24	0.61	1.77
Al ^{vi}	2.00	8.00	8.00	8.00	2.00	7.89	7.94	8.00
Ti	0.03	0.00	0.03	0.51	0.07	0.00	0.00	0.33
Fe ³⁺	0.01	0.01	0.01	0.04	0.01	0.01	0.02	0.06
Fe ²⁺	-	0.27	0.18	0.55	-	0.34	0.58	0.81
Mg	0.81	3.69	3.74	2.42	0.73	3.67	3.27	1.74
Mn	0.28	1.08	1.17	1.52	0.33	1.15	1.25	2.00
Na	0.01	0.02	0.04	0.03	0.01	0.03	0.03	0.04
Ca	5.07	5.07	5.17	5.06	5.20	5.20	5.15	4.98
K	0.03	0.04	0.07	0.28	0.03	0.09	0.09	0.34
	0.85	1.94	1.83	1.94	0.84	1.91	1.92	2.02
	0.00	0.01	0.01	0.15	0.00	0.00	0.00	0.20
	2.02	1.99	1.91	2.36	2.02	2.00	2.01	2.56
100 Mg	74.3	73.2	73.5	53.9	68.9	71.1	64.1	38.3
Mg + Fe*								

* Fe = Fe Total

TABLE 4.5 Analysis of specimen 687 C. There is a compositional break between 2/3.

ANALYSIS NO.	1				2	
	1	2	3	4*	5	6
MINERAL	ACTINO LITE	ACTINO LITE	MAGNESIO-HORNBLLENDE	MAGNESIO-HORNBLLENDE	ACTINO LITE	EDENITE
Na ₂ O	0.21	0.26	1.09	1.04	0.33	1.02
MgO	17.26	16.49	10.81	9.93	16.08	11.07
Al ₂ O ₃	1.30	1.63	9.20	8.97	2.33	8.97
SiO ₂	55.95	55.32	45.48	43.65	55.49	45.92
K ₂ O	0.02	0.08	0.77	0.81	0.05	2.03
CaO	12.49	12.51	11.98	11.64	11.82	11.85
TiO ₂	0.05	0.08	0.30	2.06	0.08	0.12
MnO	0.25	0.29	0.25	0.23	0.28	0.22
Fe ₂ O ₃	0.00	0.00	1.07	0.00	0.00	0.00
FeO	11.46	11.79	15.65	16.74	11.89	15.97
H ₂ O	2.13	2.10	1.98	1.94	2.12	1.99
Total	101.12	100.55	98.58	97.01	100.47	99.16
Si	7.88	7.85	6.85	6.73	7.86	6.91
Al ^{iv}	0.12	0.15	1.15	1.27	0.14	1.09
	8.00	8.00	8.00	8.00	8.00	8.00
Al ^{vi}	0.09	0.13	0.49	0.36	0.25	0.50
Ti	0.01	0.01	0.03	0.24	0.01	0.01
Fe ³⁺	0.00	0.00	0.12	0.00	0.00	0.00
Mg	3.62	3.49	2.42	2.28	3.40	2.48
Fe ²⁺	1.35	1.40	1.97	2.16	1.41	2.01
Mn	0.03	0.04	0.03	0.03	0.03	0.03
	5.10	5.07	5.06	5.07	5.10	5.03
Na	0.06	0.07	0.32	0.31	0.09	0.30
Ca	1.88	1.90	1.94	1.92	1.79	1.91
K	0.00	0.01	0.15	0.16	0.01	0.39
	1.94	1.98	2.41	2.39	1.89	2.60
<u>100 Mg</u> Mg + Fe**	72.8	71.4	53.7	51.4	70.7	55.2

* Primary brown hornblende inside actinolite

** Fe = Fe Total

TABLE 4.6 Electron probe microanalysis of specimen 604 C and 655 C.

SPECIMEN		604 C				655 C			
NO.		1	2	3	4	5	6	7	8
ANALYSIS		ACTINOLITE		MAGNESIO- HORNBLLENDE	MAGNESIO- HORNBLLENDE	CPX	ACTINOLITE	ACTINOLITIC HORNBLLENDE	FERRO HORNBLLENDE
MINERAL NAME	CPX	ACTINOLITE	MAGNESIO- HORNBLLENDE	MAGNESIO- HORNBLLENDE	CPX	ACTINOLITE	ACTINOLITIC HORNBLLENDE	FERRO HORNBLLENDE	FERRO HORNBLLENDE
Na ₂ O	0.14	0.52	0.76	1.05	0.54	0.22	0.41	0.93	0.93
MgO	12.74	16.52	13.66	12.27	12.60	16.07	13.13	10.68	10.68
Al ₂ O ₃	1.38	4.55	7.71	9.89	2.40	2.42	5.73	8.65	8.65
SiO ₂	52.97	53.08	47.58	45.94	51.21	53.80	49.82	45.51	45.51
K ₂ O	-	0.10	0.41	0.51	-	0.06	0.35	0.58	0.58
CaO	22.70	11.60	11.55	11.60	21.23	12.35	12.19	12.05	12.05
TiO ₂	0.40	0.16	0.29	0.43	0.41	0.04	0.26	0.41	0.41
MnO	0.39	0.37	0.34	0.32	0.30	0.27	0.21	0.27	0.27
Fe ₂ O ₃	-	0.00	1.10	0.52	-	1.42	0.82	4.88	4.88
FeO	10.10	10.88	12.31	13.59	11.46	12.02	13.80	14.97	14.97
H ₂ O	-	2.10	2.01	2.01	-	2.09	2.03	2.00	2.00
Total	100.82	99.88	97.72	98.13	100.15	100.76	98.75	100.93	100.93
Si	1.97	7.56	7.07	6.85	1.93	7.67	7.345	6.74	6.74
Al ^{iv}	0.03	0.44	0.93	1.15	0.07	0.33	0.655	1.26	1.26
Al ^{vi}	2.00	8.00	8.00	8.00	2.00	8.00	8.00	8.00	8.00
Ti	0.03	0.32	0.42	0.58	0.04	0.08	0.34	0.25	0.25
Fe ³⁺	0.01	0.02	0.03	0.05	0.01	0.00	0.03	0.05	0.05
Mg	0.71	3.51	3.02	2.73	-	0.15	0.09	0.55	0.55
Fe ²⁺	0.31	1.30	1.53	1.66	0.71	3.42	2.88	2.35	2.35
Mn	0.01	0.04	0.04	0.04	0.36	1.43	1.70	1.86	1.86
Na	0.01	5.19	5.16	5.15	0.01	0.03	0.03	0.03	0.03
Ca	0.91	0.14	0.22	0.31	0.04	0.06	0.12	0.27	0.27
K	-	1.77	1.84	1.86	0.86	1.88	1.93	1.92	1.92
	1.99	0.02	0.08	0.10	-	0.01	0.07	0.11	0.11
		1.93	2.14	2.27	2.03	1.95	2.12	2.30	2.30
100 Mg Mg + Fe*	69.6	73.0	64.7	60.9	66.4	68.4	61.7	49.4	49.4

* Fe = Fe Total

TABLE 4.7 Electron probe microanalyses of 657 C.

Grain 1 shows a compositional break between point 2 and 3.
Grain 2 shows a continuous trend from actinolite through hornblende.

ANALYSIS No.	1					2							
	1	2	3	4	5	6	7	8	9	10	11	12	
MINERAL	ACTINO-LITE	ACTINO-LITE	MAGNESIO-HORNBLLENDE	MAGNESIO-HORNBLLENDE	EDENITIC HORNBLLENDE	CPX	ACTINO-LITE	ACTINOLITIC HORNBLLENDE	ACTINOLITIC HORNBLLENDE	ACTINOLITIC HORNBLLENDE	MAGNESIO HORNBLLENDE	EDENITE	FERRO EDENITIC HORNBLLENDE
Na ₂ O	0.32	0.35	0.88	0.80	1.19	0.43	0.34	0.49	0.79	0.86	1.12	1.28	1.28
MgO	14.40	13.76	11.93	10.64	9.72	11.68	14.41	12.81	10.78	10.50	9.80	9.40	9.40
Al ₂ O ₃	3.32	3.79	7.44	8.57	10.37	1.19	2.93	4.23	7.11	7.51	8.36	9.62	9.62
SiO ₂	52.38	50.88	47.32	45.48	44.22	52.21	51.81	49.47	48.91	45.72	44.38	43.98	43.98
K ₂ O	0.22	0.42	0.59	0.72	1.00	-	0.18	0.32	0.59	0.70	1.14	1.08	1.08
CaO	12.28	12.16	11.97	11.99	11.88	22.71	12.01	12.07	11.63	11.72	11.82	11.52	11.52
TiO ₂	0.24	0.27	0.64	0.76	0.90	0.16	0.25	0.46	0.71	0.69	0.87	1.06	1.06
MnO	0.29	0.29	0.28	0.30	0.29	0.39	0.32	0.29	0.39	0.30	0.30	0.33	0.33
Fe ₂ O ₃	0.00	0.00	1.09	1.88	0.54	-	0.00	0.81	0.00	1.07	0.79	0.00	0.00
FeO	13.49	14.09	15.02	15.35	17.27	10.33	12.86	14.52	16.43	16.49	17.47	18.47	18.47
H ₂ O	2.05	2.02	2.01	1.98	1.98	-	2.02	1.99	2.02	1.96	1.95	1.96	1.96
Total	98.99	98.03	99.17	98.47	99.36	99.10	97.13	97.46	99.26	97.52	98.00	98.70	98.70
Si	7.64	7.55	7.04	6.86	6.67	1.98	7.69	7.435	7.25	6.99	6.82	6.72	6.72
Al ^{iv}	0.36	0.45	0.96	1.14	1.33	0.02	0.31	0.565	0.75	1.01	1.18	1.28	1.28
Al ^{vi}	8.00	8.00	8.00	8.00	8.00	2.00	8.00	8.00	8.00	8.00	8.00	8.00	8.00
Ti	0.22	0.21	0.35	0.39	0.52	0.04	0.20	0.18	0.50	0.34	0.33	0.45	0.45
Fe ³⁺	0.03	0.03	0.07	0.09	0.10	0.00	0.03	0.05	0.08	0.08	0.10	0.12	0.12
Fe ²⁺	0.00	0.00	0.12	0.21	0.06	-	0.00	0.09	0.00	0.12	0.09	0.00	0.00
Mg	3.13	3.04	2.64	2.40	2.19	0.66	3.19	2.86	2.38	2.39	2.25	2.14	2.14
Mn	1.65	1.75	1.87	1.94	2.18	0.33	1.60	1.82	2.04	2.11	2.24	2.36	2.36
Na	0.04	0.04	0.04	0.04	0.04	0.01	0.04	0.04	0.04	0.04	0.04	0.04	0.04
Ca	5.07	5.07	5.09	5.07	5.09	-	5.06	5.04	5.04	5.08	5.05	5.11	5.11
K	0.09	0.10	0.25	0.24	0.35	0.03	0.10	0.14	0.23	0.26	0.33	0.38	0.38
	1.92	1.93	1.91	1.94	1.92	0.93	1.91	1.95	1.85	1.92	1.95	1.89	1.89
	0.04	0.08	0.11	0.14	0.19	-	0.03	0.06	0.11	0.14	0.22	0.21	0.21
	2.05	2.11	2.27	2.32	2.46	2.00	2.04	2.15	2.19	2.32	2.50	2.48	2.48
100 + Mg	65.5	63.5	57.0	52.7	49.4	66.7	66.6	60.0	53.8	51.7	49.1	47.1	47.1
Mg + Fe Total													

TABLE 4.8 Electron probe microanalysis of 652 C. There are compositional breaks between 3/4 and 8/9.

ANALYSIS No.	1					2			
	1	2	3	4	5	6	7	8	9
MINERAL	ACTINO- LITE	ACTINO- LITE	ACTINOLITIC HORNBLENDE	EDENITIC HORNBLENDE	FERRO- EDENITIC HORNBLENDE	CPX	ACTINO- LITE IN CPX	ACTINOLITE	EDENITE
Na ₂ O	0.33	0.45	0.74	1.13	1.31	0.65	0.35	0.34	1.10
MgO	14.92	14.31	13.12	9.96	9.38	12.16	14.82	14.61	9.85
Al ₂ O ₃	2.64	3.01	5.11	9.10	9.70	1.45	1.71	3.22	8.72
SiO ₂	52.19	51.64	49.91	44.01	43.30	51.90	53.78	53.90	44.33
K ₂ O	0.14	0.15	0.35	0.91	0.98	-	0.09	0.16	0.86
CaO	12.21	12.03	11.70	11.51	11.57	20.75	11.74	12.79	11.61
TiO ₂	0.16	0.24	0.23	0.22	0.43	0.28	0.14	0.13	0.42
MnO	0.30	0.29	0.35	0.33	0.31	0.41	0.29	0.25	0.29
Fe ₂ O ₃	-	-	-	2.90	1.84	-	0.00	0.00	2.38
FeO	13.07	13.54	15.08	16.04	17.12	10.56	13.55	12.94	16.46
H ₂ O	2.03	2.02	2.02	1.94	1.94	-	2.05	2.09	1.94
Total	97.99	97.68	98.61	98.05	97.88	98.16	98.52	100.43	97.96
Si	7.69	7.65	7.40	6.74	6.57	1.98	7.86	7.72	6.79
Al ^{IV}	0.31	0.35	0.60	1.26	1.43	0.02	0.14	0.28	1.21
Al ^{VI}	8.00	8.00	8.00	8.00	8.00	2.00	8.00	8.00	8.00
Ti	0.14	0.18	0.29	0.38	0.40	0.05	0.15	0.26	0.37
Fe ³⁺	0.02	0.03	0.03	0.03	0.07	0.01	0.02	0.01	0.05
Fe ²⁺	-	-	-	0.34	0.31	-	0.00	0.00	0.27
Mg	3.27	3.16	2.90	2.27	2.05	0.69	3.23	3.12	2.25
Fe ²⁺	1.61	1.68	1.87	2.06	2.21	0.34	1.66	1.55	2.11
Mn	0.04	0.04	0.04	0.04	0.04	0.03	0.04	0.03	0.04
Na	5.08	5.09	5.13	5.12	5.08	-	5.10	4.97	5.09
Ca	0.09	0.13	0.21	0.34	0.39	0.05	0.10	0.09	0.33
K	1.93	1.91	1.86	1.89	1.93	0.85	1.84	1.96	1.91
	0.03	0.03	0.07	0.18	0.21	-	0.02	0.03	0.17
	2.05	2.07	2.14	2.41	2.53	2.02	1.96	2.08	2.41
Mg x 100 Mg + Fe	67.0	65.3	60.8	52.4	48.1	67.0	66.0	66.8	51.6

TABLE 4.9 EPMA of Clinopyroxene and traverse across actinolite and hornblende of specimen 603 C.

Grain 1 shows a continuous trend from actinolite through hornblende.
Grain 2 shows a compositional break between points 9 and 10.

ANALYSIS No.	1						2			
	1	2	3	4	5	6	7	8	9	10
MINERAL	CPX	ACTINO-LITE	ACTINO-LITE	ACTINO-LITIC HORNBLende	MAGNESIO HORNBLende	EDENITIC HORNBLende	CPX	ACTINOLITE (IN CPX)	ACTINO-LITE	EDENITIC HORNBLende
Na ₂ O	0.47	0.45	0.47	0.84	0.93	1.24	0.03	0.16	0.41	1.19
MgO	13.12	14.20	12.94	12.46	11.32	9.47	13.34	15.63	14.08	10.21
Al ₂ O ₃	1.24	2.74	3.57	5.76	7.25	10.08	1.74	1.78	3.40	9.23
SiO ₂	51.99	51.77	49.79	48.85	46.32	43.24	52.72	53.01	51.12	44.05
K ₂ O	0.08	0.12	0.21	0.36	0.49	0.83	0.06	0.01	0.18	0.75
CaO	22.40	12.19	12.07	11.96	12.03	11.93	22.76	12.47	12.29	11.69
TiO ₂	0.18	0.20	0.21	0.38	0.48	0.62	0.22	0.13	0.31	1.04
MnO	0.40	0.26	0.22	0.26	0.25	0.22	0.40	0.25	0.26	0.27
Fe ₂ O ₃	-	0.00	0.00	0.00	1.61	1.57	-	0.27	0.27	1.35
FeO	10.53	13.23	14.78	15.12	14.68	16.22	9.29	12.00	13.29	16.11
H ₂ O	-	2.02	1.98	2.00	1.96	1.94	-	2.04	2.02	1.96
Total	100.41	97.18	96.24	97.99	97.32	97.36	100.56	97.75	97.63	97.85
Si	1.95	7.70	7.56	7.31	7.03	6.65	1.96	7.78	7.585	6.73
Al ^{iv}	0.05	0.30	0.44	0.69	0.97	1.35	0.04	0.22	0.415	1.27
Al ^{vi}	2.00	8.00	8.00	8.00	8.00	8.00	2.00	8.00	8.00	8.00
Ti	0.01	0.18	0.20	0.32	0.34	0.49	0.04	0.09	0.19	0.39
Fe ³⁺	0.01	0.02	0.02	0.04	0.06	0.07	0.01	0.01	0.03	0.12
Fe ²⁺	-	0.00	0.00	0.00	0.18	0.18	-	0.03	0.03	0.15
Mg ²⁺	0.74	3.15	2.93	2.78	2.56	2.17	0.74	3.42	3.12	2.32
Mn	0.33	1.65	1.88	1.89	1.87	2.09	0.29	1.47	1.65	2.06
Na	0.01	0.03	0.03	0.03	0.03	0.03	0.01	0.03	0.03	0.04
Ca	5.03	5.06	5.06	5.06	5.04	5.03	5.05	5.05	5.05	5.08
K	0.03	0.13	0.14	0.24	0.27	0.37	0.00	0.05	0.12	0.35
100 + Mg	0.90	1.94	1.96	1.92	1.96	1.97	0.91	1.96	1.96	1.91
Mg + Fe Total	0.00	0.02	0.04	0.07	0.09	0.16	0.00	0.00	0.03	0.15
	2.03	2.09	2.14	2.23	2.32	2.50	2.00	2.01	2.11	2.41
100 + Mg	69.2	65.6	60.9	59.5	55.5	48.9	71.8	69.5	65.0	51.2

TABLE 4.10 EPMA data for clinopyroxene, pseudomorphous actinolite and surrounding, primary brown hornblende (3-6) in 602 C.

SPECIMEN						
NO.	602 C					
ANALYSIS						
NO.	1	2	3	4	5	6
MINERAL	CPX	ACTINOLITE (IN CPX)	MAGNESIO- HORNBLLENDE	EDENITIC HORNBLLENDE	EDENITIC HORNBLLENDE	FERROAN PARGASITIC HORNBLLENDE
Na ₂ O	0.63	0.60	0.64	1.30	1.37	1.32
MgO	12.02	15.37	12.65	10.35	10.45	9.02
Al ₂ O ₃	1.09	1.20	5.73	8.86	8.89	10.82
SiO ₂	52.02	53.69	48.27	43.87	43.69	42.15
K ₂ O	0.00	0.00	0.38	0.93	0.90	1.16
CaO	22.86	12.63	11.86	11.42	11.58	11.59
TiO ₂	0.12	0.06	0.79	1.88	1.96	1.03
MnO	0.43	0.32	0.32	0.33	0.35	0.32
Fe ₂ O ₃	-	0.00	1.90	0.27	1.35	2.64
FeO	10.01	13.76	14.29	17.32	16.36	16.93
H ₂ O		2.06	2.01	1.96	1.97	1.94
Total	99.18	99.69	98.84	98.49	98.87	98.92
Si	1.98	7.80	7.18	6.70	6.64	6.46
Al ^{iv}	0.02	0.20	0.82	1.30	1.36	1.54
	2.00	8.00	8.00	8.00	8.00	8.00
Al ^{vi}	0.03	0.00	0.18	0.28	0.23	0.46
Ti	0.00	0.01	0.09	0.22	0.23	0.12
Fe ³⁺	-	0.00	0.21	0.03	0.15	0.31
Mg	0.68	3.33	2.81	2.35	2.37	2.06
Fe ²⁺	0.32	1.67	1.78	2.21	2.08	2.17
Mn	0.01	0.04	0.04	0.04	0.05	0.04
		5.05	5.11	5.13	5.11	5.06
Na	0.05	0.17	0.19	0.38	0.40	0.40
Ca	0.93	1.97	1.89	1.87	1.88	1.91
K	0.00	0.00	0.07	0.18	0.17	0.23
	2.02	2.14	2.15	2.43	2.45	2.54
100 Mg Mg + Fe*	68.0	66.6	58.5	51.2	51.5	45.4

* Fe = Fe Total

TABLE 4.11 Analyses of cummingtonite, clinopyroxene, pseudomorphose actinolite and surrounding bluish-green hornblende (2, 4, 5, 8) in 601 C.

ANALYSIS No.	1		2			3			
	1	2	CUMMING-TONITE	FERROAN-PARGASITIC HORNBLLENDE	3	4	5	6	7
MINERAL	CUMMING-TONITE	FERROAN-PARGASITIC HORNBLLENDE	CUMMING-TONITE	FERROAN-PARGASITIC HORNBLLENDE	FERROAN-PARGASITIC HORNBLLENDE	FERROAN-PARGASITIC HORNBLLENDE	CPX	ACTINOLITE	TSCHERMAKITIC HORNBLLENDE
Na ₂ O	0.09	1.23	0.10	1.43	1.56	0.49	0.22	1.30	
MgO	17.77	9.93	17.45	9.89	9.16	12.88	16.33	9.12	
Al ₂ O ₃	0.69	11.53	0.93	13.02	13.25	1.51	1.96	12.72	
SiO ₂	53.71	42.58	53.43	42.03	40.41	52.26	53.75	41.57	
K ₂ O	0.00	1.05	0.00	0.84	0.99	-	0.03	0.29	
CaO	1.88	11.40	2.31	11.51	11.47	21.44	12.22	11.62	
TiO ₂	0.06	0.20	0.07	0.30	0.38	0.25	0.17	0.25	
MnO	0.65	0.22	0.77	0.18	0.18	0.31	0.19	0.20	
Fe ₂ O ₃	-	2.65	-	3.23	3.68	-	0.28	5.03	
FeO	22.12	15.29	23.17	14.60	14.80	11.45	11.84	14.19	
H ₂ O	2.04	1.95	2.05	1.97	1.93	-	2.07	1.95	
Total	99.01	98.03	100.28	99.00	97.81	100.59	99.06	98.24	
Si	7.90	6.50	7.82	6.34	6.21	1.96	7.765	6.32	
Al ^{iv}	0.10	1.50	0.18	1.66	1.79	0.04	0.235	1.68	
Al ^{vi}	8.00	8.00	8.00	8.00	8.00	2.00	8.00	8.00	
Al ^{vi}	0.02	0.57	0.00	0.65	0.62	0.03	0.10	0.60	
Ti	0.01	0.02	0.01	0.04	0.04	0.01	0.02	0.03	
Fe ³⁺	-	0.31	-	0.37	0.43	-	0.03	0.58	
Mg	3.90	2.26	3.81	2.22	2.10	0.72	3.52	2.06	
Fe ²⁺	2.72	1.95	2.84	1.84	1.90	0.36	1.43	1.80	
Mn	0.08	0.03	0.10	0.02	0.02	0.01	0.02	0.03	
Mn	6.73	5.14	6.76	5.14	5.11	-	5.12	5.10	
Na	0.03	0.37	0.03	0.42	0.47	0.03	0.06	0.39	
Ca	0.30	1.87	0.36	1.87	1.89	0.86	1.89	1.90	
K	0.00	0.21	0.00	0.16	0.20	-	0.01	0.06	
K	0.33	2.45	0.39	2.45	2.56	2.02	1.96	2.35	
100 Mg Mg + Fe Total	58.9	50.0	57.3	50.1	47.4	66.7	70.7	46.4	

from core towards contact with hornblende. CaO and MnO remain unchanged. Actinolite contains low Al^{iv} (0.14 to 0.60) and high 100 Mg/(Mg + Fe²⁺) ratio (60.8 - 76.1)

Hornblende

Primary brown hornblende mantling actinolite containing relict pyroxene is presented in table 4.10 from specimen 602 C, and in Table 4.5 (analysis 4) as relict inside actinolite lacking relict pyroxene. These primary hornblendes are distinguished from green to bluish-green metamorphic amphibole by their remarkably high Ti content which is in agreement with the opinion (Leake 1965, Bard 1970, Helz 1973, and Raase 1974) that high Ti is an indicator of high temperature and gives the brown tints in hornblende. Al^{iv}/Al^{vi} ratios of primary hornblende are also higher than metamorphic ones (≥ 3.3 as suggested by Fleet and Barnett, (1978) as a limiting boundary for the field of igneous amphibole).

Transition from actinolite core to green or bluish-green hornblende is characterized by an abrupt increase in Al₂O₃ and (FeO + Fe₂O₃) with simultaneous decrease in SiO₂ and MgO (Figs. 4.11, 4.12). CaO generally very slightly decreases or remains unchanged. Na₂O, K₂O and TiO₂ increase while MnO has a constant concentration. Gradational contacts between actinolite core and rimming hornblende are also found in some specimens by changing through actinolitic hornblende. (e.g. analysis 9 Table 4.7, analysis 4 Table 4.9). These two distinct types of contacts can also be observed in the same specimens (e.g. 603 C, 652 C). Hornblende shows stronger zoning than actinolite cores but in the same manner with continuous increase in Fe₂O₃, FeO, Al₂O₃, Na₂O, K₂O, TiO₂ and decrease in MgO and SiO₂ from actinolite boundaries towards contacts with

plagioclase. There is no significant change of CaO and MnO throughout. Al^{iv} in hornblende ranges from 0.60 to 1.77 and is always more than Al^{vi} , and both are in sharp contrast to Al contents of actinolite cores. $100 \text{ Mg}/(\text{Mg} + \text{Fe}^{\text{total}})$ ratios in hornblende are systematically lower than in actinolite and decrease outward, with variation from 66.0 to 46.5. Alkali content of hornblende is high where $100 \text{ Mg}/(\text{Mg} + \text{Fe}^{\text{total}})$ ratio is high.

Rimming hornblende around cummingtonite in specimen 601 C (Table 4.11) is also slightly zoned with Al_2O_3 , Na_2O , $FeO + Fe_2O_3$ and K_2O increasing and SiO_2 and MgO decreasing outwards. $100 \text{ Mg}/(\text{Mg} + \text{Fe}^{\text{total}})$ ratios are generally lower than in cummingtonite cores, similar to the fractionation observed by Kisch and Warnars (1969). There is no significant difference between fringing hornblendes around cummingtonite and those around actinolite in the same specimen, except that the former one has higher K_2O content. $100 \text{ Mg}/(\text{Mg} + \text{Fe}^{\text{total}})$ ratios are virtually identical in both hornblendes. With continuity from actinolite, hornblende compositions vary by two coupled substitutions, the edenite ($Na^A Al^{iv} \rightleftharpoons \square^A Si^{iv}$) and the Tschermakite ($Al^{vi} Al^{iv} \rightleftharpoons Mg^{vi} Si^{iv}$).

Cummingtonite

There is no significant change in the compositions of cummingtonite towards contacts with hornblende. Cummingtonite is characterized by higher SiO_2 , MgO , FeO , and lower Al_2O_3 , K_2O , CaO and Na_2O than edging hornblende. Alkali contents are low or practically undetectable. Al_2O_3 varies from 0.69 to 0.93 weight percent. The maximum value of CaO (2.31) is slightly higher than those reported in the literature. (Klein 1968, Stout 1972, Kanisawa 1974 and Sampson and Fawcett, 1977).

TABLE 4.12 Partial analysis of plagioclase, presented as numbers of atoms based on 8 oxygens.

SPECIMEN	685C	683C	678C	601C	601C	652C	652C	604C	656C	657C	687C	602C	603C
NO.	1	2	3	4	5	6	7	8	9	10	11	12	13
Si	2.66	2.641	2.619	2.686	2.668	2.682	2.617	2.629	2.656	2.630	2.663	2.720	2.704
Al	1.34	1.359	1.381	1.318	1.332	1.318	1.383	1.371	1.344	1.370	1.337	1.280	1.296
	4.00	4.00	4.00	4.00	4.00	4.00	4.00	4.00	4.00	4.00	4.00	4.00	4.00
Na	0.652	0.676	0.619	0.666	0.651	0.671	0.606	0.622	0.647	0.620	0.652	0.711	0.697
Ca	0.340	0.311	0.381	0.317	0.332	0.318	0.383	0.371	0.344	0.370	0.338	0.280	0.296
K	0.008	0.013	0.000	0.018	0.017	0.011	0.011	0.007	0.009	0.010	0.010	0.009	0.007
	1.00	1.00	1.00	1.00	1.00	1.00	1.00	1.00	1.00	1.00	1.00	1.00	1.00
% An	34.0	31.1	38.1	31.7	33.2	31.8	38.3	37.1	34.4	37.0	33.8	28.0	29.6

TABLE 4.13 Analyses of epidote (all iron treated as ferric) of specimen 678 C.

	1	2
MgO	0.08	0.08
Al ₂ O ₃	21.54	21.96
SiO ₂	37.97	37.95
CaO	23.17	22.77
MnO	0.04	0.07
Fe ₂ O ₃	15.83	14.80
FeO	-	-
H ₂ O	1.88	1.87
Total	100.51	99.50
Si	6.05	6.08
Al	0.00	0.00
	6.05	6.08
Al	4.05	4.15
Fe	1.90	1.78
	5.95	5.93
Mg	0.02	0.02
Mn	0.01	0.01
Ca	3.96	3.91
	3.99	3.94
$\frac{\text{Fe}^{3+}}{\text{Fe}^{3+} + \text{Al}}$	31.9	30.1

Plagioclase

Partial analyses for Ca, Na and K were carried out for plagioclase in contact with hornblende. Ca, Na, and K are converted to An, Ab and Or contents using calibrations stored in a microcomputer and so the Al and Si contents (Table 4.12) are calculated from assumed stoichiometry. Plagioclase is generally zoned with composition ranging from An₂₃₋₄₈, with increasing An content towards cores (An₃₀₋₅₀). Table 4.12 shows representative analyses of plagioclase, next to analysed hornblende presented in Table 4.3-4.11.

Epidote

A few grains of epidote in specimen 678 C were analysed and are presented in Table 4.13. It is found that composition of epidote is uniform and zoning was not detected. Pistacite value of epidote is 30-32 %. Similar observations have been reported for synthetic and regional metamorphic epidote; in low-temperature environments, epidote tends to have a composition close to Ps₃₃ (Strens, 1965 and Liou, 1973).

4.4.2 Morven-Cabrach intrusion

A number of Ca-pyroxenes were analysed (analyses 9 in Table 4.14; 6,8 in Table 4.15; 3 in Table 4.16; 1 in Table 4.17; 4 in Table 4.19; 1, 4 in Table 4.21; 2 in Table 4.22). Analysis 2 in Table 4.22 of specimen 746 C is a very coarse bleb of clinopyroxene in orthopyroxene (analysis 1 Table 4.22). Comparison of the analyses, among clinopyroxenes from different rock types in this mass, shows small differences in the compositions. In quartz-biotite norite from Craig Wood Quarry (62 P), clinopyroxene is salite of composition Wo_{46.5} En_{36.5} Fs₁₇. Clinopyroxene in hypersthene

TABLE 4.14 EPHA of coexisting minerals in 62 P.
 Analyses across 3 grains in specimen 62 P showing very slight zoning in cummingtonite (analyses 2, 3) and in
 edging hornblende (analyses 7, 8; Mg-rich). There is a compositional break between 11/12.

ANALYSIS No.	1			2			3					
	1	2	3	4	5	6	7	8	9	10	11	12
MINERAL	OPX	CUMMING- TONITE	CUMMING- TONITE	MAGNESIO HORNBLENDE	OPX	CUMMING- TONITE	MAGNESIO HORNBLENDE	MAGNESIO HORNBLENDE	CPX	ACTINO- LITE	ACTINOLITIC HORNBLENDE	MAGNESIO HORNBLENDE
Na ₂ O	0.00	0.02	0.48	1.13	0.00	0.01	0.63	0.68	0.17	0.23	0.34	0.61
MgO	18.10	17.88	17.77	11.16	18.10	17.59	13.57	13.31	12.61	15.21	14.55	10.98
Al ₂ O ₃	0.67	0.78	0.69	11.08	0.58	0.96	7.30	8.15	0.97	3.72	4.72	9.64
SiO ₂	52.69	55.26	55.29	45.46	52.98	54.84	49.16	49.40	53.89	52.95	51.64	47.63
K ₂ O	0.00	0.00	0.00	0.47	0.00	0.00	0.36	0.33	-	0.12	0.18	0.13
CaO	0.67	1.24	0.99	11.27	0.68	1.13	10.71	10.94	22.35	10.65	11.30	11.51
TiO ₂	0.09	0.09	0.30	0.48	0.09	0.04	0.51	0.13	0.14	0.32	0.42	0.82
MnO	0.58	0.44	0.44	0.17	0.58	0.45	0.17	0.16	0.24	0.19	0.17	0.15
Fe ₂ O ₃	-	-	-	0.00	-	-	0.00	0.00	-	0.00	0.00	0.00
FeO	27.85	22.45	22.71	15.41	27.38	22.48	15.19	14.13	10.58	14.29	13.91	15.69
H ₂ O	-	2.07	2.08	2.01	-	2.06	2.05	2.06	-	2.08	2.06	2.03
Total	100.87	100.23	100.75	98.64	100.39	99.56	99.65	99.29	100.95	99.76	99.29	99.19
Si	2.00	7.99	7.97	6.77	2.01	7.98	7.18	7.20	2.00	7.64	7.50	7.02
Al ^{iv}	0.00	0.01	0.03	1.23	0.00	0.02	0.82	0.80	0.00	0.36	0.50	0.98
Al ^{vi}	2.00	8.00	8.00	8.00	2.01	8.00	8.00	8.00	2.00	8.00	8.00	8.00
Al ^{vi}	0.03	0.12	0.08	0.72	0.03	0.15	0.44	0.60	0.04	0.27	0.31	0.69
Ti	0.00	0.01	0.03	0.05	0.00	0.00	0.06	0.02	0.00	0.04	0.05	0.09
Fe ³⁺	-	-	-	0.00	-	-	0.00	0.00	-	0.00	0.00	0.00
Mg	1.02	3.85	3.82	2.48	1.02	3.82	2.96	2.89	0.70	3.27	3.15	2.41
Fe ²⁺	0.88	2.71	2.74	1.92	0.87	2.74	1.86	1.72	0.33	1.72	1.69	1.93
Mn	0.02	0.05	0.05	0.02	0.02	0.06	0.02	0.02	0.01	0.02	0.02	0.02
Na	0.00	6.74	6.72	5.19	0.00	6.77	5.34	5.25	0.01	5.32	5.22	5.14
Ca	0.00	0.01	0.13	0.33	0.00	0.00	0.18	0.19	0.01	0.06	0.10	0.18
K	0.02	0.19	0.15	1.80	0.03	0.18	1.68	1.71	0.89	1.65	1.76	1.82
K	0.00	0.00	0.00	0.09	0.00	0.00	0.07	0.06	-	0.02	0.03	0.03
K	1.97	0.20	0.28	2.22	1.97	0.18	1.93	1.96	1.98	1.73	1.89	2.03
100 + Mg Mg + Fe Total	53.7	58.7	58.2	56.4	54.0	58.2	61.4	62.7	67.9	65.5	65.1	55.5

TABLE 4.15 EPMA of orthopyroxene, clinopyroxene, cummingtonite, actinolite and hornblende of 724 C.

	1			2		3	
ANALYSIS NO.	1	2	3	4	5	6	7
MINERAL	OPX	CUM.	FERROAN-PARGASITE	CUM.	FERROAN-PARGASITIC HORNBLLENDE	CPX	ACTINO-LITE *
Na ₂ O	-	0.11	1.65	0.12	1.59	0.29	0.21
MgO	15.75	14.62	5.08	13.66	7.84	11.43	13.47
Al ₂ O ₃	1.01	0.83	16.62	0.80	12.84	2.15	1.81
SiO ₂	50.09	51.82	39.02	51.78	42.62	49.70	52.36
K ₂ O	-	-	0.86	-	0.43	-	-
CaO	1.16	0.87	11.37	1.90	11.43	19.61	12.32
TiO ₂	0.19	0.05	0.03	0.04	0.51	0.43	0.15
MnO	0.67	0.76	0.17	0.88	0.23	0.34	0.17
Fe ₂ O ₃	-	-	-	-	1.06	-	1.37
FeO	30.10	26.70	19.44	26.78	18.92	14.53	14.79
H ₂ O	-	1.97	1.90	1.99	1.97	-	2.02
Total	98.97	97.73	96.15	97.95	99.44	98.48	98.67
Si	1.97	7.89	6.16	7.90	6.46	1.93	7.73
Al ^{iv}	0.03	0.11	1.84	0.10	1.54	0.07	0.27
	2.00	8.00	8.00	8.00	8.00	2.00	8.00
Al ^{vi}	0.02	0.04	1.25	0.05	0.76	0.03	0.05
Ti	0.01	0.01	0.00	0.00	0.06	0.01	0.02
Fe ³⁺	-	-	-	-	0.12	-	0.15
Mg	0.92	3.32	1.19	3.11	1.78	0.66	2.97
Fe ²⁺	0.99	3.40	2.57	3.42	2.40	0.47	1.83
Mn	0.02	0.10	0.02	0.11	0.03	0.01	0.02
		6.87	5.03	6.69	5.15		5.04
Na	-	0.03	0.51	0.04	0.47	0.02	0.06
Ca	0.05	0.14	1.92	0.31	1.86	0.82	1.95
K	-	-	0.17	-	0.08	-	-
	2.01	0.17	2.60	0.35	2.41	2.02	2.01
100 Mg	48.2	49.4	31.6	47.6	41.4	58.4	60.0
Mg + Fe ^{**}							

* Lamellae in host CPX

** Fe = Fe Total

TABLE 4.16 EPMA of specimen 84 P. There is a compositional break between 4/5.

1			2		
ANALYSIS NO.	1	2	3	4	5
MINERAL	CUMMING-TONITE	FERRO-HORNBLENDE	CPX	ACTINO-LITE	FERRO-HORNBLENDE
Na ₂ O	0.10	1.00	0.38	0.16	1.27
MgO	14.93	10.19	11.14	13.11	8.42
Al ₂ O ₃	0.65	8.82	1.27	2.16	11.80
SiO ₂	52.53	44.84	51.21	52.58	44.48
K ₂ O	-	0.65	-	0.00	0.33
CaO	1.24	11.46	21.40	13.42	11.81
TiO ₂	0.03	0.24	0.23	0.09	0.19
MnO	0.85	0.28	0.46	0.31	0.25
Fe ₂ O ₃	-	3.19	-	1.67	2.18
FeO	27.59	16.16	13.90	14.25	18.29
H ₂ O	2.00	1.96		2.04	2.01
Total	99.92	98.79	99.99	99.79	101.06
Si	7.86	6.80	1.96	7.69	6.605
Al ^{iv}	0.12	1.20	0.04	0.31	1.395
	7.98	8.00	2.00	8.00	8.00
Al ^{vi}	0.00	0.36	0.02	0.07	0.68
Ti	0.00	0.03	0.01	0.01	0.02
Fe ³⁺	-	0.37	-	0.18	0.24
Mg	3.33	2.30	0.64	2.86	1.87
Fe ²⁺	3.45	2.05	0.44	1.74	2.27
Mn	0.11	0.04	0.02	0.04	0.03
	6.89	5.15		4.90	5.11
Na	0.03	0.30	0.03	0.05	0.37
Ca	0.20	1.86	0.88	2.10	1.88
K	-	0.13		0.00	0.06
	0.23	2.29	2.04	2.15	2.31
<u>100 Mg</u> Mg + Fe*	50.9	48.70	59.3	59.8	42.7

* Fe = Fe Total

TABLE 4.17 EPMA of clinopyroxene, cummingtonite, actinolite and hornblende of 81 P.

ANALYSIS NO.	1					2	
	1	2	3	4	5	6	7
MINERAL NAME	CPX	ACTINOLITE	ACTINOLITIC HORNBLLENDE	FERRO HB	FERRO TSCHERMAKITIC	CUMMINGTONITE	FERROAN PARGASITE
Na ₂ O	0.31	0.25	0.38	0.90	1.22	0.06	1.57
MgO	10.21	11.85	10.86	8.63	5.39	12.46	6.29
Al ₂ O ₃	2.01	1.80	3.48	8.57	15.71	0.50	14.90
SiO ₂	50.42	52.40	49.93	46.72	40.73	52.22	40.39
K ₂ O	-	0.01	0.08	0.45	0.20	0.02	0.67
CaO	21.18	11.70	11.01	11.59	10.75	0.75	10.86
TiO ₂	0.40	0.24	0.22	0.38	0.14	0.01	0.40
MnO	0.46	0.35	0.38	0.32	0.30	0.73	0.30
Fe ₂ O ₃	-	2.21	3.27	2.74	3.44	-	2.91
FeO	16.10	18.55	19.00	20.40	20.39	30.45	19.96
H ₂ O	-	2.04	2.00	2.20	1.96	1.97	1.95
Total	101.09	101.40	100.61	102.90	100.23	99.17	100.20
Si	1.93	7.68	7.43	6.88	6.19	7.96	6.155
Al iv	0.07	0.31	0.57	1.12	1.81	0.04	1.845
Al v1	2.00	8.00	8.00	8.00	8.00	8.00	8.00
Ti	0.02	0.00	0.04	0.37	0.99	0.05	0.83
Fe 3+	0.01	0.03	0.02	0.04	0.02	0.00	0.05
Fe	-	0.24	0.37	0.31	0.40	-	0.34
Mg	0.58	2.59	2.41	1.90	1.22	2.83	1.43
Fe 2+	0.51	2.27	2.36	2.52	2.59	3.88	2.54
Mn	0.02	0.04	0.05	0.04	0.04	0.10	0.04
Na	0.02	5.17	5.25	5.18	5.26	6.86	5.23
Ca	0.87	1.84	1.76	1.83	1.75	0.02	0.47
K	-	0.00	0.01	0.09	0.04	0.12	1.78
	2.03	1.91	1.88	2.18	2.15	-	0.13
100 Mg / Mg + Fe*	53.2	50.8	46.9	40.2	29.0	42.2	33.2

* Fe = Fe Total

TABLE 4.18 EPMA of actinolite, cummingtonite and surrounding hornblende of 741 C.

ANALYSIS NO.	1				2	
	1	2	3	4	5	6
MINERAL NAME	ACTINOLITE *	CUMMINGTONITE	FERROAN PARGASITIC HORNBLLENDE	FERROAN PARGASITE	ACTINOLITE	FERROAN PARGASITE
Na ₂ O	0.29	0.31	0.92	0.84	0.12	0.92
MgO	12.86	11.37	7.53	5.97	13.29	5.21
Al ₂ O ₃	2.48	2.69	13.45	16.27	1.68	17.41
SiO ₂	52.82	50.18	41.27	39.16	53.53	38.36
K ₂ O	0.11	0.10	1.71	1.70	-	1.14
CaO	11.52	3.87	11.28	11.43	11.28	11.57
TiO ₂	-	-	-	-	-	-
MnO	0.50	0.80	0.18	0.20	0.27	0.22
Fe ₂ O ₃	0.00	-	2.37	4.20	0.00	5.00
FeO	17.39	27.07	18.21	17.81	17.33	17.53
H ₂ O	2.04	1.95	1.94	1.93	2.04	1.93
Total	100.01	98.34	98.86	99.51	99.54	99.29
Si	7.75	7.70	6.34	6.01	7.85	5.895
Al ^{iv}	0.25	0.30	1.66	1.99	0.15	2.105
Al ^{vi}	8.00	8.00	8.00	8.00	8.00	8.00
Ti	0.17	0.19	0.78	0.95	0.15	1.05
Fe ³⁺	-	0.00	0.27	0.49	0.00	0.58
Mg ²⁺	2.81	2.60	1.73	1.37	2.91	1.20
Mn	2.13	3.48	2.34	2.29	2.13	2.25
Na	0.06	0.10	0.02	0.03	0.03	0.03
Ca	5.18	6.37	5.14	5.13	5.22	5.11
K	0.08	0.09	0.28	0.25	0.03	0.28
	1.81	0.64	1.86	1.88	1.77	1.91
	0.02	0.02	0.34	0.33	-	0.23
	1.91	0.75	2.48	2.46	1.80	2.42
100 Mg Mg + Fe**	56.9	42.8	39.9	33.0	57.7	29.80

* patch in cummingtonite, which probably represents former clinopyroxene bleb in primary OPX.

** Fe = Fe Total

TABLE 4.19 Analysis of clinopyroxene actinolite, cummingtonite and surrounding hornblende of 757 C and 758 C.

SPECIMEN NO.	757 C			758 C				
	1	2	3	4	5	6	7	8
ANALYSIS NO.	CUMMING-TONITE	FERRO ACTINO-LITE	FERRO HB	CPX	FERRO ACTINO-LITE	FERRO ACTINO-LITIC HORNBLLENDE	CUMMING-TONITE	FERRO-EDENITIC HORNBLLENDE
Na ₂ O	0.00	0.30	0.63	0.19	0.38	0.52	0.15	1.43
MgO	11.83	10.48	9.16	9.93	10.26	9.72	11.83	7.82
Al ₂ O ₃	0.52	2.98	5.92	0.52	3.53	5.34	0.88	10.25
SiO ₂	51.82	49.84	47.60	50.51	49.82	48.59	51.22	43.44
K ₂ O	-	0.10	0.23	-	0.12	0.28	-	0.36
CaO	1.55	11.45	11.62	21.14	11.01	11.50	0.92	9.54
TiO ₂	0.07	0.29	0.60	0.11	0.19	0.18	0.06	0.59
MnO	0.74	0.26	0.26	0.36	0.31	0.30	0.79	0.34
Fe ₂ O ₃	-	1.07	1.07	-	0.27	1.36	-	1.85
FeO	30.58	19.46	20.05	15.78	20.37	19.48	30.83	21.81
H ₂ O	1.96	1.97	1.97	-	1.97	1.98	1.95	1.95
Total	99.07	98.20	99.11	98.54	98.23	99.25	98.63	99.38
Si	7.94	7.58	7.22	1.98	7.575	7.33	7.89	6.66
Al ^{iv}	0.06	0.42	0.78	0.02	0.425	0.67	0.11	1.34
Al ^{vi}	8.00	8.00	8.00	2.00	8.00	8.00	8.00	8.00
Ti	0.03	0.11	0.28	0.00	0.21	0.28	0.05	0.51
Fe ³⁺	0.01	0.03	0.07	0.00	0.02	0.02	0.01	0.07
Fe ²⁺	-	0.12	0.12	-	0.03	0.15	-	0.21
Mg	2.70	2.37	2.07	0.58	2.33	2.18	2.72	1.79
Fe ²⁺	3.92	2.47	2.54	0.52	2.59	2.46	3.97	2.80
Mn	0.10	0.03	0.03	0.01	0.04	0.04	0.10	0.05
Na	6.76	5.13	5.11	0.02	5.22	5.13	6.85	5.43
Ca	0.00	0.09	0.19	0.02	0.11	0.15	0.05	0.43
K	0.26	1.87	1.89	0.89	1.79	1.86	0.15	1.56
	-	0.02	0.05	-	0.02	0.05	-	0.07
	0.26	1.98	2.13	2.01	1.92	2.06	0.20	2.06
100 Mg Mg + Fe**	40.8	47.8	43.8	52.7	47.1	45.5	40.7	37.3

** Fe = Fe Total

TABLE 4.20 Analysis of orthopyroxene, cummingtonite and surrounding hornblende.

SPECIMEN NO.	725 C					67 P			63P		
	MAGNESIO HORNBLLENDE *	CUMMING-TONITE	FERRO-TSCHER-HAKTIC HB	FERROAN PARGASITIC HORNBLLENDE	CUMMING-TONITE	FERROAN PARGASITE	OPX	CUMMING-TONITE	FERRO-TSCHER-MAKITE		
Na ₂ O	0.89	0.08	1.09	1.44	0.18	1.91	-	0.01	1.25		
MgO	10.33	13.85	7.29	6.08	13.24	6.84	14.68	14.26	4.68		
Al ₂ O ₃	8.26	0.76	13.75	15.89	1.82	17.10	0.68	1.02	18.32		
SiO ₂	46.94	53.18	42.37	41.25	51.79	39.88	50.00	52.82	39.76		
K ₂ O	0.14	0.06	0.49	0.41	0.03	0.18	-	-	0.24		
CaO	11.42	1.42	11.55	11.35	1.81	10.04	1.02	0.42	10.52		
TiO ₂	0.25	0.00	0.09	0.19	0.04	0.31	0.21	0.02	0.05		
MnO	0.17	0.76	0.16	0.15	0.65	0.28	0.72	0.70	0.25		
Fe ₂ O ₃	0.53	-	1.07	-	-	1.06	-	-	0.79		
FeO	17.33	26.87	18.22	19.47	27.38	19.30	33.16	29.73	20.73		
H ₂ O	1.99	1.99	1.95	1.96	1.98	1.96	-	2.01	1.95		
Total	98.25	98.97	98.03	98.19	98.92	98.86	100.47	100.99	98.54		
Si	7.07	7.99	6.48	6.32	7.83	6.07	1.96	7.86	6.10		
Al iv	0.93	0.01	1.52	1.68	0.17	1.93	0.03	0.14	1.90		
Al vi	8.00	8.00	8.00	8.00	8.00	8.00	1.99	8.00	8.00		
Ti	0.54	0.12	0.96	1.19	0.15	1.15	0.00	0.03	1.41		
Fe 3+	0.03	0.00	0.01	0.02	0.00	0.04	0.01	0.00	0.01		
Fe 2+	0.06	-	0.12	0.00	-	0.12	-	-	0.09		
Mn	2.32	3.10	1.67	1.39	2.98	1.56	0.86	3.16	1.07		
Na	2.19	3.38	2.33	2.49	3.46	2.46	1.09	3.70	2.66		
Ca	0.02	0.10	0.02	0.02	0.08	0.04	0.02	0.09	0.03		
K	5.15	6.70	5.11	5.11	6.67	5.37	-	6.98	5.27		
	0.26	0.02	0.32	0.43	0.05	0.57	-	-	0.37		
	1.85	0.23	1.90	1.86	0.29	1.64	0.04	0.07	1.73		
	0.03	0.01	0.10	0.08	0.01	0.04	-	-	0.05		
	2.14	0.26	2.32	2.37	0.35	2.25	2.02	0.07	2.15		
100 Mg / Mg + Fe**	50.8	47.8	40.5	35.8	46.3	37.7	44.1	46.1	28.0		

* Bleb of green hornblende inside cummingtonite, representing small lath of plagioclase in pre-existing orthopyroxene.

** Fe = Fe Total

TABLE 4.21 Analysis of clinopyroxene, actinolite and hornblende. There is a compositional break between 5/6.

SPECIMEN NO.	73 P			733 C			733C	
	1	2	3	4	5	6	7	8
ANALYSIS NO.	CPX	ACTINOLITE*	FERRO HB	CPX	ACTINOLITE	FERRO PARGASITE	CUMMING- TONITE	FERRO TSCHERMUKITE
Na ₂ O	0.32	0.30	1.14	0.23	0.13	1.66	0.11	0.67
MgO	12.10	13.57	7.88	10.57	12.79	3.97	13.97	3.60
Al ₂ O ₃	2.37	2.86	10.59	2.13	0.92	19.46	1.29	17.43
SiO ₂	49.62	52.80	44.70	50.20	53.39	37.81	52.64	39.06
K ₂ O	-	0.15	0.66	-	-	0.35	-	0.67
CaO	20.70	11.39	11.51	21.19	11.16	9.93	2.22	11.51
TiO ₂	0.49	0.04	0.39	0.36	0.29	0.06	0.29	0.06
MnO	0.27	0.19	0.20	0.23	0.40	0.22	0.32	0.23
Fe ₂ O ₃	-	0.00	0.80	-	0.00	1.58	-	0.77
FeO	11.76	15.93	20.52	13.35	16.80	21.84	25.20	21.00
H ₂ O	-	2.05	1.98	-	2.01	1.93	1.99	1.90
Total	97.63	99.28	100.37	98.26	97.89	98.81	98.03	96.90
Si	1.92	7.74	6.74	1.95	7.95	5.85	7.93	6.14
Al ^{iv}	0.08	0.26	1.26	0.05	0.05	2.15	0.07	1.86
Al ^{vi}	2.00	8.00	8.00	2.00	8.00	8.00	8.00	8.00
Ti	0.03	0.23	0.62	0.04	0.12	1.39	0.16	1.33
Fe ³⁺	0.01	0.01	0.04	0.01	0.03	0.01	0.03	0.01
Fe ²⁺	-	0.00	0.09	-	0.00	0.18	-	0.09
Mn	0.70	2.96	1.78	0.61	2.84	0.92	3.14	0.84
Na	0.38	1.95	2.58	0.43	2.09	2.83	3.18	2.76
Ca	0.01	0.02	0.03	0.01	0.05	0.03	0.04	0.03
K	0.02	5.17	5.14	0.02	5.13	5.36	6.55	5.06
	0.86	0.09	0.33	0.88	0.04	0.50	0.03	0.21
	-	1.79	1.86	-	1.78	1.64	0.36	1.94
	2.02	0.03	0.13	-	-	0.07	-	0.13
	64.8	1.90	2.32	2.00	1.82	2.11	0.39	2.28
100 Hg Mg + Fe**	64.8	60.3	40.0	58.7	57.6	23.4	49.7	22.8

* Actinolite occurs as coarse lamellae in clinopyroxene

** Fe = Fe Total

TABLE 4.22 Analysis of pyroxenes, cummingtonite and hornblende.

SPECIMEN NO.	746 C				735 C			
	1	2	3	4	5	6	7	8
ANALYSIS								
MINERAL NAME	OPX	CPX*	CUMMING-TONITE	FERRO-TSCHERMAKITIC HB	OPX	CUMMING-TONITE	MAGNESIO HORNBLENDE	MAGNESIO HORNBLENDE
Na ₂ O	-	0.34	0.07	1.23	0.03	0.16	0.73	0.81
MgO	15.03	11.02	14.73	6.68	19.41	16.53	13.65	13.17
Al ₂ O ₃	0.91	1.86	0.95	14.49	0.90	1.20	8.27	10.01
SiO ₂	49.04	50.46	52.55	41.38	52.04	54.40	48.22	46.15
K ₂ O	-	-	-	0.29	-	-	0.50	0.79
CaO	0.94	20.61	0.90	11.35	0.82	3.47	11.90	11.46
TiO ₂	0.19	0.36	0.15	0.08	0.14	0.04	0.30	1.19
MnO	0.74	0.34	0.65	0.19	0.52	0.36	0.16	0.17
Fe ₂ O ₃	-	-	-	2.12	-	-	0.83	1.11
FeO	31.44	13.85	26.11	18.15	24.91	20.53	12.35	12.88
H ₂ O	-	-	1.98	1.94	-	2.04	2.04	2.04
Total	98.29	98.84	98.09	97.90	98.77	98.73	98.95	99.78
Si	1.96	1.95	7.93	6.36	1.99	7.97	7.07	6.75
Al ^{iv}	0.04	0.05	0.07	1.64	0.01	0.03	0.93	1.25
Al ^{vi}	2.00	2.00	8.00	8.00	2.00	8.00	8.00	8.00
Ti	0.00	0.03	0.10	0.98	0.03	0.18	0.49	0.49
Fe ³⁺	0.01	0.01	0.02	0.01	0.00	0.01	0.03	0.13
Fe ²⁺	-	-	-	0.24	-	-	0.09	0.12
Mn	0.89	0.63	3.31	1.53	1.11	3.61	2.98	2.87
Na	1.05	0.45	3.30	2.33	0.80	2.52	1.52	1.57
Ca	0.03	0.01	0.08	0.03	0.02	0.05	0.02	0.02
K	-	-	6.81	5.12	0.00	6.37	5.13	5.20
100 Mg / Mg + Fe**	-	0.03	0.02	0.37	0.00	0.05	0.21	0.23
	0.04	0.85	0.15	1.87	0.03	0.55	1.87	1.80
	-	-	-	0.06	-	-	0.09	0.15
	2.02	2.01	0.17	2.30	1.99	0.60	2.17	2.18
	45.9	58.3	50.1	37.3	58.1	58.9	64.9	62.9

* Inclusion in orthopyroxene

** Fe = Fe Total

gabbro (81 P) is classified as augite of composition $Wo_{44} En_{30} Fs_{26}$. There is a variation of clinopyroxene composition in noritic rocks from $Wo_{44} En_{36} Fs_{20}$ to $Wo_{45} En_{29} Fs_{26}$. K_2O is not detected in all cases. Compositions of clinopyroxene blebs in orthopyroxene are almost identical to those of separate single grains of clinopyroxene.

Orthopyroxene

Compositions of orthopyroxene from 5 specimens, three of which contain clinopyroxene were determined and classified as hypersthene (analyses 1, 5 in Table 4.14; 1 in Table 4.15; 1 of 65 P in Table 4.20, 1 and 5 in Table 4.22). There is a chemical variation of orthopyroxene in quartz-biotite norites from $Wo_2 En_{53} Fs_{45}$ in specimen 62 P to $Wo_2 En_{43} Fs_{55}$ in specimen 65 P. Orthopyroxene in noritic rocks is also classified as hypersthene of composition varying from $Wo_2 En_{57} Fs_{41}$ to $Wo_2 En_{45} Fs_{53}$. Al_2O_3 is relatively low and shows good correlation with coexisting clinopyroxene. Orthopyroxene always has lower Al_2O_3 content than clinopyroxene which contains 0.52-2.37% Al_2O_3 . Conversely MnO is normally higher in orthopyroxene than clinopyroxene and ranges from 0.58 to 0.78% in orthopyroxene. TiO_2 values are normally low. Consistent and homogeneous values of MnO and Al_2O_3 are found. Zoning is not detected in either pyroxene.

Cummingtonite

Some selected cummingtonite analyses are presented with their coexisting orthopyroxenes and rimming hornblende in Tables 4.14-4.22. Slight zoning is detected in cummingtonite with increases in Na_2O and TiO_2 from core towards rim while major elements remain more or less constant. Cummingtonites coexisting with orthopyroxenes

have compositions ranging from 46.1 to 58.9 percent $Mg/(Mg + Fe^{total})$ depending on compositions of orthopyroxene. For all compositions, cummingtonite has slightly higher $Mg/(Mg + Fe^{total})$ ratios than coexisting orthopyroxene. There are no systematic distributions of CaO and Al_2O_3 among coexisting orthopyroxene and cummingtonite. In specimen 62 P, CaO and Al_2O_3 are higher in cummingtonite, while CaO is higher in orthopyroxene but Al_2O_3 is higher in cummingtonite in specimen 65 P, or alternatively, both CaO and Al_2O_3 are higher in orthopyroxene (724 C) or equivalent in both minerals (746 C). Unusually high CaO (3.47% and 3.87%) in cummingtonite of 735 C and 741 C is probably due to fine lamellae of Ca-amphibole.

Orthopyroxene-free cummingtonite has $Mg/(Mg + Fe^{total})$ ratios ranging from 42.2 to 50.9%, and lower in specimen 757 C (40.8%) and specimen 758 C (40.7%) where coarse cummingtonite aggregates are partly replaced by hornblende.

Actinolite

Generally, compositions of pseudomorphing actinolite show slightly lower $Mg/(Mg + Fe^{total})$ ratios than relict clinopyroxene, both MgO and FeO being higher. SiO_2 of actinolite is slightly higher than clinopyroxene in some specimens (733 P, 73 P, 724 C, 81 P, 84 P) but slightly lower in others (757 C, 62 P). Al_2O_3 content is normally higher in actinolite, ranging from 0.92 up to 5.34% in actinolitic hornblende. Actinolite is continuously zoned by slightly increasing Al_2O_3 , (FeO + Fe_2O_3) and decreasing MgO, SiO_2 from actinolite core to actinolite hornblende towards the contact with hornblende.

Actinolite also occurs as patches in cummingtonite in specimen

741 C (analysis 1, Table 4.18), and between cummingtonite and edging hornblende (analysis 2, Table 4.19) of specimen 757 C. There is no compositional difference between different generations of actinolite in the same specimen. In all cases, the $Mg/(Mg + Fe^{total})$ ratio in actinolite is significantly higher than in coexisting cummingtonite and hornblende.

Hornblende

Analyses of rimming hornblende around actinolite and cummingtonite from 14 specimens are presented in Tables 4.14-4.22. Hornblende compositions vary markedly within the intrusion. They can not be simply selected to compositions of primary pyroxenes, cummingtonite or associated plagioclase. There is no significant compositional variation between edging hornblendes around cummingtonite and those surrounding actinolite in the same specimen, suggesting that compositions of hornblende are not controlled by pre-existing phases.

Usually the $Mg/(Mg + Fe^{total})$ ratio is lower in hornblende (ranging from 28 to 48.7%) than in the cummingtonite core. But in some specimens (62 P, 735 C and 757 C), it is slightly higher than in cummingtonite. In 62 P and 735 C, cummingtonite is Mg-rich compared with cummingtonite in the other specimens. Al_2O_3 varies greatly from 5.92% in ferro-hornblende of specimen 757 C to 18.32% in ferrotschermakite of specimen 65 P. No systematic variations for CaO and MnO were observed. The high Al, Fe amphiboles usually exhibit bluish-green or blue colour, while the lower Al ones are green.

Compositions of hornblende around actinolite also have lower $Mg/(Mg + Fe^{total})$ ratios (which range from 23.4-55.5%) than

TABLE 4.23 Partial analysis of plagioclase, presented as numbers of atoms based on 8 oxygens.

SPECIMEN NO.	73 P	741 C	757 C	758 C	746 C	725 C	724 C	733 C	62 P ₁	62 P ₂
Si	2.446	2.484	2.571	2.477	2.466	2.442	2.446	2.458	2.341	2.426
Al	1.554	1.516	1.429	1.523	1.534	1.558	1.554	1.542	1.659	1.574
	4.00	4.00	4.00	4.00	4.00	4.00	4.00	4.00	4.00	4.00
Na	0.437	0.479	0.563	0.467	0.454	0.439	0.441	0.448	0.341	0.419
Ca	0.554	0.516	0.429	0.523	0.534	0.558	0.554	0.542	0.659	0.574
K	0.009	0.005	0.008	0.010	0.012	0.003	0.005	0.010	0.00	0.007
	1.00	1.00	1.00	1.00	1.00	1.00	1.00	1.00	1.00	1.00
% An	55.4	51.6	42.9	52.3	53.4	55.8	55.4	54.2	65.9	57.4

actinolite. Al_2O_3 values vary from 5.34% in ferro-actinolitic hornblende of specimen 757 C to 19.46% in ferropargasite of specimen 733 C.

Rimming hornblendes around both cummingtonite and actinolite are slightly zoned in the same manner with increasing NaO, Al_2O_3 and ($\text{Fe}_2\text{O}_3 + \text{FeO}$), and decreasing SiO_2 and MgO, towards plagioclase, except in specimen 62 P in which hornblende is quite homogeneous with only slight increase in Al_2O_3 and decreasing SiO_2 towards plagioclase.

Plagioclase

Table 4.23 shows some analyses of plagioclase next to hornblende. Zoning is very weak. Plagioclase compositions range from An_{43} in specimen 757 C to An_{54} in most of the studied specimens. In 62 P, plagioclase is An_{59-66} .

4.4.3 Belhelvie intrusion

Pyroxenes

Analytical data for coexisting clinopyroxene and orthopyroxene and their pseudomorphing amphiboles, from the Balmedie Quarry, are given in Tables 4.24 to 4.26. Orthopyroxenes range from hyperthene ($\text{Wo}_2 \text{En}_{63} \text{Fs}_{35}$) in specimen 19 D to bronzite ($\text{Wo}_3 \text{En}_{72} \text{Fs}_{25}$) in specimen 38 P. Clinopyroxene is salite of $\text{Wo}_{46} \text{En}_{42} \text{Fs}_{12}$ to $\text{Wo}_{47} \text{En}_{43} \text{Fs}_{10}$. For coexisting pyroxenes, Belhelvie pyroxenes are Mg-rich compared with the pyroxenes from Morven-Cabrach and Glen Scaddle intrusions. Al_2O_3 content in orthopyroxene (1.10-1.35%) is generally higher than those in the Morven-Cabrach mass while MnO in both pyroxenes is lower. The alkali content in both pyroxenes is less than 0.5

TABLE 4.24 EPMA of pyroxenes, pseudomorphing amphiboles and surrounding hornblende.

SPECIMEN NO.	19D						19E		
	1	2	3	4	5	6	7	8	9*
ANALYSIS	OPX	CUMMING TONITE	ACTINOLITE HORNBLLENDE	CPX	ACTINOLITE	MAGNESIO HB	CUMMING TONITE	FERROAN PARGASITIC HORNBLLENDE	MAGNESIO HB
Na ₂ O	0.44	0.35	0.76	0.33	0.21	0.69	0.11	1.79	0.75
MgO	22.93	20.23	17.59	15.26	18.27	13.08	21.28	12.99	15.79
Al ₂ O ₃	1.01	5.05	7.12	1.51	1.78	8.67	1.26	14.29	6.97
SiO ₂	53.95	53.40	51.80	51.52	54.28	48.92	56.19	45.14	49.70
K ₂ O	-	0.15	0.12	-	0.01	0.27	-	0.19	0.45
CaO	0.95	1.62	9.69	23.51	13.23	13.19	0.73	11.52	11.86
TiO ₂	0.41	0.37	0.57	0.40	0.06	0.12	0.04	0.23	1.39
MnO	0.44	0.16	0.16	0.21	0.15	0.15	0.41	0.16	0.21
FeO**	22.35	18.68	10.99	7.99	10.14	13.04	19.31	12.62	11.13
H ₂ O		2.14	2.13		2.11	2.07	2.13	2.09	2.09
Total	102.48	102.15	100.93	100.73	100.24	100.20	101.46	101.02	100.34
Si	1.96	7.47	7.28	1.92	7.71	7.08	7.89	6.48	7.14
Al ^{iv}	0.04	0.53	0.72	0.07	0.29	0.92	0.11	1.52	0.86
	2.00	8.00	8.00	1.99	8.00	8.00	8.00	8.00	8.00
Al ^{vi}	0.01	0.31	0.45	0.00	0.00	0.56	0.10	0.90	0.30
Ti	0.01	0.04	0.06	0.01	0.01	0.01	0.01	0.03	0.15
Mg	1.24	4.22	3.68	0.85	3.87	2.82	4.45	2.78	3.37
Fe	0.68	2.19	1.29	0.25	1.20	1.58	2.27	1.52	1.33
Mn	0.01	0.02	0.02	0.01	0.02	0.02	0.05	0.02	0.03
Na	0.03	6.78	5.50	0.02	5.10	4.99	6.88	5.25	5.18
Ca	0.04	0.09	0.21	0.02	0.06	0.19	0.03	0.50	0.21
K	0.00	0.24	1.46	0.94	2.01	2.05	0.11	1.77	1.82
		0.03	0.02	-	0.00	0.05	-	0.04	0.08
	2.02	0.36	1.69	2.08	2.07	2.29	0.14	2.31	2.11
100 Mg	64.6	65.8	74.0	77.3	76.3	64.1	66.2	64.7	71.7
Mg + Fe***									

* Primary brown hornblende

** FeO is total Fe

*** Fe = Fe total

TABLE 4.25 EPMA of pyroxenes and amphiboles of 38 P showing transitional composition from actinolite to hornblende.

ANALYSIS No.	1			2			3							
	1	2	3	4	5	6	7	8	9	10	11	12	13	14
MINERAL NAME	OPX	CUMMING-TONITE	FERROAN PARGASITE	OPX	CUMMING-TONITE	ACTINOLITIC HORNBLende	MAGNESIO HORNBLende	CPX	ACTINO-LITE	ACTINO-LITE	ACTINOLITIC HORNBLende	MAGNESIO HORNBLende	MAGNESIO HORNBLende	MAGNESIO HORNBLende
Na ₂ O	-	0.00	2.61	-	0.22	0.54	1.26	0.26	0.08	0.42	0.36	0.88	0.95	1.27
MgO	26.71	23.25	12.31	26.39	21.80	18.06	17.29	15.37	19.11	18.98	17.98	15.48	15.06	14.90
Al ₂ O ₃	1.16	0.93	16.44	1.17	2.03	5.33	10.53	1.67	1.95	3.01	3.80	6.29	7.62	8.56
SiO ₂	53.46	55.77	41.37	54.09	55.61	50.47	49.03	52.46	54.57	53.13	51.51	47.34	46.66	46.65
K ₂ O	-	0.00	0.23	-	0.00	0.11	0.35	-	0.07	0.12	0.30	0.36	0.41	0.29
CaO	1.90	0.89	11.58	1.74	2.01	11.47	11.71	23.05	12.47	12.03	12.34	11.84	11.84	11.87
TiO ₂	0.17	0.52	0.21	0.18	0.03	0.32	0.09	0.30	0.21	0.46	0.63	0.87	0.78	0.77
MnO	0.31	0.38	0.12	0.34	0.24	0.14	0.14	0.18	0.17	0.14	0.13	0.14	0.16	0.17
Fe ₂ O ₃	-	-	0.00	-	-	2.37	1.74	-	1.14	1.71	2.32	2.17	2.17	1.37
FeO	14.49	15.71	10.48	15.70	17.05	6.54	7.49	5.95	7.05	7.01	6.96	8.56	8.94	9.61
H ₂ O	-	2.12	2.01	-	2.14	2.06	2.14	-	2.11	2.10	2.07	1.99	2.00	2.02
Total	98.20	99.57	97.36	99.61	101.13	97.41	101.77	99.24	98.93	99.11	98.40	96.11	96.59	97.48
Si	1.96	7.87	6.16	1.965	7.79	7.31	6.83	1.95	7.74	7.55	7.41	7.07	6.95	6.90
Al ^{iv}	0.04	0.13	1.84	0.035	0.21	0.69	1.17	0.05	0.26	0.45	0.59	0.93	1.05	1.10
Al ^{vi}	2.00	8.00	8.00	2.00	8.00	8.00	8.00	2.00	8.00	8.00	8.00	8.00	8.00	8.00
Ti	0.01	0.02	1.05	0.02	0.13	0.21	0.57	0.03	0.07	0.06	0.06	0.19	0.30	0.38
Fe ³⁺	0.01	0.06	0.00	0.01	0.00	0.04	0.01	0.01	0.02	0.05	0.07	0.10	0.09	0.09
Fe ²⁺	1.46	4.89	2.73	1.43	4.55	3.90	3.60	0.85	4.04	4.02	3.86	3.45	3.34	3.28
Mn	0.45	1.85	1.31	0.48	2.00	0.80	0.87	0.19	0.84	0.83	0.84	1.07	1.12	1.19
Na	0.01	0.05	5.13	0.01	6.71	5.23	5.25	0.01	5.11	5.16	5.10	5.07	5.11	5.11
Ca	-	0.00	0.75	-	0.06	0.15	0.34	0.02	0.02	0.12	0.10	0.26	0.28	0.36
K	0.08	0.14	1.85	0.07	0.30	1.78	1.75	0.92	1.90	1.83	1.90	1.93	1.89	1.88
	-	0.00	0.04	-	0.00	0.02	0.06	-	0.01	0.02	0.06	0.07	0.08	0.06
	2.02	0.14	2.64	2.02	0.36	1.95	2.15	2.03	1.93	1.97	2.06	2.26	2.25	2.30
100 + Mg / Mg + Fe Total	76.4	72.6	67.6	74.9	69.5	78.6	77.4	81.7	80.8	79.9	78.0	72.5	71.1	71.0

TABLE 4.26 Analyses of pyroxenes and amphiboles of 33 P.

ANALYSIS No.	1				2			3			4	
	1	2	3	4	5	6	7	8	9	10	11	
MINERAL NAME	OPX	CUMMING- TONITE	CUMMING- TONITE	FERROAN PARGASITE	CUMMING- TONITE	ACTINOLITIC HORNBLLENDE	FERROAN PARGASITE	CPX	ACTINO- LITE	ACTINOLITIC HORNBLLENDE	PRIMARY MAGNESIO HORNBLLENDE	
Na ₂ O	0.26	0.01	0.01	1.85	0.00	0.66	1.73	0.00	0.14	0.47	0.54	
MgO	24.48	22.83	20.99	10.91	21.19	16.61	10.04	14.50	17.02	14.00	13.69	
Al ₂ O ₃	1.32	0.67	0.40	16.39	0.28	6.33	16.68	1.19	1.00	5.73	6.50	
SiO ₂	53.25	55.53	55.27	41.02	55.15	50.60	40.47	53.02	53.07	49.48	48.76	
K ₂ O	-	0.13	0.00	0.10	-	0.27	0.12	-	0.24	0.22	0.26	
CaO	1.32	0.41	0.70	11.36	0.81	11.56	11.79	23.17	12.57	12.30	12.22	
TiO ₂	0.12	0.03	0.01	0.15	0.02	0.16	0.07	0.17	0.13	0.72	1.14	
MnO	0.39	0.40	0.45	0.12	0.56	0.14	0.14	0.22	0.22	0.19	0.18	
Fe ₂ O ₃	-	-	-	1.61	-	1.42	3.21	-	1.38	1.55	0.27	
FeO	19.46	17.64	19.41	11.35	18.89	9.35	11.30	7.24	9.56	12.30	12.75	
H ₂ O	-	2.11	2.08	1.98	2.08	2.08	1.98	-	2.04	2.03	2.03	
Total	100.60	99.76	99.32	96.84	98.98	99.18	97.56	99.51	97.37	98.99	98.34	
Si	1.95	7.89	7.95	6.165	7.95	7.27	6.08	1.98	7.77	7.30	7.185	
Al ^{iv}	0.05	0.11	0.05	1.835	0.05	0.73	1.92	0.02	0.17	0.70	0.815	
Al ^{vi}	2.00	8.00	8.00	8.00	8.00	8.00	8.00	2.00	7.94	8.00	8.00	
Al ^{vi}	0.01	0.00	0.02	1.07	0.00	0.34	1.04	0.03	0.00	0.30	0.31	
Ti	0.00	0.00	0.00	0.02	0.00	0.02	0.01	0.01	0.01	0.08	0.13	
Fe ³⁺	-	-	-	0.18	-	0.15	0.37	-	0.15	0.06	0.03	
Mg	1.34	4.83	4.50	2.44	4.55	3.56	2.25	0.81	3.72	3.08	3.01	
Fe ²⁺	0.60	2.10	2.34	1.43	2.28	1.12	1.42	0.23	1.17	1.52	1.57	
Mn	0.01	0.05	0.06	0.02	0.07	0.02	0.02	0.01	0.03	0.02	0.02	
Na	0.02	0.00	0.00	0.54	0.00	5.21	5.11	-	5.08	5.06	5.07	
Ca	0.05	0.06	0.11	1.83	0.12	1.78	1.90	0.00	0.04	0.13	0.15	
K	-	0.02	0.00	0.02	-	0.05	0.02	0.93	1.97	1.95	1.93	
	2.03	0.08	0.11	2.39	0.12	2.01	2.43	2.02	2.05	2.12	2.13	
100 Mg Mg + Fe Total	69.2	69.7	65.8	60.2	66.6	73.7	55.7	77.9	73.8	66.1	65.3	

weight percent. There is no significant change in composition of pyroxenes towards contacts with secondary amphiboles.

Cummingtonite

The composition of cummingtonite differs from that of coexisting orthopyroxene in being higher in SiO_2 and lower in MgO , while FeO is lower in 33 P and 19 D but slightly higher in 38 P. The $\text{Mg}/(\text{Mg} + \text{Fe}^{\text{total}})$ ratio is virtually identical for the two minerals (76.4-69.5%) except in 38P where it is slightly lower in cummingtonite. Cummingtonite is slightly zoned with increasing FeO and decreasing MgO from the orthopyroxene contact outwards. Since CaO , Al_2O_3 and Na_2O are very low in both cummingtonite and orthopyroxene, no systematic relations can be observed. CaO content ranges from 0.41-2.10%. Al_2O_3 is also low, ranging from 0.93-2.03% except in analysis 2, Table 4.24 in which Al_2O_3 is unusually high (5.06%), probably due to very fine lamellae of an Al-rich phase.

Actinolite

The data indicate that replacing actinolites after clinopyroxenes have higher MgO , FeO but much lower CaO than clinopyroxene. SiO_2 is also higher, but remains constant in specimen 33 P (analyses 8, 9 Table 4.26). However, $\text{Mg}/(\text{Mg} + \text{Fe}^{\text{total}})$ is similar in both minerals (77.3-81.7%). Actinolite inherited the Al_2O_3 and MnO content of the clinopyroxene TiO_2 is slightly lower in actinolite. It is continuously zoned with Al_2O_3 , $(\text{FeO} + \text{Fe}_2\text{O}_3)$, TiO_2 and Na_2O generally increasing, and SiO_2 and MgO decreasing outwards from actinolite core through actinolite hornblende, which shows a compositional break with rimming magnesio-hornblende where there is an abrupt rise in Al_2O_3 , $(\text{FeO} + \text{Fe}_2\text{O}_3)$, Na_2O and fall in MgO , SiO_2 (between analyses 11 and

12 in Table 4.25).

Hornblende

Compositions of hornblende vary greatly even within the same thin section. Primary brown hornblende is classified as magnesio-hornblende of high MgO, TiO₂, SiO₂ and low Al₂O₃, Na₂O and (FeO + Fe₂O₃) content (analysis 11, Table 4.26 and analysis 9, Table 4.24). Edging hornblendes around cummingtonite differ greatly from those surrounding actinolitic cores in the same specimen. Cummingtonite is rimmed by actinolitic hornblende (19 D), ferroan pargasite (19 E and grain 1 of 33 P) or a transition, from actinolitic hornblende to ferroan pargasite (33 P, grain 2) or magnesio hornblende (38 P). Al₂O₃ is much higher in ferroan pargasite (14.29-16.68%) compared with other types of rimming hornblende. (6.33-7.12% in actinolitic hornblende to 10.53% in magnesio hornblende. The Mg/(Mg + Fe^{total}) ratio in pargasitic hornblende is lower than in cummingtonite core while this ratio is higher in actinolitic hornblende and magnesio hornblende.

Pseudomorphing actinolite is bordered by either actinolitic hornblende (analysis 10, Table 4.26) or magnesio hornblende (analysis 6, Table 4.24) or a transition from actinolitic hornblende through magnesio hornblende outwards (analyses 11-14, Table 4.25). Magnesio hornblende is continuously zoned with rising (FeO + Fe₂O₃), Na₂O, Al₂O₃ and MnO, and falling MgO and SiO₂ towards plagioclase contacts.

Plagioclase

Table 4.27 shows analyses of plagioclase next to rimming hornblende. It is found that plagioclase is zoned of composition An₇₉₋₈₆, with

TABLE 4.27 Compositions of plagioclase from 4 specimens from the Belhelvie Quarry.

SPECIMEN NO.	19 D	19 E	38 P	33 P
Si	2.184	2.202	2.150	2.173
Al	1.816	1.798	1.850	1.827
	4.00	4.00	4.00	4.00
Na	0.182	0.205	0.148	0.172
Ca	0.816	0.793	0.850	0.827
K	0.002	0.002	0.002	0.001
	1.00	1.00	1.00	1.00
% An	81.6	79.3	85.0	82.7

decreasing An content to An₇₃₋₇₆ at the cores.

4.5 INTERPRETATION AND DISCUSSION

4.5.1 Solidus and Subsolidus Compositional Relationships of Some Coexisting Pyroxenes from the Studied Areas

The major element distributions in single pyroxenes and between coexisting pyroxenes of the present study, from the Morven-Cabrach intrusion, the Belhelvie intrusion and the Glen Scaddle mass are plotted in the pyroxene quadrilateral in Figures 4.13, 4.14 and 4.15 respectively.

Coexisting orthopyroxene and clinopyroxenes are connected by tie lines. The tie line of specimen 746 C in Figure 4.13 joins coexisting clinopyroxene bleb and orthopyroxene host. In addition to data presented in this study, one pair of coexisting pyroxenes in a Morven-Cabrach rock from Allan (1970) is also plotted in Figure 4.13. Examination of Figures 4.13 and 4.14 reveals that the miscibility gap between coexisting pyroxenes is very broad with Wo of orthopyroxene approximately 2% and clinopyroxene > 40% Wo. The long tie lines between coexisting pyroxenes are essentially coincident with those connecting the compositions of coexisting pyroxenes from many metamorphic rocks. (Huebner, 1982).

Also plotted in figure 4.14 are analyses of clinopyroxene in specimens studied for coronas (Chapter 3), in which clinopyroxenes have not been replaced by secondary amphiboles, and previous analyses of coexisting pyroxenes by Wadsworth et. al. (1966). Wadsworth et.al.'s specimens came from troctolitic, gabbroic and noritic units of the

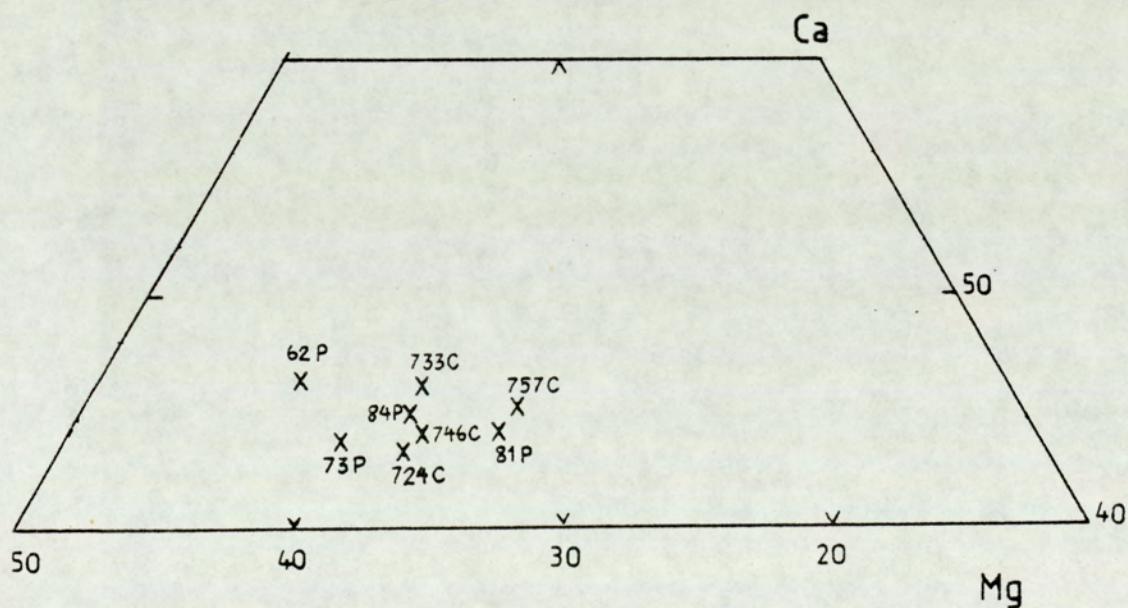
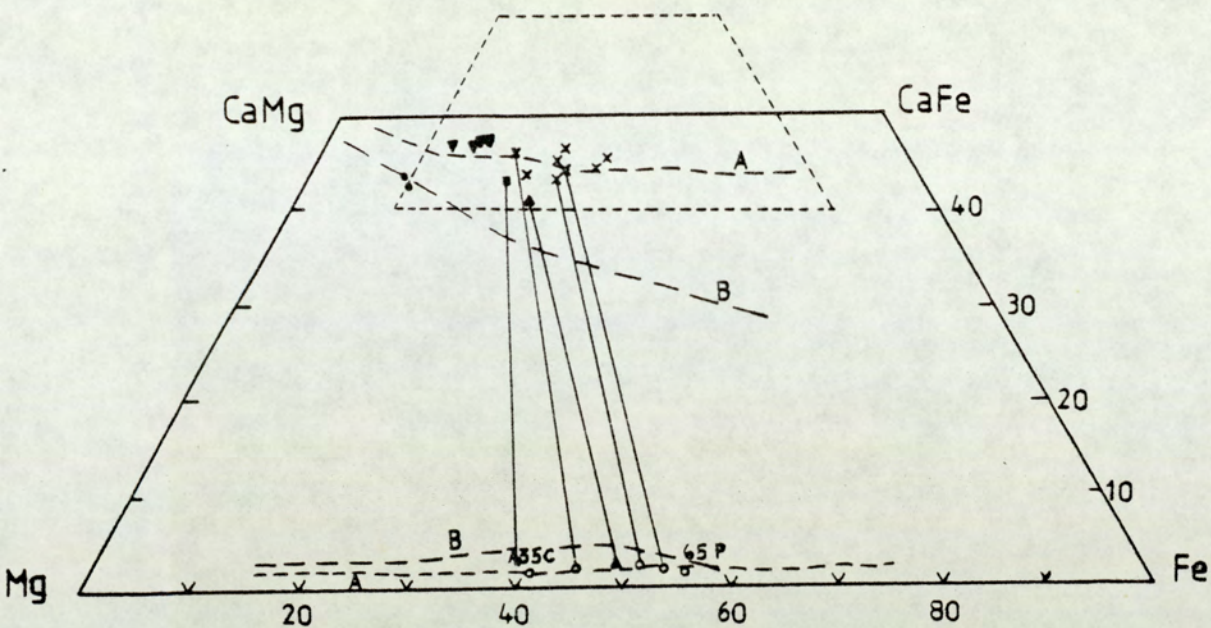


Fig 4.13 Ca-Fe-Mg diagram of pyroxenes from the Morven-Cabrach area and comparable areas. Dotted lines A and B are metamorphic and igneous trends from Huebner (1980). Tie-lines join coexisting pairs.

- x Morven-Cabrach mass (this study)
- △—▲ Morven-Cabrach mass (Allan, 1970)
- Insh mass (Clarke & Wadsworth, 1970)
- ▼ Portsoy mass
- Huntly mass

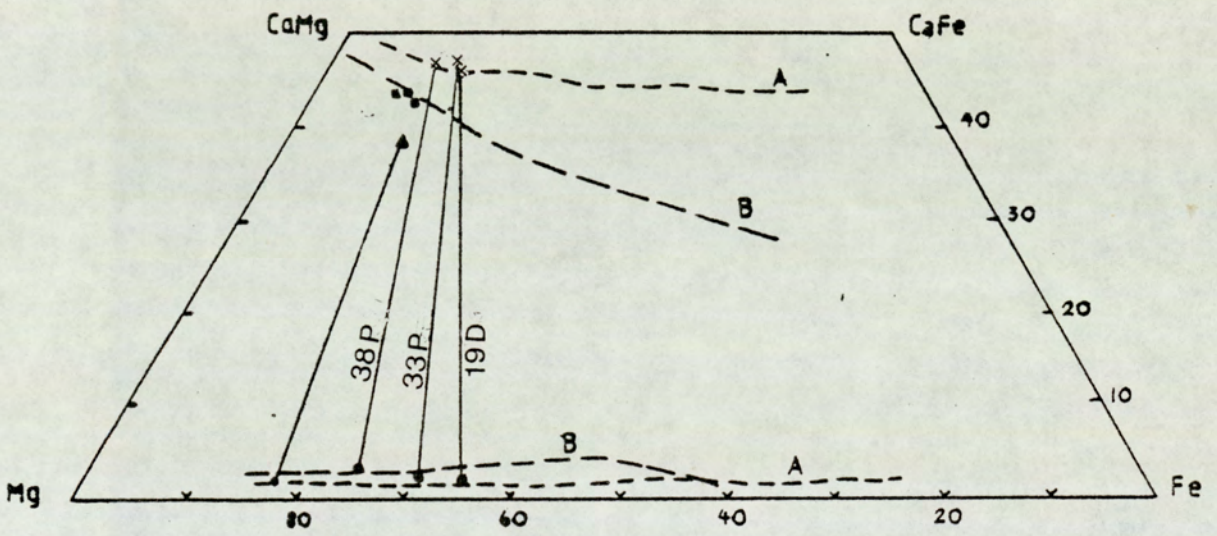


Fig 4.14 Ca-Fe-Mg diagram of pyroxenes from Belhelvie area.

- x Uralitised pyroxenes
- Unaltered pyroxene from coronites
- ▲ Data from Wadsworth et. al.

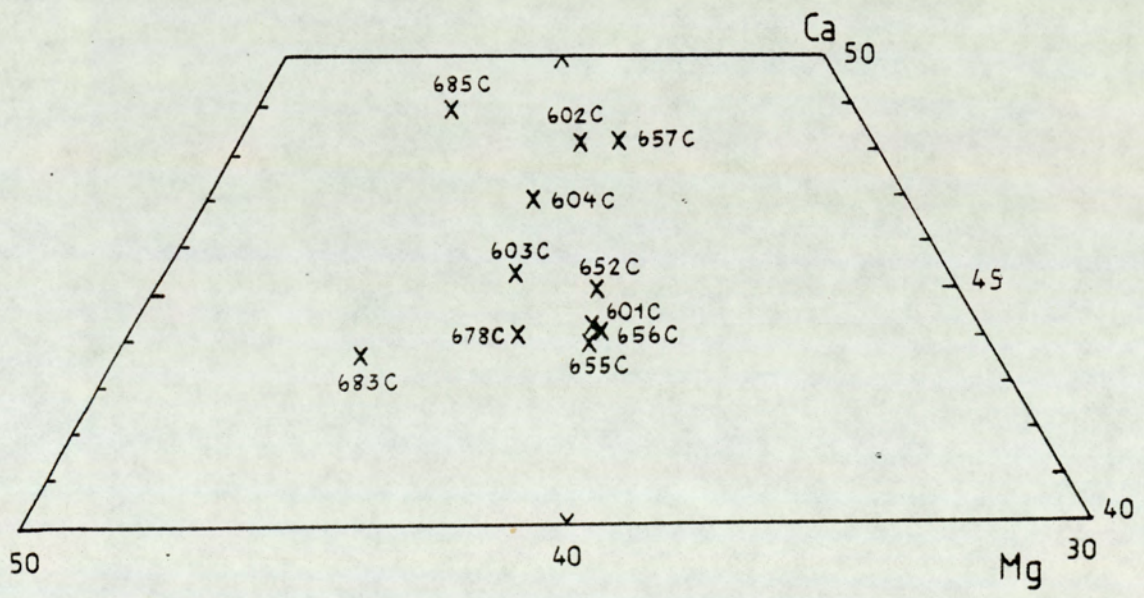
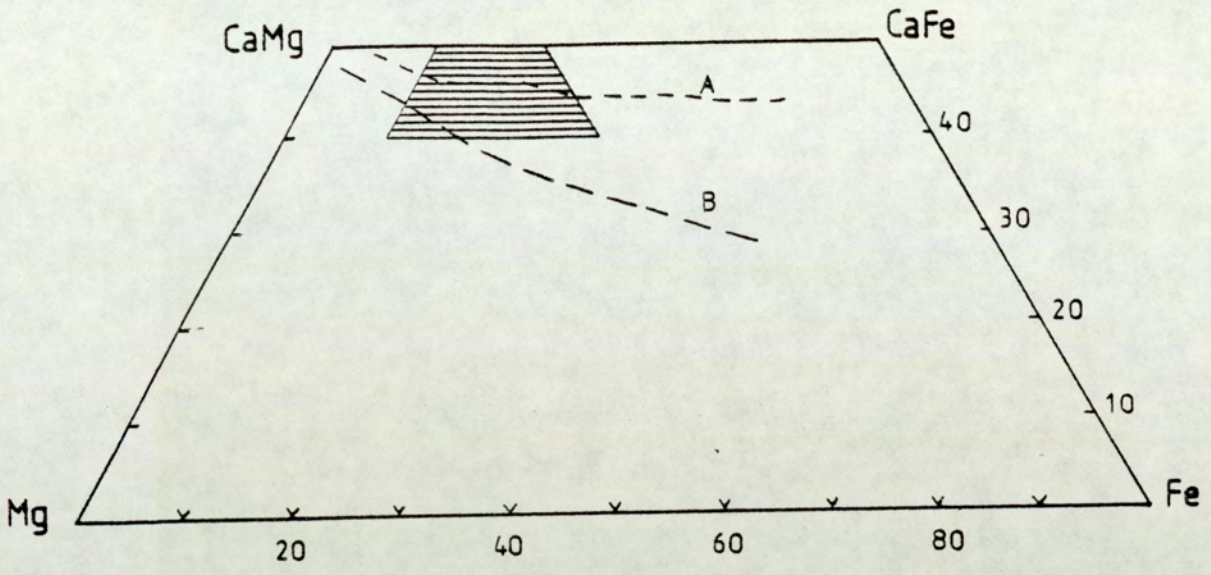


Fig 4.15 Ca-Fe-Mg diagram of pyroxenes from the Glen Scaddle area.

other septum of the intrusion. Specimen B.H.8 is hypersthene gabbro, augite showing very fine exsolution lamellae of orthopyroxene along (100) plane (Smith, 1977). It is found that pyroxenes from the Belhelvie intrusion are controlled by the two types of tie line in the pyroxene quadrilateral. Wadsworth et.al.'s data and 'unuralitized' clinopyroxene in coronites are found to lie close to a solidus trend of coexisting pyroxenes that crystallized contemporaneously from a melt at equilibrium (line B). Uralitized pyroxenes from the Balmedie Quarry essentially coincide with the trend of metamorphic pyroxene or sub-solidus trend (line A).

The compositions of pyroxenes from other intrusions of the 'younger' basic complexes are also plotted in Figure 4.13 for comparison with the present ~~study~~ study. Data from ^{the} Insch mass were obtained from Clarke and Wadsworth (1970). Analyses of clinopyroxene from the Portsoy and the Huntly masses were carried out in the present study. Their analyses are tabulated in Appendix 2. Portsoy specimens contain uralitized pyroxene while pyroxene from Huntly is unaltered. Figure 4.13 also suggests two types of pyroxene trends, one of which is a subsolidus trend, the other is a crystallization trend consistent with an igneous origin. The compositions, in terms of their major constituents, of the analysed clinopyroxene from the Glen Scaddle mass are graphically presented in Figure 4.15. Once again, they scatter along the subsolidus trend.

Figures 4.13 to 4.15 strongly suggest that extensive sub-solidus chemical readjustment has occurred in some of these pyroxenes. Since these intrusions are very slow-cooled, (Stoker, 1980 and Pankhurst, 1970), the re-equilibration of pyroxenes after initial

crystallization could be possible. Also, the presence of coarse lamellae or blebs is a clear indication of sub-solidus re-equilibration (exsolution). However, exsolution lamellae are absent from most of the studied specimens, so other subsolidus changes must have affected the composition.

It is clear from the present analyses that pyroxenes that have undergone uralitization always lie along the sub-solidus trend while fresh, unaltered pyroxene is still unchanged, and lies along the solidus trend. This picture indicates pyroxene reequilibration took place during the uralitization process, so the uralitization is a retrograde, regional metamorphic phenomenon.

Geothermometry of coexisting pyroxenes was attempted using the method of Wood and Banno (1973) based on three types of solvus; enstatite-diopside solvus determined at 30 kbar by Davis and Boyd (1966), by Nehru and Wyllie (1974) at 30 kbar and Lindsley and Dixon (1976) at 20 kbar. Temperatures calculated using all three sets of parameters are listed in Table 4.28 as T_1 , T_2 and T_3 respectively. Temperature estimations by these methods are found to be unrealistically and unacceptably high for metamorphic temperatures. All these solvi were determined at very high pressure. For the rocks studied, lower pressure parameters would have been more appropriate. However, one pair of igneous pyroxenes from the Belhelvie mass analysed by Wadsworth et. al. (1966) gives reasonable igneous temperatures of 1127° , 1120° and 1283° by these methods.

Recently, Lindsley and Anderson (1983) introduced a useful graphical two-pyroxene thermometer on the quadrilateral diagram at low pressure ($P < 2$ kbar). In Figure 4.16, their isotherms are plotted along with

TABLE 4.28 Comparisons of estimated temperature of coexisting pyroxenes using Wood and Banno (1973) calculation method based on enstatite-diopside solvus determined at 30 kbar by Davis and Boyd (1966) as T₁; Nehru and Wyllie (1974) as T₂; Lindsley and Dixon (1976) at 20 kbar as T₃.

LOCALITY	SPECIMEN NO.	T ₁	T ₂	T ₃
BELHELVIE	33 P	880°	752°	792°
	38 P	970°	850°	919°
	19 D	955°	910°	1034°
	BH 8*	1127°	1120°	1283°
MORVEN- CABRACH	62 P	810°	700°	740°
	724 C	917°	917°	1074°
	746 C	856°	810°	915°

* analyses from Wadsworth et al (1966)

$$T_1 = (10202.0 / (\ln (a^{cpx}/a^{opx}) - 7.65 \times^{opx} + 3.88 \times^{opx} - 4.6) - 273)$$

$$T_2 = (-5006.0 / (\ln (a^{cpx}/a^{opx}) - 3.75 \times^{opx} + 1.90 \times^{opx} \times^{opx} - 1.72) - 273)$$

$$T_3 = (-3951.0 / (\ln (a^{cpx}/a^{opx}) - 2.96 \times^{opx} + 1.50 \times^{opx} \times^{opx} - 0.75) - 273)$$

(after Henry and Medaris parameter in Stormer and Whitney, 1977).

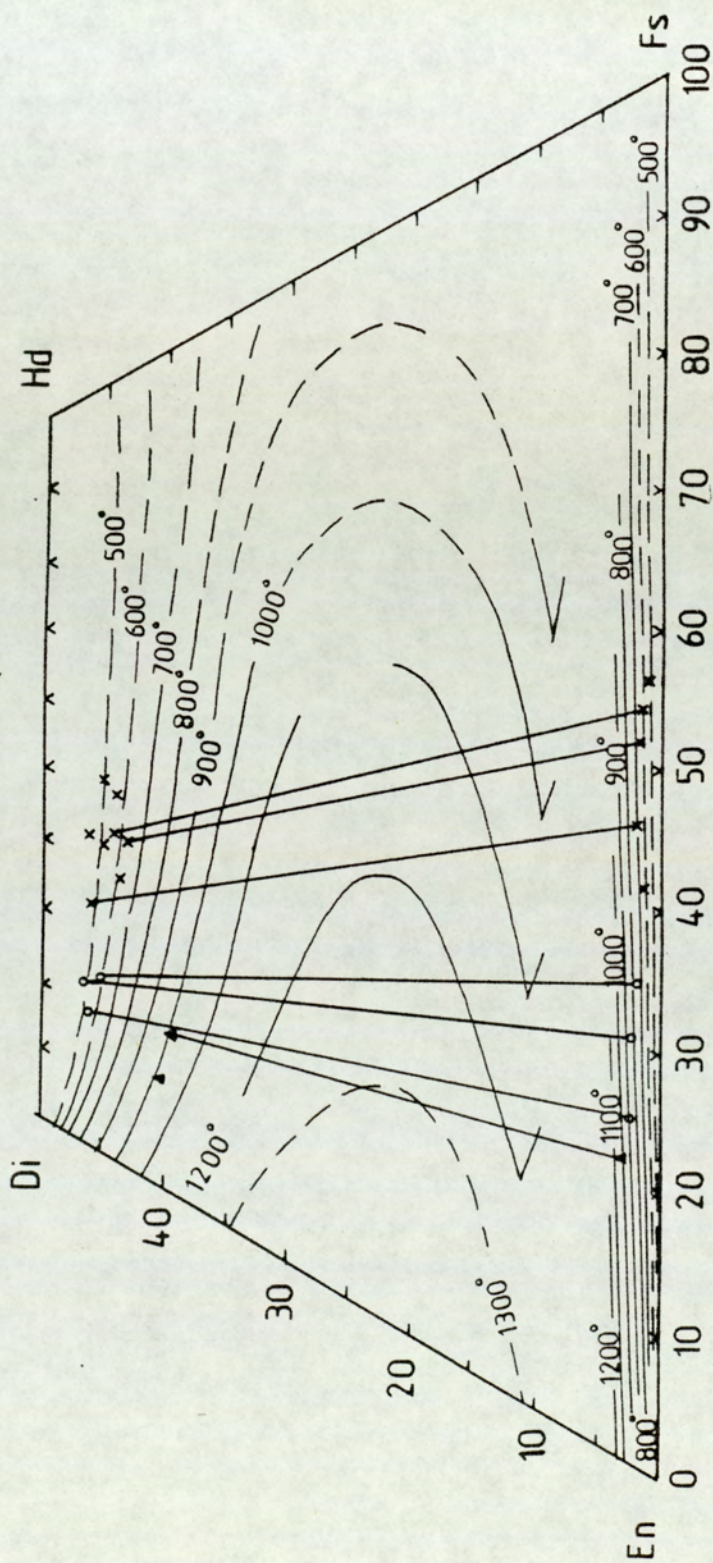


Fig 4.16 Graphical pyroxene geothermometer of Lindsley and Anderson (1983).

- o—o Belhelvie pyroxenes (this study)
 - ▲—▲ Belhelvie pyroxene
 - x—x Morven-Cabrach pyroxenes
- (data from Wadsworth et. al.)

the pyroxenes studied for estimation of metamorphic temperatures. Although the proper method of projecting on to the MgSiO_3 - CaSiO_3 - FeSiO_3 plane is required before an accurate geothermometer is possible (Lindsley and Anderson, 1983), the present pyroxene analyses contain very small or negligible amounts of Fe^{3+} , Al and Ti, which do not have much effect on the projection. Therefore, Wo, En, Fs were plotted from the atomic ratios of Ca, Mg and Fe atoms directly. Any accurate two-pyroxene geothermometer must also be pressure-dependent, but the pyroxenes studied are low-pressure ones, so pressure correction for the projection is unnecessary.

Coexisting pyroxenes from the Morven-Cabrach intrusion projected on to the graphical thermometer (Fig 4.16) indicate temperatures ranging from approximately 500° to 600°C for clinopyroxene and 600° to 700°C for orthopyroxene. Clinopyroxenes from the Belhelvie mass indicate temperatures of 500° - 600°C from uralitised pyroxenes in this study and 1000° - 1050°C for igneous pyroxenes from Wadsworth et. al. (1966). Lack of pyroxene pairs prevents use of their thermometer for the Glen Scaddle and Portsoy intrusions. However, the clinopyroxenes lie along the 500° - 600° isotherms of the pyroxene geothermometer.

Two-pyroxene geothermometers are very sensitive to small differences in compositions, particularly for orthopyroxene because the lines are close together (Fig 4.16). Very small uncertainty in the compositions could contribute to large error in the temperature estimation. Moreover, both subsolidus and solidus orthopyroxene, based upon experimental data and natural compositions, contain very similar Wo content. (Lindsley and Dixon, 1976; Bohlen and Essene, 1978). It is therefore very difficult to determine whether the composition of primary

orthopyroxene has changed during the cummingtonite replacement. This perhaps explains the higher temperature for orthopyroxene in the geothermometer graphs compared with coexisting clinopyroxene.

4.5.2 Replacement of Clinopyroxene by Actinolite

Clinopyroxenes and the amphiboles replacing them generally have b, c and a* parallel. On the basis of structural and compositional similarity between single-chain clinopyroxene and double-chain actinolite (both are monoclinic, of C 2/c space group for clinopyroxene and C 2/m for actinolite), and the retaining of the b and c crystallographic axes, it would appear generally that the conversion can occur simply by rotating of alternate single tetrahedral chains of clinopyroxene to double chains of actinolite concomitant with some cation movements (Rodgers, 1973, Nakajima and Ribbe 1981). Changing from T_4O_{12} to T_4O_{11} (where T represents tetrahedrally coordinated Si, Al) leaves one spare oxygen for hydrogen atoms to bond with (hydroxylation). There is no need, or minimum need, for breaking T-O bonds. This transformation would appear therefore to be the rearrangement of the oxygen pattern accompanied by cation migrations through the octahedral and polyhedral sites. The preservation of oxide inclusion patterns of clinopyroxene in pseudomorphing actinolite suggests the minimum structural rearrangement of oxygen atoms. Law and Whittaker (1980) also propose that theoretically stacking sequences of oxygen atoms in pyroxene are closely analogous to amphiboles, corresponding to the above model. An alternative mechanism, in which submicroscopic lamellae ("zippers") of amphibole propagate into pyroxene (Veblen and Buseck, 1981) is possible where the product is an intimate mixture of pyroxene and amphibole, but perhaps less likely where there is a sharp reaction boundary between

pyroxene and amphibole as in the present study. The proposed mechanism suggests that Si and Al may be approximately conserved in the reaction, in which case (Ca + Fe + Mg) decrease from 9 in pyroxene to 7 in amphibole (per 24 oxygens).

In order to understand the chemical changes in this alteration, the differences in number of atoms of each element per 24 (O, OH) between relict clinopyroxene and actinolite are shown in Table 4.29. The number of atoms in actinolite are from analyses next to or within relict clinopyroxene. The amounts of Si and Al are essentially similar in both minerals corresponding to the above model of minimum disturbance of tetrahedral T-O bonds. However, there is an increase in replacement of Si by Al in tetrahedral sites and incoming of Al in octahedral sites in actinolite further from the interface with pyroxene, towards hornblende contacts.

From Table 4.29, the major chemical differences between pyroxene and actinolite are Ca, Fe and Mg; Ca is much higher in clinopyroxene while Fe and Mg are higher in actinolite. At first glance, the main cation movements during the transformation appear to be removal of more than 1 Ca per 24 oxygens from, and introducing Fe, Mg into the system to achieve the net change of -1 in (Ca + Fe + Mg). However such a view is not favoured in the present study for the following reasons. There is compositional evidence that clinopyroxenes once had lower Ca content than they now contain. The solidus trend (line B in Fig 4.13) contains primary clinopyroxenes of lower Ca content than those in the metamorphic trend (line A in Fig 4.13), which are the present compositions of studied clinopyroxenes. Many natural pyroxene assemblages support the concept that tie-lines between pyroxene pairs become longer as temperature falls. This picture suggests increasing Ca content in clinopyroxene after

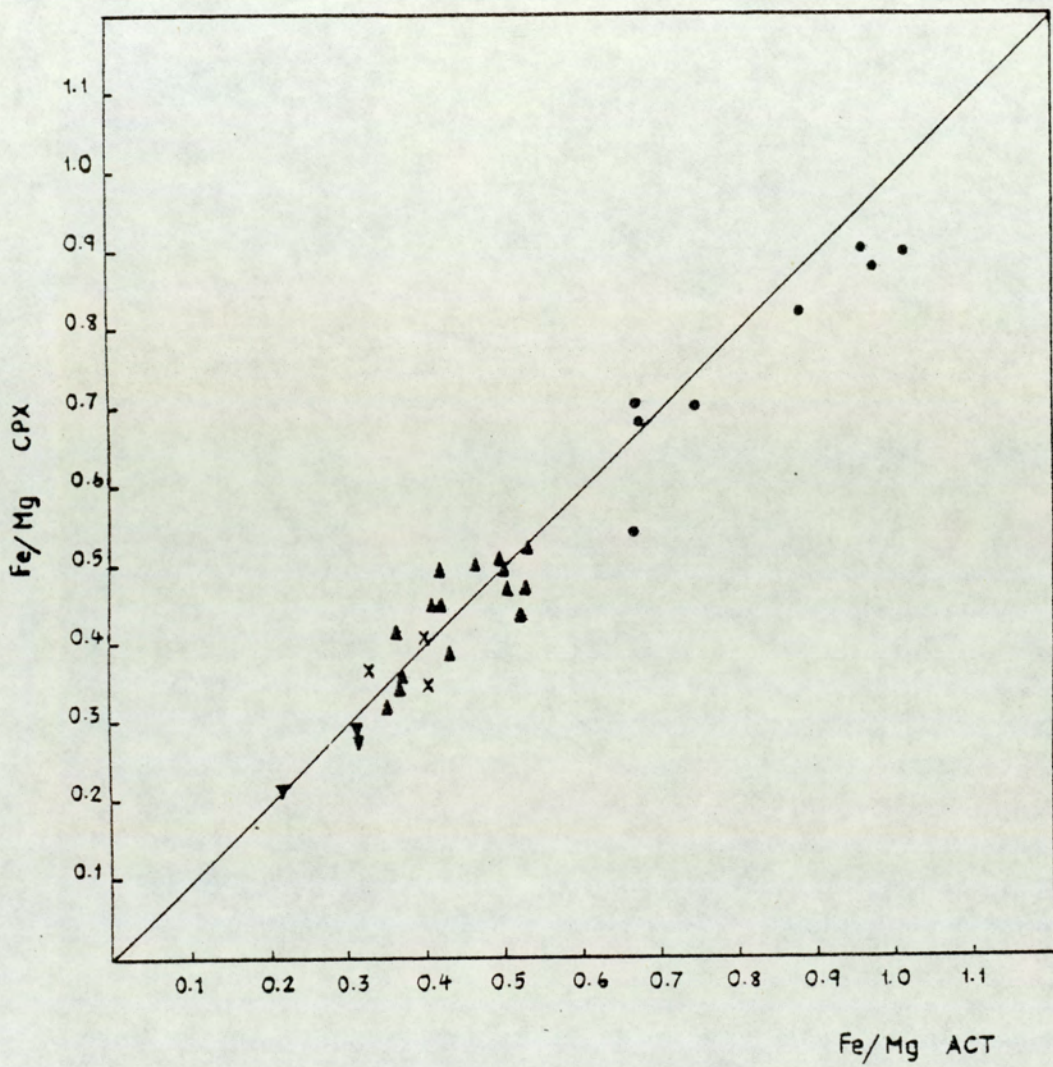


Fig 4.17 Fe/Mg partition between clinopyroxene and replacing actinolite.

- ▲ Glen Scaddle
- ▼ Belhelvie
- Morven-Cabrach
- x Portsoy

metamorphism from igneous compositions. Ca then must move into clinopyroxene at the beginning of actinolite pseudomorphing, rather than being released. However, since Ca content is nearly constant in each grain, despite different amounts of replacement by actinolite within a single thin section, at one stage during the actinolite producing reaction, Ca must be released to maintain this consistent content in pyroxene (see Section 4.5.4 below). Fe/Mg ratios between metamorphic pyroxene and actinolite are similar (Fig 4.17). Thus, Fe²⁺ and Mg could well be 'equilibrated' among these minerals, although the phases themselves may not be in stable equilibrium.

In a dry system, pyroxenes undergo two kinds of structural and chemical changes on cooling from igneous or metamorphic temperature in order to remain in equilibrium; intra crystalline exsolution exchange of Ca, Mg and Fe or the inversion of pigeonite. Clearly, the transformation of clinopyroxene to actinolite is characteristic of pyroxene re-equilibration in the hydrous environment, by the similar process of Ca, Mg and Fe exchange with environment. Unlike the exsolution process in the dry system, this mechanism presumably involves the exchange across the broad reaction front. The degree of transformation depends mainly on the availability of H₂O. The extent of Fe, Mg and Ca exchange with the environment of the clinopyroxene-actinolite system will be considered when hornblende producing reactions are dealt with.

4.5.3 Replacement of Hypersthene by Cummingtonite

Because of the differences in their structures, the transformation of hypersthene to cummingtonite is more complicated than clinopyroxene-actinolite transformation. The hypersthene-cummingtonite transformation involved not only change from the orthorhombic (PaCa) to the

monoclinic (C2/m) system, but also the development of aggregate and fibrous habits of replacing cummingtonite. These habits are very characteristic of cummingtonite in both deformed and undeformed rocks, suggesting internal control.

Since cummingtonite is the amphibole analogue of pigeonite (Ross et. al. 1968, 1969) and clinoenstatite, this process may be analogous to the inversion of orthoenstatite (PbCa) to clinoenstatite (P2₁/c). In the case when cummingtonite forms good, single crystals which is rare, it retains the b and c crystallographic axes of relict hypersthene. In transformation from orthoenstatite to clinoenstatite, a*, b and c crystallographic directions are also unchanged (Smyth 1974, Coe and Kirby 1975). Principally, the hypersthene-cummingtonite transformation requires not only the rotation of alternate single chain as in clinopyroxene-actinolite transformation, but also the translation of the Si chains parallel to c as in orthoenstatite-clinoenstatite transformation (Coe and Kirby, 1975). The process studied by Coe and Kirby (1975) is deformational and produces a bulk shear of the crystal, so cannot completely describe the present case. The minimum movements of oxygen atoms are involved, since the opaque inclusions in hypersthene are generally still remain their positions in cummingtonite after completely pseudomorphing. Bulk shape change may be avoided partly by twinning of the cummingtonite. It is also noteworthy that the cummingtonite usually forms aggregates of misoriented grains, implying a complex mechanism, presumably involving nucleation.

In spite of the differences in structure, in chemistry both minerals are comparable. Table 4.30 shows the comparisons in terms of differences in numbers of atoms of each element per 24 (O, OH) between relict hypersthene and associated cummingtonite. The major

TABLE 4.30 Comparison between relict orthopyroxenes and replacing cummingtonite in terms of differences in numbers of atoms of each element per 240 (OH).

+ means higher in cummingtonite.
 - means higher in orthopyroxene.

LOCALITY	BELHELVIE				MORVEN-CABRACH			
	SPECIMEN NO.	33 P	38 P	62 P	724 C	65 P	746 C	735 C
Si		+0.09	+0.03	-0.01	+0.01	+0.02	+0.09	+0.01
Al		-0.12	-0.05	-0.01	-0.05	+0.05	+0.01	+0.05
Ti		0.00	+0.02	+0.01	0.00	-0.04	-0.02	+0.01
Mg		-0.53	-0.95	-0.23	-0.36	-0.28	-0.25	+0.83
Fe		-0.30	+0.05	-0.81	-0.56	-0.66	-0.90	-0.68
Mn		+0.01	+0.01	-0.03	+0.02	+0.01	-0.04	-0.03
Na		-0.08	0.00	+0.01	+0.03	-	+0.02	-0.05
Ca		-0.14	-0.18	+0.11	-0.06	-0.09	-0.01	+0.43
K		+0.02	-	-	-	-	-	-

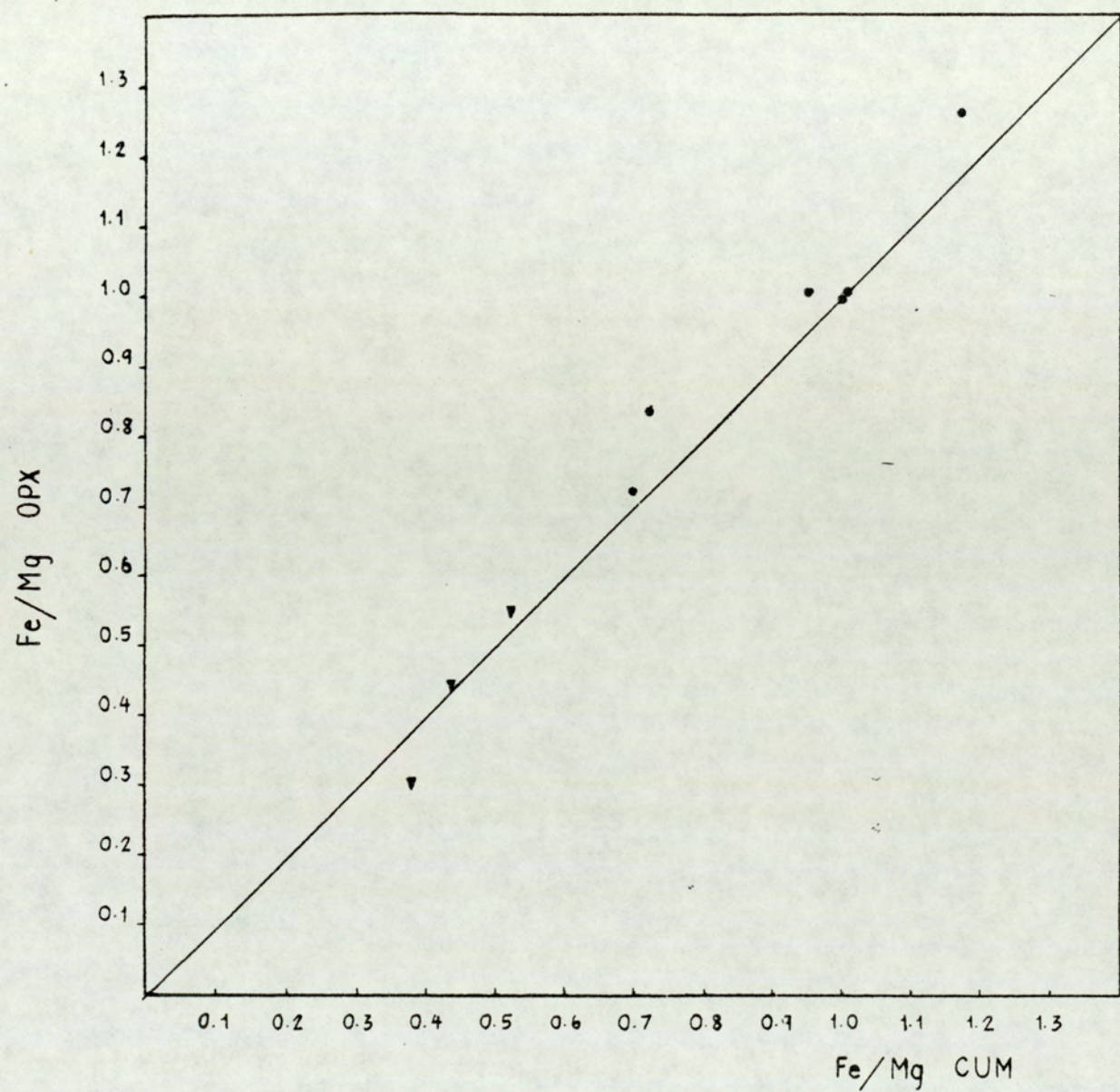


Fig 4.18 Fe/Mg partition between orthopyroxene and pseudomorphing cummingtonite.

- Morven-Cabrach
- ▼ Belhelvie

differences are Fe and Mg. Fe/Mg partition between hypersthene and cummingtonite is plotted in Fig 4.18. Generally, this ratio is quite similar in both minerals. The slightly lower ratio in cummingtonite in some specimens may be consistent with the presence of dustyopaque oxide, which is commonly associated with cummingtonite, and which may be exsolved from it.

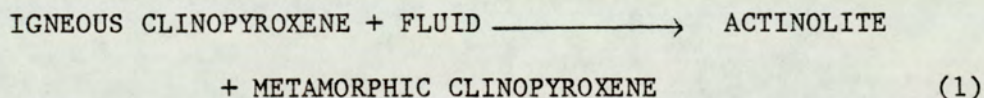
Due to the similarity in chemistry between hypersthene and cummingtonite and lack of zoning in both minerals, it is suggested that the transformation may be more rapid than the clinopyroxene-actinolite transformation, which requires longer time for the ion exchanges because the large Ca^{2+} ion will diffuse slower than the smaller $(\text{Mg}, \text{Fe})^{2+}$. Clinopyroxene, therefore still remains in many specimens while co-existing orthopyroxene is completely replaced by cummingtonite.

4.5.4 Model Reactions for the Formation of Actinolite, Cummingtonite and Hornblende

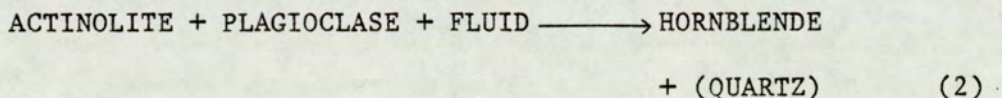
In many terrains, actinolite cores inside hornblende rims can be interpreted as relics of an earlier, low-grade metamorphism (Grapes and Graham, 1978). Such an interpretation would be possible for the Glen Scaddle area in the present study. However, in NE Scotland, the metamorphic history of the basic intrusions is simply retrograde. Interpreting the actinolite as a low-temperature product separately from the hornblende would mean it was later, with the hornblende an early product of a reaction between plagioclase and clinopyroxene. Analogously cummingtonite would have to be interpreted as later than its rimming hornblende, accepting that replacement of relic pyroxenes by actinolite and cummingtonite may have gone on to a late stage. It is noted here that there is textural evidence for replacement of

cummingtonite by hornblende, and that the sequence of assemblages with increasing metamorphic reaction (promoted by shearing) at Belhelvie suggests replacement of actinolite by hornblende. If actinolite formed separately from hornblende it would be difficult to accommodate the chemical changes discussed earlier. The interpretation offered here is that hornblende formed while cummingtonite and actinolite were simultaneously replacing pyroxenes. The simultaneous reactions cannot be modelled exactly because they are too complicated, but some suggestions will now be made.

From the existing textural evidence of core-rim relationships, a plausible model of chemical reactions consistent with the mineralogy and textures can simply be written as:-

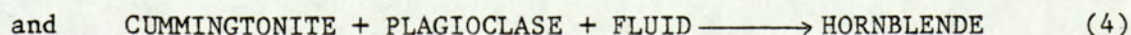


with simultaneous formation of hornblende:-



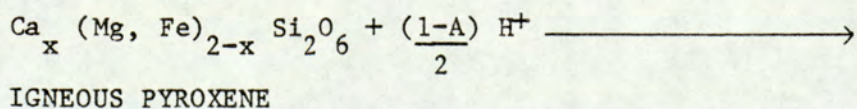
because small quartz grains are present as inclusions in actinolite and hornblende (mostly in the Glen Scaddle specimens). All studied specimens also contain free quartz. On textural grounds, it should be entered on the product side of the reaction.

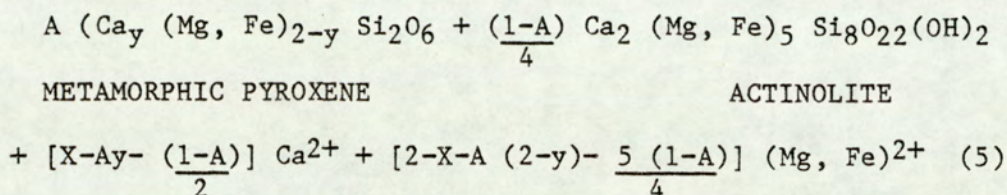
The transformation of orthopyroxene to cummingtonite, contemporaneously with the rimming hornblende formation can be written by the following simplified reactions:-



It is not possible to write these equations quantitatively like those in corona formation (c.f. Chapter 3), since there are so many uncertainties; the compositions of primary pyroxenes are not known, and the ratio of products and reactants can not be measured due to their variations within a single thin section or even within the same grain. Zoning also causes uncertainty in estimating the compositions of product minerals. However, from the data available, mainly the compositions of products and structural relationships between product and reactant, some possible reactions can be modelled from these data based on ideal assumptions.

In the clinopyroxene-actinolite transformation, extending from section 4.5.2, it is assumed, based on structural and chemical relationships that Si is unchanged while Fe, Mg and Ca moved during the reaction. At the beginning of the reaction, when a small amount of actinolite is produced, Ca must move into the system concomitant with releasing Fe, Mg. Since the composition of metamorphic pyroxene is constant within the scale of a thin section whether the amount of clinopyroxene is small or large, there must be one stage during the transformation when metamorphic pyroxene is produced to certain amount, that Ca is released from the system while introducing Fe, Mg. We can estimate this stage by writing the reaction using estimated primary pyroxene composition from the Ca, Fe, Mg diagram (Figs. 4.13-4.15) calculated from igneous trends as they cross the metamorphic tie-line bundles. From the assumption of constant Si and concomitantly constant oxygen, allowing Ca^{2+} , Fe^{2+} , Mg^{2+} and H^+ to move across the interface, neglecting minor elements, the reaction can be proposed as:





Here A is the fraction of reactant clinopyroxene that remains as metamorphic pyroxene. Since the Fe/Mg ratio in igneous pyroxene is unknown, Mg and Fe are treated together. If any Ca^{2+} is released by this reaction, then $X - Ay - \frac{(1-A)}{2} > 0$

The plausible value of X is estimated from the composition of pyroxene from the igneous trend to be 0.8. The value of y is taken from the analyses which give an average of 0.89 for the Glen Scaddle specimens, 0.93 for the Belhelvie and 0.86 for the Morven-Cabrach pyroxenes. Therefore, Ca^{2+} is released if:

A < 0.77 in the Glen Scaddle pyroxene

A < 0.70 in the Belhelvie pyroxene and

A < 0.83 in the Morven-Cabrach pyroxene

$$(\text{Mg}, \text{Fe})^{2+} \text{ are released if } 2 - X - A(2-y) - \frac{5(1-A)}{4} > 0,$$

then $(\text{Mg}, \text{Fe})^{2+}$ must be released when the amounts of metamorphic pyroxene produced are as follows:

A > 0.36 for Glen Scaddle

A > 0.28 for Belhelvie and

A > 0.45 for Morven-Cabrach pyroxenes

The directions of Ca^{2+} and $(\text{Mg}, \text{Fe})^{2+}$ movements across the interface related to the approximate amount of metamorphic pyroxene produced can be shown in Fig 4.19. Since Fe/Mg is similar in clinopyroxene

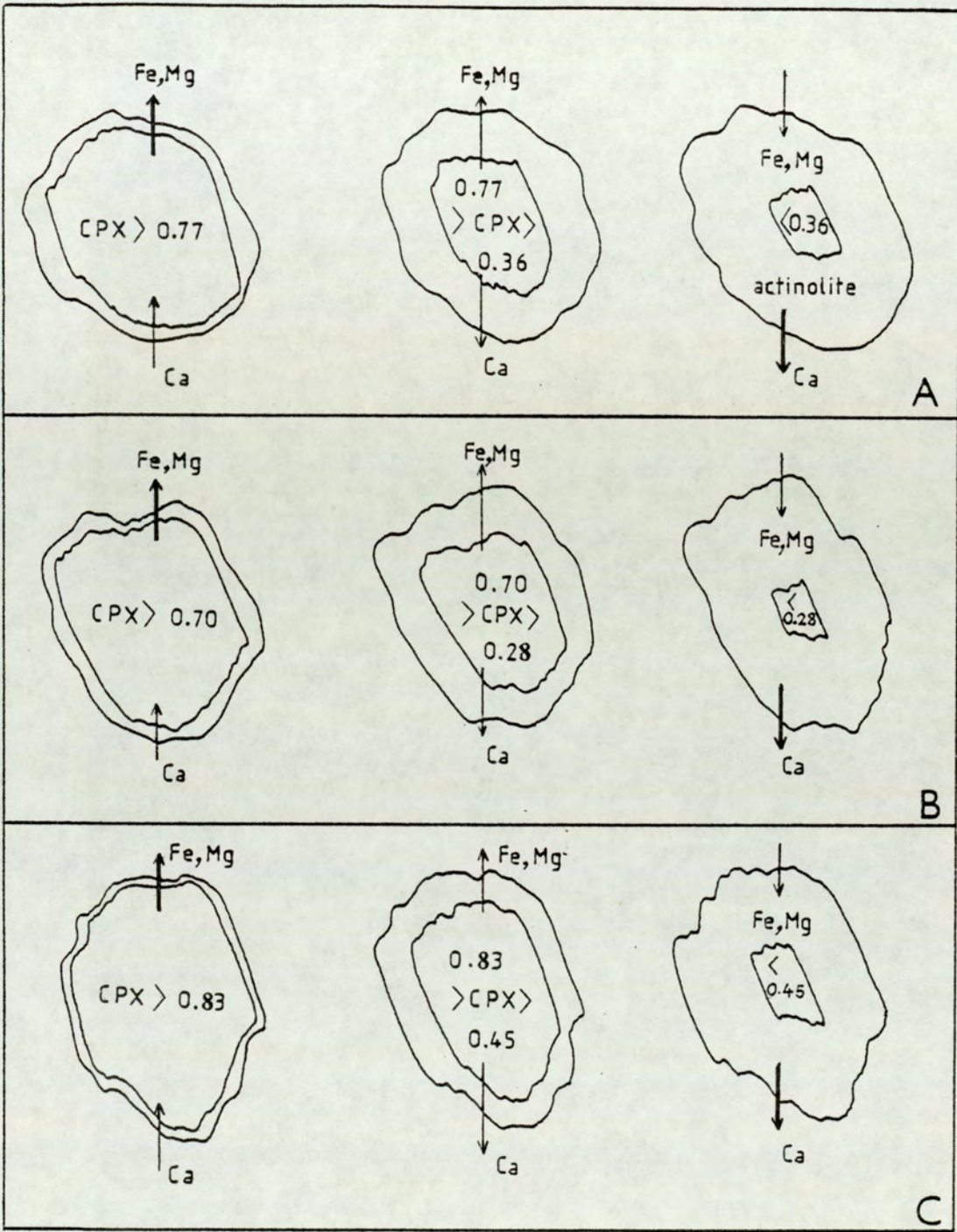


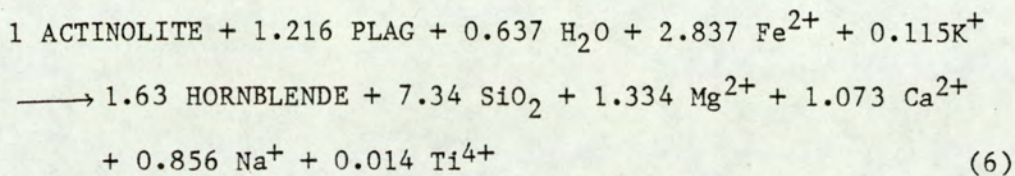
Fig 4.19 Diagram of Ca and Mg, Fe movements in the reaction, igneous pyroxene + fluid \longrightarrow actinolite + metamorphic pyroxene related to the amount of metamorphic pyroxene produced.

- (A) Glen Scaddle (B) Belhelvie
 (C) Morven-Cabrach

and actinolite (Section 4.5.2), these elements are probably released or consumed in approximately the ratio in which they are found in the minerals.

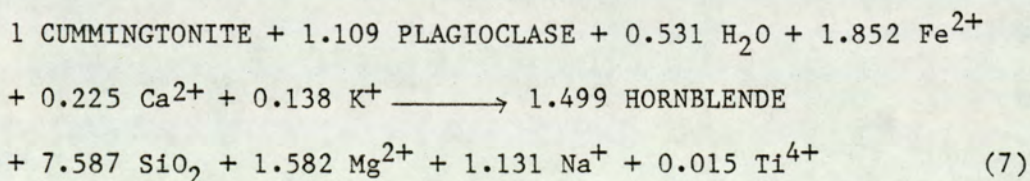
The likely source of Ca is plagioclase. The possibility that $(\text{Fe}, \text{Mg})^{2+}$ released at the initial stage of actinolite forming reaction goes to form hornblende by simultaneous reaction of actinolite and plagioclase will be examined next. This model reaction can be written allowing some constraints to be placed. The obvious assumption of Al and Si closure can not be applied within small volumes here. The Al/Si ratio is much lower in most of the hornblendes than associated plagioclase. There is a weight of evidence that Al in plagioclase is definitely moved during hornblende formation. Actinolite contains noticeable amounts of Al; and hornblende is zoned. The occurrence of quartz inclusions in actinolite and hornblende also indicates Si movement but perhaps still within the system. Nevertheless, ^{the} Al/Si ratio of bluish-green hornblende of pargasitic or tschermakitic compositions in some of the Morven-Cabrach samples, particularly in the area next to plagioclase, is almost similar to associated plagioclase. As already mentioned, these bluish-green hornblendes form at an early stage of the reaction, and they provide evidence that Al and Si movements are restricted at the beginning of the reaction. We can use the composition of hornblende produced at this stage, to write the reactions based on assumption of Al, Si immobility, with H and O also constrained (to move only as H_2O), in order to make the equation soluble.

Using the data from specimen 733 C in which Al/Si plagioclase = 0.627, Al/Si hornblende = 0.605 (treating all phases except SiO_2 on a basis of 24 oxygens)



Part of the Ca^{2+} released in reaction (6) might go to form metamorphic pyroxenes, which are still preserved in this rock. Fe and Mg should be available from the actinolite-forming reaction. However, reaction (6) consumes Fe but produces Mg. The different behaviour for these two elements is due to the much higher Fe/Mg in hornblende than in actinolite (Section 4.5.5 below). Since the actinolite forming reaction probably releases Fe and Mg in approximately the proportions present in the actinolite, we cannot have a closed system to these elements.

If the system on the scale of ^a hand specimen is closed, Mg^{2+} and Na^+ must move to react in the simultaneous reactions occurring in different parts of the thin section such as hornblende formation around cummingtonite. Compositions of hornblende from both locations in the same thin section are very similar, reflecting the limit of $\text{Mg} \rightarrow \text{Al}$ substitution. The Al/Si ratio of this hornblende is 0.629. Based on Al, Si closure, this reaction can be written as:

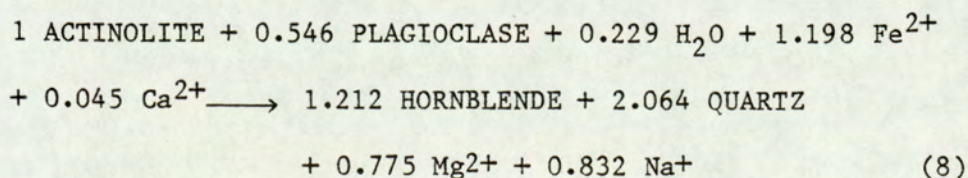


This reaction consumes Ca, which may be supplied from the actinolite \longrightarrow hornblende reaction. This reaction again consumes Fe and releases Mg, again because of the higher Fe/Mg in hornblende than in the reactant amphibole (see Section 4.5.6 below). Thus the production of hornblende involves a definite exchange of Fe and Mg with a larger

system. However, some specimens have higher Fe/Mg in cummingtonite than hornblende (Section 4.5.6 below). In general, it is possible that the hornblende-forming reactions interact with reactions producing silicates from primary Fe oxide minerals, to balance out Fe and Mg. Fe/Mg of pyroxene may also have changed during metamorphism, by an unknown amount. Bulk metasomatism of the rock is also possible. Many of the Morven-Cabrach specimens contain "uralite" veinlets, which in the case of 733 C under discussion are identified as chlorite. These may be the pathways of ionic exchange.

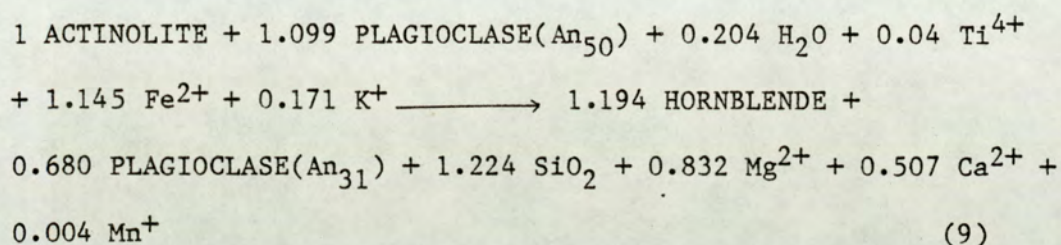
Restricted movement of Al, Si at this stage causes a wide discontinuity between actinolite and hornblende. As has already been described in corona formation, when more H₂O gets into the system, Al can be more mobile. Reactions evolved further and produced ordinary hornblende of the amphibolite facies. More Al can move into actinolite, reducing the width of the compositional gap.

In the Glen Scaddle area most of the hornblendes approach equilibrium hornblende composition, and SiO₂ is present as quartz inclusions. Based on the data from specimen 683 C, neglecting minor elements, the reaction can be proposed as:-



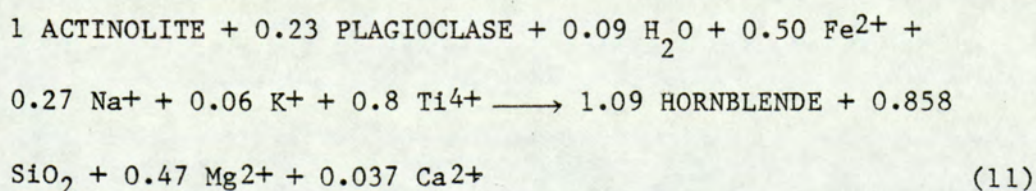
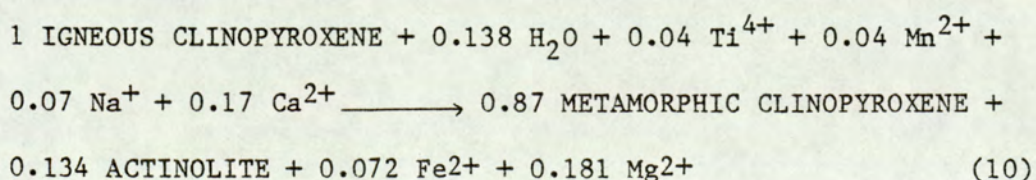
However, it should be borne in mind that the present plagioclase composition (An₃₁) is probably not primary, so we can consider

this plagioclase as a product in a reaction with igneous plagioclase as a reactant. Reasonable coefficients are obtained if this primary plagioclase is given a composition in the range An₅₀₋₆₀, similar to Morven-Cabrach plagioclase. Taking primary plagioclase as An₅₀, constrains the system to be closed to Al, Si, O, H and Na, allowing Fe, Mg and Ca to move around, the reaction can be written as:

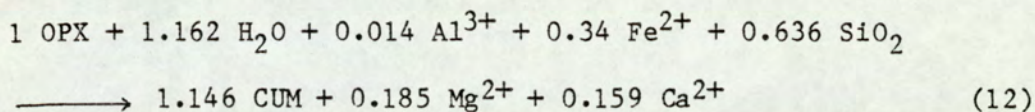


Ca²⁺ released from this reaction was taken up presumably by the concomitant metamorphic clinopyroxene formation, but Mg²⁺ is problematic, it might be removed from the system as discussed above.

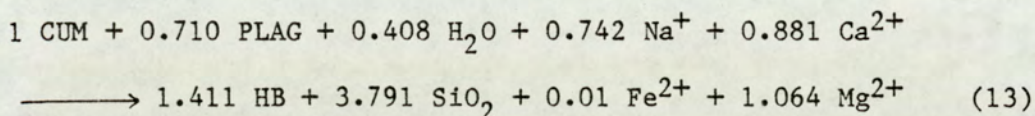
In the Belhelvie specimens we have a good idea of primary plagioclase composition, still represented in the rocks as An₈₀. Again we can write the model reactions based on the ideal assumption of overall closure to Al, Si among several minerals although Al/Si ratio is much lower in hornblende than plagioclase. The igneous clinopyroxene composition is estimated from the igneous trend with the same Fe/Mg ratio as metamorphic composition. From the data from specimen 38 P, the following net reactions can be proposed:-



Using the present composition of orthopyroxene, cummingtonite formation can be expressed by:-



Meanwhile, hornblende around cummingtonite is produced by:-



It is impossible to link these reactions. However Mg^{2+} is released in all reactions while Na^+ is consumed. SiO_2 is present as quartz.

Although many ideal assumptions are proposed for the plausible reactions, it is likely that these reactions showed open-system behaviour as shown above. Retrograde metamorphism is generally thought of as a broadly isochemical process. In many metamorphic terrains of retrograde environment, metasomatism has also been reported. Beach (1974) found that amphibolitization of granulite has resulted in some loss of Ca and Mg and a gain in Na. Hanan (1976) studied uralitized Baltimore gabbros and concluded that FeO/MgO ratios are high relative to unuralitized gabbros. A loss of K_2O and FeO, and higher Na/Na + K ratios with increasing retrogression in retrograde metamorphism of a high grade terrain has also been reported (Corbett and Phillips, 1981). It would be interesting for future work to do whole rock analyses for the studied areas. Some has been done in the Morven-Cabrach rocks containing "uralite" veins (Allan, 1970) which surprisingly showed an isochemical system.

4.5.5 Coexisting Actinolite and Hornblende

Calcic amphibole grains in the studied areas occur as layers around pyroxene with chemical zoning within actinolite core and hornblende rim, rather than single grains showing exsolution lamellae (Tagiri 1977) or as separate grains (Brady, 1974) which are the best evidence for equilibrium assemblages or a miscibility gap between actinolite and hornblende. According to geological evidence (section 2.1.1, 2.2.1) zoning in calcic amphibole in the studied areas reflects an attempt to attain equilibrium perhaps by reacting with plagioclase which is the main non-ferromagnesian mineral. Textural evidence (section 4.2.1, 4.2.2) indicates that hornblende generally developed when actinolite is in contact with plagioclase. Plagioclase, then must play an important role in the formation of hornblende (section 4.5.4). Most of the rapid transitions from actinolite core to hornblende rim reported in the literature occur in the transitional prograde zone from greenschist to amphibolite facies, associated with changing plagioclase compositions from low An (albite) to higher An (oligoclase and andesine) in the amphibolite facies (e.g. Cooper and Lovering 1970, Graham 1974, Kuniyoshi and Liou 1976, Sampson and Fawcett 1977). Recognition that the production of more calcic plagioclase during the actinolite-hornblende transition needs more Al in plagioclase itself, brings into question the source of Al for the abrupt increase in Al content of hornblende from actinolite, although the final breakdown of epidote and chlorite can be contributed to this problem (Grapes and Graham, 1978 Harte and Graham 1975). This solution can not apply to the present study and mineralogy, because of difference in geological setting ^Chlorite is also present in various amounts especially in the Glen Scaddle intrusion, where there is also a little epidote. However, the reaction being

studied is retrograde and differs from the literature studies because plagioclase changes from more calcic (e.g. An₈₀ igneous plagioclase preserved in the Belhelvie area) to less calcic (e.g. An₃₀ metamorphic plagioclase at Glen Scaddle).

It was deduced in the last section that the actinolite hornblende reaction releases Ca derived from reactant plagioclase. This is similar to the process studied by Grapes et al (1977) except that they interpret their reaction sequence as prograde.

Unlike the prograde reactions which involved not only plagioclase but also usually epidote and chlorite from lower grade of greenschist facies to produce hornblende, hornblende in retrograde environment are formed simultaneously with actinolite by direct reaction with plagioclase. Their chemical relationships will now be compared with those formed by prograde metamorphism.

According to the recent classification of calcic amphibole by Leake (1978), actinolite is characterized by (Na + K) in A site < 0.50, Ti < 0.50 whereas Si content varies from 7.50 - 8.00 atoms per 23 oxygens (anhydrous) with Mg/(Mg + Fe)²⁺ ratios ranging from 0.0 - 0.50 for ferro-actinolite and 0.50 - 0.90 for actinolite. Actinolitic hornblende is the intermediate phase between actinolite and hornblende, containing 7.25 - 7.50 Si atoms per formulae unit. In Fig. 4.20, actinolite, actinolitic hornblende and hornblende from cores towards rims in three studied areas are plotted. The dominant chemical difference between the three studied areas are the high Mg content in ^{the} Belhelvie area relative to Glen Scaddle and particularly Morven-Cabrach which contains the highest Fe contents.

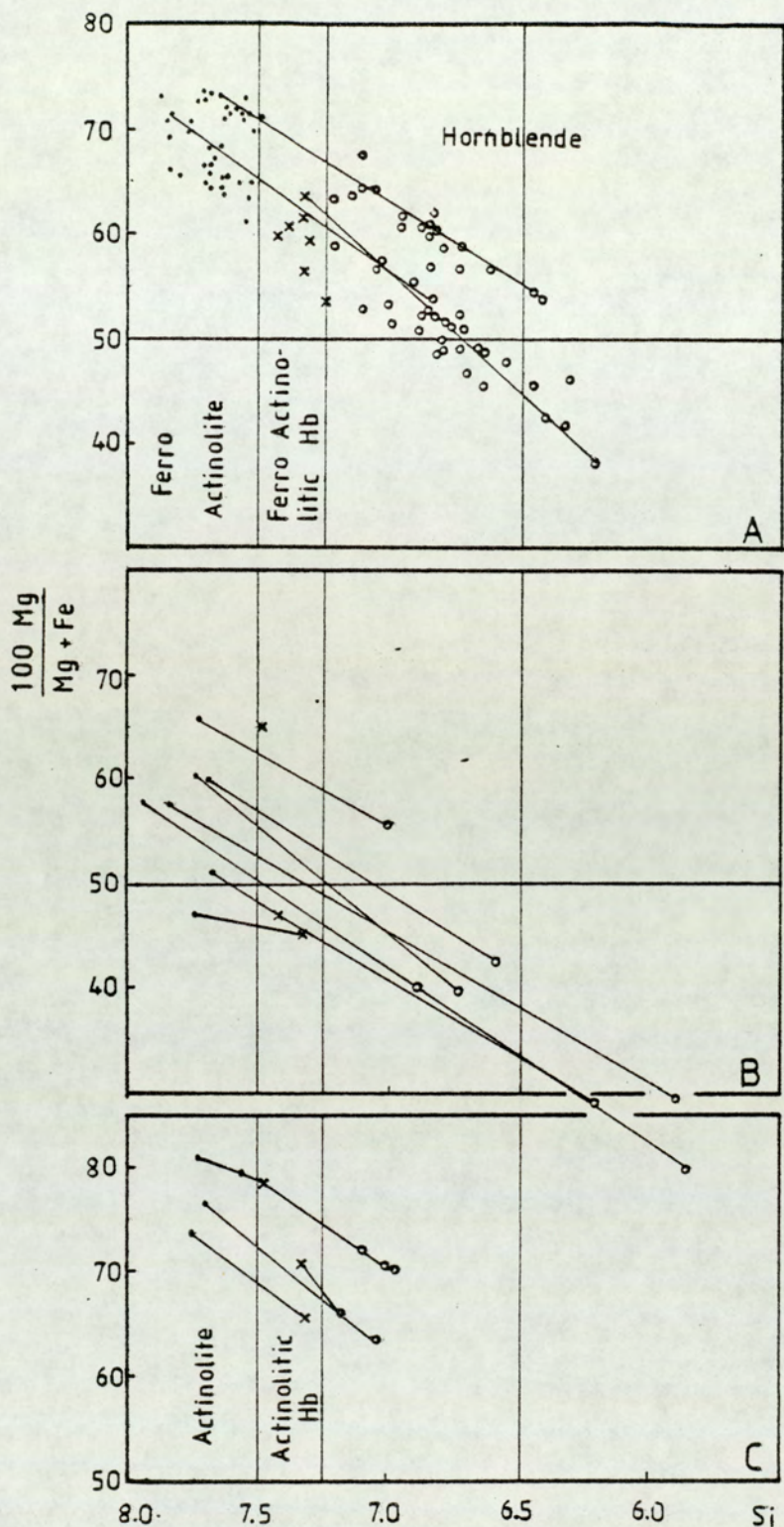


Fig 4.20

Actinolite and hornblendes plotted in terms of $100\text{Mg}/\text{Mg} + \text{Fe}$ and Si. Nomenclature is according to Leake (1978). Tie lines for Glen Scaddle (A) indicate coexisting amphiboles across a sharp compositional break. Tie lines for Morven-Cabrach (B) and Belhelvie (C) areas indicate sequential analyses within one grain replacing clinopyroxene, not necessarily with any compositional break.

Neglecting Fe^{3+} , chemical variations from actinolite to hornblende can be described in terms of two independent major substitutions within the basic tremolite-actinolite formulae,

$\square^{\text{A}} \text{Ca}_2\text{Mg}_5\text{Si}_8\text{O}_{22}(\text{OH})_2$ (Cooper and Lovering 1970, Robinson et al 1971):-

$\text{Na}^{\text{A}}\text{Al}^{\text{iv}} = \square^{\text{A}}\text{Si}^{\text{iv}}$ the edenite substitution

and $\text{Mg}^{\text{vi}}\text{Si}^{\text{iv}} = \text{Al}^{\text{iv}}\text{Al}^{\text{vi}}$ the tschermakite substitution.

Linear combination of these derives the pargasite substitution

$(\text{Na}^{\text{A}}\text{Al}^{\text{vi}}\text{Al}_2^{\text{iv}} = \square^{\text{A}}\text{Mg}\text{Si}_2)$.

Increasing Fe with decreasing Mg from actinolite to hornblende (Fig. 4.20) suggests that $\text{Fe} \rightleftharpoons \text{Mg}$ is also an important substitution. The amounts of edenite and tschermakite substitutions can be employed to describe the solid solution behaviour between actinolite and hornblende. If the gap does exist, there should be a discontinuous substitution relation between coexisting phases. Due to the chemical complexity of calcic amphibole, many different types of solvus have been proposed to illustrate the compositional relations or define the gap. Form and position of each solvus is uncertain from area to area, or even within the same area in different geological settings.

In Fig. 4.21 and 4.22, actinolite and hornblende are plotted in a Mg vs Al^{iv} diagram defined by Shido and Miyashiro (1959), who indicate a composition gap intervening between the field of greenschist and epidote-amphibolite facies. The present data are plotted within and across the defined miscibility gap (Fig. 4.21). Sharply coexisting pairs show also an inconsistent composition gap within each area or even within the same thin section (Fig. 4.22). Similar observations are also found in prograde metamorphic sequences in both low pressure terrains; e.g. Hidaka, Southern Abukuma and in medium

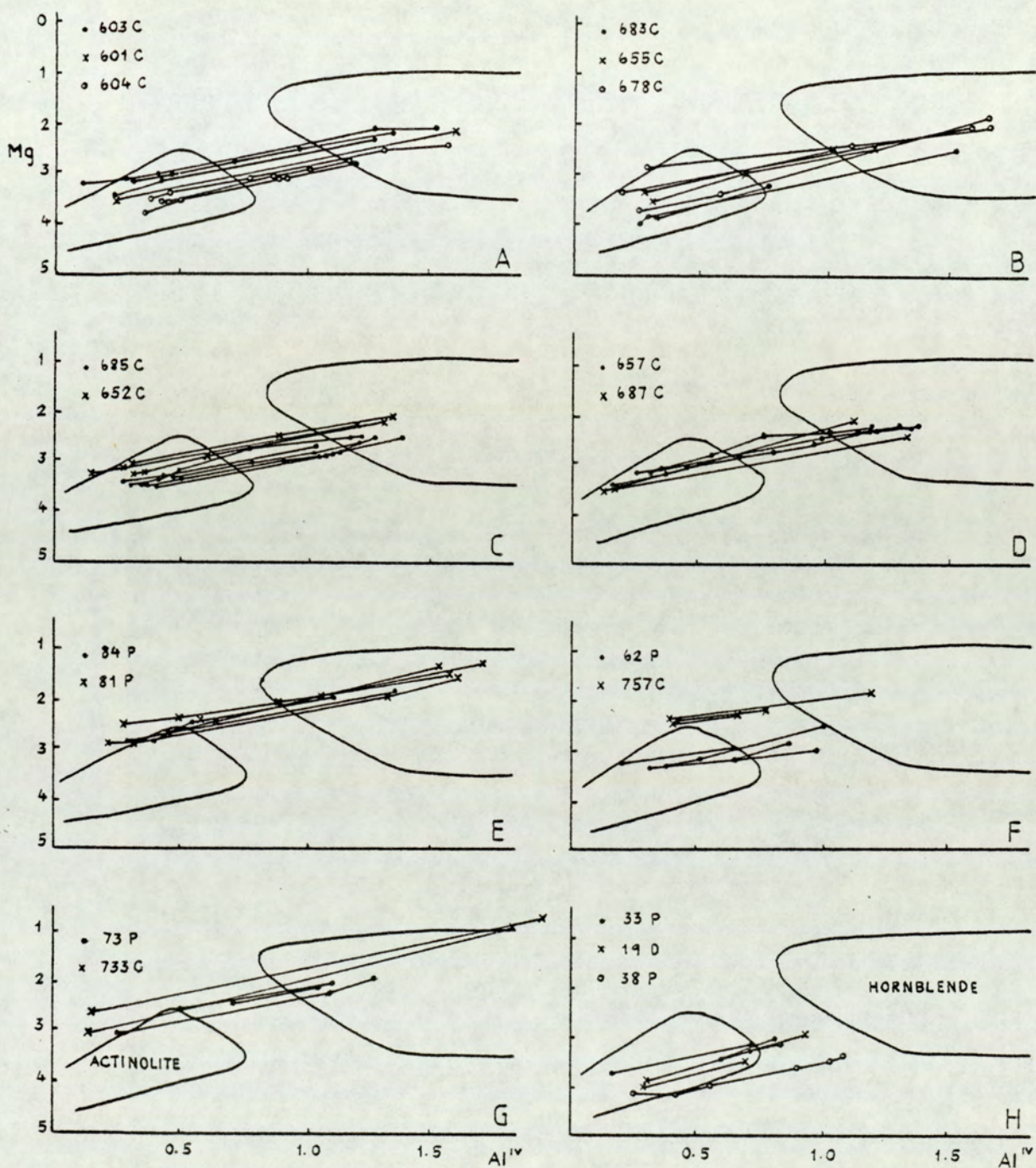


Fig 4.21 Plot of Mg against Al^{IV} for coexisting actinolite-hornblende from:-
 (A-D) = Glen Scaddle, (E-G) = Morven-Cabrach, H = Belhelvie
 Fields of actinolite and hornblende from Shido and Miyashiro (1959).

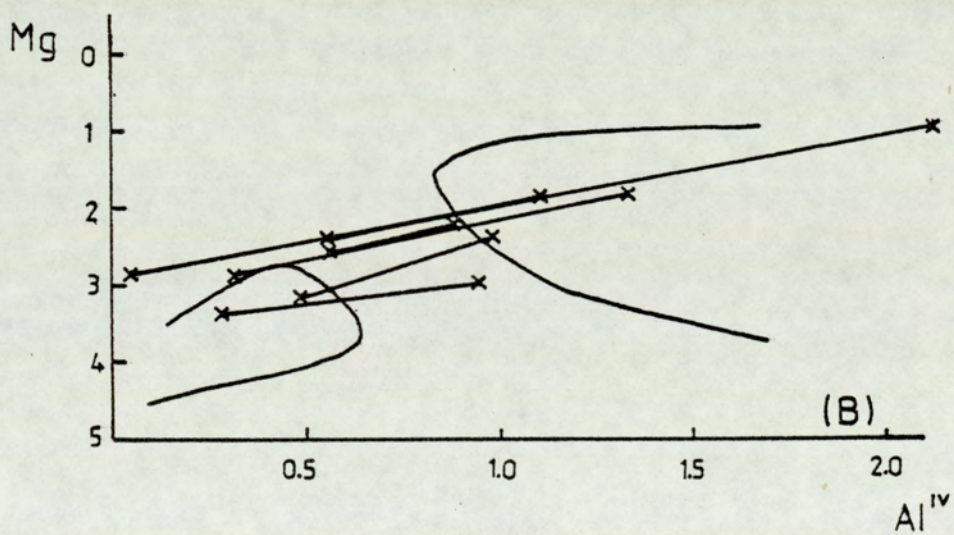
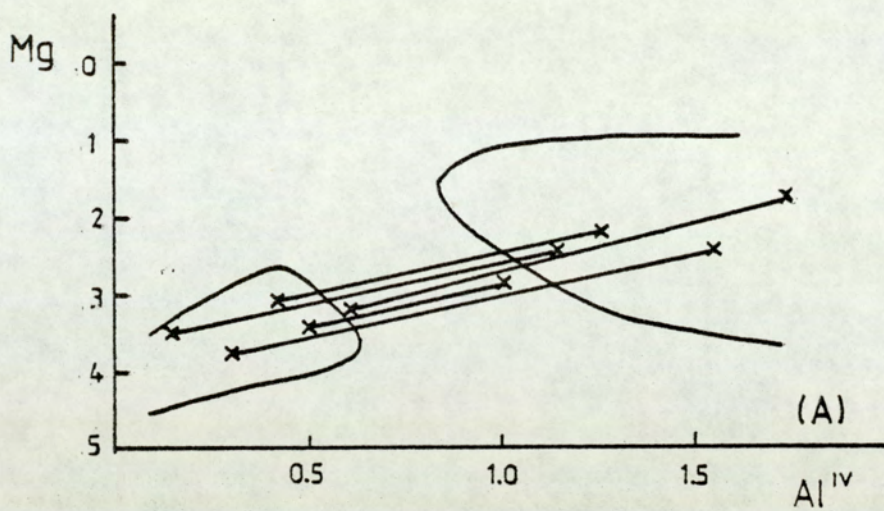


Fig 4.22 Intimately coexisting actinolite-hornblende pairs plotted in the diagram of Shido and Miyashiro (1959).

to high pressure terrains; e.g. Scottish Highlands and Sambagawa. (Grapes & Graham 1978, Fig. 3).

Choudhuri (1974) pointed out that the distribution coefficient of Fe and Mg between coexisting actinolite and hornblende may vary with Al content of hornblende. Tagiri (1977) found that Fe-Mg partition (of coexisting calcic amphiboles as lamellae intergrowths in low-medium pressure metamorphism) depends on the Al^{iv} content of hornblende, and proposed a shape of the solvus based on his method in terms of an Mg-Fe- Al^{iv} diagrams. He noted that Fe-rich calcic amphibole shows a wider gap than Mg-rich one. In Fig. 4.23, the present data are plotted. Although Fe and Mg are more or less well-behaved in Glen Scaddle and Belhelvie masses, no systematic relationships between Fe/Mg ratio and Al^{iv} are observed in the coexisting amphiboles. Continuous compositional zoning across the "solvus" is also common in all studied area. Fe/Mg is systematically higher in hornblende than in actinolite (Fig. 4.24) as expected (Tagiri 1977).

In the Portsoy and Belhelvie areas (Fig. 4.24B) and Glen Scaddle area (Fig. 4.24C) there is some regularity of Fe-Mg partition but no systematic distributions are found in the Morven-Cabrach area (Fig. 4.24A) except in 62 P.

One of the major chemical differences between actinolite and hornblende is the nearly empty A site and very low tetrahedral Al content in actinolite (Hawthorne, 1981). These are plotted, along with Al^{vi} , against $Fe^{2+}/(Fe^{2+} + Mg)$ in Figs. 4.25 and 4.26. Again there is a continuous trend (Fig. 4.25) while co-existing actinolite and hornblende pairs fail to define the expected gap

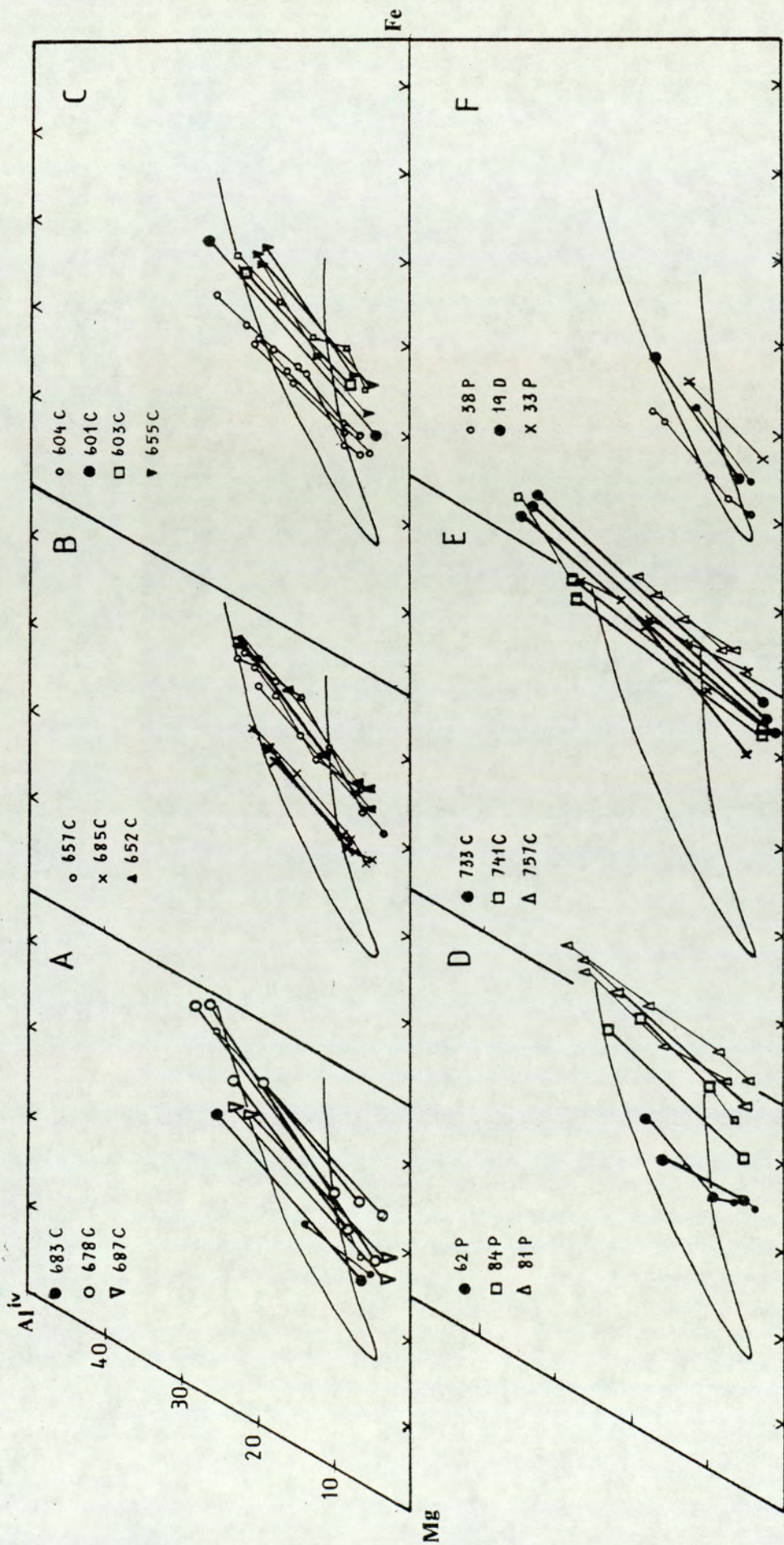


Fig 4.23 The Mg-Fe-Al^{iv} diagram of coexisting actinolite-hornblende. Heavy symbols indicate sharp coexistence across a compositional break. The compositional gap is from the pairs from the high grade parts of the epidote amphibolite facies of Hitachi district. (Tagiri, 1977).
 (A) - (C) Glen Scaddle; (D), (E) Morven-Cabrach (F) Belhelvie

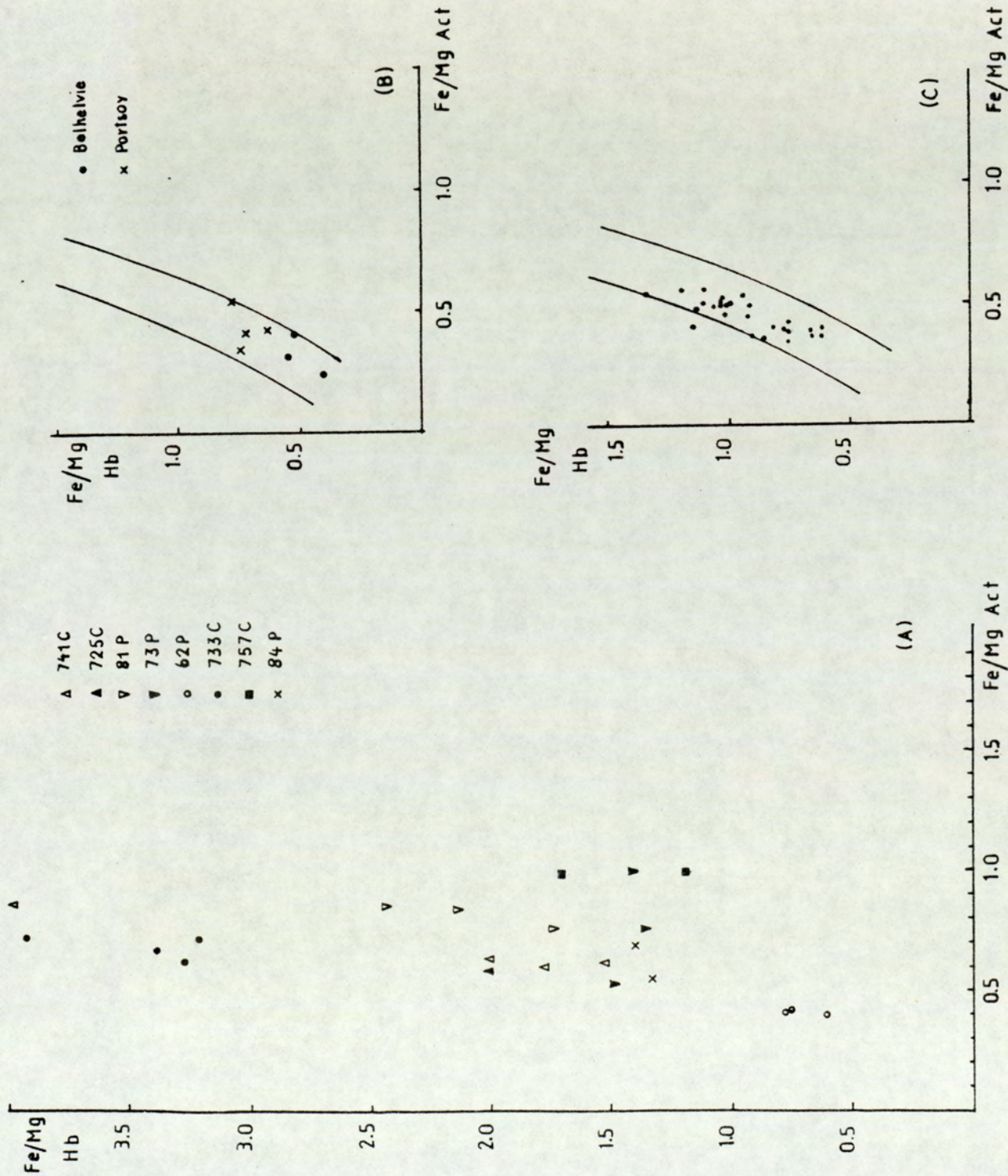


Fig 4.24

Fe-Mg partition between
coexisting actinolite-hornblende
from:-
(A) Morven-Cabrach area
(B) Belhelvie and Portsoy areas
(C) Glen Scaddle area
compared Tagiri (1977)

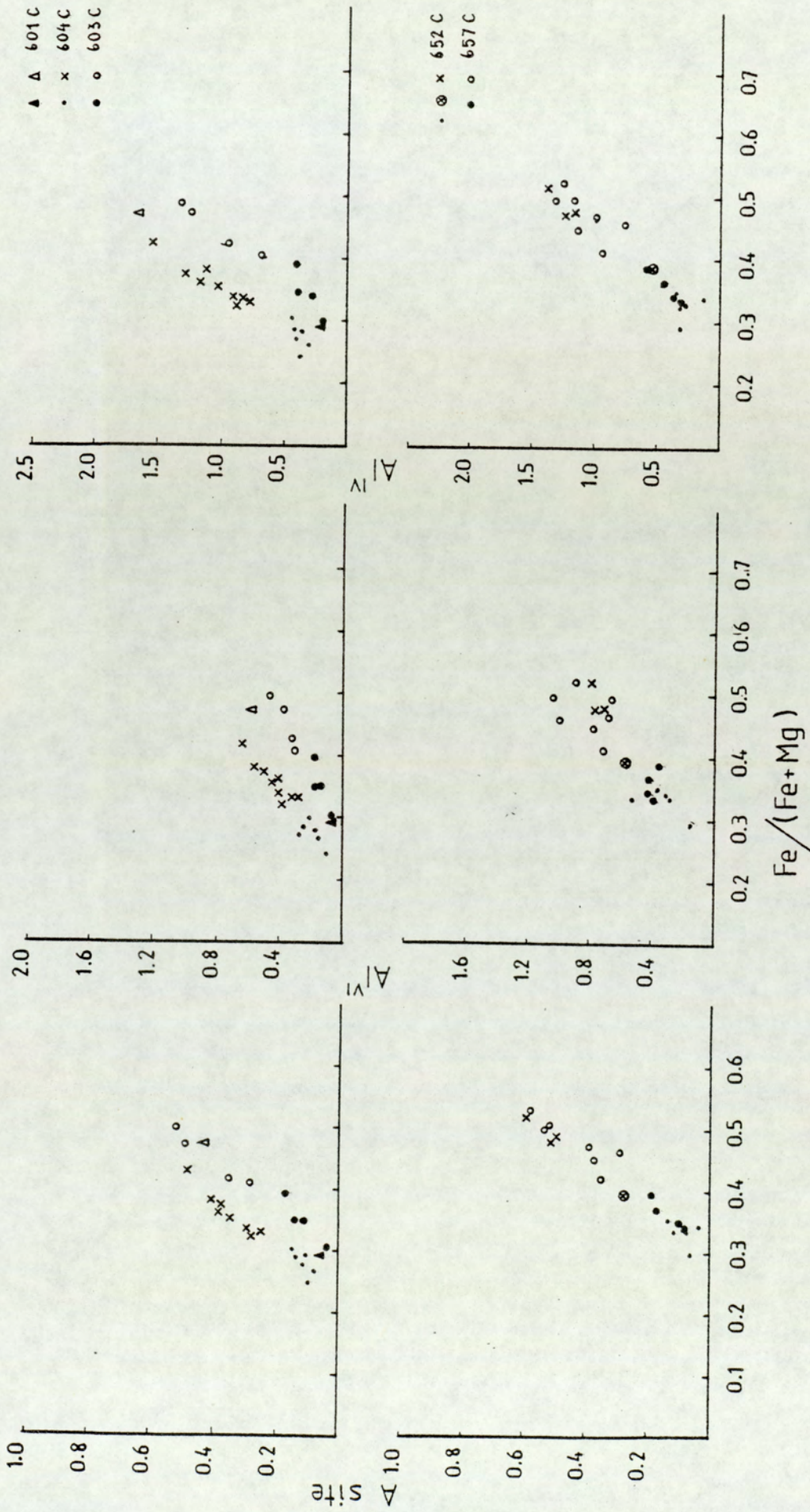


Fig 4.25 A-site occupancy, Alvi and Aliv versus $Fe/(Fe + Mg)$ for Glen Scaddle actinolite and hornblende.

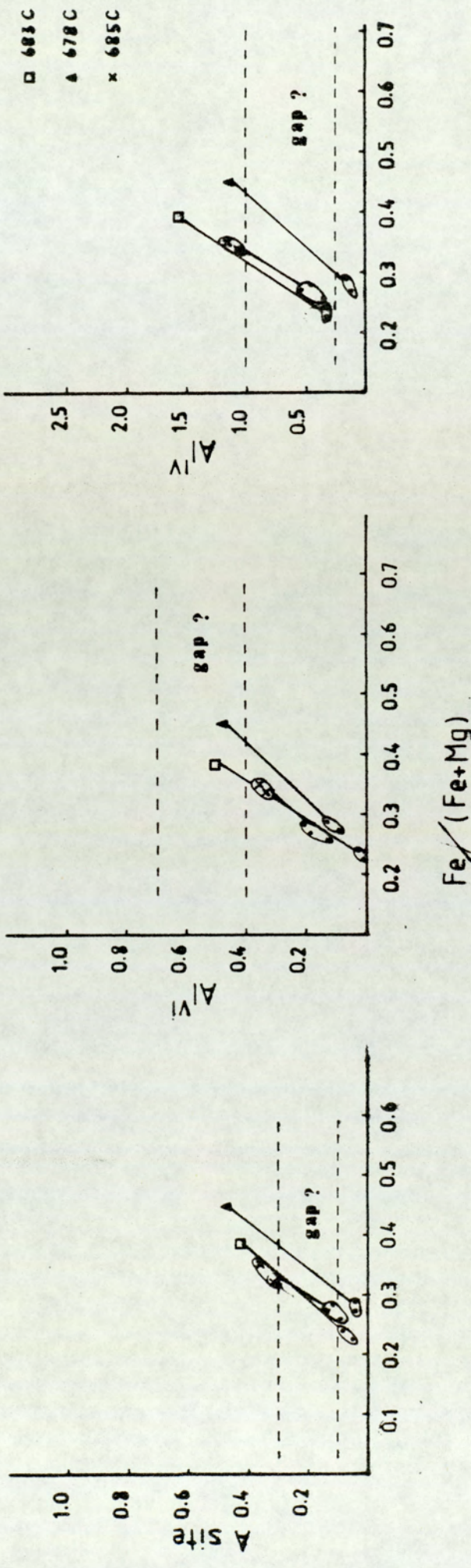


Fig 4.26 Coexisting actinolite and hornblende (across compositional break) in Glen Scaddle area, compared with miscibility gap suggested by the data of Misch and Rice (1975).

(Fig. 4.26). A-site occupancy is sensitive to errors introduced in estimating Fe^{3+} , so total alkalis are better used (Hietanen, 1974). The ratio of total alkalis to tetrahedral Al content remains constant and close to 1:3 (Fig. 4.27). This trend illustrates the combined edenite and the tschermakite substitutions leading to the intermediate compositions of hornblende between pargasite and tschermakite. The solid line drawn through actinolite and hornblende in Fig. 4.27 represents these substitutions in the ratios 7:3 as found by Hietanen (1974) and Hanan (1980). In Fig. 4.27, most of the points fall close to this line, and show a continuous trend. Clear separation of two or three compositional areas has not been found. This observation contrasts with the two fields found by Sampson and Fawcett (1977) and the three fields reported by Hietanen (1974). Hanan (1980) studied metamorphic reactions in the Baltimore igneous complex and found two separate fields in the Baltimore Block of the complex and three fields in the Susquehanna Block in this diagram. The continuous compositional variation along this trend, similar to the present study is reported by Thomson et al (1981) and in the Scottish Highlands by Grapes and Graham (1978).

One other method to demonstrate the continuous solid solution between actinolite and hornblende is the series of Al content. This relationship is plotted in terms of tetrahedral Al against total Al. Figs. 4.28 to 4.30 show a good, systematic continuous correlation between total Al and Al^{iv} from low Al actinolite to high Al hornblende in all studied areas. Values before and after recalculation for Fe^{3+} (which causes an increase in Al^{iv}) are plotted for each point for comparison. There is only a very slight shift of the trend. The slope of $\text{Al total}/\text{Al}^{\text{iv}}$ in the Glen Scaddle

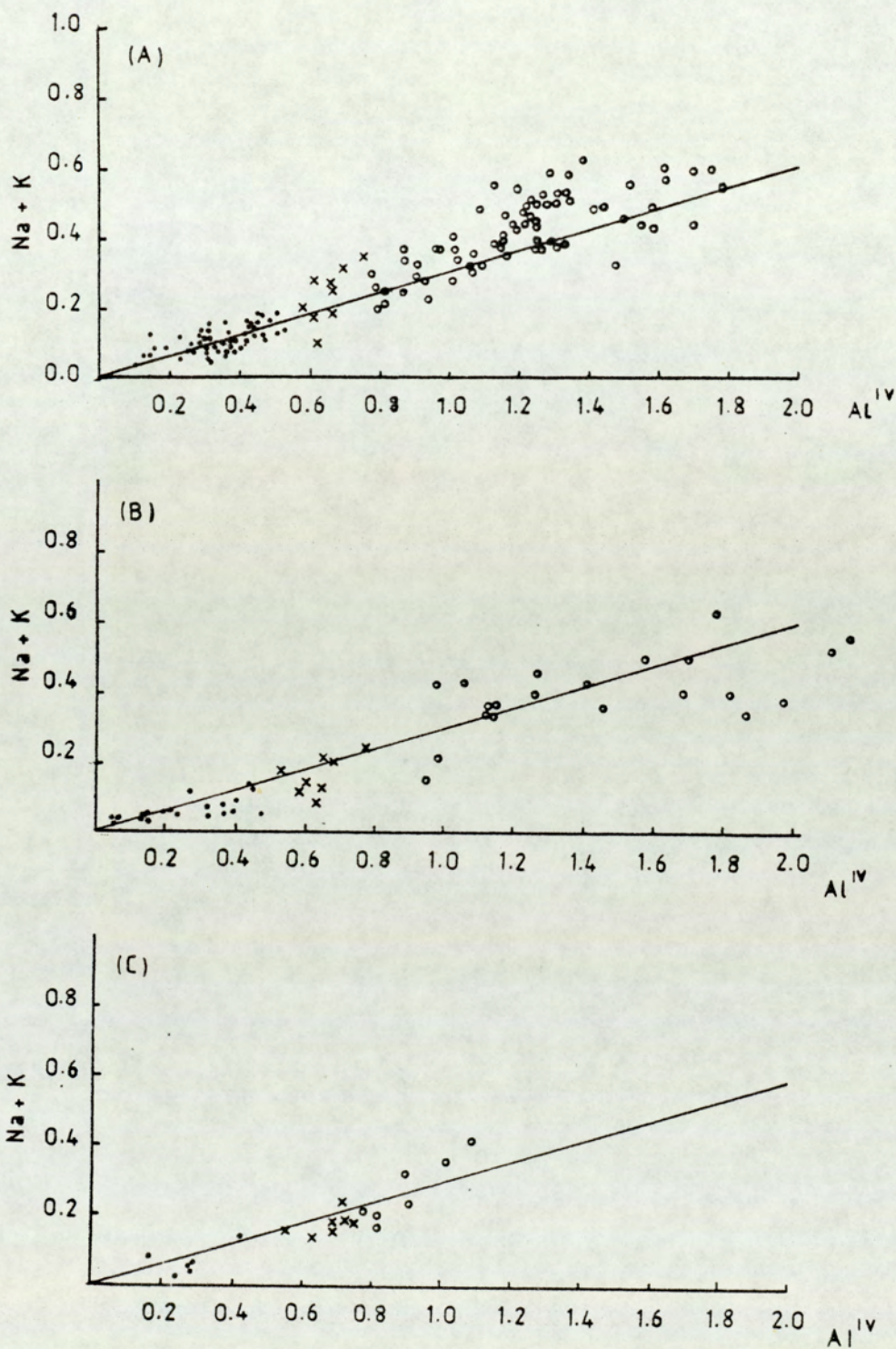


Fig 4.27 Plot of total alkalis against tetrahedral Al (after estimating Fe^{3+}) for
 • actinolite, x actinolite hornblende, o hornblende.
 (A) Glen Scaddle area
 (B) Morven-Cabrach area
 (C) Belhelvie area

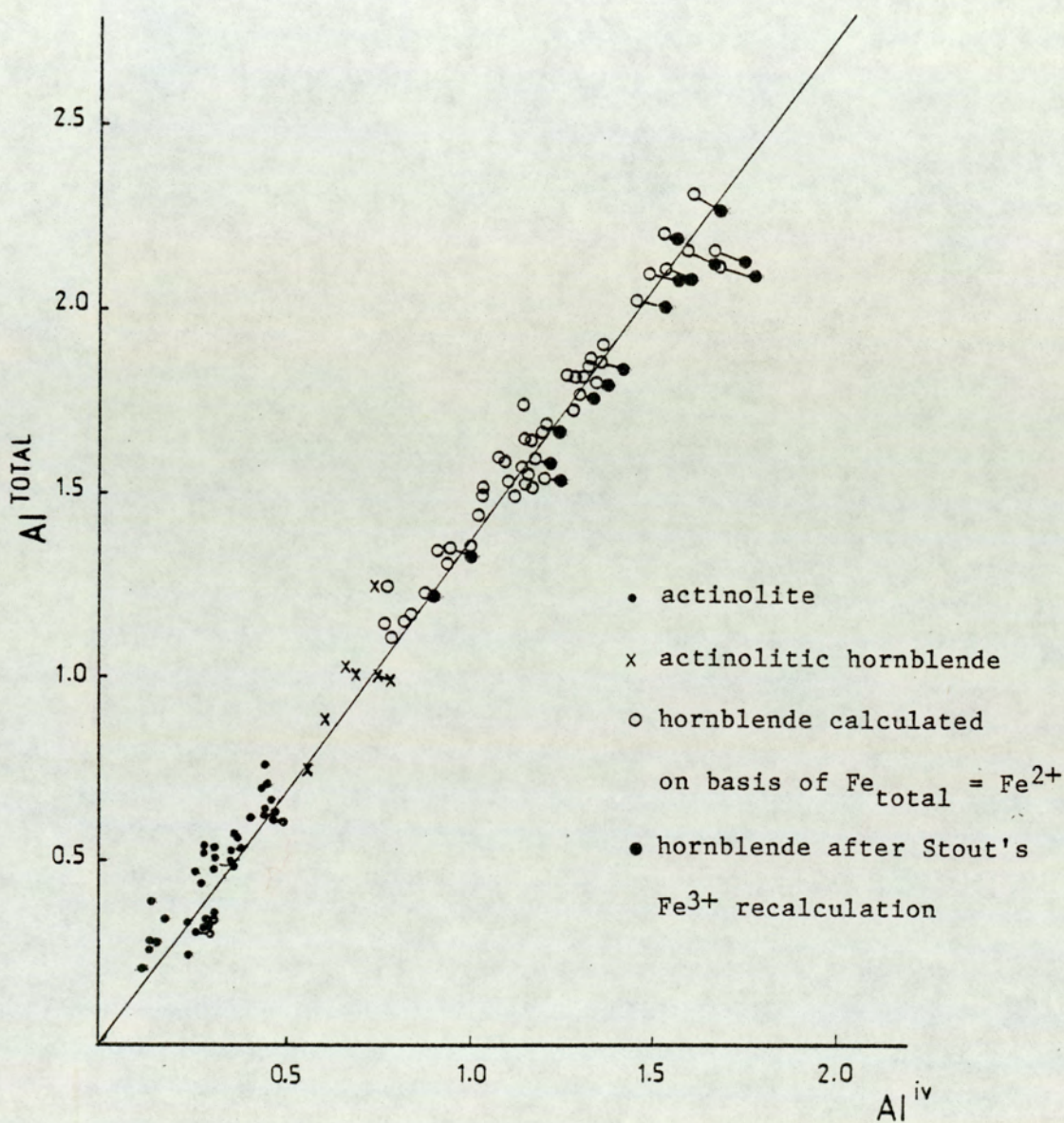


Fig 4.28 Tetrahedral Al plotted against total Al for calcic amphiboles from Glen Scaddle area, showing continuous solid solution from low Al actinolite to high Al hornblende.

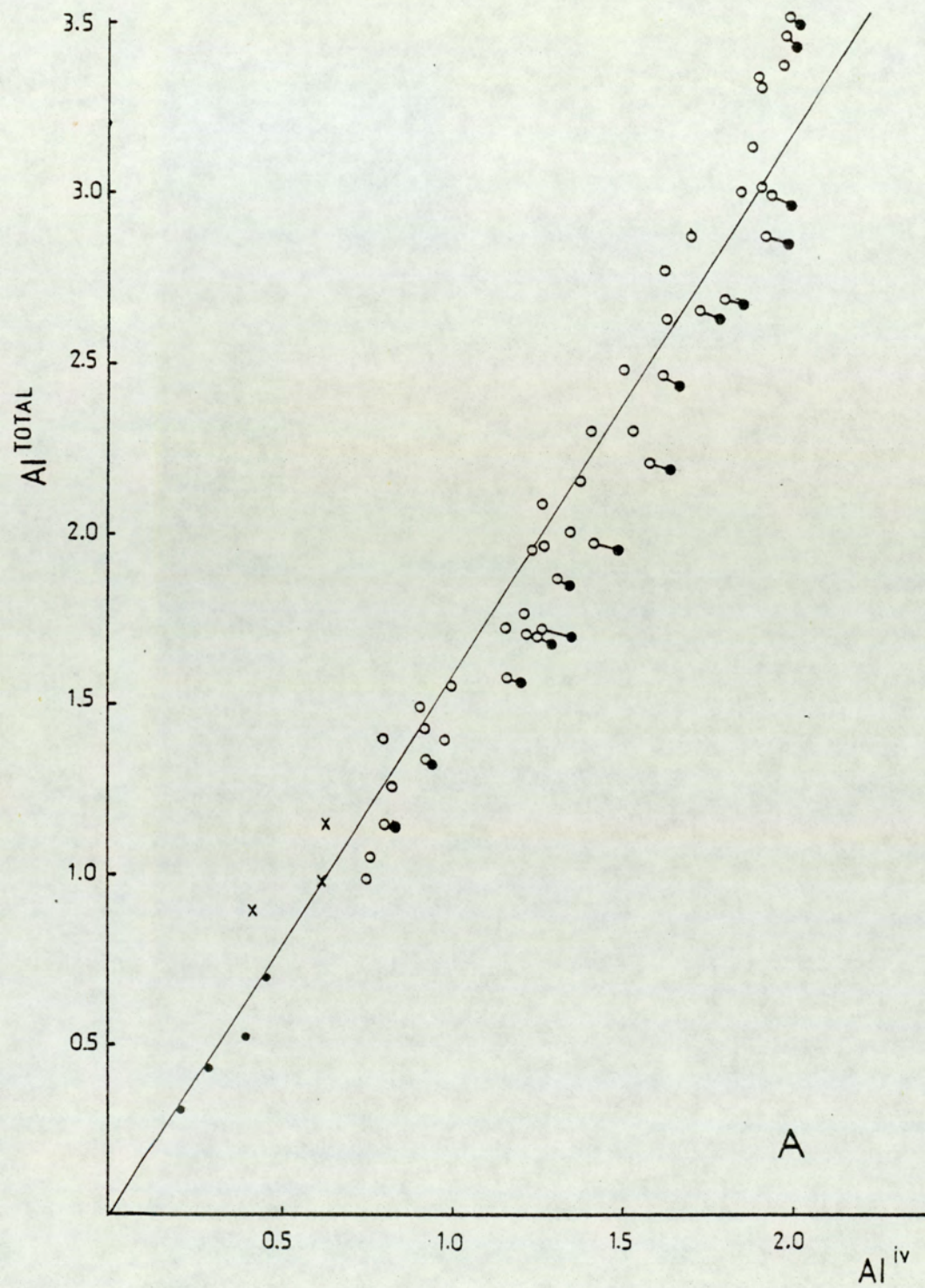
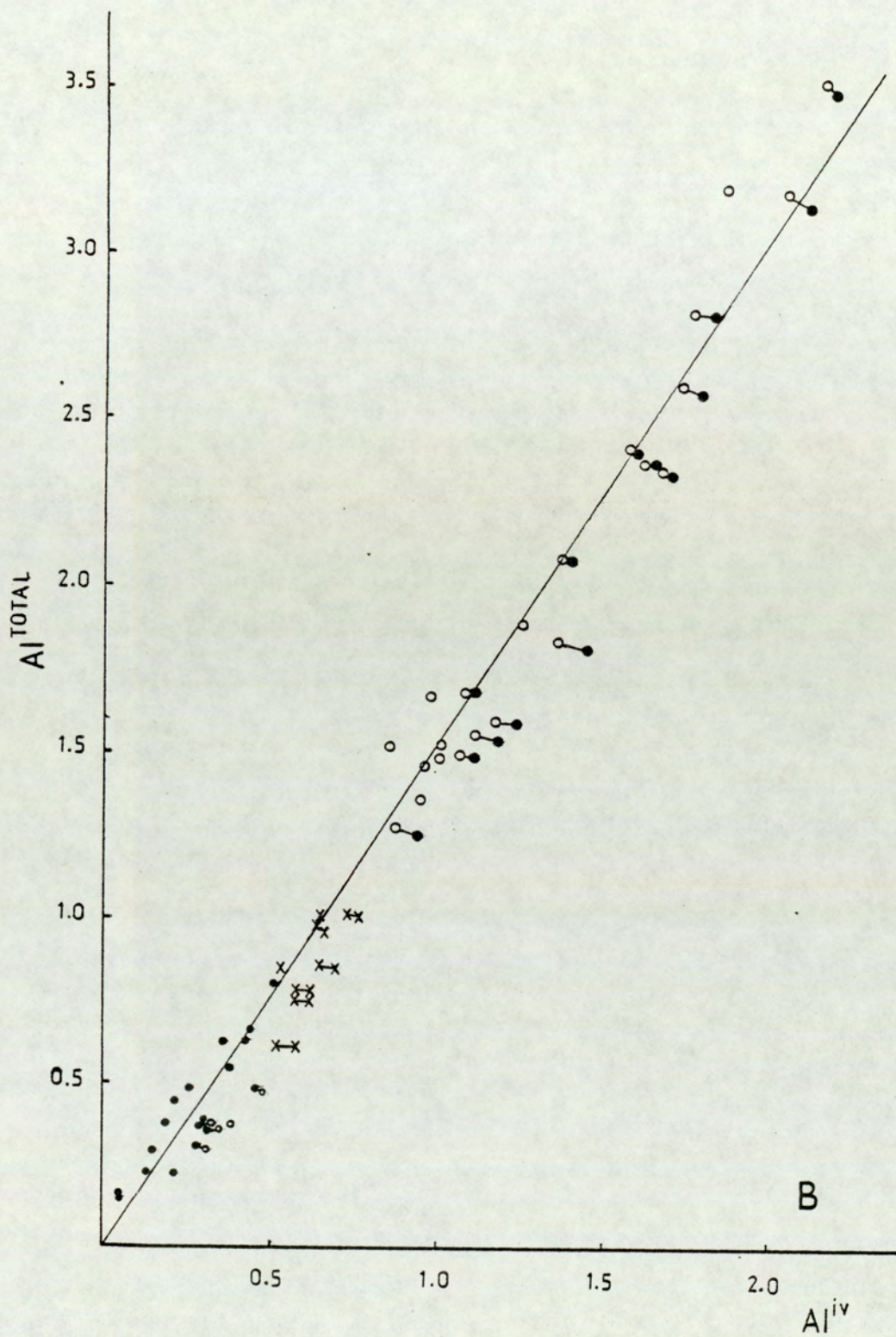


Fig 4.29

Tetrahedral Al plotted against Al^{IV} for calcic amphibole from Morven-Cabrach area.

(A) Actinolite-hornblende with cummingtonite. Actinolite occurs as patches or narrow zone between cummingtonite and fringing hornblende.



(B) Actinolite-hornblende as zoned mineral showing continuous solid solution, without cummingtonite.

(Symbols are the same as Fig 4.28)

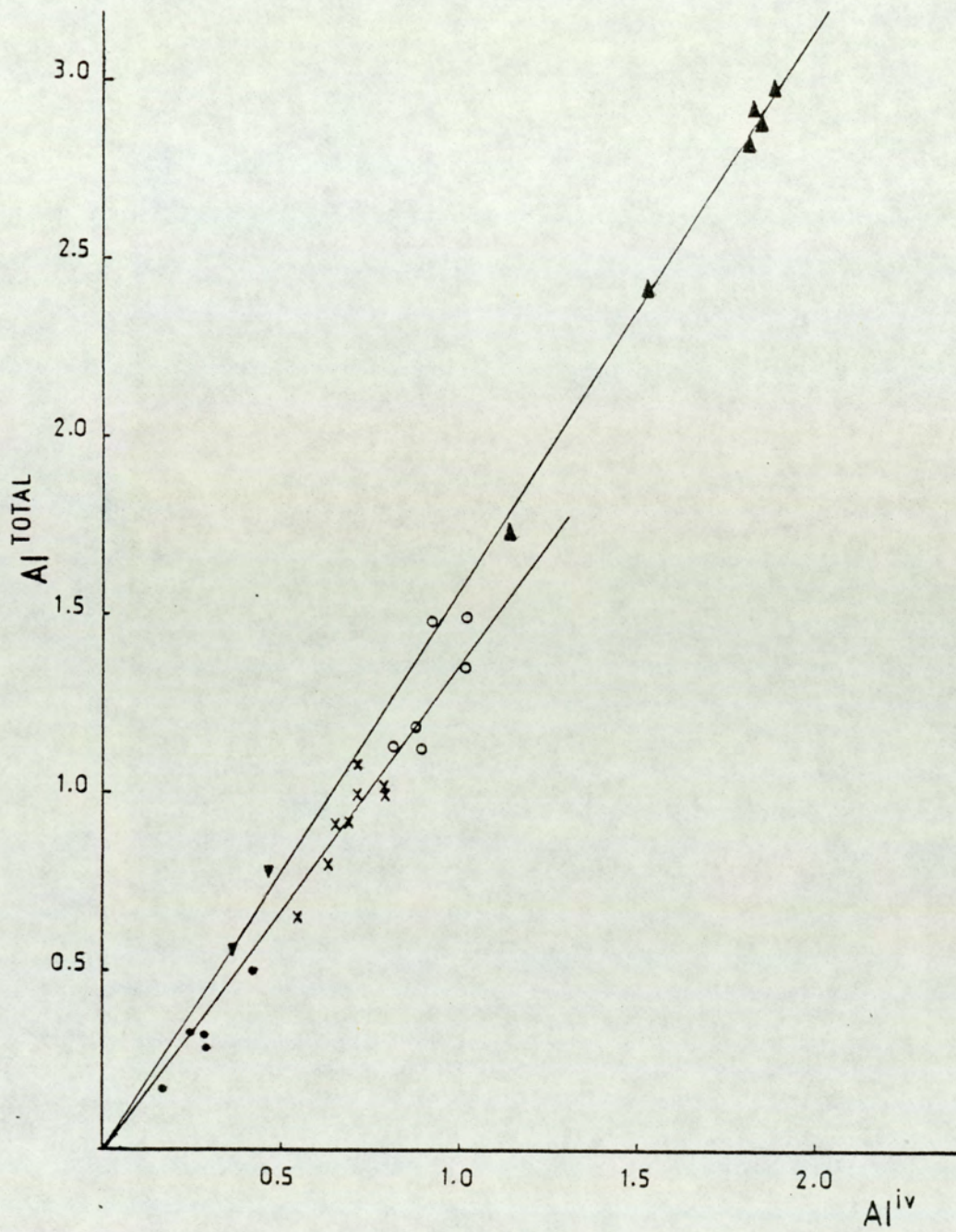


Fig 4.30 Tetrahedral Al plotted against Al for calcic amphibole from the Belhelvie area

▲ rimming hornblende around cummingtonite

▼ actinolite with cummingtonite

(Symbols are the same as Fig. 4.28)

area (Fig. 4.28) is close to 1.4 which is very similar to that of upper amphibolite facies reported by Misch and Rice (1975). In the Morven-Cabrach area (Fig. 4.29), this ratio is approximately 1.55 for coexisting actinolite and hornblende around relict clinopyroxene and 1.6 for those with cummingtonite (actinolite occurs as patches inside cummingtonite which is rimmed by hornblende). The Al^{total}/Al^{iv} slope in the Belhelvie mass (Fig. 4.30), is 1.38 for actinolite and hornblende zones around clinopyroxene and is 1.6 for those coexisting with cummingtonite. Al^{total} is much higher in hornblende around cummingtonite than those rimming actinolite in the same specimen.

Textural and chemical data presented above clearly indicate that actinolite and hornblende in the studied areas are not equilibrium pairs. The chemical discontinuity between these amphiboles is not consistent in each single thin section. Strongly zoned hornblende most readily shows the evidence of disequilibrium. The reaction must be very sluggish, particularly the Al movement. The observations are consistent with those in prograde terrains although the nature of reaction is different. During retrograde metamorphism, the reaction rates are also ~~also~~ slower than prograde reactions.

4.5.6 Coexisting Cummingtonite and Calcic Amphibole

From the textural relations of the hornblende rims around cummingtonite cores wherever in contact with plagioclase it can be reasonably proposed that the origin of hornblende is reaction between cummingtonite and plagioclase. Although the sharp, parallel contact between these amphiboles is likely to define the original orthopyroxene and plagioclase contact, the textural evidence presented

in section 4.2 suggests that hornblende forms simultaneously with the development of cummingtonite (Section 4.5.4). In other words, they formed under the same physical conditions. In the Morven-Cabrach area, actinolite occurs as blebs or patches in cummingtonite presumably representing the pre-existing blebby clinopyroxene exsolution in orthopyroxene.

Calcic amphibole and cummingtonite miscibility gap is defined by a compositional discontinuity, mainly influenced by the sizes of ions, in the occupancy of the M_4 site, similar to the gap between Mg-Fe pyroxene and calcic pyroxene. In calcic amphibole the M_4 site tends to contain mostly Ca while cummingtonite, like pigeonite, shows a strong preference for Fe^{2+} in this site (Robinson et al 1982). Relationships between cummingtonite and calcic amphibole, showing a wide miscibility gap, can be illustrated by the Ca, Fe and Mg distributions, plotted in the pyroxene quadrilateral (Fig. 4.31). The tie lines connecting cummingtonite and hornblende are crossed even within the same specimen, due to zoning in hornblende and the effect of Fe^{3+} content in hornblende. The partition of Mg-Fe between coexisting cummingtonite and hornblende can be investigated by plotting on a diagram of $[Mg/(Mg + Fe)]_{ca-am}$ against $[Mg/(Mg + Fe)]_{cum}$. (Fig. 4.32). It is found that there is no systematic distribution of Fe, Mg related to co-existing plagioclase as proposed by Kisch and Warnaars (1969). This presumably reflects disequilibrium (next section). In Morven-Cabrach specimens of the same plagioclase composition there is variation, usually with lower $Mg/(Mg + Fe)$ ratios in hornblende while in some specimens of ordinary hornblende composition (e.g. 62 P, 84 P, 735 C), this ratio is similar or slightly higher in hornblende. However, it is found that the distribution coefficient (K_D hb-cum) of Fe^{total} and Mg partition

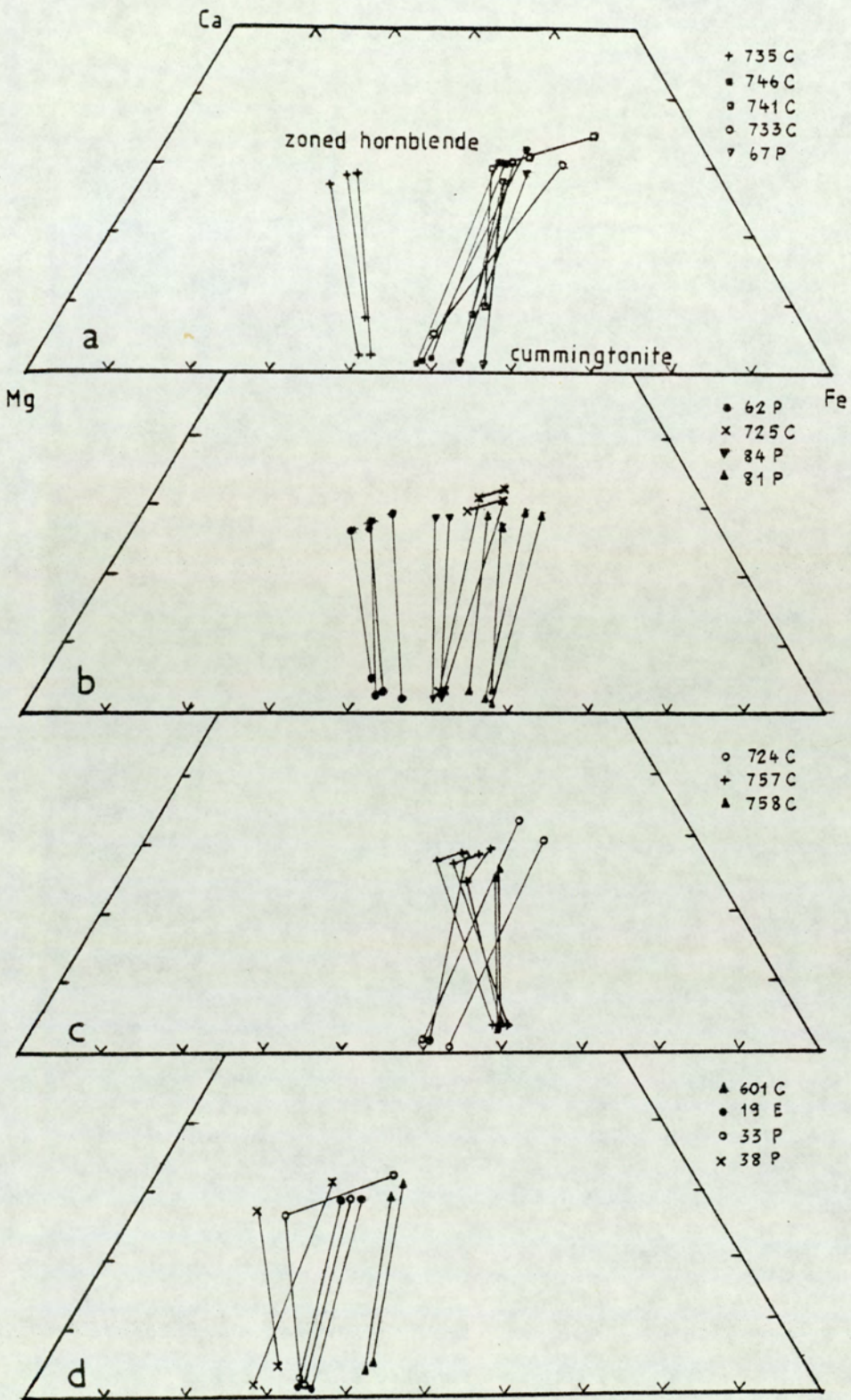


Fig 4.31 Ca-Mg-Fe plots of coexisting cummingtonite and hornblende.
 (a) - (c) Morven-Cabrach
 (d) Belhelvie and Glen Scaddle

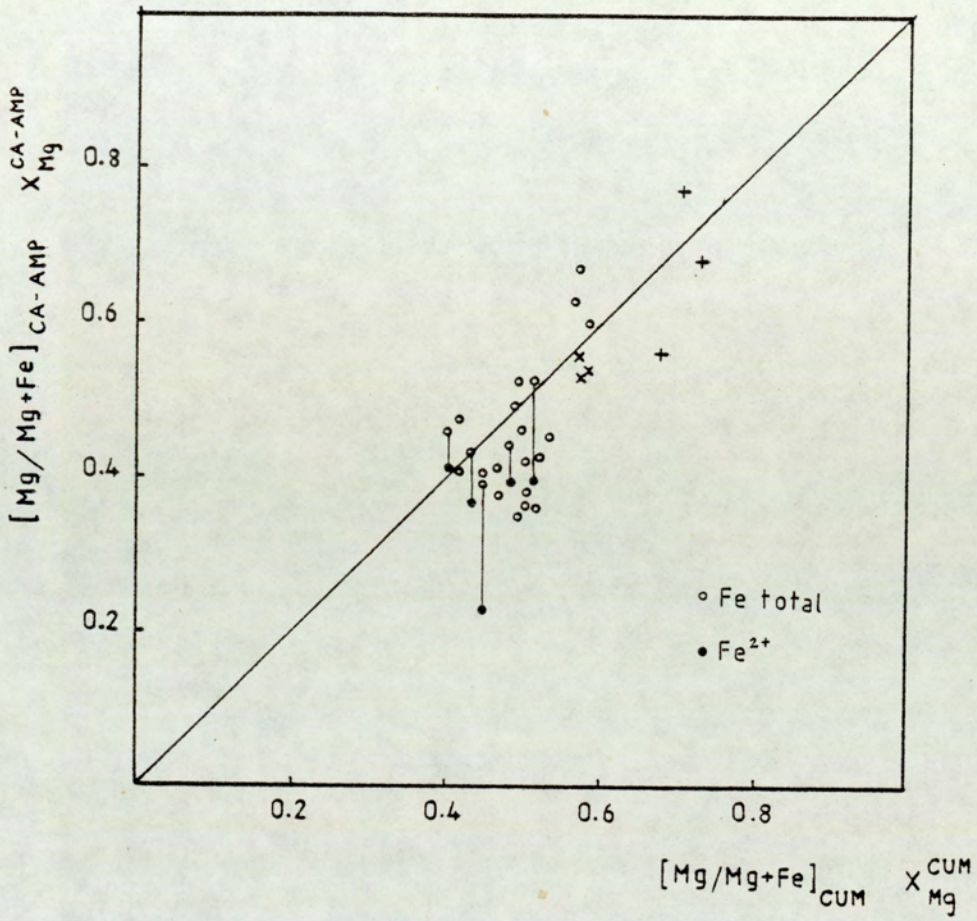


Fig 4.32 Mg-Fe partition between cummingtonite and hornblende after Kisch and Warnaars (1969).

- ° Morven-Cabrach area
- × Glen Scaddle area
- + Belhelvie area

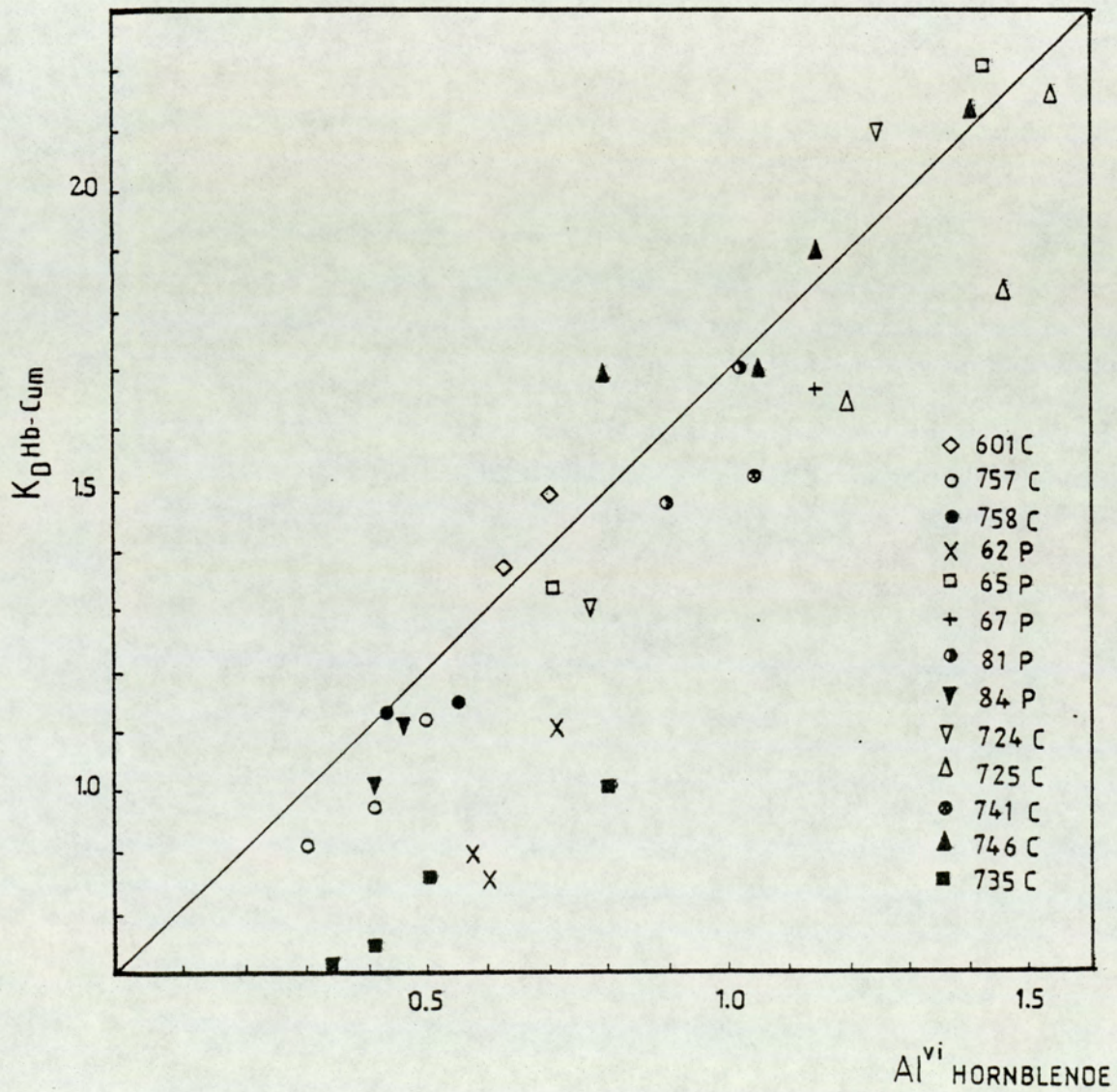


Fig 4.33 Dependence of the distribution coefficient for the partition of Fe, Mg between hornblende and cummingtonite on Al^{vi} content of hornblende.

has some dependence on Al^{vi} content of hornblende (Fig. 4.33) as suggested by Fleet et. al. (1978). From the analytical data of zoned hornblende, Mg decreases with Fe, Al increase outward, and the tschermakite substitution in hornblende then is dominantly $Al^{vi} Al^{iv}$ for MgSi substitution. In the initial stage of the reaction, it is thought that Al movement is very restricted, during the transformation to hornblende (tschermakitic) causing limited replacement of Mg by Al^{vi} .

The occurrence of a thin actinolite zone between cummingtonite and hornblende with irregular contacts in some specimens in both Morven-Cabrach and Belhelvie areas is thought to be due to slow diffusion of Al compared with the other elements, notably Ca.

As noted in the last section, in the Belhelvie area cummingtonite coexists with more aluminous hornblende than does actinolite. The obvious interpretation of the difference in Al content in both hornblendes is the limited movement of Al into cummingtonite which Al can move more easily into actinolite.

4.5.7 Hornblende-Plagioclase relations

Differences in the total Al content in hornblende in all studied areas, or even within the same intrusion cannot be simply related to the composition of co-existing plagioclase. However, between the Glen Scaddle and the Morven-Cabrach areas, the lower total Al content of the Glen Scaddle hornblende can be related to lower An content of the Glen Scaddle plagioclase (An_{28-38}) compared with those of the Morven-Cabrach area (An_{43-66}).

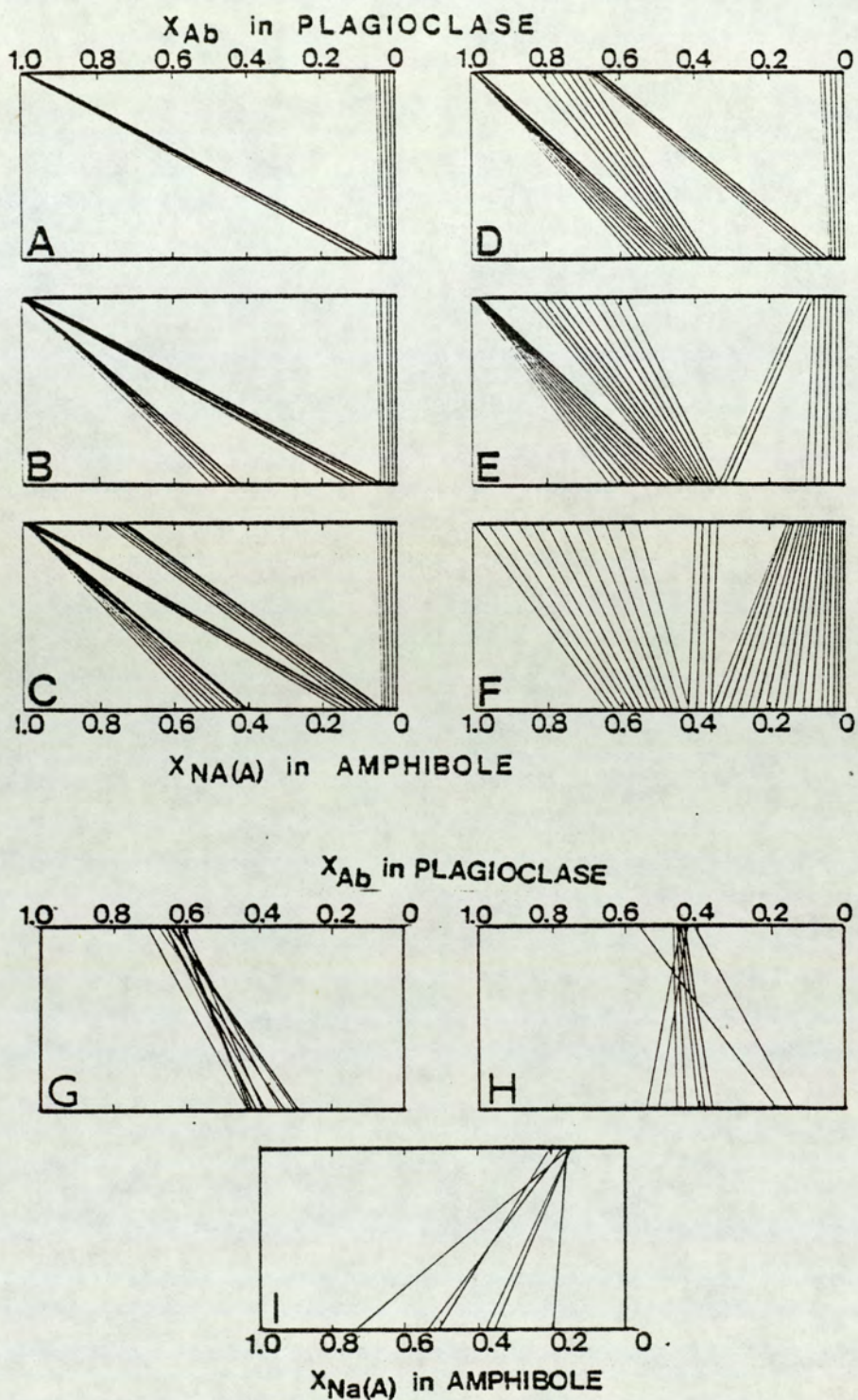


Fig 4.34

Relationships between hornblende and associated plagioclase in terms of Na distribution in plagioclase and M_4 in hornblende. A to F are expected equilibrium amphibole-plagioclase coexistence from Chlorite zone (A) to Sillmanite zone (F) after Spear (1981).

(G) Glen Scaddle, (H) Morven-Cabrach

(I) Belhelvie

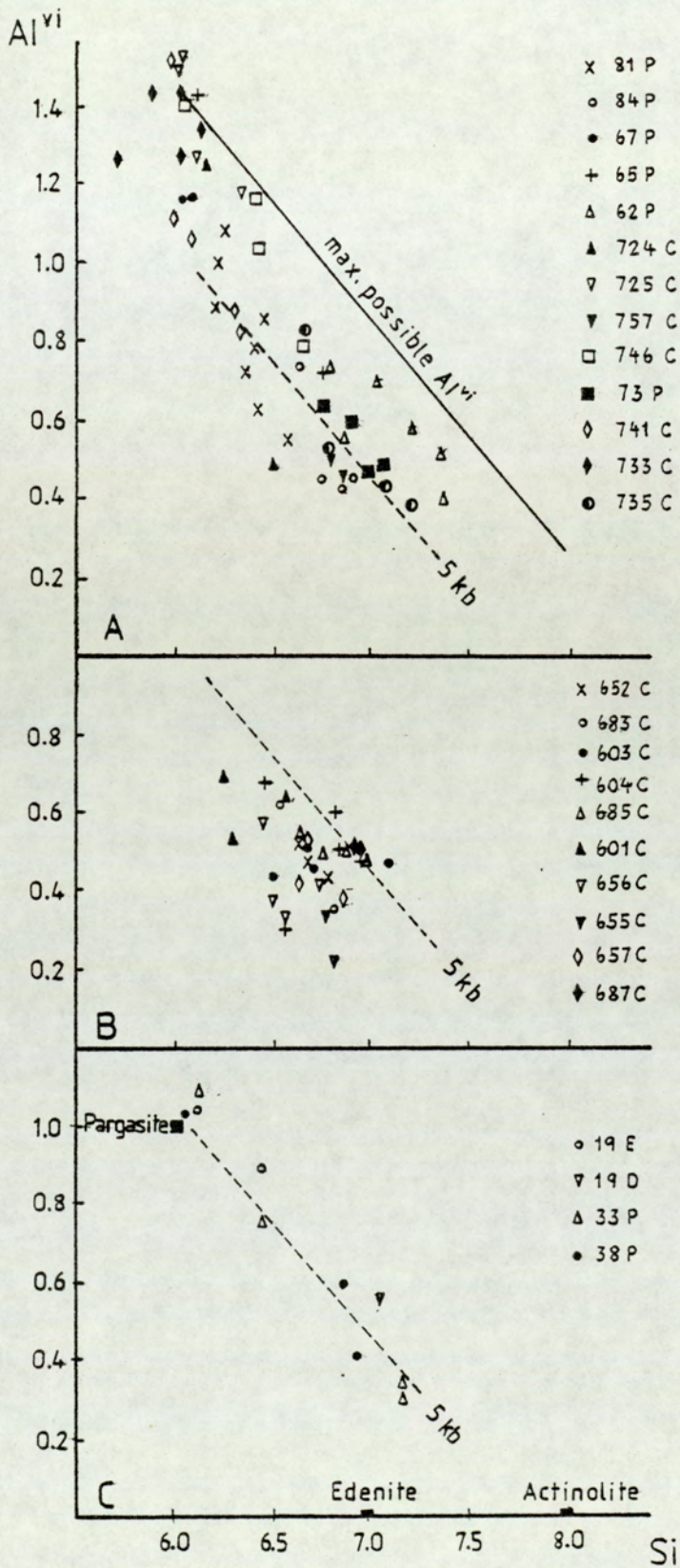


Fig 4.35 Relations between Al^{vi} and Si of hornblende compared with Raase (1974)

(A) Morven-Cabrach

(B) Glen Scaddle

(C) Belhelvie

Similar hornblendes are formed in all the areas, but only in the Glen Scaddle area has the plagioclase been thoroughly re-equilibrated. This can be seen from Figure 4.34, in which the Na distribution is plotted following Spear (1981). The Glen Scaddle hornblende-plagioclase pairs are consistent with equilibrium in the amphibolite facies. A few Morven-Cabrach specimens may also be close to equilibrium, but most are not. The Belhelvie plagioclase-hornblende relations represent gross disequilibrium. Figure 4.35 shows the Al^{iv} and Si contents of hornblende which according to Raase (1974) can be used as a geobarometer. Among the present data, only those for Glen Scaddle should be so used because they approach equilibrium with plagioclase. They suggest a metamorphic pressure less than 5 kbars.

4.6 CONCLUSIONS

Pyroxene compositions have re-equilibrated under the metamorphic conditions in the hydrous environment, by exchanging Ca, Fe and Mg and homogenization of these elements through the crystal. If metamorphic clinopyroxene predominates over actinolite, the reaction producing both minerals consumes Ca. On the other hand Ca is released by the reaction actinolite + plagioclase \longrightarrow hornblende + quartz, because the reactant plagioclase is calcic. This Ca may partly be fixed in the metamorphic pyroxene but can also contribute to the reaction cummingtonite + plagioclase \longrightarrow hornblende. Hornblende usually has higher Fe/Mg than cummingtonite and actinolite, implying exchange of these elements with the environment. Fe/Mg partition among minerals shows variations within a specimen, but tends towards equilibrium; in particular, systematic dependence on Al content of amphibole in the expected manner is found. Al content of hornblende does not systematically vary with plagioclase composition between areas; only ⁱⁿ the Glen Scaddle

area do hornblende and plagioclase closely approach equilibrium as the plagioclase composition has become more sodic. Even in this area, actinolite hornblende pairs show inconsistent Al partition indicating mutual disequilibrium. In all areas, disequilibrium coexistence is found along with continuous variation from actinolite to Al-rich hornblende and continuous zoning of individual grains across the supposed miscibility gap. Thus metastable equilibrium is approached for Fe/Mg partition among amphiboles whose Al contents are kinetically constrained. Actinolite-hornblende pairs occur because Al diffusion is slow: actinolite is a kinetically determined intermediate phase in the reaction from clinopyroxene to hornblende. Actinolite sometimes also occurs between cummingtonite and hornblende, because Ca diffuses more easily than Al. Thus all boundaries between aluminous and non-aluminous amphibole are inherited (may be modified greatly) from the original plagioclase/pyroxene interface. These boundaries are somewhat analogous to the "migrating central boundary" in the coronas around olivine (Chapter 3) but the present case is more complicated because some Al, Si movement is required in all cases and the boundary between actinolite and hornblende may become smeared out into a continuous zoning profile.

CHAPTER FIVE

EXSOLUTION OF ILMENITE AND RUTILE IN HORNBLLENDE

5.1 INTRODUCTION

Oxide inclusions in silicate minerals have been widely reported in the literature, concerning their orientation relationships and the modes of occurrence. In pyroxene, spinel and ilmenite inclusions have been originally studied by Bown and Gay (1959), followed by the description of rutile (Moore, 1968 and Griffin et. al. 1971) as well as spinel (Goode and Moore, 1975) and titanomagnetite (Elsdon, 1971). Recently, oriented magnetite inclusions in pyroxenes have been examined in detail by Fleet et. al. (1980). Ilmenite and spinel lamellae in pyroxenes have been interpreted as the products of subsolidus exsolution (Garrison and Taylor, 1981). Feldspar can exsolve hematite-like inclusions of various orientations (Copley and Gay, 1979). In olivine, ilmenite inclusions (Moseley, 1981) and spinel group inclusions (Champness, 1970 and Ashworth, 1979) have also been found.

Although the oxide inclusions in hornblende have been noticed (e.g. Fleet et. al. 1980), apparently, they have never been investigated in detail. As it is generally accepted that Ti content in hornblende tends to increase with increasing temperature of equilibration (e.g. Leake 1965, Bard 1970, Helz 1973 and Raase 1974), the exsolving of Ti phases during the cooling of hornblende could be possible.

The present study reports on oriented ilmenite and rutile inclusions

in hornblendes from the Glen Scaddle and the Glen Loy basic intrusions in NW Scotland. Similar oriented inclusions in hornblende have also been noticed in other intrusions associated with this thesis such as Portsoy and Morven-Cabrach intrusions. The techniques include the scanning electron microscope, electron probe microanalyser, universal stage measurements and single crystal X-ray oscillation photography.

5.2 SPECIMEN LOCALITIES

Three specimens examined in this study were collected from two slowly cooled basic intrusions in Argyllshire, NW Scotland. Two specimens (610 C and 612 C) came from the Glen Scaddle intrusion (c.f. section 2.1). The other specimen (659 C) is from the Glen Loy intrusion, which is of Caledonian synorogenic age (Institute of Geological Sciences, 1975). Their specimen localities are tabulated in Appendix 1.

5.3 PETROGRAPHY

Hornblende is the major mineral in all specimens with some plagioclase and small amounts of chlorite, sphene and ilmenite. Hornblende crystals are more or less oriented with generally euhedral forms. Plagioclase is fresh. Chlorite occurs as small flakes or less commonly along cracks in hornblende.

Oriented inclusions are densely distributed in the central parts of hornblende grains, leaving clear narrow margins (Fig. 5.1). The variation in colour within hornblende grains is from green in inclusion-bearing areas to brown in inclusion-free areas. Grains



20 μm



10 μm

Fig. 5.1

Optical micrographs of oriented inclusions in hornblende from Glen Scaddle specimen (612 C).

- (a) Transmitted plane polarized light micrographs, showing an array of inclusions (bottom right of the hornblende grain) while the majority of inclusions are scattered. Pale areas of hornblende are green, the darker are brown.
- (b) Reflected light micrograph.

generally have green inclusion-free edges. The majority of inclusions in the Glen Scaddle specimens are brown thin plates, varying in longest dimension from 1 to 10 μm , with minor acicular or rod like inclusions of stronger colour. The Glen Loy specimen contains finer grains of hornblende and the dark, dust-like, mostly acicular inclusions are also finer. Apart from scattered inclusions in the interior part of hornblende, the inclusions are also occasionally found as arrays or trains of small separate particles within hornblende grains (Fig. 5.1).

5.4 SCANNING ELECTRON MICROSCOPY (SEM)

The scanning electron microscopy combined with X-ray analyses was used (c.f. section 3.6). Two types of inclusion have been found, the pure Ti phase or rutile and the Ti-Fe phase (Fig. 5.2) which is identified using the transmission electron diffraction pattern to be ilmenite. Ilmenite is seen optically as brown thin plates while the acicular or rod-like inclusions are rutile. The analyses by SEM indicate that most of the inclusions in the Glen Scaddle specimens are ilmenite with minor rutile, while rutile predominates over ilmenite in hornblende from the Glen Loy specimen.

In order to obtain high contrast between these two phases, the back-scattered electron detector of the silicon diode system (Hall and Lloyd, 1981) has been used. Fig. 5.3 shows the SEM image with bright areas of ilmenite of higher atomic number than rutile (grey) and hornblende (black). Generally, rutile and ilmenite form separately, but intergrowths of rutile and ilmenite are occasionally seen (Fig. 5.3).

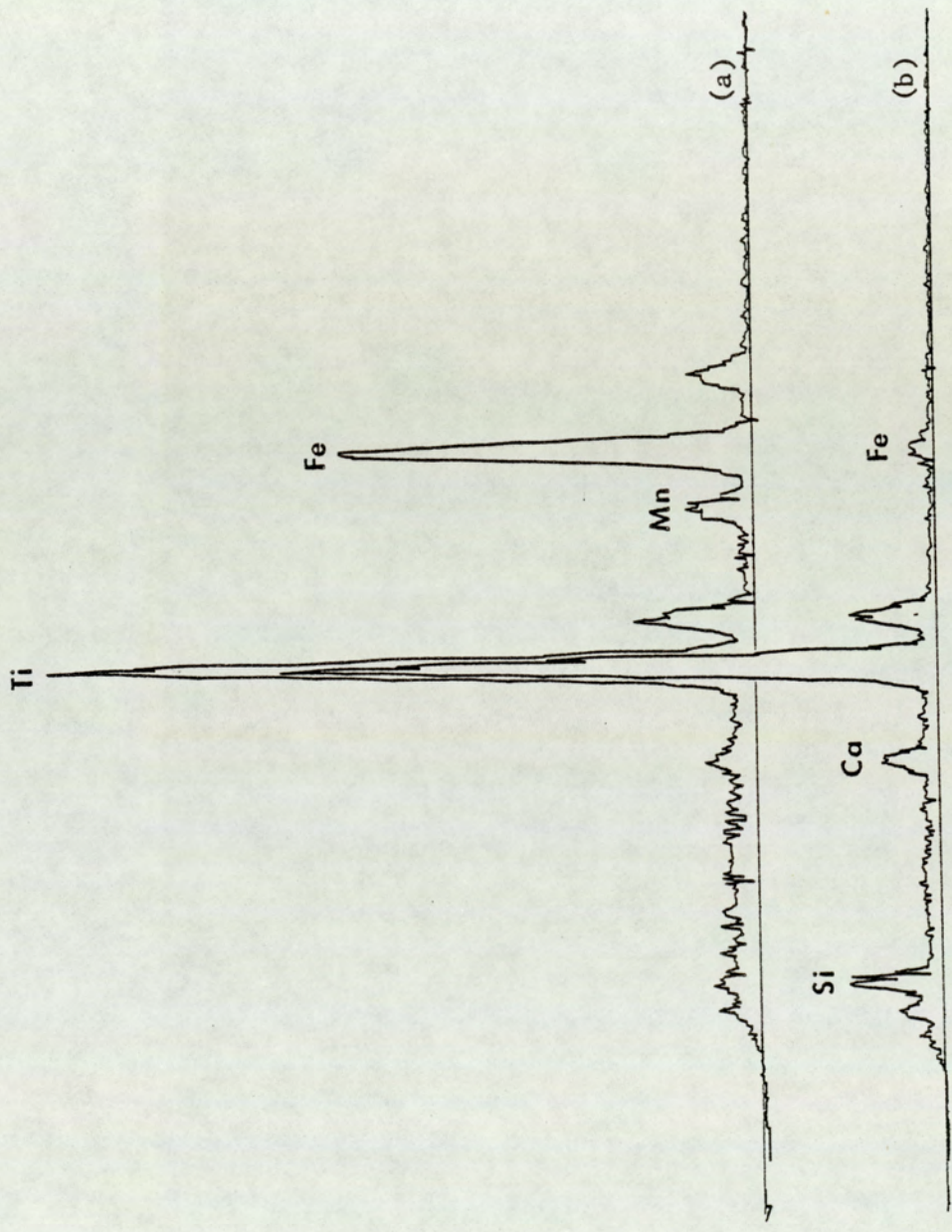


Fig. 5.2 Energy dispersive X-ray spectra of ilmenite inclusion (a) and a rutile inclusion (b) which is slightly contaminated by host hornblende

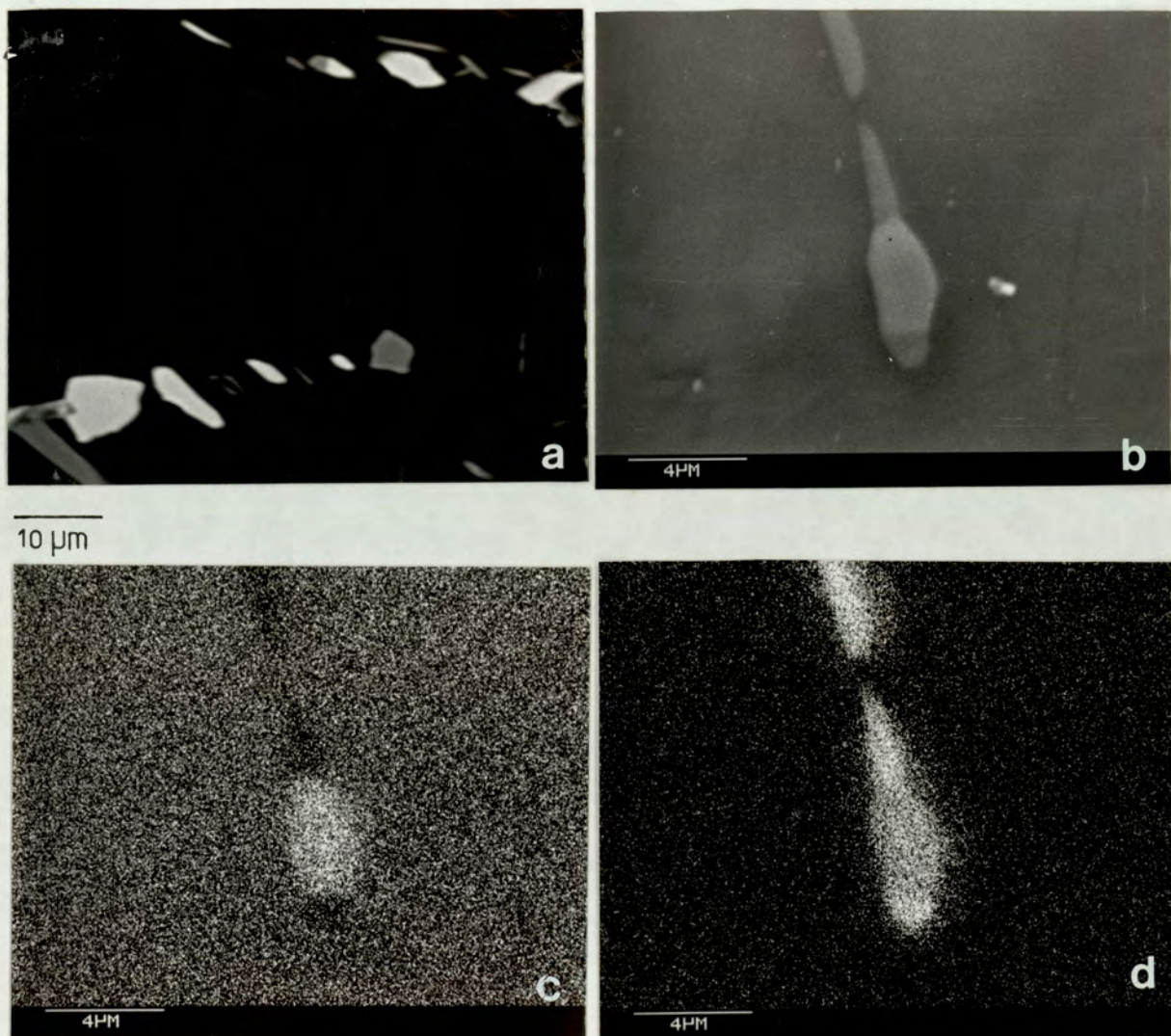


Fig. 5.3 SEM micrographs showing ilmenite and rutile inclusions.

- (a) Electron image obtained with a silicon-diode back-scattered electron detector, showing strong atomic number contrast between ilmenite (white) rutile (grey) and hornblende (black). This particular photograph shows two arrays of inclusions.
- (b) Electron image of ilmenite (white) and rutile (grey) intergrowth, obtained with a conventional detector. Note the much lower contrast than from (a), (c) and (d) are X-ray images of Fe and Ti respectively as the same areas as (b).

5.5 MINERAL COMPOSITIONS

The analysis of hornblende and ilmenite were made with the electron probe microanalyser under the same conditions as those described in section 3.5.1.

Although it was generally difficult to avoid the inclusions to get pure hornblende analyses, compositions of the Glen Scaddle hornblende were obtained separately from the ilmenite inclusions. Table 5.1 is representative of several grains analysed in specimen 612 C. The beam was focussed and optically visible inclusions were carefully avoided in the inclusion-bearing area. Analysis 1 represents the green, inclusion bearing area. Analysis 2 denotes the brown, inclusion free area and analysis 3 is the green, clear margin. The primary ilmenite (analysis 5) was also analysed for comparison with inclusion ilmenite (analysis 4). Their compositions are very similar.

The low Ti content of hornblende within the inclusion-bearing area compared with the brown, inclusion-free area, strongly indicates that excess Ti content in primary hornblende was thrown out to form rutile and ilmenite during cooling, an exsolution process. The brown areas in which the Ti-phase exsolution failed to develop perhaps represent the original hornblende compositions. However, the similar Fe-content in both green inclusion-bearing and brown inclusion-free areas suggest that the original amphibole must have been zoned. This is also confirmed by the green, Ti-poor, inclusion-free edges. Zoning in primary brown hornblende, without inclusions, having thin, green margins is also found in specimen 602 C of the Glen Scaddle intrusion (Table 4.10 in chapter 4).

TABLE 5.1. Electron microprobe analyses of hornblende and ilmenite

SPECIMEN No.	612 C					659 C	
MINERAL	AMPHIBOLE			ILMENITE		AMPHIBOLE	
ANALYSIS No*	1	2	3	4	5	6	7
Na ₂ O	1.94	1.91	1.82	-	-	2.44	2.58
MgO	11.91	11.70	11.20	0.12	0.05	13.46	13.73
Al ₂ O ₃	13.15	12.86	14.10	-	-	12.53	12.78
SiO ₂	42.19	41.93	41.11	-	-	41.76	42.91
K ₂ O	0.67	0.67	0.49	-	-	0.70	0.58
CaO	11.62	11.51	11.60	0.02	0.19	11.47	11.25
TiO ₂	1.56	2.46	1.23	49.41	49.56	3.52	2.56
MnO	0.18	0.17	0.14	1.05	1.36	0.22	0.17
FeO**	13.82	13.89	14.76	48.76	47.88	12.05	11.92
H ₂ O+	2.01	2.01	1.99	-	-	2.04	2.06
Total	99.05	99.09	98.33	99.36	99.04	100.19	100.54

Formula to 23 oxygens				to 6 oxygens		to 23 oxygens	
Si	6.29	6.26	6.20	-	-	6.14	6.26
Aliv	1.71	1.74	1.80	-	-	1.86	1.74
	8.00	8.00	8.00			8.00	8.00
Alvi	0.61	0.52	0.71	-	-	0.31	0.45
Ti	0.18	0.28	0.13	1.88	1.89	0.39	0.28
Fe ³⁺	-	-	-	0.24++	0.22++	-	-
Fe ²⁺	1.72**	1.73**	1.86**	1.83	1.82	1.48**	1.45**
Mg	2.65	2.60	2.52	0.01	0.00	2.95	2.98
Mn	0.02	0.02	0.02	0.05	0.06	0.03	0.02
	5.18	5.15	5.24			5.16	5.18
Na	0.56	0.55	0.53	-	-	0.70	0.73
Ca	1.86	1.84	1.88	0.00	0.01	1.81	1.76
K	0.13	0.13	0.10	-	-	0.13	0.11
	2.55	2.52	2.51			2.64	2.60

- * 1: green hornblende in inclusion-bearing area
 2: brown hornblende of inclusion-free area
 3: green margin (without inclusions) of hornblende
 4: primary ilmenite
 5: ilmenite inclusion in hornblende
 6: amphibole plus inclusions of rutile
 7: green margin, inclusion-free hornblende

** Total Fe as FeO

+ H₂O calculated from ideal formula

++ Fe³⁺ estimated from stoichiometry

It is impossible to analyse pure hornblende in the inclusion-bearing areas of the Glen Loy specimen: analysis 6 thus represents hornblende plus rutile inclusions using defocussed beam. This analysis should serve as an estimate of primary hornblende composition. The green, inclusion-free edge of the same grain is also tabulated in Table 5.1 (analysis 7).

According to the I.M.A. nomenclature of amphiboles (Leake, 1978) and taking total Fe as Fe^{2+} , the pure amphiboles (analyses 1, 2, 3 and 7) are classified as ferroan pargasitic hornblende. The analysis of amphibole plus inclusions (analysis 6), which should be the primary amphibole composition, indicates it was a ferroan pargasite.

5.6 ESTIMATION OF VOLUME PROPORTIONS OF ILMENITE INCLUSIONS IN A HORNBLLENDE

The proportions of ilmenite inclusions in hornblende in the Glen Scaddle specimen have been determined using the digitizer (c.f. section 3.7). Seven reflected-light photomicrographs of two grains of hornblende were analysed. Each photograph contains evenly scattered inclusions (Fig. 5.1 b) of area approximately $150 \times 100 \mu m$. The two grains digitized were both analysed by EPMA and one of them gave the results tabulated in Table 1. The other gave inferior but very similar analyses. The inclusions are known to be almost all ilmenite (from SEM work). The data indicate the presence of 1.99 to 3.34%, averaging 2.60, modal % ilmenite. This is a minimum estimate since very small particles (seen in TEM) may not be resolved in optical photomicrographs, but these are probably only a very small additional ilmenite volume.

Although the appearance of ilmenite inclusions under the microscope is numerous, the inclusion/host volume ratio is very low. The analysis of hornblende plus inclusion also shows a reasonable hornblende composition. It is then reasonable to suggest that the inclusions were produced by exsolution from the original hornblende in a closed system. The predominance of ilmenite over rutile inclusions in the Glen Scaddle hornblende is probably due to higher Fe content in primary amphibole (analysis 1) compared with the Glen Loy amphibole (analysis 6, 7) of higher Ti but lower Fe contents which alternatively exsolved more rutile than ilmenite.

5.7 ORIENTATION RELATIONSHIPS BETWEEN ILMENITE AND HORNBLENDE HOST

5.7.1 Universal-stage Measurements

Although the inclusions are precipitated in consistent orientations (Fig. 5.1), only ilmenite of platy morphology and coarser grains can be oriented using the four-axis universal stage. The poles of normals of platy ilmenites relative to crystallographic directions of hornblende ($C2/m$ setting) are plotted in Fig. 5.4. Due to the very small sizes and irregular shapes of some ilmenites, only three simple orientations apart from the scattered orientations have been observed. They are concentrated near a^* , b and c of hornblende indicating that the platy habit plane of ilmenite (0001) is approximately in (010), (100) and (001) planes of hornblende. Other orientations are scattered, though they seem to concentrate in the upper half of the stereogram ($\bar{h}kl$ and $\bar{h}\bar{k}l$ positions) which are equivalent by the (010) mirror plane of hornblende. The universal stage measurements do not provide complete results for

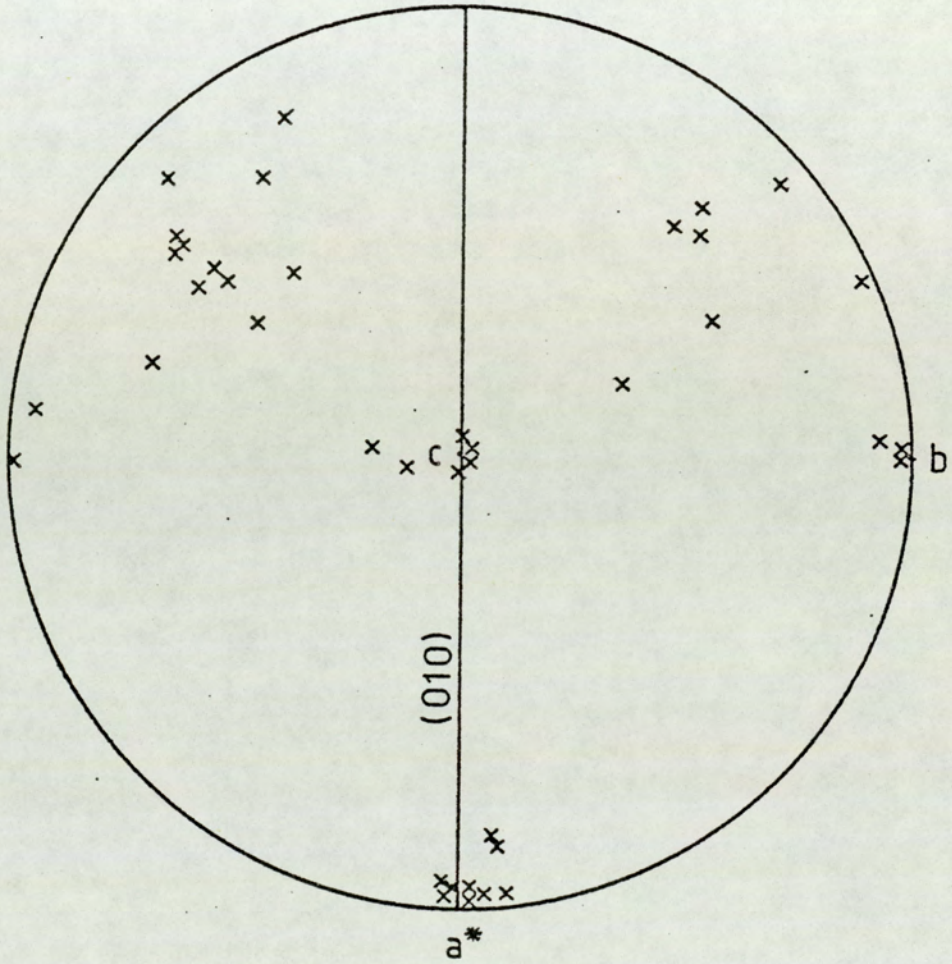


Fig. 5.4

Upper hemisphere stereogram, showing the poles of normals to plate-like ilmenite inclusions relative to crystallographic directions for the host hornblende ($C2/m$ setting) measured by universal stage microscopy.

the purpose of the study. Further studies including transmission electron microscopy and X-ray diffraction were undertaken.

5.7.2 Transmission Electron Microscopy (TEM)

A thin section of specimen 612 C was double polished and demounted. Parts of the specimen which contain hornblendes with a large amount of inclusions were selected and mounted on titanium mesh support grids. They were thinned by ion bombardment until there were holes in the specimen, to be able to study the thin areas around the holes. The specimens were examined using a JEOL JEM 100B instrument operating at 100kV. These observations are supplementary to a more extensive study by Dr. Ashworth using the more specialized technique of high-voltage TEM (Mongkoltip and Ashworth, 1983).

In describing crystallographic relations, the $C2/m$ setting of hornblende is used and ilmenite is set on hexagonal axes. All oxide particles were identified as mainly ilmenite with minor rutile. Ilmenite, which has (0001) platy habit, is found in orientations which fit the four relationships to hornblende established in the high voltage TEM work: (0001) of ilmenite is parallel to hornblende (100), (001), ($\bar{2}61$) and (26 $\bar{1}$). Therefore, there are two distinct orientations of the form $\{\bar{2}61\}$. These four orientations can be found close together and they are true whether ilmenites are scattered or form small arrays. Some of the diffraction patterns used for interpretation are shown in Fig. 5.5. The incomplete coherence between these two structures can be observed as misfit dislocations along interfaces of ilmenite particles in contact with hornblende (Fig. 5.6). In some ilmenite inclusion, fine platelets presumed to be hematite are found in

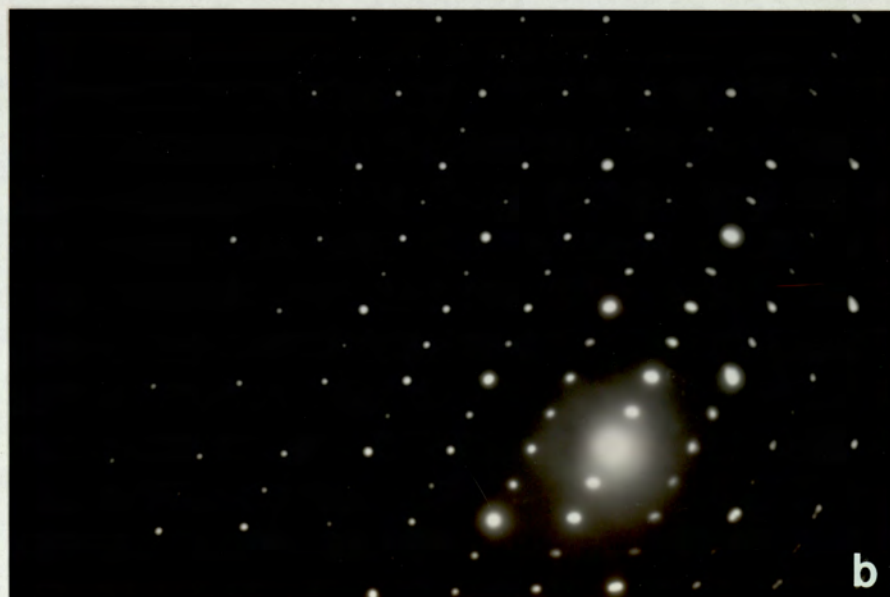
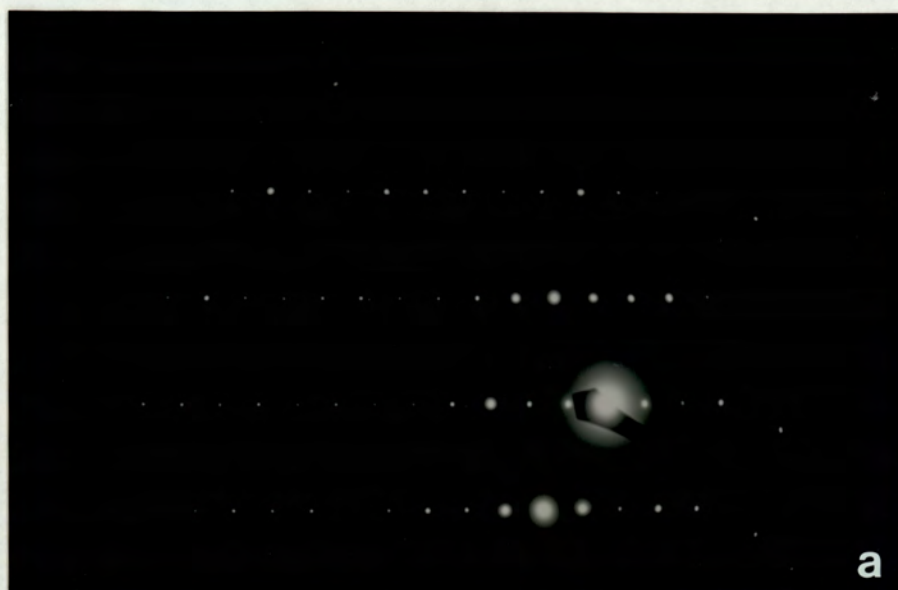
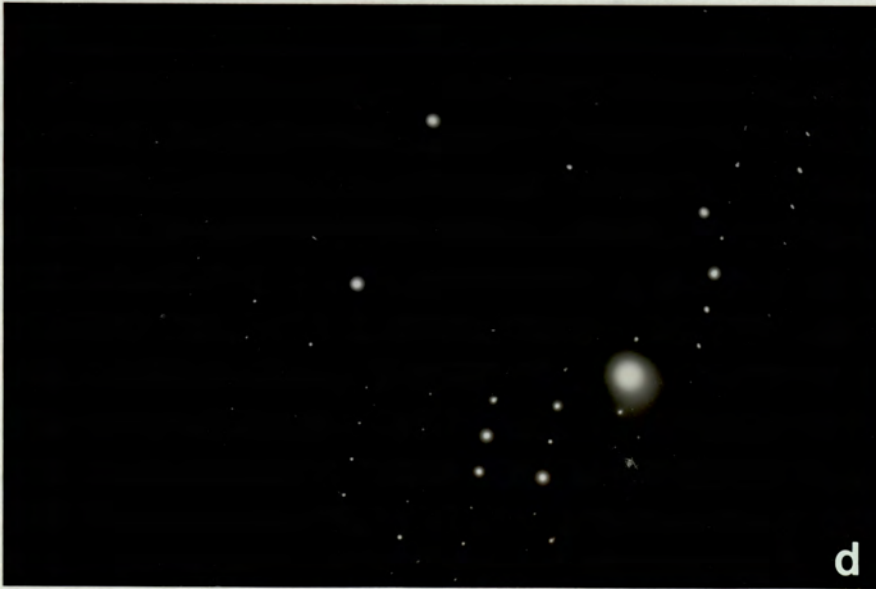


Fig. 5.5 Electron diffraction patterns of hornblende host and ilmenite inclusions

- (a) [116] zone of hornblende
(b) [100] zone of hornblende



- (c) $\bar{1}11$ zone of ilmenite
- (d) Superimposed ilmenite $[13, 2, 4)$ and hornblende $[112]$ diffraction patterns of (261) type orientation. $((0001)$ ilmenite // (261) of hornblende).

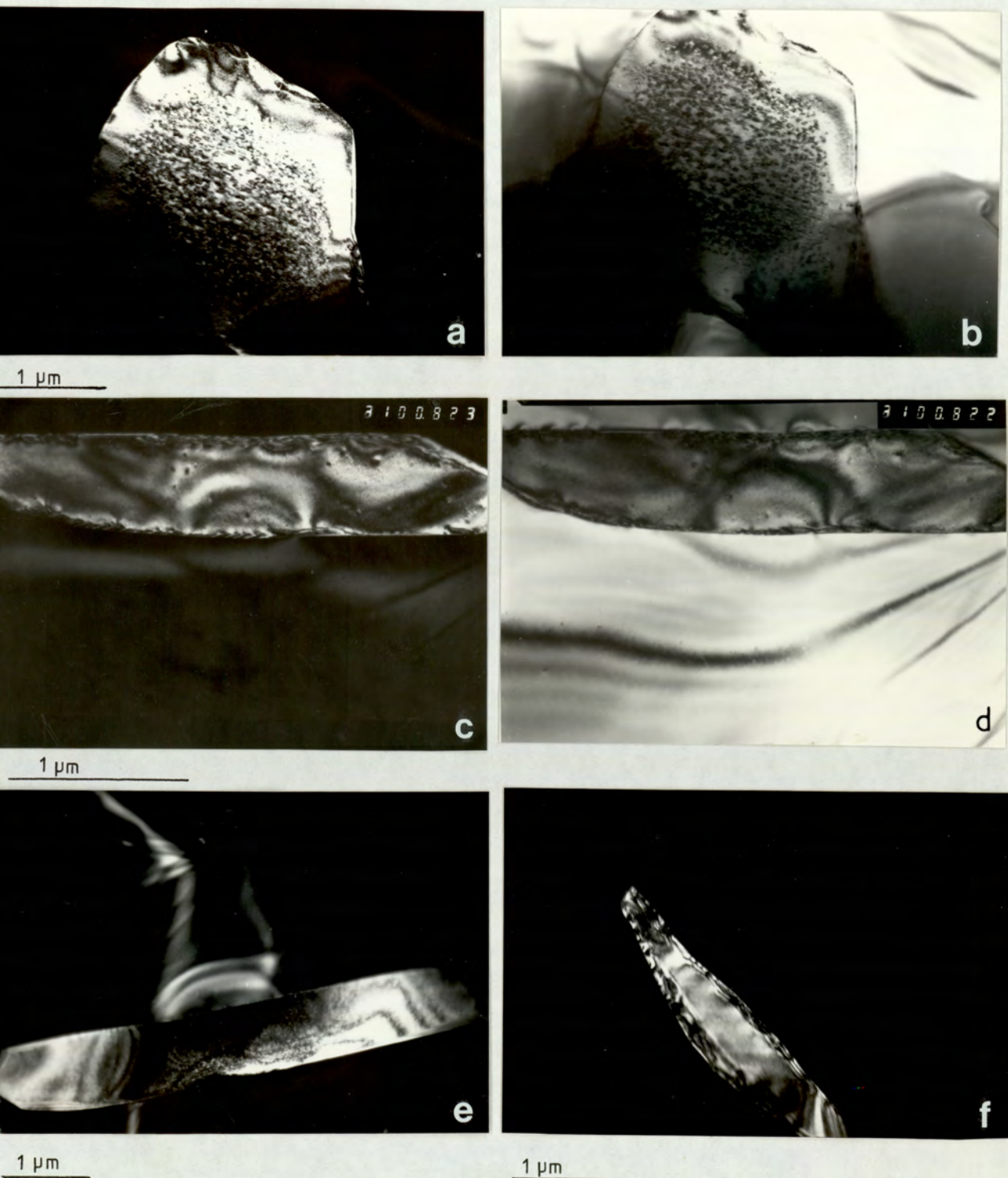


Fig. 5.6

TEM micrographs showing shapes and sizes of ilmenite inclusions in hornblende.

(a), (b): dark and bright field images showing platelets substructure in the inner part of an ilmenite inclusion.

(c), (d): dark and bright field images showing misfit dislocations in the interfaces with hornblende.

(e), (f): dark field images of ilmenite inclusions.

the central part of the grain (Fig. 5.6).

5.7.3 Single-crystal X-ray Diffraction

A hornblende single crystal showing good crystal form was selected from specimen 610 C. The length of the crystal along the C axis is less than 1 mm. The crystal was mounted on the end of a thin glass fibre with araldite. By using the morphology of the crystal, the C axis was set approximately parallel to the long direction of the glass fibre. Once the mounted crystal was placed in a goniometer head, the two arcs on the goniometer head were adjusted until the C rotation axis were made parallel to the goniometer axis. The method of alignment correction by Davies (in Zussman, 1977) was used. The photographs were taken with the crystal oscillating through a 20° angle using the Cr tube. The exposures of each photograph are around 6 to 10 hours.

The interpretation of orientation relations between hornblende and ilmenite inclusions would be very difficult without previous work (universal stage measurement and TEM). The purpose of the single-crystal oscillation X-ray diffraction is to check the consistency of ilmenite lattice orientations throughout a larger volume than could be studied in the TEM work.

For the four main orientations, the ilmenite zone axes approximately parallel to the C-axis of hornblende are as follows: for $(0001)_{ilm}$ // $(\bar{2}61)_{hb}$, $[261]_{ilm}$ // C_{hb} ; for $(0001)_{ilm}$ // $(\bar{2}\bar{6}1)_{hb}$, $[\bar{4}21]_{ilm}$ // C_{hb} ; for $(0001)_{ilm}$ // $(001)_{hb}$, $[111]_{ilm}$ // C_{hb} ; and for $(0001)_{ilm}$ // $(100)_{hb}$, $[110]_{ilm}$ // C_{hb} . So, the reciprocal lattice of hornblende oscillates about the C-axis and four reciprocal lattices

of ilmenite about $[261]$, $[\bar{4}21]$, $[111]$ and $[110]$. Each lattice of ilmenite is in a pair related by hornblende symmetry specifically by reflection in the (010) mirror plane, therefore there are 8 reciprocal lattices altogether.

Using the Hewlett-Packard 85 microcomputer, the ξ , and η value in each reciprocal-lattice layer and the horizontal distance in mm, $/x/$, from a vertical line through the central spot were tabulated for hornblende and ilmenite. First, the hornblende spots were identified to find the centre of oscillation. Then the ilmenite spots were indexed. The sets of ilmenite axes used to index the X-ray photographs differ from (but are equivalent to) those used by Mongkoltip and Ashworth (1983); they merely represent a different arbitrary choice of a_1 , a_2 and a_3 axes within (0001) plane of ilmenite. The $[261]_1$, $[110]_1$, and $[111]_1$, settings used here correspond exactly to $[261]$, $[110]$, $[111]$, of Mongkoltip and Ashworth (1983). The $[\bar{4}21]_1$, setting corresponds to their $[\bar{2}\bar{6}1]$. The $[261]_2$, $[110]_2$, $[111]_2$ and $[421]_2$ correspond respectively to $[\bar{2}\bar{6}\bar{1}]$, $[\bar{1}\bar{1}0]$, $[\bar{1}\bar{1}\bar{1}]$ and $[26\bar{1}]$.

Two photographs are presented from two different oscillation ranges (Fig. 5.7). Most of the predicted ilmenite spots in each orientations of ilmenite are found, some being unrecorded probably due to their low intensity. Ilmenite layer lines are found on the photographs because of the coincidence of the rational zone axis of ilmenite with C axis of hornblende. The displacements of some ilmenite spots from the first layer line (Fig. 5.7b) are presumably related to inexactness of this coincidence due to the misfit between ilmenite and hornblende oxygen planes (Fig. 5.8). All 8 orientations found by TEM work are confirmed by the X-ray

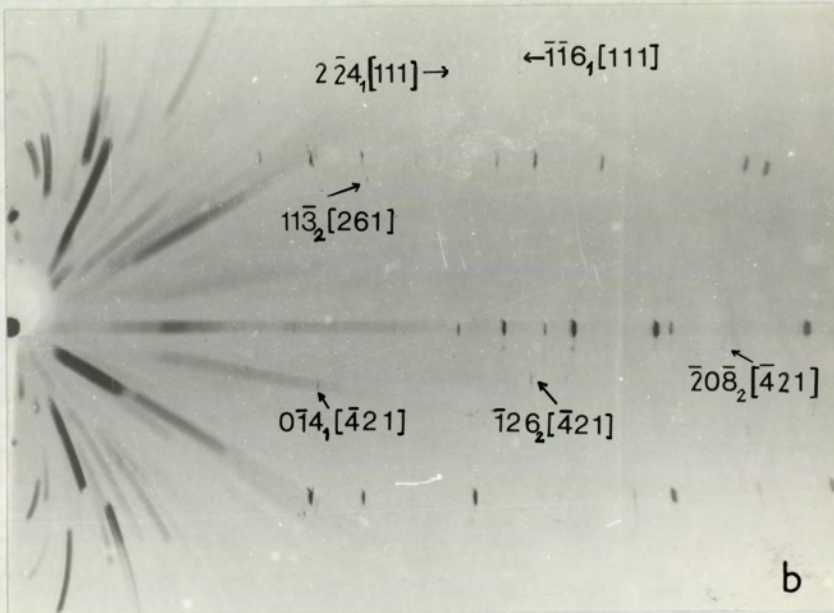
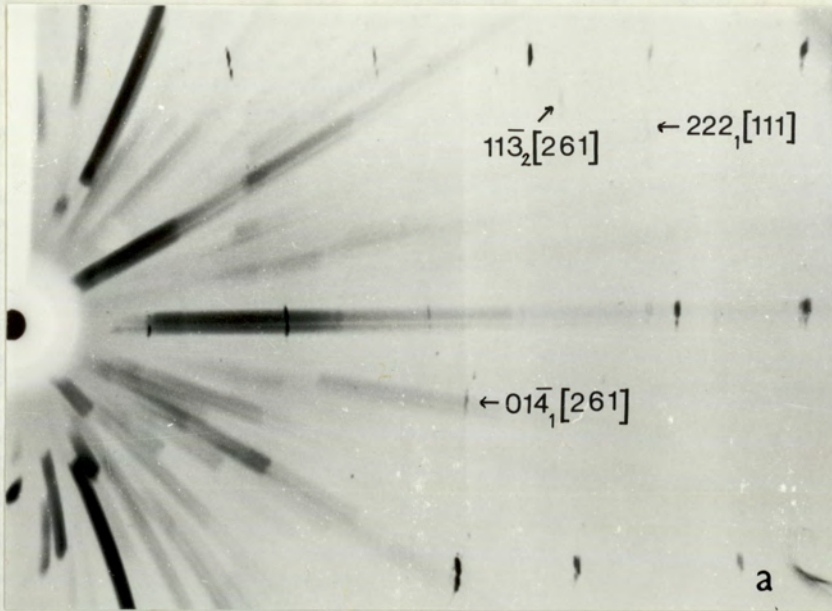


Fig. 5.7 X-ray oscillation photographs of hornblende of specimen 610 C, taken with centre of oscillation about

- (a) 20° away from a^* toward $-b^*$, 10 hours exposure.
- (b) 30° away from a^* toward b^* , 6 hours exposure. The displacements of some ilmenite spots from the first layer line are presumably related to the misfit between ilmenite and hornblende structures.

TABLE 5.2 INDEXED ILMENITE SPOTS RELATED TO ILMENITE ZONE AXIS
WHICH IS APPROXIMATELY PARALLEL TO C OF HOST HORNBLENDE

Photograph No.	Oscillation Centre	hkl of ilmenite spot	Orientation of ilmenite lattice*
1	35° away from b* towards -a*	$2\bar{2}4$	$[111]_1$
		$\bar{1}14$	$[111]_2$
		$21\bar{2}$	$[111]_1$
		$\bar{1}\bar{1}6$	$[111]_1$
		$1\bar{2}9$	$[\bar{4}21]_1$
		$3\bar{3}0$	$[110]_1$
		$00\bar{6}$	$[110]_1$
		$10\bar{8}$	$[110]_1$
		018	$[110]_2$
2	30° away from a* towards b*	$\bar{2}04$	$[111]_1$
		$2\bar{2}4$	$[111]_1$
		$\bar{1}\bar{1}6$	$[111]_1$
		$\bar{3}24$	$[111]_2$
		$\bar{1}14$	$[110]_1$
		$\bar{1}0\bar{4}$	$[\bar{4}21]_1$
		104	$[110]_1$
		$2\bar{1}0$	$[110]_1$
		$11\bar{3}$	$[261]_2$
		$\bar{2}3\bar{8}$	$[261]_2$
		$\bar{2}0\bar{5}$	$[\bar{4}21]_1$
		$\bar{2}\bar{1}\bar{1}$	$[\bar{4}21]_2$
		$0\bar{1}4$	$[\bar{4}21]_1$
		$\bar{1}\bar{2}1$	$[\bar{4}21]_2$
$\bar{1}2\bar{5}$	$[\bar{4}21]_2$		
3	20° away from a* towards -b*	10 (10)	$[110]_1$
		$\bar{2}34$	$[110]_1$
		$\bar{3}24$	$[111]_1$
		$\bar{2}37$	$[110]_1$
		$1\bar{3}4$	$[111]_2$
		$\bar{2}22$	$[111]_1$
		$1\bar{2}3$	$[111]_1$
		$01\bar{4}$	$[261]_1$
		$0\bar{1}4$	$[\bar{4}21]_2$
		$\bar{3}06$	$[261]_2$
		$\bar{2}1\bar{6}$	$[\bar{4}21]_1$
$\bar{1}0\bar{4}$	$[\bar{4}21]_2$		
$\bar{1}3\bar{2}$	$[\bar{4}21]_2$		

* 1, 2 represent lattice pair by hornblende symmetry.

oscillation diffraction study. Table 5.2 is the list of identified ilmenite spots from Fig. 5.7 and another photograph which was taken at 35° away from b^* toward $-a^*$ of hornblende.

For rutile, which is the minority of the inclusions, a few intense spots can be identified. A few unidentified spots could be reflections from the platy ilmenite on (010) of hornblende, observed by the universal stage (Fig. 5.4), and chlorite which is occasionally found as patchy alteration in hornblende.

5.8 COMPARISON OF ILMENITE AND HORNBLLENDE CRYSTAL STRUCTURES

The observed orientation relationships between the two minerals can be interpreted in terms of their crystal structures.

In the normal ilmenite structure the layers of oxygen atoms are arranged in approximately hexagonal close packing (Fig. 5.8 d). In the exsolution of ilmenite, the oxygen stacking sequence of hornblende must rearrange itself into the hexagonal close packed. Theoretically, close packed oxygen atoms in amphibole can be generated by the full O^- rotation of the double SiO_4 chains (Thompson, 1970). It was observed by Papike et. al. (1973) that in the amphibole structure, a complete S^- rotation results in hexagonal close-packing of oxygen atoms and a complete O^- rotation in cubic close packing of oxygen atoms. In the real structure, the hornblende is partly O^- rotated (Cameron and Papike, 1979) and it is closer to the fully extended than the fully rotated theoretical structures (Law and Whittaker, 1980). Therefore, the oxygen stacking sequence of hornblende had to change from approximately cubic to hexagonal closed-packed during the ilmenite exsolution process. This transformation generates a misfit between

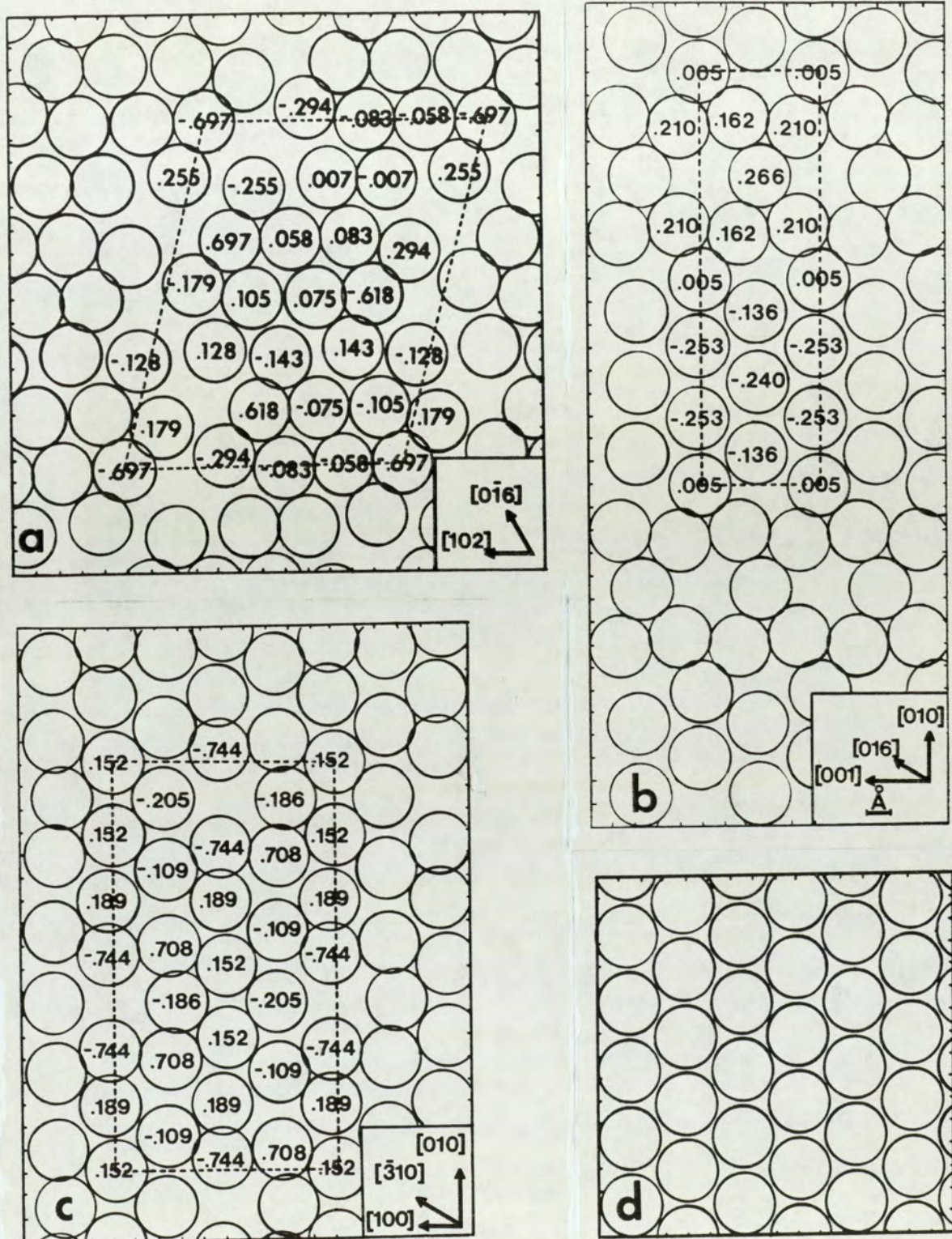


Fig. 5.8

The arrangement of oxygen atoms in the nearly close-packed planes of hornblende.

- (a) $\{\bar{2}61\}$
- (b) (100)
- (c) (001)
- (d) the hexagonal arrangement in (0001) of ilmenite

ilmenite and hornblende structures. This contributes to the mismatch along ilmenite interfaces (Fig. 5.6). The arrangements of oxygen atoms in hornblende structure along (100), (001) and $\{\bar{2}61\}$ planes, derived from the unit cell parameters and atomic co-ordinates given by Papike et. al. (1969), are shown in Fig. 5.8. In the theoretical fully O-rotated structure, these are the four close-packed planes. Although the oxygen atoms are arranged in approximately hexagonal configuration in the real structure, there is a discrepancy between the oxygen layer in ilmenite (Fig. 5.8) and the corresponding distances in hornblende, causing a misfit between them.

In conclusion, hornblende can exsolve ilmenite during the cooling to accommodate the Ti equilibration content which tends to decrease with decreasing temperature. Like oxides exsolved from most of the silicate minerals, the orientations of ilmenite were controlled by the packing of oxygen atoms in hornblende. The misfit dislocations along ilmenite interfaces are due to the discordance between the two structures.

APPENDIX 1

SPECIMEN LIST AND LOCALITY MAPS

1. GLEN SCADDLE INTRUSION

SPECIMEN NO.	GRID REFERENCES
598 C	NN 000691
599 C	NN 000691
600 C	NN 001690
* 601 C	NM 988688
* 602 C	NM 992690
* 603 C	NM 992690
* 604 C	NM 989689
605 C	NM 986688
606 C	NM 986688
607 C	NM 986688
608 C	NM 986688
609 C	NM 985688
610 C	NM 983685
611 C	NM 983685
* 612 C	NM 983685
613 C	NM 983685
651 C	NM 997696
* 652 C	NM 995696
653 C	NM 995696
654 C	NM 988698
* 655 C	NM 982698
* 656 C	NM 978700
* 657 C	NM 967698
658 C	NM 963685
673 C	NN 003684
674 C	NN 004683
675 C	NN 004683
676 C	NN 004682
677 C	NN 003679
* 678 C	NN 003679
679 C	NM 999677
680 C	NM 996676
681 C	NM 996676
682 C	NM 995677
* 683 C	NM 994677
684 C	NM 994680
* 685 C	NN 007653
686 C	NN 004653
* 687 C	NN 005655
688 C	NN 005656
689 C	NN 008659
690 C	NN 008659
691 C	NN 008659
692 C	NN 011662
693 C	NN 012663
694 C	NN 012663
695 C	NN 012663
696 C	NN 012660

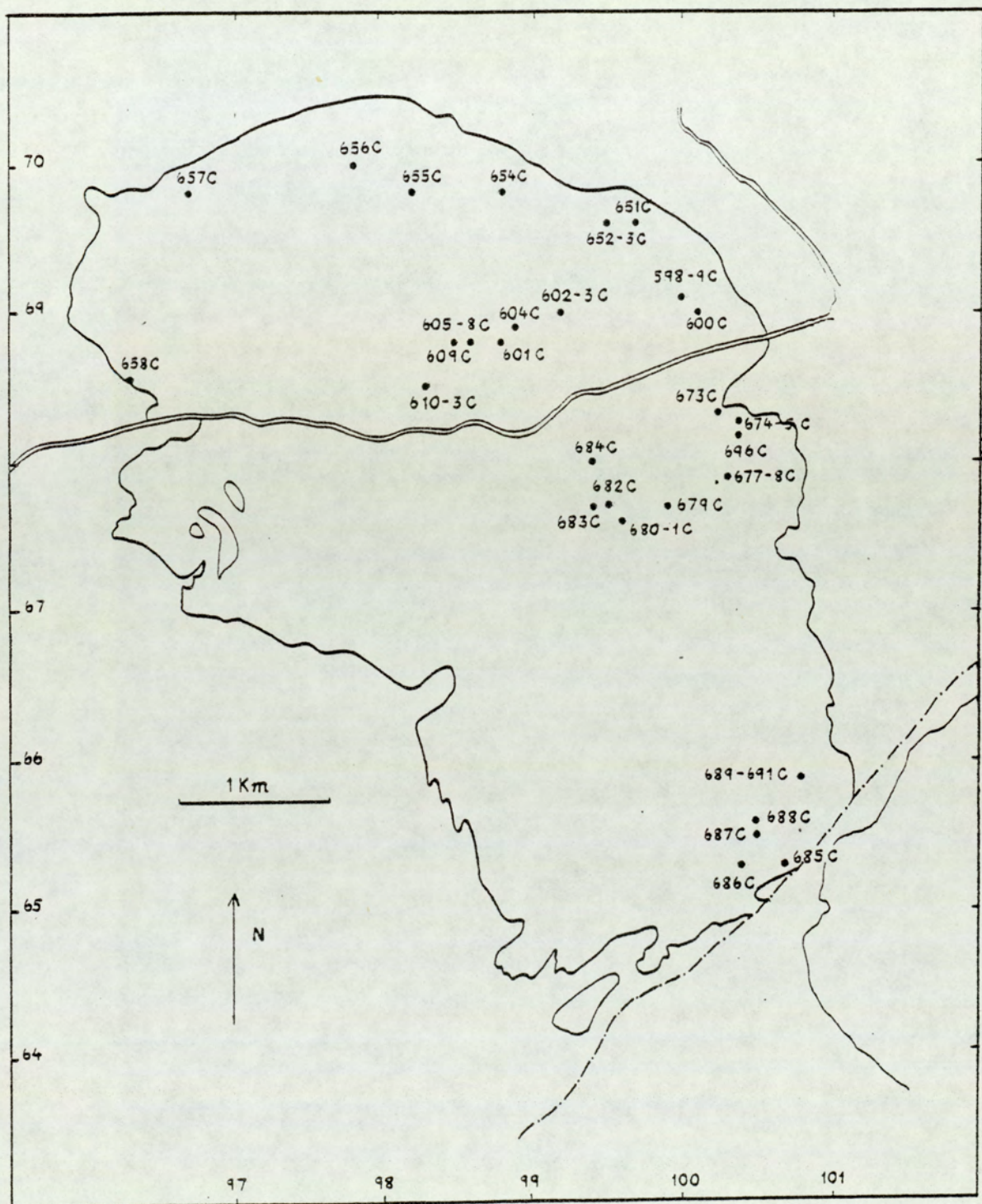


Fig. 1. Specimen location map of the Glen Scaddle intrusion.

2. MORVEN-CABRACH INTRUSION

SPECIMEN NO	GRID REFERENCES
* 62 P	373164
63 P	373164
64 P	373167
* 65 P	373165
66 P	373165
* 67 P	386081
68 P	386081
69 P	386081
70 P	379068
71 P	380067
72 P	380064
* 73 P	384078
74 P	362137
75 P	362137
76 P	362137
77 P	359123
78 P	348125
79 P	348125
80 P	348125
* 81 P	348125
82 P	375128
83 P	375128
* 84 P	376126
719 C	393093
720 C	392091
721 C	391089
722 C	388087
723 C	388086
* 724 C	388086
* 725 C	348089
726 C	347084
727 C	346084
728 C	345077
729 C	345076
730 C	379063
731 C	376062
732 C	374061
* 733 C	367055
734 C	365054
* 735 C	361052
736 C	353057
737 C	347057
738 C	347057
739 C	355053
740 C	357052
* 741 C	359049
742 C	361049
743 C	368053
744 C	399066
745 C	397066
* 746 C	397063
747 C	395061

2. MORVEN-CABRACH INTRUSION (CONTINUED)

SPECIMEN NO.	GRID REFERENCES
748 C	393055
749 C	393055
750 C	384051
751 C	380050
752 C	372047
753 C	379047
754 C	380063
755 C	381064
756 C	381064
* 757 C	387021
* 758 C	385021
759 C	373026
760 C	369026
761 C	364026
762 C	360026
763 C	353028
764 C	361023
765 C	383028
766 C	384035
767 C	388037
768 C	402028

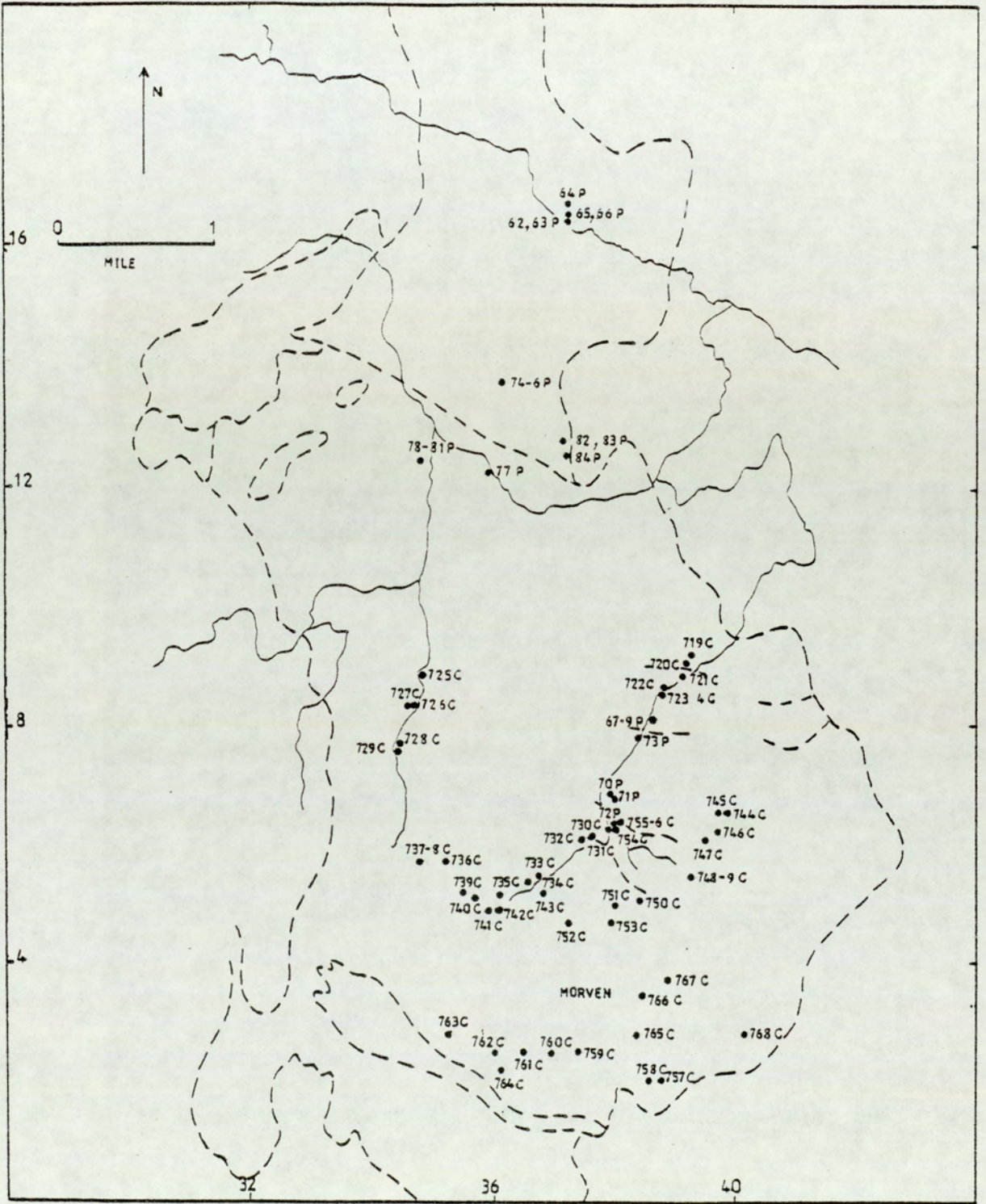


Fig. 2. Specimen location map of the Morven-Cabrach mass.

3. BELHELVIE INTRUSION

SPECIMEN NO.

GRID REFERENCES

* 11 P - 39 P,
19 E, 19 D

(BALMEDIÉ QUARRY)
NJ 944181

50 P	939187
51 P	940187
52 P	928189
* 53 P	932196
54 P	932196
55 P	923193
56 P	923193
57 P	921191
58 P	921191
59 P	909211
60 P	912206
61 P	912206
708 C	934197
709 C	934197
* 710 C	931198
711 C	931198
712 C	930197
713 C	928198
714 C	927195
715 C	931196
716 C	931196
717 C	929172
718 C	929172
* 15/18763	UNKNOWN

(Department Collection)
BR 2.1.1/7

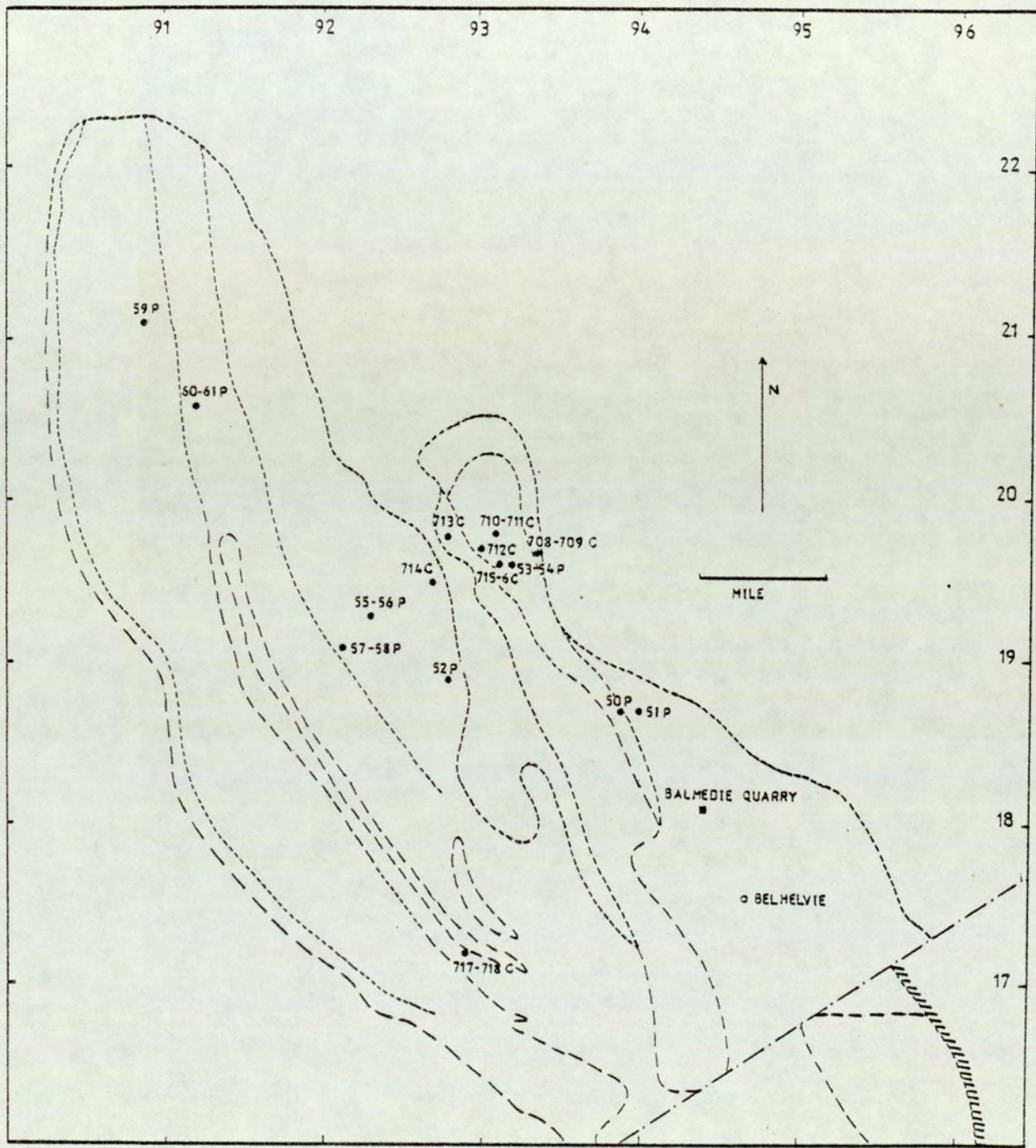


Fig. 3. Specimen location map of the Belhelvie mass.

4. HUNTLY MASS

SPECIMEN NO.	GRID REFERENCES
770 C	495409
771 C	494411
772 C	499421
* 773 C	493423
* 774 C	501408
775 C	496406
776 C	487416
777 C	490440
778 C	490440
779 C	490440
780 C	490440
781 C	498431
782 C	498431
783 C	498431
784 C	498431
785 C	498431
786 C	498431
787 C	474385
788 C	474385
789 C	474385
790 C	474385
791 C	474385
792 C	475386
793 C	475386
794 C	475386
795 C	424369
796 C	424369
797 C	424369
798 C	604495
799 C	604495
800 C	602495
* 28/19763	UNKNOWN (Department Collection) BR 2.1.1/1

5. PORTSOY MASS

SPECIMEN NO.	GRID REFERENCES
* 626 C	UNKNOWN (Department Collection)
* 625 C	

* PROBE ANALYSED ROCKS

APPENDIX 2

SUPPLEMENTARY ELECTRON MICROPROBE ANALYSES
OF PYROXENES AND AMPHIBOLES

TABLE 1 Supplementary electron probe microanalysis of pyroxenes and amphiboles from the Glen Scaddle intrusion

SPECIMEN NO.	603 C					603 C		
	ACTINO-LITE	ACTINO-LITE	ACTINO-LITE	FERRO HB	FERRO TSCHERMAKITIC HORNBLENDE	ACTINO-LITE	ACTINO-LITE	FERRO EDENITIC HORNBLENDE
Na ₂ O	0.13	0.21	0.42	0.74	0.78	0.35	0.46	1.17
MgO	14.65	14.43	14.04	9.21	8.83	14.75	12.27	8.90
Al ₂ O ₃	0.78	1.63	2.79	9.45	10.72	2.66	4.46	9.86
SiO ₂	53.65	53.21	52.58	43.89	42.07	52.48	52.62	44.53
K ₂ O	0.00	0.04	0.10	0.91	1.07	0.11	0.19	1.00
CaO	12.18	12.65	12.71	11.54	11.48	13.57	12.87	11.93
TiO ₂	0.06	0.19	0.22	0.52	0.47	0.24	0.36	0.87
MnO	0.35	0.09	0.31	0.26	0.26	0.24	0.25	0.29
Fe ₂ O ₃	0.00	2.25	1.68	3.70	6.34	0.00	0.00	1.62
FeO	14.32	14.16	14.24	16.75	15.98	13.57	15.54	18.83
H ₂ O	2.03	2.06	2.07	1.95	1.94	2.06	2.08	1.99
Total	98.15	100.92	101.16	98.92	99.94	100.03	101.10	100.99
Si	7.90	7.68	7.58	6.68	6.39	7.61	7.59	6.67
Al ^{iv}	0.10	0.28	0.42	1.32	1.61	0.39	0.41	1.33
	8.00	7.96	8.00	8.00	8.00	8.00	8.00	8.00
Al ^{vi}	0.04	0.00	0.06	0.38	0.31	0.07	0.35	0.42
Ti	0.01	0.02	0.02	0.06	0.04	0.03	0.04	0.09
Fe ³⁺	0.00	0.24	0.18	0.43	0.72	0.00	0.00	0.18
Mg	3.22	3.10	3.02	2.09	2.00	3.19	2.64	1.99
Fe ²⁺	1.77	1.71	1.72	2.13	2.03	1.65	1.87	2.37
Mn	0.04	0.01	0.04	0.03	0.03	0.03	0.03	0.04
	5.08	5.08	5.04	5.12	5.13	4.97	4.93	5.09
Na	0.04	0.06	0.12	0.22	0.23	0.10	0.13	0.34
Ca	1.92	1.96	1.96	1.88	1.87	2.11	1.99	1.91
K	0.00	0.01	0.02	0.18	0.21	0.02	0.03	0.19
	1.96	2.03	2.10	2.28	2.31	2.23	2.15	2.44
$\frac{100 \text{ Mg}}{\text{Mg} + \text{Fe}^*}$	64.5	61.4	61.4	44.9	42.1	66.9	58.5	43.8

* Fe = Fe total

SPECIMEN NO.	604 C			604 C			
	ACTINO- LITE	MAGNESIO HB	MAGNESIO HB	ACTINO- LITE	ACTINO- LITE	MAGNESIO HB	MAGNESIO HB
Na ₂ O	0.30	0.73	0.77	0.52	0.25	0.76	1.05
MgO	17.16	14.00	12.26	16.52	16.73	13.66	12.27
Al ₂ O ₃	2.85	7.48	9.25	4.55	2.87	7.71	9.89
SiO ₂	52.67	47.71	44.75	53.08	52.74	47.58	45.94
K ₂ O	0.13	0.40	0.81	0.10	0.07	0.41	0.51
CaO	11.70	11.60	11.87	11.60	11.70	11.55	11.60
TiO ₂	0.15	0.30	0.59	0.16	0.08	0.29	0.43
MnO	0.34	0.29	0.22	0.37	0.34	0.34	0.32
Fe ₂ O ₃	1.40	1.08	0.00	0.00	0.29	1.10	0.52
FeO	9.67	11.68	13.54	10.88	10.63	12.31	13.59
H ₂ O	2.06	2.01	1.96	2.10	2.10	2.01	2.01
Total	98.43	97.28	96.02	99.88	97.80	97.72	98.13
Si	7.62	7.10	6.84	7.56	7.69	7.07	6.85
Al ^{iv}	0.38	0.90	1.16	0.44	0.31	0.93	1.15
	8.00	8.00	8.00	8.00	8.00	8.00	8.00
Al ^{vi}	0.10	0.41	0.51	0.32	0.17	0.42	0.58
Ti	0.02	0.03	0.07	0.02	0.01	0.03	0.05
Fe ³⁺	0.15	0.12	0.00	0.00	0.03	0.12	0.09
Mg	3.70	3.10	2.79	3.51	3.63	3.02	2.73
Fe ²⁺	1.17	1.45	1.73	1.30	1.29	1.53	1.65
Mn	0.04	0.04	0.03	0.04	0.04	0.04	0.04
	5.18	5.15	5.13	5.19	5.17	5.16	5.14
Na	0.08	0.21	0.23	0.14	0.07	0.22	0.31
Ca	1.81	1.84	1.94	1.77	1.83	1.83	1.86
K	0.02	0.08	0.16	0.02	0.01	0.08	0.10
	1.91	2.13	2.33	1.93	1.91	2.13	2.27
$\frac{100 \text{ Mg}}{\text{Mg} + \text{Fe}^*}$	73.7	66.5	61.7	73.0	73.3	64.3	60.9

* Fe = Fe total

SPECIMEN NO.	604 C		604 C				
	ACTINO- LITE	MAGNESIO HB	ACTINO- LITE	ACTINO- LITE	MAGNESIO HB	MAGNESIO HB	TSCHERMAKITIC HORNBLLENDE
Na ₂ O	0.41	0.90	0.26	0.36	0.66	0.87	1.09
MgO	15.96	12.89	16.12	15.32	13.59	11.87	10.36
Al ₂ O ₃	4.04	8.53	3.27	3.83	6.55	10.21	12.16
SiO ₂	51.74	46.44	52.67	51.09	47.72	44.63	41.95
K ₂ O	0.08	0.47	0.11	0.10	0.33	0.60	0.80
CaO	11.42	11.54	12.27	12.09	11.65	11.64	11.46
TiO ₂	0.12	0.37	0.29	0.29	0.55	0.70	0.98
MnO	0.38	0.33	0.28	0.33	0.31	0.30	0.29
Fe ₂ O ₃	0.00	1.62	0.00	0.00	1.61	2.16	1.85
FeO	11.47	12.47	11.33	11.86	12.13	12.67	13.64
H ₂ O	2.05	2.00	2.07	2.03	1.99	1.98	1.94
Total	97.67	97.56	98.67	97.30	97.09	97.63	96.52
Si	7.57	6.94	7.63	7.54	7.14	6.70	6.44
Al ^{iv}	0.43	1.06	0.37	0.46	0.86	1.30	1.56
	8.00	8.00	8.00	8.00	8.00	8.00	8.00
Al ^{vi}	0.27	0.45	0.19	0.21	0.30	0.51	0.64
Ti	0.01	0.04	0.03	0.03	0.06	0.08	0.11
Fe ³⁺	0.00	0.18	0.00	0.00	0.18	0.24	0.21
Mg	3.48	2.88	3.48	3.37	3.03	2.66	2.37
Fe ²⁺	1.40	1.56	1.37	1.46	1.52	1.60	1.75
Mn	0.05	0.04	0.04	0.04	0.04	0.04	0.04
	5.21	5.15	5.11	5.11	5.13	5.13	5.12
Na	0.12	0.26	0.07	0.10	0.19	0.26	0.33
Ca	1.79	1.85	1.91	1.91	1.87	1.87	1.88
K	0.02	0.09	0.02	0.02	0.06	0.12	0.16
	1.93	2.20	2.00	2.03	2.12	2.25	2.37
$\frac{100 \text{ Mg}}{\text{Mg} + \text{Fe}^*}$	71.3	62.3	71.7	69.7	64.1	59.1	54.7

* Fe = Fe total

SPECIMEN NO.	652 C				657 C			
	ACTINO- LITE	ACTINO- LITE	MAGNESIO HB	FERRO EDENITIC HB	CPX	ACTINO- LITE	MAGNESIO HB	EDENITE
Na ₂ O	0.36	0.41	0.89	1.35	0.55	0.19	0.76	1.29
MgO	14.12	13.99	10.77	8.99	11.68	15.39	12.16	10.31
Al ₂ O ₃	2.51	2.74	6.75	9.81	1.53	1.51	6.37	8.25
SiO ₂	52.12	50.94	46.08	42.75	51.86	53.44	48.14	44.70
K ₂ O	0.14	0.19	0.54	1.06	-	0.04	0.32	0.86
CaO	12.07	11.95	11.56	11.63	21.99	12.06	12.01	11.70
TiO ₂	0.27	0.20	0.33	0.45	0.18	0.11	0.67	0.93
MnO	0.29	0.28	0.30	0.30	0.36	0.35	0.28	0.31
Fe ₂ O ₃	0.00	0.00	1.05	1.83	-	0.00	0.00	0.00
FeO	14.03	14.10	16.24	17.47	10.75	12.26	15.09	16.75
H ₂ O	2.03	2.00	1.94	1.92		2.04	2.00	1.95
Total	97.94	96.80	96.45	97.56	98.90	97.39	97.80	97.05
Si	7.71	7.65	7.10	6.63	1.98	7.86	7.22	6.88
Al ^{iv}	0.29	0.35	0.90	1.37	0.02	0.14	0.78	1.12
	8.00	8.00	8.00	8.00	2.00	8.00	8.00	8.00
Al ^{vi}	0.15	0.13	0.33	0.42	0.04	0.12	0.35	0.38
Ti	0.03	0.02	0.04	0.05	0.01	0.01	0.08	0.11
Fe ³⁺	0.00	0.00	0.12	0.21	-	0.00	0.00	0.00
Mg	3.11	3.13	2.47	2.08	0.66	3.37	2.72	2.37
Fe ²⁺	1.74	1.77	2.09	2.27	0.34	1.51	1.89	2.16
Mn	0.04	0.04	0.04	0.04	0.01	0.04	0.04	0.04
	5.07	5.09	5.09	5.07		5.05	5.08	5.06
Na	0.10	0.12	0.27	0.41	0.04	0.05	0.22	0.39
Ca	1.91	1.92	1.91	1.93	0.90	1.90	1.93	1.93
K	0.03	0.04	0.11	0.21	-	0.01	0.06	0.17
	2.04	2.08	2.29	2.55	2.00	1.96	2.21	2.48
$\frac{100 \text{ Mg}}{\text{Mg} + \text{Fe}^*}$	64.2	63.9	52.8	45.6	66.0	69.1	58.9	52.3

*Fe = Fe total

SPECIMEN NO.		685 C						685 C	
MINERAL	ACTINO-LITE	ACTINO-LITE	MAGNESIO HB	ACTINO-LITE	MAGNESIO HB				
Na ₂ O	0.29	0.40	0.71	0.74	0.80	0.84	1.15	0.29	1.00
MgO	16.55	16.23	13.78	13.00	13.07	12.80	11.44	16.23	11.69
Al ₂ O ₃	3.05	3.97	6.90	8.03	8.14	8.22	10.64	2.55	8.82
SiO ₂	52.27	51.62	47.89	46.67	46.75	46.06	43.65	52.77	45.32
K ₂ O	0.08	0.12	0.35	0.52	0.53	0.57	0.71	0.11	0.65
CaO	12.31	12.28	12.08	12.24	12.08	12.02	11.82	12.47	11.87
TiO ₂	0.22	0.32	0.60	0.73	0.62	0.69	0.69	0.20	0.60
MnO	0.27	0.25	0.25	0.24	0.26	0.26	0.27	0.27	0.30
Fe ₂ O ₃	1.40	1.68	2.20	2.47	1.91	2.17	2.68	0.00	1.26
FeO	9.59	9.76	11.39	11.84	12.02	12.11	12.84	10.27	14.56
H ₂ O	2.06	2.06	2.01	2.01	2.01	1.99	1.97	2.05	1.98
Total	98.09	98.69	98.16	98.49	98.19	97.73	97.86	97.21	98.05
Si	7.595	7.48	7.08	6.92	6.95	6.89	6.59	7.73	6.82
Al ^{iv}	0.405	0.52	0.92	1.08	1.05	1.11	1.41	0.27	1.18
	8.00	8.00	8.00	8.00	8.00	8.00	8.00	8.00	8.00
Al ^{vi}	0.12	0.16	0.29	0.33	0.37	0.35	0.48	0.17	0.38
Ti	0.03	0.04	0.07	0.08	0.07	0.08	0.08	0.02	0.07
Fe ³⁺	0.15	0.18	0.24	0.27	0.21	0.24	0.31	0.00	0.27
Mg	3.59	3.51	3.04	2.87	2.90	2.86	2.57	3.54	2.62
Fe ²⁺	1.16	1.18	1.41	1.47	1.50	1.52	1.62	1.25	1.70
Mn	0.03	0.03	0.03	0.03	0.03	0.03	0.03	0.03	0.04
	5.08	5.10	5.08	5.05	5.08	5.08	5.09	5.01	5.08
Na	0.08	0.11	0.20	0.21	0.23	0.25	0.34	0.08	0.29
Ca	1.91	1.90	1.92	1.95	1.92	1.93	1.91	1.96	1.91
K	0.02	0.02	0.07	0.10	0.10	0.11	0.14	0.02	0.13
	2.01	2.03	2.19	2.26	2.25	2.29	2.39	2.06	2.33
$\frac{100 \text{ Mg}}{\text{Mg} + \text{Fe}^*}$	73.1	72.0	64.8	62.2	62.9	61.8	57.2	73.9	57.0

* Fe = Fe total

SPECIMEN NO.

685 C

MINERAL	CPX	ACTINO- LITE	ACTINO- LITE	MAGNESIO HB	ACTINO- LITE	ACTINO- LITE	MAGNESIO HB	MAGNESIO HB
Na ₂ O	0.41	0.22	0.41	0.83	0.29	0.35	0.77	0.90
MgO	12.84	15.89	15.61	12.07	16.30	15.87	13.04	11.72
Al ₂ O ₃	0.94	2.70	4.16	8.44	3.08	3.69	8.14	9.35
SiO ₂	52.61	53.17	52.20	46.24	52.04	51.65	46.68	44.77
K ₂ O	-	0.11	0.17	0.59	0.07	0.10	0.40	0.54
CaO	23.21	12.49	12.25	11.77	12.16	12.22	11.89	12.03
TiO ₂	0.13	0.17	0.28	1.08	0.22	0.26	0.65	0.79
MnO	0.35	0.25	0.25	0.25	0.25	0.25	0.24	0.24
Fe ₂ O ₃	-	0.00	0.00	0.00	1.11	1.11	2.16	2.47
FeO	8.27	10.57	10.85	13.87	10.10	10.48	11.95	12.58
H ₂ O		2.06	2.06	1.99	2.05	2.05	2.00	1.97
Total	98.76	97.63	98.24	97.13	97.67	98.03	97.92	97.36
Si	1.99	7.75	7.58	6.97	7.60	7.54	6.94	6.76
Al ^{iv}	0.01	0.25	0.42	1.03	0.40	0.46	1.06	1.24
	2.00	8.00	8.00	8.00	8.00	8.00	8.00	8.00
Al ^{vi}	0.03	0.22	0.29	0.47	0.14	0.18	0.38	0.43
Ti	0.00	0.02	0.03	0.12	0.02	0.03	0.07	0.09
Fe ³⁺	-	0.00	0.00	0.00	0.12	0.12	0.24	0.27
Mg	0.72	3.45	3.38	2.71	3.55	3.45	2.90	2.63
Fe ²⁺	0.26	1.29	1.32	1.75	1.23	1.27	1.49	1.59
Mn	0.01	0.03	0.03	0.03	0.03	0.03	0.03	0.03
		5.01	5.05	5.08	5.09	5.08	5.11	5.04
Na	0.03	0.06	0.12	0.24	0.08	0.10	0.22	0.26
Ca	0.94	1.95	1.91	1.90	1.91	1.92	1.90	1.95
K	-	0.02	0.03	0.11	0.01	0.02	0.08	0.11
	1.99	2.03	2.06	2.25	2.00	2.04	2.20	2.32
<u>100 Mg</u> Mg+Fe*	73.5	72.8	71.9	60.8	72.3	71.1	62.6	58.5

* Fe = Fe total

SPECIMEN NO.	678 C			683 C			683 C				
	MINERAL	ACTINOLITE	FERRON PARCASITIC HORNBLLENDE	ACTINOLITE	ACTINOLITE	MAGNESIO HORNBLLENDE	MAGNESIO HORNBLLENDE	MAGNESIO HORNBLLENDE	CPX	MAGNESIO HORNBLLENDE	MAGNESIO HORNBLLENDE
Na ₂ O	0.27	1.19		0.21	0.29	0.35	0.77	0.90	0.38	0.82	0.93
MgO	14.77	8.44		16.11	16.30	15.87	13.04	11.72	14.43	14.23	13.42
Al ₂ O ₃	1.96	11.84		2.80	3.08	3.69	8.14	9.35	1.83	8.95	8.78
SiO ₂	52.80	41.11		51.98	52.04	51.65	46.68	44.77	51.72	46.93	45.47
K ₂ O	-	1.22		0.08	0.07	0.10	0.40	0.54	0.01	0.52	0.78
CaO	11.36	11.85		12.48	12.16	12.22	11.89	12.03	21.02	12.05	11.54
TiO ₂	0.07	0.13		0.23	0.22	0.26	0.65	0.79	0.27	1.07	1.10
MnO	0.24	0.24		0.24	0.25	0.25	0.24	0.24	0.27	0.18	0.24
Fe ₂ O ₃	0.00	4.96		1.94	1.11	1.11	2.16	2.47	-	3.35	2.46
FeO	13.70	15.66		9.46	10.10	10.48	11.95	12.58	8.78	10.44	11.80
H ₂ O	2.02	1.92		2.04	2.05	2.05	2.00	1.97	-	2.06	2.00
Total	97.19	98.56		97.57	97.67	98.03	97.92	97.36	98.71	100.60	98.52
Si	7.82	6.33		7.605	7.60	7.54	6.94	6.76	1.95	6.78	6.76
Al ^{iv}	0.18	1.67		0.395	0.40	0.46	1.06	1.24	0.05	1.22	1.24
	8.00	8.00		8.00	8.00	8.00	8.00	8.00	2.00	8.00	8.00
Al ^{vi}	0.16	0.47		0.09	0.14	0.18	0.38	0.43	0.03	0.30	0.30
Ti	0.01	0.02		0.03	0.02	0.03	0.07	0.09	0.01	0.12	0.12
Fe ³⁺	0.00	0.58		0.21	0.12	0.12	0.24	0.27	-	0.36	0.27
Mg	3.26	1.94		3.51	3.55	3.45	2.90	2.63	0.81	3.07	2.97
Fe ²⁺	1.70	2.01		1.16	1.23	1.27	1.49	1.59	0.28	1.26	1.47
Mn	0.03	0.03		0.03	0.03	0.03	0.03	0.03	0.01	0.02	0.03
	5.16	5.05		5.03	5.09	5.08	5.11	5.04		5.13	5.16
Na	0.08	0.36		0.06	0.08	0.10	0.22	0.26	0.03	0.23	0.27
Ca	1.80	1.96		1.96	1.91	1.92	1.90	1.95	0.85	1.86	1.84
K	-	0.24		0.02	0.01	0.02	0.08	0.11	0.00	0.10	0.15
	1.88	2.56		2.04	2.00	2.04	2.20	2.32	2.02	2.19	2.26
100 Mg Mg + Fe*	65.8	42.8		71.9	72.3	71.1	62.6	58.5	74.5	65.3	63.0

* Fe = Fe total

TABLE 2 Supplementary electron probe microanalyses of pyroxenes and amphiboles from the Morven-Cabrach intrusion

SPECIMEN NO.	62 P			62 P				
	CUMMING-TONITE	MAGNESIO HB	MAGNESIO HB	CPX	ACTINO-LITE (IN CPX)	ACTINO-LITE	ACTINO-LITE	ACTINOLITIC HORNBLLENDE
Na ₂ O	0.05	0.63	0.73	0.21	0.39	0.18	0.19	0.58
MgO	17.04	13.51	12.64	12.77	13.84	15.11	15.20	13.29
Al ₂ O ₃	0.91	6.91	8.65	1.28	3.86	2.26	2.69	5.83
SiO ₂	54.78	48.11	48.61	51.69	51.49	54.56	54.33	50.12
K ₂ O	0.00	0.30	0.36	-	0.03	0.04	0.06	0.28
CaO	1.23	10.96	11.27	21.98	11.60	11.84	11.00	11.23
TiO ₂	0.04	0.50	0.39	0.14	0.70	0.27	0.25	0.38
MnO	0.50	0.18	0.17	0.23	0.15	0.16	0.17	0.18
Fe ₂ O ₃	-	1.91	0.00	-	0.00	0.00	0.00	0.00
FeO	23.48	13.39	15.06	10.44	14.51	14.00	14.15	15.20
H ₂ O	2.06	2.01	2.05		2.04	2.09	2.09	2.04
Total	100.09	98.41	99.93	98.74	98.61	100.51	100.13	99.13
Si	7.97	7.13	7.09	1.97	7.56	7.81	7.79	7.36
Al ^{iv}	0.03	0.87	0.91	0.03	0.44	0.19	0.21	0.64
	8.00	8.00	8.00	2.00	8.00	8.00	8.00	8.00
Al ^{vi}	0.13	0.33	0.58	0.03	0.23	0.19	0.24	0.37
Ti	0.00	0.06	0.04	0.00	0.08	0.03	0.03	0.04
Fe ³⁺	-	0.21	0.00	-	0.00	0.00	0.00	0.00
Mg	3.70	2.98	2.75	0.73	3.03	3.22	3.25	2.91
Fe ²⁺	2.86	1.66	1.84	0.33	1.78	1.68	1.70	1.87
Mn	0.06	0.02	0.02	0.01	0.02	0.02	0.02	0.02
	6.75	5.26	5.23		5.14	5.14	5.24	5.21
Na	0.01	0.18	0.21	0.02	0.11	0.05	0.05	0.16
Ca	0.19	1.74	1.76	0.90	1.83	1.82	1.69	1.77
K	0.00	0.06	0.07		0.01	0.01	0.01	0.05
	0.20	1.98	2.04	2.02	1.95	1.88	1.75	1.98
<u>100 Mg</u>	56.4	61.4	60.0	68.6	62.9	65.8	65.7	60.9
Mg + Fe*								

*Fe = Fe total

SPECIMEN NO.	62 P			62 P			62 P	
MINERAL	CPX	ACTINOLITIC HORNBLLENDE	MAGNESIO HB	ACTINO-LITE	ACTINO-LITE	MAGNESIO HB	CUMMING-TONITE	MAGNESIO HB
Na ₂ O	0.20	0.46	0.65	0.18	0.17	0.67	0.05	0.73
MgO	12.92	14.38	12.67	15.37	15.25	13.42	17.24	12.64
Al ₂ O ₃	1.68	5.69	8.74	2.20	2.29	7.78	0.88	8.65
SiO ₂	51.47	50.14	48.58	52.44	52.29	47.78	52.88	48.61
K ₂ O	-	0.16	0.33	0.03	0.03	0.28	-	0.36
CaO	20.65	11.38	11.21	11.62	11.14	11.30	1.30	11.27
TiO ₂	0.18	0.35	0.55	0.23	0.21	0.48	0.04	0.39
MnO	0.23	0.16	0.13	0.16	0.19	0.17	0.51	0.17
Fe ₂ O ₃	-	0.00	0.00	1.32	1.72	2.62	-	0.00
FeO	10.40	13.49	13.03	12.93	13.03	12.84	23.76	15.06
H ₂ O		2.04	2.03	2.04	2.03	2.03	2.02	2.05
Total	97.73	98.25	97.92	98.52	98.35	99.37	98.68	99.93
Si	1.97	7.37	7.15	7.675	7.67	7.01	7.86	7.09
Al ^{iv}	0.03	0.63	0.85	0.325	0.33	0.99	0.14	0.91
	2.00	8.00	8.00	8.00	8.00	8.00	8.00	8.00
Al ^{vi}	0.05	0.36	0.67	0.07	0.05	0.35	0.01	0.58
Ti	0.01	0.04	0.06	0.02	0.03	0.05	0.00	0.04
Fe ³⁺	-	0.00	0.00	0.15	0.18	0.29		
Mg	0.74	3.15	2.78	3.34	3.36	2.93	3.82	2.75
Fe ²⁺	0.33	1.66	1.61	1.64	1.54	1.58	2.95	1.84
Mn	0.01	0.02	0.02	0.02	0.02	0.02	0.06	0.02
		5.23	5.14	5.24	5.18	5.22	6.84	5.23
Na	0.02	0.13	0.19	0.05	0.05	0.19	0.01	0.21
Ca	0.85	1.79	1.77	1.75	1.82	1.78	0.21	1.76
K	-	0.03	0.06	0.01	0.01	0.05	-	0.07
	2.01	1.95	2.02	1.81	1.88	2.02	0.22	2.04
<u>100 Mg</u> Mg + Fe*	69.2	65.5	63.4	66.1	65.1	61.1	56.4	59.9

* Fe = Fe total

SPECIMEN NO.		81 P				81 P			
MINERAL	CPX	ACTINO-LITE	FERRO ACTINOLITIC HORNBLLENDE	FERROAN PARGASITIC HORNBLLENDE	CPX	FERRO ACTINOLITIC HORNBLLENDE	FERRO HB	FERROAN PARGASITIC HORNBLLENDE	
Na ₂ O	0.00	0.04	0.16	1.15	0.00	0.15	0.22	0.85	
MgO	10.08	11.97	10.78	5.81	10.70	10.79	9.97	6.65	
Al ₂ O ₃	1.72	2.75	4.87	13.26	1.62	4.48	7.36	13.28	
SiO ₂	50.58	50.34	49.16	41.57	49.84	50.00	48.30	42.04	
K ₂ O	0.19	0.20	0.34	0.81	0.19	0.27	0.49	0.80	
CaO	19.22	11.21	11.49	11.49	20.86	11.86	11.74	11.60	
TiO ₂	0.40	0.32	0.37	0.51	0.40	0.27	0.36	0.46	
MnO	0.57	0.35	0.29	0.28	0.55	0.31	0.33	0.31	
Fe ₂ O ₃	-	0.00	2.72	1.58	-	2.71	3.32	4.28	
FeO	15.84	20.55	17.97	20.79	15.08	17.87	18.11	18.94	
H ₂ O		2.00	2.00	1.94		2.01	2.09	1.97	
Total	98.60	99.73	100.15	99.19	99.24	100.72	102.29	101.18	
Si	1.97	7.54	7.31	6.40	1.93	7.38	7.06	6.32	
Al ^{iv}	0.03	0.46	0.69	1.60	0.07	0.62	0.94	1.68	
	2.00	8.00	8.00	8.00	2.00	8.00	8.00	8.00	
Al ^{vi}	0.05	0.03	0.17	0.82	0.01	0.17	0.33	0.68	
Ti	0.01	0.04	0.04	0.06	0.01	0.03	0.04	0.05	
Fe ³⁺	-	0.00	0.30	0.18	-	0.30	0.37	0.49	
Mg	0.58	2.67	2.38	1.34	0.62	2.37	2.17	1.49	
Fe ²⁺	0.52	2.57	2.24	2.67	0.49	2.21	2.21	2.38	
Mn	0.02	0.04	0.04	0.04	0.02	0.04	0.04	0.04	
		5.35	5.17	5.11		5.12	5.16	5.13	
Na	0.00	0.01	0.05	0.34	0.00	0.04	0.06	0.25	
Ca	0.80	1.80	1.83	1.89	0.87	1.88	1.83	1.87	
K	0.01	0.04	0.07	0.16	0.01	0.05	0.09	0.15	
	1.99	1.85	1.95	2.39	2.03	1.97	1.98	2.27	
$\frac{100 \text{ Mg}}{\text{Mg} + \text{Fe}^*}$	53.1	50.9	48.4	31.8	55.9	48.6	45.7	34.2	

*Fe = Fe total

SPECIMEN NO.	81 P			81 P				
MINERAL	CUMMING-TONITE	FERROAN PARGASITE	FERROAN PARGASITE	CPX	ACTINO-LITE	ACTINO-LITE	FERRO HB	FERRO TSCHERMAKITIC HORNBLLENDE
Na ₂ O	0.07	1.67	1.53	0.22	0.13	0.22	1.21	1.49
MgO	12.95	5.75	6.44	10.39	12.99	12.69	7.75	7.21
Al ₂ O ₃	0.66	15.77	15.52	1.75	1.31	2.08	10.04	13.15
SiO ₂	51.96	39.50	41.19	50.46	53.22	51.97	42.65	41.76
K ₂ O	-	0.63	0.53	-	0.05	0.01	0.00	0.33
CaO	0.41	10.62	10.50	21.03	10.61	10.87	11.10	11.22
TiO ₂	0.00	0.21	0.17	0.34	0.08	0.11	0.55	0.40
MnO	0.86	0.36	0.36	0.37	0.51	0.36	0.28	0.29
Fe ₂ O ₃	-	3.96	2.96	-	1.95	2.49	5.23	4.55
FeO	31.67	20.40	20.27	15.36	18.69	17.65	18.02	18.53
H ₂ O	1.98	1.95	1.98	0.00	2.05	2.03	1.92	1.97
Total	100.56	100.82	101.45	99.92	101.59	100.48	98.75	100.90
Si	7.86	6.02	6.17	1.94	7.74	7.64	6.55	6.29
Al ^{iv}	0.12	1.98	1.83	0.06	0.23	0.36	1.45	1.71
	7.98	8.00	8.00	2.00	7.97	8.00	8.00	8.00
Al ^{vi}	0.00	0.86	0.92	0.02	0.00	0.00	0.37	0.63
Ti	0.00	0.02	0.02	0.01	0.01	0.01	0.07	0.05
Fe ³⁺	-	0.45	0.34	-	0.21	0.27	0.60	0.52
Mg	2.92	1.31	1.44	0.60	2.82	2.78	1.78	1.62
Fe ²⁺	4.00	2.57	2.54	0.49	2.27	2.17	2.32	2.33
Mn	0.11	0.05	0.05	0.01	0.06	0.05	0.04	0.04
	7.03	5.26	5.31		5.37	5.28	5.18	5.19
Na	0.02	0.50	0.44	0.02	0.04	0.06	0.35	0.43
Ca	0.07	1.73	1.69	0.87	1.65	1.71	1.83	1.81
K	-	0.12	0.10	-	0.01	0.00	0.00	0.06
	0.09	2.35	2.23	2.02	1.70	1.77	2.18	2.30
<u>100 Mg</u> <u>Mg + Fe*</u>	42.2	30.2	33.3	54.7	53.1	53.2	37.8	36.2

*Fe = Fe total

SPECIMEN NO.	84 P		84 P			
MINERAL	CUMMINGTONITE	FERRO HB	CPX	ACTINOLITE	ACTINOLITIC HORNBLLENDE	FERRO HB
Na ₂ O	0.09	0.98	0.22	0.18	0.39	0.70
MgO	14.55	9.19	11.45	13.11	11.48	8.55
Al ₂ O ₃	0.74	9.30	0.79	2.19	4.29	8.73
SiO ₂	52.13	42.86	51.71	51.60	50.00	45.56
K ₂ O	0.00	0.54	0.06	0.07	0.16	0.47
CaO	1.33	11.42	21.92	12.08	11.62	11.97
TiO ₂	0.06	0.25	0.18	0.10	0.14	0.32
MnO	0.94	0.30	0.35	0.30	0.28	0.27
Fe ₂ O ₃	0.00	4.41	-	0.00	2.46	4.06
FeO	27.67	15.70	13.92	18.82	17.42	18.21
H ₂ O	1.99	1.91		2.03	2.01	1.98
Total	99.50	96.86	100.60	100.48	100.25	100.82
Si	7.85	6.65	1.97	7.53	7.40	6.82
Al ^{iv}	0.13	1.35	0.03	0.38	0.60	1.18
	7.98	8.00	2.00	7.91	8.00	8.00
Al ^{vi}	0.00	0.35	0.00	0.00	0.15	0.37
Ti	0.01	0.03	0.01	0.01	0.01	0.04
Fe ³⁺	0.00	0.51	-	0.46	0.27	0.45
Mg	3.27	2.13	0.65	2.85	2.54	1.91
Fe ²⁺	3.48	2.04	0.44	1.84	2.15	2.28
Mn	0.12	0.04	0.01	0.04	0.04	0.03
	6.88	5.10		5.20	5.16	5.08
Na	0.03	0.30	0.02	0.05	0.11	0.21
Ca	0.21	1.90	0.89	1.89	1.84	1.92
K	0.00	0.10	0.00	0.01	0.03	0.09
	0.24	2.30	2.02	1.95	1.98	2.22
$\frac{100 \text{ Mg}}{\text{Mg} + \text{Fe}^*}$	48.4	45.4	59.4	55.4	51.0	41.4

* Fe = Fe total

SPECIMEN NO.	73 P			73 P			
	CPX	FERRO ACTINOLITE	FERRO HB	CPX	ACTINOLITIC HORNBLLENDE	FERRO HB	FERRO HB
Ca ₂ O	0.31	0.55	0.89	0.35	0.48	1.03	1.01
MgO	12.54	9.87	8.69	12.10	11.26	8.32	8.44
Al ₂ O ₃	2.21	5.69	8.22	2.20	4.84	9.34	9.37
SiO ₂	50.51	47.05	45.52	50.51	50.24	44.88	45.63
K ₂ O	-	0.42	0.81	-	0.21	0.28	0.32
CaO	19.55	11.51	11.75	20.27	11.70	11.45	11.51
TiO ₂	0.41	0.04	0.20	0.52	0.27	0.10	0.12
MnO	0.26	0.17	0.23	0.28	0.20	0.20	0.21
Fe ₂ O ₃	-	0.00	0.00	-	0.00	1.86	1.62
FeO	12.77	19.78	20.48	12.24	17.83	19.12	19.33
H ₂ O		1.94	1.96		2.01	1.95	1.98
Total	98.56	97.02	98.75	98.47	99.04	98.53	99.54
Si	1.94	7.28	6.97	1.94	7.48	6.86	6.89
Al ^{iv}	0.06	0.72	1.03	0.06	0.52	1.14	1.11
	2.00	8.00	8.00	2.00	8.00	8.00	8.00
Al ^{vi}	0.04	0.31	0.46	0.04	0.33	0.54	0.57
Fi	0.01	0.01	0.02	0.02	0.03	0.01	0.01
Fe ³⁺	-	0.00	0.00	-	0.00	0.21	0.18
Mg	0.72	2.28	1.98	0.69	2.50	1.89	1.90
Fe ²⁺	0.41	2.56	2.62	0.39	2.22	2.44	2.44
Mn	0.01	0.02	0.03	0.01	0.03	0.03	0.03
		5.18	5.11		5.11	5.12	5.13
Na	0.02	0.16	0.27	0.03	0.14	0.31	0.30
Ca	0.80	1.91	1.93	0.83	1.87	1.87	1.86
K	-	0.08	0.16	-	0.04	0.06	0.06
	2.01	2.15	2.36	2.01	2.04	2.24	2.22
100 Mg / Mg + Fe*	63.6	47	43.1	63.9	52.9	41.6	41.95

* Fe = Fe total

SPECIMEN NO.	67 P		65 P			724 C	
MINERAL	CUMMING-TONITE	TSCHERMAKITIC HORNBLLENDE	OPX	CUMMING-TONITE	TSCHERMAKITIC HORNBLLENDE	CPX	ACTINO-LITE
Na ₂ O	0.14	2.10	0.00	0.00	0.67	0.27	0.26
MgO	14.33	6.22	15.00	15.25	8.62	11.30	11.71
Al ₂ O ₃	0.26	17.25	0.68	0.61	11.16	1.87	2.90
SiO ₂	52.21	40.28	50.32	53.14	44.84	50.71	50.77
K ₂ O	0.03	0.22	-	0.00	0.60	-	-
CaO	0.63	10.27	0.87	0.64	10.83	20.61	12.07
TiO ₂	0.05	0.41	0.20	0.01	0.28	0.32	0.11
MnO	0.64	0.31	0.70	0.66	0.21	0.37	0.21
Fe ₂ O ₃	0.00	0.00	-	0.00	2.70	-	1.62
FeO	29.32	21.11	33.19	28.15	18.73	13.79	17.00
H ₂ O	1.98	1.98		2.02	2.00		1.99
Total	99.59	100.15	100.96	100.48	100.64	99.24	98.64
Si	7.89	6.09	1.96	7.89	6.68	1.95	7.60
Al ^{iv}	0.05	1.91	0.03	0.11	1.32	0.05	0.40
	7.94	8.00	1.99	8.00	8.00	2.00	8.00
Al ^{vi}	0.00	1.17	0.00	0.00	0.65	0.03	0.11
Ti	0.01	0.05	0.01	0.01	0.03	0.01	0.01
Fe ³⁺	0.00	0.00	-	0.00	0.30	-	0.18
Mg	3.23	1.40	0.87	3.37	1.92	0.65	2.61
Fe ²⁺	3.71	2.67	1.08	3.50	2.34	0.44	2.13
Mn	0.08	0.04	0.02	0.08	0.03	0.01	0.03
	7.03	5.33		6.96	5.27		5.07
Na	0.04	0.62	0.00	0.00	0.19	0.02	0.08
Ca	0.10	1.66	0.04	0.10	1.73	0.85	1.93
K	0.01	0.04	-	0.00	0.11	-	0.00
	0.15	2.32	2.02	0.10	2.03	2.01	2.01
$\frac{100 \text{ Mg}}{\text{Mg} + \text{Fe}^*}$	46.5	34.9	44.6	49.1	42.0	59.4	53.1

* Fe = Fe total

SPECIMEN NO.	741 C				741 C	
	CUMMINGTONITE	ACTINOLITE	FERROAN PARGASITE	FERRO TSCHERMAKITE	ACTINOLITE	FERROAN PARGASITE
Na ₂ O	0.18	0.24	1.16	0.96	0.06	1.07
MgO	12.13	12.20	6.55	3.05	13.31	6.49
Al ₂ O ₃	2.03	2.42	14.40	18.54	0.92	14.04
SiO ₂	50.72	50.72	40.08	38.23	53.55	39.87
K ₂ O	0.10	0.10	0.81	0.63	0.00	1.48
CaO	3.43	8.10	11.30	11.44	10.80	11.36
TiO ₂	0.00	0.00	0.00	0.00	0.00	0.00
MnO	0.65	0.74	0.23	0.25	0.28	0.19
Fe ₂ O ₃	-	0.00	3.89	1.30	0.00	2.84
FeO	26.81	21.24	17.48	20.86	17.24	18.42
H ₂ O	1.95	1.97	1.91	1.90	2.02	1.90
Total	98.00	97.73	97.81	97.16	98.18	97.66
Si	7.78	7.71	6.22	6.00	7.95	6.23
Al ^{iv}	0.22	0.29	1.78	2.00	0.05	1.77
	8.00	8.00	8.00	8.00	8.00	8.00
Al ^{vi}	0.15	0.15	0.85	1.44	0.12	0.81
Ti	0.00	0.00	0.00	0.00	0.00	0.00
Fe ³⁺	-	0.00	0.45	0.15	0.00	0.34
Mg	2.77	2.77	1.52	0.72	2.95	1.51
Fe ²⁺	3.44	2.70	2.27	2.74	2.14	2.40
Mn	0.08	0.10	0.03	0.03	0.04	0.03
	6.44	5.72	5.12	5.08	5.25	5.09
Na	0.05	0.07	0.35	0.29	0.02	0.33
Ca	0.56	1.32	1.88	1.92	1.72	1.90
K	0.02	0.02	0.16	0.13	0.00	0.30
	0.63	1.41	2.39	2.34	1.74	2.53
$\frac{100 \text{ Mg}}{\text{Mg} + \text{Fe}^*}$	44.6	50.6	35.7	22.3	57.9	35.5

* Fe = Fe total

SPECIMEN NO.	746 C				746 C			
MINERAL	OPX	CPX	CUMMING-TONITE	FERRO-TSCHERMAKITIC HORNBLLENDE	OPX	CPX	CUMMING-TONITE	FERRO HB
Na ₂ O	0.00	0.34	0.07	1.23	0.00	0.32	0.09	1.11
MgO	15.03	11.02	14.73	6.68	15.50	11.18	15.49	7.29
Al ₂ O ₃	0.91	1.86	0.95	14.49	0.95	1.95	1.07	11.77
SiO ₂	49.04	50.46	52.55	41.38	48.82	49.86	52.09	42.39
K ₂ O	-	-	-	0.29	-	-	-	0.26
CaO	0.94	20.61	0.90	11.35	0.73	21.38	0.57	11.46
TiO ₂	0.19	0.36	0.15	0.08	0.20	0.49	0.15	0.12
MnO	0.74	0.34	0.65	0.19	0.69	0.31	0.63	0.19
Fe ₂ O ₃	-	-	-	2.12	-	-	-	2.05
FeO	31.44	13.85	26.11	18.15	30.73	12.91	25.48	18.18
H ₂ O			1.98	1.94			1.98	1.92
Total	98.29	98.84	98.09	97.90	97.62	98.40	97.55	96.74
Si	1.96	1.95	7.93	6.36	1.96	1.93	7.89	6.595
Al ^{iv}	0.04	0.05	0.07	1.64	0.04	0.07	0.11	1.505
	2.00	2.00	8.00	8.00	2.00	2.00	8.00	8.00
Al ^{vi}	0.00	0.03	0.10	0.98	0.00	0.02	0.08	0.74
Ti	0.01	0.01	0.02	0.01	0.01	0.01	0.02	0.02
Fe ³⁺	-	-	-	0.25	-	-	-	0.24
Mg	0.89	0.63	3.31	1.53	0.93	0.65	3.49	1.67
Fe ²⁺	1.05	0.45	3.30	2.33	1.03	0.42	3.23	2.38
Mn	0.03	0.01	0.08	0.03	0.02	0.01	0.08	0.03
			6.81	5.13			6.90	5.09
Na	0.00	0.03	0.02	0.37	0.00	0.02	0.03	0.34
Ca	0.04	0.85	0.15	1.87	0.03	0.89	0.09	1.91
K	-	-	-	0.06	-	-	-	0.05
	2.02	2.01	0.17	2.30	2.02	2.02	0.12	2.30
<u>100 Mg</u> Mg + Fe*	46.0	58.6	50.1	37.2	47.3	60.7	52.0	38.9

*Fe = Fe total

SPECIMEN NO.		733 C		735 C					
MINERAL	CPX	ACTINO-LITE	FERRO-TSCHERMAKITE	OPX	CUMMING-TONITE	MAGNESIO HB	OPX	CUMMING-TONITE	MAGNESIO HB
Na ₂ O	0.32	0.15	0.83	-	0.12	0.76	0.01	0.14	0.78
MgO	11.15	13.77	4.32	19.04	16.94	13.13	19.42	17.41	13.96
Al ₂ O ₃	2.37	1.17	18.89	0.92	1.00	8.85	0.96	0.99	7.60
SiO ₂	51.03	52.67	35.35	52.15	54.47	47.25	51.70	54.52	47.41
K ₂ O	-	0.00	0.44	-	0.00	0.68	-	-	0.69
CaO	19.56	7.30	9.44	1.14	0.87	11.69	1.49	0.68	11.53
TiO ₂	0.35	0.27	0.08	0.16	0.05	0.21	0.17	0.09	0.15
MnO	0.27	0.44	0.19	0.59	0.56	0.14	0.50	0.53	0.16
Fe ₂ O ₃	-	0.00	8.60	-	-	0.55	-	-	1.64
FeO	13.61	20.60	17.24	25.01	21.87	12.90	23.57	22.12	11.69
H ₂ O		2.00	1.86		2.03	2.02		2.04	2.01
Total	98.66	98.37	97.24	99.01	97.91	98.18	97.82	98.52	97.62
Si	1.96	7.87	5.56	1.99	8.04	7.00	1.99	8.00	7.05
Al ^{iv}	0.04	0.13	2.44	0.01	0.00	1.00	0.01	0.00	0.95
	2.00	8.00	8.00	2.00	8.04	8.00	2.00	8.00	8.00
Al ^{vi}	0.07	0.08	1.06	0.03	0.17	0.55	0.03	0.17	0.39
Ti	0.01	0.03	0.01	0.01	0.01	0.02	0.01	0.01	0.02
Fe ³⁺	-	0.00	1.02	-	-	0.06	-	-	0.18
Mg	0.64	3.07	1.02	1.08	3.73	2.89	1.11	3.81	3.10
Fe ²⁺	0.44	2.57	3.27	0.80	2.70	1.60	0.76	2.72	1.45
Mn	0.01	0.06	0.03	0.02	0.07	0.02	0.02	0.07	0.02
		5.81	5.41		6.68	5.14		6.78	5.16
Na	0.02	0.04	0.25	-	0.03	0.22	0.00	0.04	0.23
Ca	0.81	1.17	1.59	0.05	0.14	1.86	0.06	0.11	1.84
K	-	0.00	0.09	-	0.00	0.13	-	-	0.13
	2.00	1.21	1.93	1.99	0.17	2.21	2.00	0.15	2.20
100 Mg	59.3	54.4	23.6	57.6	58.0	63.6	59.5	58.4	65.4
Mg + Fe*									

* Fe = Fe total

SPECIMEN NO.	725 C				725 C				725 C				
	MAGNESIO HORNBLLENDE*	CUMMING-TONITE	FERRO TSCHERMAKITE		CUMMING-TONITE	ACTINOLITE	ACTINOLITE	FERRO TSCHERMAKITE	CUMMING-TONITE	FERRO HORNBLLENDE	FERROAN PARGASITE		
Na ₂ O	0.92	0.08	1.26		0.13	0.43	0.20	1.26	0.11	0.90	2.75		
MgO	10.56	14.23	6.34		14.51	12.18	13.25	5.37	14.76	9.22	5.92		
Al ₂ O ₃	8.76	0.73	17.43		1.03	3.93	1.82	18.53	0.79	11.75	19.81		
SiO ₂	46.95	52.40	40.45		52.87	50.27	52.73	39.08	53.10	44.67	40.71		
K ₂ O	0.19	0.02	0.36		0.02	0.07	0.03	0.48	0.03	0.85	0.44		
CaO	11.04	0.90	11.21		1.36	11.39	12.14	11.33	1.07	11.53	10.80		
TiO ₂	0.23	0.03	0.06		0.28	0.17	0.07	0.09	0.03	0.21	0.10		
MnO	0.20	0.77	0.17		0.69	0.57	0.17	0.17	0.68	0.15	0.12		
Fe ₂ O ₃	1.35	-	2.42		-	0.28	0.27	0.80	-	0.00	0.00		
FeO	17.25	27.36	18.02		26.09	16.51	16.20	18.64	25.76	17.43	18.90		
H ₂ O	2.01	1.98	1.98		2.00	1.99	2.03	1.94	1.99	1.99	2.03		
Total	99.46	98.50	99.70		98.98	97.79	98.91	97.69	98.32	98.70	101.58		
Si	7.00	7.93	6.09		7.92	7.55	7.79	6.02	7.98	6.73	6.01		
Al ^{iv}	1.00	0.07	1.91		0.08	0.45	0.21	1.98	0.02	1.27	1.99		
	8.00	8.00	8.00		8.00	8.00	8.00	8.00	8.00	8.00	8.00		
Al ^{vi}	0.53	0.06	1.19		0.10	0.24	0.10	1.38	0.12	0.82	1.46		
Ti	0.03	0.00	0.01		0.03	0.02	0.01	0.01	0.00	0.02	0.01		
Fe ³⁺	0.15	-	0.27		-	0.03	0.03	0.09	-	0.00	0.00		
Mg	2.34	3.21	1.42		3.24	2.73	2.92	1.23	3.31	2.07	1.30		
Fe ²⁺	2.15	3.46	2.27		3.27	2.08	2.00	2.40	3.24	2.20	2.33		
Mn	0.03	0.10	0.02		0.09	0.07	0.02	0.02	0.09	0.02	0.02		
	5.23	6.83	5.18		6.73	5.17	5.08	5.13	6.76	5.13	5.12		
Na	0.27	0.02	0.37		0.04	0.12	0.06	0.38	0.03	0.26	0.79		
Ca	1.76	0.15	1.81		0.22	1.83	1.92	1.87	0.17	1.86	1.71		
K	0.04	0.01	0.07		0.00	0.01	0.01	0.09	0.01	0.16	0.08		
	2.07	0.18	2.25		0.26	1.96	1.99	2.34	0.21	2.28	2.58		
100 Mg Mg + Fe**	50.5	48.1	35.9		50.0	56.4	59.0	33.0	50.5	48.5	35.8		

* Bleb of hornblende inside cummingtonite

**Fe = Fe total

SPECIMEN NO.	757 C					757 C					757 C				
	MINERAL	CUMINGTONITE	CUMINGTONITE	FERRO HORNBLENDE	FERRO HORNBLENDE	CPX	FERRO ACTINOLITE	FERRO HORNBLENDE	CUMINGTONITE	CUMINGTONITE	FERRO HORNBLENDE	CUMINGTONITE	CUMINGTONITE	FERRO HORNBLENDE	
Na ₂ O	0.09	0.05	0.63	0.91	0.18	0.27	0.92	0.06	0.04	0.81	0.06	0.04	0.81		
MgO	11.66	11.32	9.32	7.44	9.67	10.28	7.31	11.38	11.41	8.20	11.38	11.41	8.20		
Al ₂ O ₃	0.51	1.02	5.45	9.26	0.93	3.04	8.60	0.71	0.63	7.66	0.71	0.63	7.66		
SiO ₂	51.38	51.14	46.80	43.51	50.06	49.76	43.16	50.64	51.28	45.41	50.64	51.28	45.41		
K ₂ O	-	-	0.31	0.53	-	0.12	0.57	-	0.00	0.47	-	0.00	0.47		
CaO	1.38	1.77	9.84	11.45	19.99	11.12	11.32	2.27	1.27	11.27	2.27	1.27	11.27		
TiO ₂	0.05	0.12	0.59	0.68	0.20	0.20	0.38	0.04	0.04	0.32	0.04	0.04	0.32		
MnO	0.70	0.65	0.31	0.21	0.36	0.28	0.25	0.73	0.72	0.23	0.73	0.72	0.23		
Fe ₂ O ₃	-	-	1.58	2.61	-	0.80	3.34	-	0.00	2.11	-	0.00	2.11		
FeO	30.97	30.30	21.20	19.61	16.12	19.75	19.43	29.93	31.13	19.95	29.93	31.13	19.95		
H ₂ O	1.94	1.94	1.94	1.92	-	1.96	1.89	1.92	1.94	1.94	1.92	1.94	1.94		
Total	98.68	98.31	97.97	98.13	97.51	97.58	97.17	97.68	98.46	98.37	97.68	98.46	98.37		
Si	7.92	7.90	7.22	6.73	1.98	7.60	6.77	7.89	7.93	6.98	7.89	7.93	6.98		
Al ^{iv}	0.08	0.10	0.78	1.27	0.02	0.40	1.23	0.12	0.07	1.02	0.12	0.07	1.02		
	8.00	8.00	8.00	8.00	2.00	8.00	8.00	8.00	8.00	8.00	8.00	8.00	8.00		
Al ^{vi}	0.02	0.08	0.21	0.43	0.02	0.15	0.36	0.02	0.04	0.38	0.02	0.04	0.38		
Ti	0.01	0.01	0.07	0.08	0.01	0.02	0.05	0.00	0.01	0.04	0.00	0.01	0.04		
Fe ³⁺	-	-	0.18	0.30	-	0.09	0.39	-	0.00	0.24	-	0.00	0.24		
Mg	2.68	2.61	2.14	1.72	0.57	2.35	1.72	2.64	2.63	1.88	2.64	2.63	1.88		
Fe ²⁺	3.99	3.91	2.74	2.54	0.53	2.52	2.55	3.90	4.02	2.57	3.90	4.02	2.57		
Mn	0.09	0.09	0.04	0.03	0.01	0.04	0.03	0.10	0.09	0.03	0.10	0.09	0.03		
	6.79	6.70	5.38	5.10	-	5.17	5.10	6.66	6.79	5.14	6.66	6.79	5.14		
Na	0.03	0.02	0.19	0.28	0.01	0.08	0.28	0.02	0.01	0.24	0.02	0.01	0.24		
Ca	0.23	0.29	1.62	1.90	0.85	1.83	1.90	0.38	0.21	1.86	0.38	0.21	1.86		
K	-	-	0.06	0.11	-	0.02	0.12	-	0.00	0.09	-	0.00	0.09		
	0.26	0.31	1.87	2.29	2.00	1.93	2.30	0.40	0.22	2.19	0.40	0.22	2.19		
<u>100 Mg</u> Mg + Fe*	40.2	40.0	42.3	37.7	51.6	47.2	36.7	40.4	39.5	40.1	40.4	39.5	40.1		

* Fe = Fe total

TABLE 3 EPMA of clinopyroxenes and amphiboles of specimen 625 C, 626 C
Portsoy intrusion

SPECIMEN NO.	625 C				625 C				
	MINERAL	CPX	ACTINO- LITE	ACTINOLITIC HORNBLLENDE	MAGNESIO HB	CPX	ACTINO- LITE	ACTINO LITE	MAGNESIO HB
	Na ₂ O	-	0.34	0.76	0.67	-	0.15	0.24	0.95
	MgO	13.30	14.21	14.06	11.39	13.23	16.83	16.56	13.78
	Al ₂ O ₃	0.79	3.04	4.90	10.45	0.72	1.62	2.60	10.00
	SiO ₂	53.47	53.36	50.27	46.29	53.69	53.80	53.27	46.44
	K ₂ O	-	0.18	0.55	0.74	-	0.04	0.12	0.98
	CaO	23.24	13.08	12.78	11.51	23.37	13.25	13.15	11.52
	TiO ₂	0.13	0.36	0.62	1.24	0.10	0.09	0.13	0.89
	MnO	0.31	0.26	0.19	0.27	0.30	0.25	0.26	0.28
	Fe ₂ O ₃	-	0.00	0.82	0.27	-	0.00	0.00	0.82
	FeO	9.06	13.57	13.19	15.60	9.83	12.05	11.82	12.37
	H ₂ O		2.08	2.05	2.04		2.09	2.09	2.05
	Total	100.30	100.48	100.19	100.47	101.24	100.18	100.24	100.08
	Si	1.99	7.68	7.315	6.785	1.99	7.72	7.63	7.77
	Al ^{iv}	0.01	0.32	0.685	1.215	0.01	0.27	0.37	1.23
		2.00	8.00	8.00	8.00	2.00	7.99	8.00	8.00
	Al ^{vi}	0.03	0.19	0.16	0.59	0.02	0.00	0.07	0.48
	Ti	0.00	0.04	0.07	0.14	0.00	0.01	0.01	0.10
	Fe ³⁺	-	0.00	0.09	0.03	-	0.00	0.00	0.09
	Mg	0.74	3.05	3.05	2.49	0.73	3.60	3.54	2.99
	Fe ²⁺	0.28	1.63	1.61	1.91	0.30	1.45	1.42	1.51
	Mn	0.01	0.03	0.02	0.03	0.01	0.03	0.03	0.03
			4.94	5.00	5.19		5.08	5.07	5.20
	Na	-	0.10	0.22	0.19	-	0.04	0.07	0.27
	Ca	0.93	2.02	2.00	1.81	0.93	2.04	2.02	1.80
	K	-	0.03	0.10	0.14	-	0.01	0.02	0.18
		1.99	2.15	2.32	2.14	1.99	2.09	2.11	2.25
	<u>100 Mg</u> Mg + Fe*	72.5	65.2	64.5	56.2	70.9	71.3	71.4	65.2

*Fe = Fe total

SPECIMEN NO.		626 C			
MINERAL	CPX	ACTINOLITE	MAGNESIO HORNBLLENDE	CPX	MAGNESIO HORNBLLENDE
Na ₂ O	0.33	0.22	0.95	0.33	1.40
MgO	14.21	16.46	11.66	14.23	12.88
Al ₂ O ₃	0.82	2.79	9.45	0.00	10.65
SiO ₂	53.82	53.16	45.63	53.08	46.21
K ₂ O	-	0.03	0.95	0.74	0.00
CaO	22.26	12.78	12.12	22.86	12.37
TiO ₂	0.27	0.22	1.83	0.14	1.35
MnO	0.24	0.23	0.28	0.24	0.20
Fe ₂ O ₃	-	2.26	0.54	-	0.55
FeO	8.80	9.91	14.97	7.32	12.41
H ₂ O		2.09	2.03		2.06
Total	100.75	100.15	100.41	98.94	100.08
Si	1.98	7.59	6.73	2.00	6.72
Al ^{iv}	0.02	0.41	1.27	0.00	1.28
	8.00	8.00	8.00	2.00	8.00
Al ^{vi}	0.02	0.06	0.34	0.00	0.54
Ti	0.01	0.02	0.20	0.00	0.15
Fe ³⁺	-	0.24	0.06	-	0.06
Mg	0.78	3.50	2.57	0.80	2.80
Fe ²⁺	0.27	1.19	1.85	0.23	1.51
Mn	0.01	0.03	0.04	0.01	0.02
		5.04	5.06		5.08
Na	0.02	0.06	0.27	0.02	0.40
Ca	0.89	1.96	1.92	0.92	1.93
K	-	0.01	0.18	0.04	0.00
	2.00	2.03	2.37	2.02	2.33
$\frac{100 \text{ Mg}}{\text{Mg} + \text{Fe}^*}$	74.3	71.0	57.4	77.7	64.1

* Fe = Fe total

TABLE 4 EPMA of primary clinopyroxene from coronite specimens of the Belhelvie mass

SPECIMEN NO.	28/19763	773 C	15/18763
MINERAL	CLINOPYROXENE		
NaO	0.37	0.48	0.27
MgO	16.25	15.82	16.42
Al ₂ O ₃	3.92	4.04	4.08
SiO ₂	51.17	51.08	51.06
CaO	20.86	20.98	20.77
TiO ₂	1.26	0.52	0.56
MnO	0.19	0.13	0.16
FeO	5.73	5.37	4.71
Total	99.75	98.41	98.03
Si	1.88	1.90	1.90
Al ^{iv}	0.12	0.10	0.10
	2.00	2.00	2.00
Al ^{vi}	0.05	0.08	0.08
Ti	0.04	0.02	0.02
Mg	0.89	0.88	0.91
Fe	0.18	0.17	0.15
Mn	0.01	0.00	0.01
Ca	0.82	0.84	0.83
Na	0.03	0.03	0.02
	2.01	2.01	2.02
$\frac{100 \text{ Mg}}{\text{Mg} + \text{Fe}}$	83.2	83.8	85.8

REFERENCES

- Allan, W.C. 1970: The Morven-Cabrach basic intrusion. Scott. J. Geol. 6, 53-72.
- Allen, V.T. and Fahey, J.J. 1957: Some pyroxenes associated with pyrometasomatic zinc deposits in Mexico and New Mexico. Bull. Geol. Soc. Am. 68, 881-896.
- Ashcroft, W.A. and Boyd, R. 1976: The Belhelvie mafic igneous intrusion, Aberdeenshire - a re-investigation. Scott. J. Geol. 12, 1-14.
- Ashworth, J.R. 1975: The sillimanite zones of the Huntly-Portsoy area in the north-east Dalradian, Scotland. Geol. Mag. 112, 113-136.
- Ashworth, J.R. 1979: Two kinds of exsolution in chondritic olivine. Mineralog. Mag. 43, 535-538.
- Ashworth, J.R. and Chinner, G.A. 1978: Coexisting garnet and cordierite in migmatites from the Scottish Caledonides. Contrib. Mineral. Petrol. 65, 379-394.
- Austrheim, H. and Robins, B. 1981: Reactions involving hydration of orthopyroxene in anorthosite-gabbro. Lithos. 14, 275-281.
- Bancroft, G.M. 1973: Mössbauer Spectroscopy. An Introduction for Inorganic Chemists and Geochemists. McGraw-Hill Book Co., Inc., New York.
- Bancroft, G.M. and Brown, J.R. 1975: A Mössbauer study of coexisting hornblendes and biotites: Quantitative Fe^{3+}/Fe^{2+} ratios. Am. Mineral. 60, 265-272.
- Bancroft, G.M., Burns, R.G. and Maddock, A.G. 1967: Determination of the cation distribution in the cummingtonite-grunerite series by Mössbauer spectroscopy. Am. Mineral. 52, 1009-1026.
- Bard, J.P. 1970: Composition of hornblendes formed during the Hercynian progressive metamorphism of the Aracena metamorphic belt (SW Spain). Contrib. Mineral. Petrol. 28, 117-134.
- Beach, A. 1974: Amphibolitization of Scourian granulites. Scott. J. Geol. 10, 35-43.
- Bohlen, S.R. and Essene, E.J. 1978: Igneous pyroxenes from metamorphosed anorthosite massifs. Contrib. Mineral. Petrol. 65, 433-442.
- Bonnichsen, B. 1969: Metamorphic-pyroxenes and amphiboles in the Biwabik Iron Formation, Dunka River area, Minnesota. Mineral. Soc. Am. Spec. Paper 2, 217-241.
- Bown, M.G. and Gay, P. 1959: The identification of oriented inclusions in pyroxene crystals. Am. Mineral. 44, 592-602.
- Boyd, R. and Munro, M. 1978: Deformation of the Belhelvie Mass, Aberdeenshire. Scott. J. Geol. 14, 29-44.

- Brady, J.B. 1974: Coexisting actinolite and hornblende from west-central New Hampshire. Am. Mineral. 59, 529-535.
- Brophy, J.H., Rose, R.M. and Wulff, J. 1964: Structure and properties of materials V.2: Thermodynamics of structure. John Wiley & Sons Inc. London 216 pp.
- Burns, R.G. and Greaves, C.J. 1971: Correlations of infrared and Mössbauer site-population measurements of actinolites. Am. Mineral. 56, 2010-2033.
- Cameron, M. and Papike, J.J. 1979: Amphibole crystal chemistry: A review. Fortschritte der Mineralogie, 57, 28-67.
- Cawthorn, R.G. 1976: Melting relations in part of the system CaO-MgO-Al₂O₃-SiO₂-Na₂O-H₂O under 5 kb pressure. J. Petrol. 17, 44-72.
- Champness, P.E. 1970: Nucleation and growth of iron oxides in olivines, (Mg, Fe)₂ SiO₄ Mineralog. Mag. 37, 790-800.
- Chinner, G.A. and Heseltine, F.J. 1979: The Grampide andalusite/kyanite isograd. Scott. J. Geol. 15, 117-127.
- Choudhuri, A. 1974: Distribution of Fe and Mg in actinolite, hornblende and biotite in some Precambrian metagreywackes from Guyana, South America. Contrib. Mineral. Petrol. 44, 45-55.
- Clarke, P.D. and Wadsworth, W.S. 1970: The Inch layered intrusion. Scott. J. Geol. 6, 7-25.
- Coe, R.S. and Kirby, S.H. 1975: The orthoenstatite to clinoenstatite transformation by shearing and reversion by annealing: Mechanism and potential applications. Contrib. Mineral. Petrol. 52, 29-55.
- Cooper, A.F. and Lovering, J.F. 1970: Greenschist amphiboles from Haast River, New Zealand. Contrib. Mineral. Petrol. 27, 11-24.
- Copley, P.A. and Gay, P. 1979: Crystallographic studies of some Norwegian aventurinised feldspars by optical, X-ray and electron optical methods. Norsk geol. Tidsskr. 59, 229-237.
- Corbett, G.J. and Phillips, G.N. 1981: Regional retrograde metamorphism of a high grade terrain: The Willyama Complex, Broken Hill, Australia. Lithos 14, 59-73.
- Dana, E.S. 1946: in Dana's Textbook of Mineralogy, 4th edition, Ford W.E. ed., John Wiley & Sons Inc. 851 pp.
- Davies, P.T.: in Zussman, J. 1977: X-ray diffraction, 392-473. In Physical methods in determinative mineralogy. Zussman, J. ed., Academic Press, 720 pp.
- Davies, B.T.C. and Boyd, F.R. 1966: The join Mg₂Si₂O₆ - CaMgSi₂O₆ at 30 kilobars pressure and its application to pyroxenes from Kimberlites, J. geophys. Res. 71, 3567-3576,
- Dowty, E. 1980: Crystal-chemical factors affecting the mobility of ions in minerals. Am. Mineral. 65, 174-182.

- Drever, H.I. 1940: The geology of Ardgour, Argyllshire. Trans. R. Soc. Edinburgh 60, 141-170.
- Elsdon, R. 1971: Clinopyroxenes from the Upper Layered Series Kap Edvard Holm, East Greenland. Mineralog. Mag. 38, 49-57.
- Emmett, T.F. 1982: The petrography and geochemistry of corona-bearing dolerites from the Jotun Nappe, central southern Norway. Mineralog. Mag. 46, 43-48.
- England, R.N. 1974: Corona structures formed by near-isochemical reaction between olivine and plagioclase in a metamorphosed dolerite. Mineralog. Mag. 39, 816-818.
- Esbensen, K.H. 1978: Coronites from the Fongen gabbro complex, Trondheim Region, Norway: role of water in the olivine-plagioclase reaction. Neues Jb. Miner. Abh. 132, 113-135.
- Fettes, D.J. 1970: The structural and metamorphic state of the Dalradian rocks and their bearing on the age of emplacement of the basic sheet. Scott. J. Geol. 6, 108-118.
- Fleet, M.E. and Barnett, R.L. 1978: Al^{IV}/Al^{VI} partitioning in calciferous amphiboles from the Froot Mine, Sudbury, Ontario. Can. Mineral. 16, 527-532.
- Fleet, M.E., Bilcox, G.A. and Barnett, R.L. 1980: Oriented magnetite inclusions in pyroxenes from the Grenville Province. Can. Mineral. 18, 89-99.
- Friedman, G.M. 1955: Petrology of the Memesagamesing Lake norite mass, Ontario, Canada. Am. J. Sci. 253, 590-608.
- Frodesen, S. 1968: Coronas around olivine in a small gabbro intrusion, Bamble Area, South Norway. Norsk geol. Tidsskr. 88, 201-206.
- Garrison, J.R. Jr. and Taylor, L.A. 1981: Petrogenesis of pyroxene-oxide intergrowths from kimberlite and cumulate rocks: co-precipitation or exsolution. Am. Mineral. 66, 723-740.
- Goldman, D.S. 1979: A re-evaluation of the Mössbauer spectroscopy of calcic amphiboles. Am. Mineral. 64, 109-118.
- Goode, A.D.T. and Moore, A.C. 1975: High pressure crystallisation of the Ewarara, Kalka and Gosse Pile intrusions, Giles complex, central Australia. Contrib. Mineral. Petrol. 51, 77-97.
- Graham, C.M. 1974: Metabasite amphiboles of the Scottish Dalradian. Contrib. Mineral. Petrol. 47, 165-185.
- Grapes, R.H. 1975: Actinolite-hornblende pairs in metamorphosed gabbros, Hidaka Mountains, Hokkaido. Contrib. Mineral. Petrol. 49, 125-140.
- Grapes, R.H. and Graham, C.M. 1978: The actinolite-hornblende series in metabasites and the so-called miscibility gap: a review. Lithos 11, 85-97.

- Grapes, R.H., Hashimoto, S. and Miyashita, S. 1977: Amphiboles of a metagabbro-amphibolite sequence, Hidaka metamorphic belt, Hokkaido. J. Petrol. 18, 285-318.
- Gresens, R.L. 1974: Discussion of "The Mineralogy of High-Temperature Shear Zones at Scourie, N.W. Scotland" by Alistair Beach. J. Petrol. 15, 413-417.
- Gribble, C.D. 1967: The basic intrusive rocks of Caledonian age of the Haddo House and Arnage districts, Aberdeenshire. Scott. J. Geol. 3, 125-136.
- Grieve, R.A.F. and Gittins, J. 1975: Composition and formation of coronas in the Hadlington Gabbro, Ontario, Canada. Can. J. Earth Sci. 12, 289-299.
- Griffin, W.L. and Heier, K.S. 1973: Petrological implications of some corona structures. Lithos 6, 315-335.
- Griffin, W.L., Jensen, B.B. and Misra, S.N. 1971: Anomalously elongated rutile in eclogite-facies pyroxene and garnet. Norsk geol. Tidsskr. 51, 177-185.
- Grove, T.L. 1977: Structural characterization of labradorite-bytownite plagioclase from volcanic, plutonic and metamorphic environments. Contrib. Mineral. Petrol. 64, 273-302.
- Hafner, S.S. and Ghose, S. 1971: Iron and magnesium distribution in cummingtonites $(\text{Fe,Mg})_7\text{Si}_8\text{O}_{22}(\text{OH})_2$. Z. Kristallogr. 133, 301-326.
- Hall, M.G. and Lloyd, G.E. 1981: The SEM examination of geological samples with a semiconductor back-scattered electron detector Am. Mineral. 66, 362-368.
- Hanan, B.B. 1976: Geochemistry and petrology of the Baltimore complex. MSc. Thesis. Virginia Polytechnic Institute and State University.
- Hanan, B.B. 1980: The petrology and geochemistry of the Baltimore mafic complex, Maryland. Ph.D. Thesis, Virginia Polytechnic Institute and State University.
- Harte, B. and Graham, C.M. 1975: The graphical analysis of greenschist to amphibolite facies mineral assemblages in metabasites. J. Petrol. 16, 347-370.
- Hawthorne, F.C. 1981: Crystal chemistry of the Amphiboles. In Amphiboles and Other Hydrous Pyriboles - Mineralogy, Ribbe, P.H. ed., Mineral. Soc. Amer. Rev. Mineral. 9A, 1-102.
- Helz, R.T. 1973: Phase relations of basalts in their melting range at $\text{PH}_2\text{O} = 5$ kb as a function of oxygen fugacity. Part I. Mafic phases. J. Petrol. 14, 249-302.
- Henry, N.F.M. 1938: The petrology of the Morven-Cabrach area, Aberdeenshire. Ph.D. Thesis. Univ. Cambridge.

- Hietanen, A. 1974: Amphibole pairs, epidote minerals, chlorite and plagioclase in metamorphic rocks, northern Sierra Nevada, California. Am. Mineral. 59, 22-40.
- Himmelberg, G.R. and Phinney, W.C. 1967: Granulite facies metamorphism. Granite Falls-Montevideo area, Minnesota. J. Petrol. 8, 325-348.
- Huang, W.T. and Merritt, C.L. 1954: Petrography of the Troctolite of the Wichita mountains, Oklahoma. Am. Mineral. 39, 549-565.
- Hudson, N.F.C. 1980: Regional metamorphism of some Dalradian pelites in the Buchan area, N.E. Scotland. Contrib. Mineral Petrol. 73, 39-51.
- Huebner, J.S. 1980: Pyroxene phase equilibria at low pressure. In Pyroxenes, Prewitt, C.T. ed., Mineral. Soc. Amer. Rev. Mineral. 7, 213-288.
- Hynes, A. 1982: A comparison of amphiboles from medium and low pressure metabasites. Contrib. Mineral. Petrol. 81, 119-125.
- Institute of Geological Sciences, 1975: Geological Survey of Great Britain (Scotland) 1: 50,000 Solid Edition Sheet 62 E: Loch Lochy.
- Issacs, A.M., Brown, P.E., Valley, J.W., Essene, E.J. and Peacor, D.R. 1981: An analytical electron microscopic study of a pyroxene-amphibole intergrowth. Contrib. Mineral. Petrol. 77, 115-120.
- Joesten, R. 1977: Evolution of mineral assemblage zoning in diffusion metasomatism. Geochim. cosmochim. Acta. 41, 649-670.
- Johnson, M.R.W. 1962: Relations of movement and metamorphism in the Dalradians of Banffshire. Trans. Edinb. geol. Soc. 19, 29-64.
- Johnson, M.R.W. and Stewart, F.H. 1960. On Dalradian structures in north-east Scotland. Trans. Edinb. geol. Soc. 18, 94-103.
- Kanisawa, S. 1974: Zoned hornblendes and associated cummingtonites from the Numabukuro plutonic mass, Kitakami Mountains, Japan. Memoirs of the Geol. Soc. of Japan. 11, 89-93.
- Kisch, H.J. and Warnaars, F.W. 1969: Distribution of Mg and Fe in cummingtonite-hornblende and cummingtonite-actinolite pairs from metamorphic assemblages. Contrib. Mineral. Petrol. 24, 245-267.
- Klein, C. 1968: Coexisting amphiboles. J. Petrol. 9, 281-330.
- Kuniyoshi, S. and Liou, J.G. 1976: Contact metamorphism of the Karmutsen Volcanics, Vancouver Island, British Columbia. J. Petrol. 17, 73-99.
- Law, A.D. and Whittaker, E.J.W. 1980: Rotated and extended model structures in amphiboles and pyroxenes. Mineralog. Mag. 43, 565-574.
- Leake, B.E. 1965: The relationship between composition of calciferous amphibole and grade of metamorphism. In W.S. Pitcher and G.W. Flinn, eds., Controls of Metamorphism, p.299-318 Oliver and Boyd, Edinburgh.

- Leake, B.E. 1978: Nomenclature of Amphiboles. Am. Mineral. 63, 1023-1052.
- Lindsley, D.H. and Anderson, D.J. 1983: A two-pyroxene thermometer. J. geophys. Res. 88, supplement, A887-A906.
- Lindsley, D.H. and Dixon, S.A. 1976: Diopside-enstatite equilibrium at 850° - 1400°C and 5-35 kbar. Am. J. Sci. 276, 1285-1301.
- Liou, J.G. 1973: Synthesis and stability relations of epidote, $\text{Ca}_2\text{Al}_2\text{FeSi}_2\text{O}_{12}(\text{OH})$. J. Petrol. 14, 381-413.
- MacKenzie, W.S. 1957: The crystalline modifications of $\text{NaAlSi}_3\text{O}_8$. Am. J. Sci. 255, 481-516.
- Magruder, G.L. 1981: The chemical petrology of the corona growth: olivine + plagioclase \rightarrow orthopyroxene + amphibole + spinel in an anorthositic gabbro of the Wilmington Complex. MSc Thesis, University of Delaware.
- Mason, R. 1967: Electron-Probe microanalysis of coronas in a troctolite form Sulitjelma, Norway. Mineralog. Mag. 36, 504-514.
- McGregor, D.M. and Wilson, C.D.V. 1967: Gravity and magnetic surveys of the younger gabbros of Aberdeenshire. Q. Jl. geol. Soc. Lond. 123, 99-123.
- McLelland, J.M. and Whitney, P.R. 1980: A generalized garnet-forming reaction for meta-igneous rocks in the Adirondacks. Contrib. Mineral. Petrol. 72, 111-122.
- Medaris, L.G. 1969: Partitioning of Fe^{2+} and Mg^{2+} between coexisting synthetic olivine and orthopyroxene. Am. J. Sci. 267, 945-968.
- Medaris, L.G., Jr., 1975: Coexisting spinel and silicates in alpine peridotites of the granulite facies. Geochim. cosmochim. Acta. 39, 947-958.
- Mersmann, M.A. 1981: Metamorphism of a gabbronorite dike: corona development and amphibolitization, Hellroaring Lakes Area, Beartooth Mountains, Montana. MSc Thesis. University of Cincinnati.
- Miller, C. 1974: Reaction rims between olivine and plagioclase in metaperidotites, Ötztal Alps, Austria. Contrib. Mineral. Petrol. 43, 333-342.
- Misch, P. and Rice, J.M. 1975: Miscibility of tremolite and hornblende in progressive Skagit Metamorphic Suite, North Cascades, Washington. J. Petrol. 16, 1-21.
- Mongkoltip, P. and Ashworth, J.R. 1983: Exsolution of ilmenite and rutile in hornblende. Am. Mineral. 68, 143-155.
- Mongkoltip, P. and Ashworth, J.R. 1983: Quantitative estimation of an open-system symplectite-forming reaction: restricted diffusion of Al and Si in coronas around olivine. J. Petrol. in press.

- Moore, A. 1968: Rutile exsolution in orthopyroxene. Contrib. Mineral. Petrol. 17, 233-236.
- Moseley, D. 1981: Ilmenite exsolution in olivine. Am. Mineral. 66, 976-979.
- Munro, M. 1970: A re-assessment of the "younger" basic igneous rocks between Huntly and Portsoy based on new borehole evidence. Scott. J. Geol. 6, 41-52.
- Murthy, M.V.N. 1958: Coronites from India and their bearing on the origin of coronas. Bull. geol. Soc. Am. 68, 23-38.
- Nakajima, Y. and Ribbe, P.H. 1980: Alteration of pyroxenes from Hokkaido, Japan, to amphibole, clays, and other biopyriboles. Neues Jb. Miner. Monatsh. 258-268.
- Nakajima, Y. and Ribbe, P.H. 1981: Texture and structural interpretation of the alteration of pyroxene to other biopyriboles. Contrib. Mineral. Petrol. 78, 230-239.
- Nehru, C.E. and Wyllie, P.J. 1974: Electron microprobe measurement of pyroxenes coexisting with H_2O - undersaturated liquid in the join $CaMg Si_2O_6 - Mg_2 Si_2O_6 - H_2O$ at 30 kilobars with applications to geothermometry. Contrib. Mineral. Petrol. 48, 221-228.
- Neumann, E.R. 1976: Compositional relations among pyroxenes, amphiboles and other mafic phases in the Oslo Region plutonic rocks. Lithos 9, 85-109.
- Nishiyama, T. 1983: Steady diffusion model for olivine - plagioclase corona growth. Geochim. Cosmochim. Acta. 47, 283-294.
- Oba, T. 1980: Phase relations in the tremolite - pargasite join. Contrib. Mineral. Petrol. 71, 247-256.
- O'Hara, M.J. and Stewart, F.H. 1966: Olivine - liquid reaction and the depth of crystallization of the east Aberdeenshire gabbros. Nature 210, 830-831.
- Oliver, T.A. 1951: The effect of uralitization upon the chemical composition of the Sudbury norite. Am. Mineral. 36, 421-429.
- Pankhurst, R.J. 1970: The geochronology of the basic igneous complexes. Scott. J. Geol. 6, 83-107.
- Pankhurst, R.J. 1974: Rb-Sr whole-rock chronology of Caledonian events in northeast Scotland. Bull. geol. Soc. Am. 85, 345-350.
- Papike, J.J., Ross, M. and Clark, J.R. 1969: Crystal-chemical characterization of clinoamphiboles based on five new structure refinements. Mineral. Soc. Amer. Spec. Paper 2, 117-136.
- Papike, J.J., Prewitt, C.T., Sueno, S. and Cameron, M. 1973: Pyroxenes: comparison of real and ideal structural topologies. Z. Kristallogr. 138, 254-273.

- Papike, J.J. Cameron, K.L. and Baldwin, K. 1974: Amphiboles and pyroxenes: characterization of other than quadrilateral components and estimates of ferric iron from microprobe data. Geol. soc. Amer. Program Abstr. 6, 1053-1054.
- Piispanen, R. and Alapieti, T. 1977: Uralitization - an example from Kuusamo, Finland. Bull. geol. Soc. Fin. 49, 39-46.
- Pluysnina, L.P. and Ivanov, I.P. 1981: Thermodynamic regime of greenstone metamorphism of basic volcanic rocks after experimental data. Can. J. Earth. Sci. 18, 1303-1309.
- Raase, P. 1974: Al and Ti contents of hornblende, indicators of pressure and temperature of regional metamorphism. Contrib. Mineral. Petrol. 45, 231-236.
- Read, H.H. 1923: The petrology of the Arnage district in Aberdeenshire: a study of assimilation. Q. Jl. geol. Soc. Lond. 79, 446-480.
- Read, H.H. 1923: The geology of the country around Banff, Huntly and Turriff. Mem. geol. Surv. Scotland for sheets 86 and 96.
- Read, H.H. and Farquhar, O.C. 1956: The Buchan Anticline of the Banff Nappe of Dalradian rocks in north-east Scotland. Q. Jl. geol. Soc. Lond. 112, 131-156.
- Read, H.H., Sadashivaiah, M.S. and Haq, B.T. 1961: Differentiation in the Olivine - Gabbro of the Inch Mass, Aberdeenshire. Proc. Geol. Assoc. Lond. 72, 391-413.
- Reed, S.J.B. 1975: Electron Microprobe Analysis. Cambridge Univ. Press, London. 395 pp.
- Reynolds, R.C. and Frederickson, A.F. 1962: Corona development in Norwegian hyperites and its bearing on the metamorphic facies concept. Bull. geol. Soc. Am. 73, 59-71.
- Robie, R.A., Bethke, P.M., Toulmin, M.S. and Edwards, J.L. 1966: X-ray crystallographic data, densities and molar volumes of minerals. In: Handbook of physical constants. S.P. Clark, ed. Geol. Soc. Am. Mem. 97, 587 pp.
- Robinson, P., Spear, F.S., Schumacher, J.C., Laird, J., Klein, C., Evans, B.W. and Doolan, B.L. 1982: Phase relations of metamorphic amphiboles: Natural occurrence and theory. In amphibole: Petrology and experimental phase relations. Veblen D.R., and Ribbe, P.H. eds., Mineral. Soc. Amer. Rev. Mineral. 9B, 1-228.
- Rodgers, K.A. 1973: Uralites and uralitization in the ultramafic belt of southern New Caledonia. Geol. Mag. 110, 125-131.
- Rose, G. 1831, cited in Dana's Textbook of Mineralogy 4th edition. 1946: Ford, W.E. ed. John Wiley & Sons. Inc. 851 pp.
- Ross, M., Papike, J.J. and Shaw, K.W. 1969: Exsolution textures in amphiboles as indicators of subsolidus thermal histories. Mineral. Soc. Amer. Spec. Paper 2, 275-299.

- Ross, M., Papike, J.J. and Weiblen, P.W. 1968. Exsolution in clin amphiboles. Science 159, 1099-1104.
- Sampson, G.A. and Fawcett, J.J. 1977: Coexisting amphiboles from the Hastings region of southeastern Ontario. Can. Mineral. 15, 283-296.
- Sapountzis, E.S. 1975: Coronas from the Thessaloniki Gabbros (north Greece). Contrib. Mineral. Petrol. 51, 197-203.
- Seifert, F. 1977: Compositional dependence of the hyperfine interaction of ^{57}Fe in anthophyllite. Phys. Chem. Minerals. 1, 43-52.
- Shackleton, R.M. in discussion with Read and Farquhar, 1956: The Buchan anticline of the Banff nappe of Dalradian rocks in north-east Scotland. Q. Jl. geol. Soc. Lond. 112, 131-156.
- Shand, S.J. 1945: Coronas and Coronites, Bull. geol. Soc. Am. 56, 247-266.
- Shido, F. and Miyashiro, A. 1959: Hornblende of the basic metamorphic rocks. Tokyo Univ. Fac. Sci. J. Sec II, 12, 85-102.
- Smith, P.P.K. 1977: An electron microscopic study of amphibole lamellae in augite. Contrib. Mineral. Petrol. 59, 317-322.
- Smyth, J.R. 1974: Experimental study on the polymorphism of enstatite. Am. Mineral. 59, 345-352.
- Spear, F.S. 1981: Amphibole-plagioclase equilibria: an empirical model for the relation albite + tremolite = edenite + 4 quartz. Contrib. Mineral. Petrol. 77, 355-364.
- Spear, F.S. 1981: An experimental study of hornblende stability and compositional variability in amphibolite. Am. J. Sci. 281, 697-734.
- Starmer, I.C. 1969: Basic plutonic intrusions of the Risør - Söndeled area, south Norway: the original lithologies and their metamorphism. Norsk geol. Tidsskr. 49, 403-431.
- Stewart, F.H. 1947: The gabbroic complex of Belhelvie in Aberdeenshire. Q. Jl. geol. Soc. Lond. 102, 465-498.
- Stewart, F.H. 1970: The Younger basic igneous complexes of north east Scotland and their metamorphic envelope. Scott. J. Geol. 6, 3-6.
- Stewart, F.H. and Johnson, M.R.W. 1960: The structural problem of the Younger gabbros of north-east Scotland. Trans. Edinb. geol. Soc. 18, 104-112.
- Stoker, M.S. 1980: The geology of eastern Ardgour. Ph.D. Thesis, Liverpool University.
- Stormer, J.C. and Whitney, J.A. 1977: Two feldspar geothermometry. Contrib. Mineral. Petrol. 65, 123-133.

- Stout, J.H. 1972: Phase petrology and mineral chemistry of coexisting amphiboles from Telemark, Norway. J. Petrol. 13, 99-146.
- Strens, R.G.J. 1965: Stability and relations of the Al-Fe epidotes. Mineralog. Mag. 35, 464-475.
- Tagiri, M. 1977: Fe - Mg partition and miscibility gap between coexisting calcic amphiboles from the Southern Abukuma Plateau, Japan. Contrib. Mineral. Petrol. 62, 271-281.
- Thompson, J.B., Jr. 1970: Geometrical possibilities for amphibole structures: model biopyriboles. Am. Mineral. 55, 292-293.
- Thomson, M.L., Fleet, M.E. and Barnett, R.L. 1981: Amphiboles from the Renzy Lake ultramafic complex, south-western Quebec. Can. Mineral. 19, 469-477.
- van Lamoen, H. 1979: Coronas in Olivine Gabbros and Iron Ores from Susimäki and Riuttamaa, Finland. Contrib. Mineral. Petrol. 68, 259-268.
- Veblen, D.R. and Buseck, P.R. 1981: Hydrous pyriboles and sheet silicates in pyroxenes and uralites: intergrowth microstructures and reaction mechanisms. Am. Mineral. 66, 1107-1134.
- Vernon, R.H. 1972: Reactions involving hydration of cordierite and hypersthene. Contrib. Mineral. Petrol. 35, 125-137.
- Vernon, R.H. and Pooley, G.D. 1981: SEM/microprobe study of some symplectic intergrowths replacing cordierite. Lithos. 14, 75-82.
- Wadsworth, W.J., Stewart, F.H. and Rothstein, A.T.V., 1966: Cryptic layering in the Belhelvie intrusion, Aberdeenshire. Scott. J. Geol. 2, 54-66.
- Watt, W.R. 1914: Geology of the country around Huntly (Aberdeenshire). Q. Jl. geol. Soc. Lond. 70, 266-293.
- Weedon, D.S. 1965: Corona Structures in the Basic Igneous Masses of East Aberdeenshire. Nature 208, 885.
- Weedon, D.S. 1970: The ultrabasic/basic igneous rocks of the Huntly region. Scott. J. Geol. 6, 26-40.
- Wells, O.C. 1974: Scanning electron microscopy. McGraw Hill. 421 pp.
- Whitney, P.R. and McLelland, J.M. 1973: Origin of coronas in Metagabbros of the Adirondack Mountains, N.Y. Contrib. Mineral. Petrol. 39, 81-98.
- Wiseman, J.D.H. 1934: The central and southwest Highland epidiorites: a study in progressive metamorphism. Q. Jl. Geol. Soc. Lond. 90, 354-417.
- Wood, B.J. and Banno, S. 1973: Garnet-orthopyroxene and orthopyroxene-clinopyroxene relationships in simple and complex systems. Contrib. Mineral. Petrol. 42, 109-124.

Yamaguchi, Y., Akai, J. and Tomita, K. 1978: Clinoamphibole
lamellae in diopside of garnet lherzolite from Alpe Arami,
Bellinzona, Switzerland. Contrib. Mineral. Petrol. 66, 263-270.